

RENATA KOTYNIA

**FRP COMPOSITES  
FOR FLEXURAL STRENGTHENING  
OF CONCRETE STRUCTURES  
THEORY, TESTING, DESIGN**

LODZ UNIVERSITY OF TECHNOLOGY

LODZ 2019

**LODZ UNIVERSITY OF TECHNOLOGY**



**RENATA KOTYNIA**

**FRP COMPOSITES FOR FLEXURAL  
STRENGTHENING OF CONCRETE STRUCTURES  
THEORY, TESTING, DESIGN**

LODZ 2019

Reviewers:  
Prof. PhD. Eng. Joost Walraven  
Prof. PhD. Eng. Wojciech Radomski

Scientific Editor of the Faculty of Civil Engineering  
Architecture and Environmental Engineering:  
PhD. Eng. Marek Jabłoński

Cover design:  
PhD. Eng. Arch. Tomasz Krotowski  
Architectural Design Institute of Architecture and Urban Planning, TUL

Text setting:  
MSc Eng. Jacek Filipczak

@ Copyright by Lodz University of Technology 2019

LODZ UNIVERSITY OF TECHNOLOGY PRESS  
90-924 Łódź, ul. Wólczajska 223  
Tel. 42-631-20-87; 42-631-29-52  
Fax 42-631-25-38  
e-mail: [zamowienia@info.p.lodz.pl](mailto:zamowienia@info.p.lodz.pl)  
[www.wydawnictwo.p.lodz.pl](http://www.wydawnictwo.p.lodz.pl)

ISBN 978-83-7283-996-1  
DOI: 10.34658/9788372839961  
<https://doi.org/10.34658/9788372839961>

Offset printing by “Quick-Druk”, 95-100 Łódź, ul. Łąkowa 11  
Edition 100 copies  
No. 2302

---

## Contents

---

<b>Preface</b>	5
<b>Symbols</b>	9
<b>1. Introduction</b>	17
1.1. Overview	17
1.2. FRP materials	17
1.2.1. Fibres	18
1.2.2. Matrices	21
1.2.3. Adhesives	22
1.3. FRP composites	23
1.4. FRP strengthening systems.	30
<b>2. Flexural strengthening</b>	35
2.1. State of the art in research	35
2.2. Failure mechanisms of FRP strengthened RC members	36
2.3. Strengthening with prestressed FRP members	49
2.4. Preloading effect.	51
<b>3. FRP to concrete bond behaviour</b>	53
3.1. Debonding mechanisms.	53
3.2. Bond behaviour between FRP and concrete.	55
3.3. Effective bond length	61
3.3.1. <i>fib</i> Bulletin 14, 2001.	61
3.3.2. CNR–DT 200 R1, 2013.	61
3.3.3. <i>fib</i> Bulletin 90, 2019.	62
3.3.4. ACI 440.2R–08, 2008	63
3.3.5. Other approaches to the effective bond length	64
3.4. Theoretical bond models	67
3.4.1. Shear capacity based models	67
3.4.2. Concrete tooth models	70
3.4.3. Interfacial stress based models	72
<b>4. Bond strength models</b>	79
4.1. Empirical models.	79
4.2. Shear bond slip models	81
4.2.1. Fracture mechanics models.	82
4.2.2. Meso–scale finite element model	87
4.3. Parameters effecting the FRP to concrete bond behaviour	91
<b>5. Design guidelines and code formulations</b>	97
5.1. ACI 440.2R–08	97
5.2. <i>fib</i> Bulletin 14	97
5.3. <i>fib</i> Bulletin 90	100
5.4. JSCE recommendations.	105

5.5. Concrete Society TR55 . . . . .	105
5.6. CNR DT200 . . . . .	105
5.6.1. CNR DT200/2004 . . . . .	105
5.6.2. CNR DT200/2013 . . . . .	107
5.7. Swiss guide SIA166 2004 . . . . .	108
5.7.1. Strengthening with non-prestressed FRP laminates . . . . .	108
5.7.2. Strengthening with prestressed FRP laminates (Gradient method) . . . . .	111
5.8. German simplified method DAFStb (2014) . . . . .	113
5.9. The comparison of design approaches . . . . .	114
<b>6. Advanced design models . . . . .</b>	<b>117</b>
6.1. Accurate analysis of bond strength according to DAFStb . . . . .	117
6.1.1. Curvature effect on the bond behaviour . . . . .	118
6.1.2. Flexural strength analysis . . . . .	120
6.1.3. Accurate method for IC FRP debonding. . . . .	123
6.1.4. End anchorage analysis . . . . .	130
6.2. Fundamental mechanics model . . . . .	137
<b>7. Author's approach to flexural strengthening . . . . .</b>	<b>151</b>
7.1. Description of the model . . . . .	151
7.2. Comparative analysis of the tested members . . . . .	156
7.3. Parametric analysis . . . . .	159
<b>8. Chosen nonlinear finite element models . . . . .</b>	<b>167</b>
8.1. Nonlinear finite element analysis by R. Kotynia, H. Abdel Baky, K. Neale and U. A. Ebead (2009) . . . . .	167
8.1.1. Material modelling for concrete, steel and FRP . . . . .	168
8.1.2. FRP to concrete interface bond model . . . . .	170
8.1.3. Geometrical modelling . . . . .	172
8.1.4. Numerical results and discussion . . . . .	175
8.1.5. Interfacial shear slip profile . . . . .	178
8.1.6. Conclusion . . . . .	183
8.2. Nonlinear finite element analysis by Sz. Serega, R. Kotynia and K. Lasek (2018) . . . . .	184
8.2.1. Finite element model of preloaded RC beams strengthened with prestressed CFRP laminates. . . . .	184
8.2.2. Constitutive material models . . . . .	185
8.2.3. Strategy of numerical simulations. . . . .	198
8.2.4. Parametric study . . . . .	204
8.2.5. Conclusions . . . . .	212
<b>9. Conclusions . . . . .</b>	<b>215</b>
<b>References . . . . .</b>	<b>217</b>

## Preface

More than twenty years of author's research on reinforced concrete members strengthened with FRP materials ensured to write this book as a summary of the own experiences and development of modelling of concrete structures strengthened in flexure with adhesively bonded (AB) fibre reinforced polymer (FRP) materials.

The purpose of this book is to provide structural and mechanical engineers with simplified and advanced model for flexural strengthening of reinforced concrete members with externally bonded (called in the last nomenclature EB) FRP reinforcement. The review of existing bond models is to explain phenomenon of bond losing between FRP and concrete. The detailed analysis of variable parameters shows complexity this problem.

The latest bond research proved a big effect of nonaxial action on the FRP reinforcement, which is observed in the full scale RC FRP strengthened members. The new knowledge on behaviour induced necessity of revision existing design approaches to the new generation of guidelines based on more accurate design approaches.

It should be noted that this book does not specify details of the safety concept based on the accurate factors for EB FRP strengthened RC members. The scientific research summarized in this book based only on non-anchored externally applied pre-cured FRP laminates or cured in-situ FRP sheets. The near surface mounted (NSM) FRP technique is not the object of this book.

The main author's aim is to emphasize the uploaded design rules based on the simplified and more accurate design approaches. The idea to introduce more advanced approaches in comparison to the simplified ones is to change existing conservative approaches for more economically efficient design.

It should be emphasized that the book focuses only on the flexure, while the shear capacity, which is evidently connected with bending is not considered in this book. Obviously the RC members flexurally strengthened needs always shear analysis as well.

This book steers for the scientific approaches and it shows tendency of changes in designing FRP strengthened RC members than practical guidelines referring to the ultimate and serviceability limit states. The long term effects in flexural strengthening are not considered here.

This book consisting of eight chapters collecting the published results of a mount of researches and experts in applications of the FRP materials for flexural strengthening of RC structures.

Chapter 1 provides a review of the FRP materials with a special focus on their anisotropic structure, strength characteristics and exiting FRP strengthening systems. Chapter 2 gives a state of art in the published research of the flexurally strengthened RC members with an accurate analysis of the failure mechanisms. Chapter 3 delves into details of the FRP-to-concrete bond mechanisms based on

variable bond tests with the special focus on the effective bond strain and the bond length based on many published theoretical models. Chapter 4 describes bond behaviour on the simple empirical models, shear bond slip models and advanced meso-scale finite element models. Chapter 5 gives the most practical summary of design guidelines and code formulations with a special distinction on the fib Bulletins (the old and new version) and both Italian guidelines CNR-DT 200 versions (2004 and 2013). A review of the Swiss guide SIA166 (2004) was presented due to strong support of PhD thesis by Czaderski, 2012. Chapter 6 presents two advanced design models published in DafStB (2014) and Oehlers et al. (2015). One of the accurate method proposed in DafStB (2014) considers bond strength transmission at the segment of RC members between cracks. The phenomenon of this method based on effects of curvature, crack pattern and segmental behaviour of the strengthened RC element. Another much more complex model proposed by Oehlers at al., 2015 based on fundamental mechanics. The novelty of this method based on the mechanics of displacements in the three-dimensional partial-interaction moment-rotation model, however due to complexity of this model is not applicable for practical design. This book focuses on new generation guidelines, which can be recommended for practical applications. Chapter 7 presents the author's analytical model for RC members strengthened in flexure with EB FRP materials with the parametric analysis of the steel and FRP reinforcement ratio on the IC debonding failure. It confirms the important effect of the RC member stiffness on the strengthening efficiency. This analysis could be useful for practical applications. Chapter 8 presents two finite element models and comparison with the own author's experimental tests. The first one based on collaboration with Prof. K. Neale, U. Ebead and dr. H. A. Baky from Sherbrooke University. The second one is the result of collaboration with dr. Serega from Krakow University of Technology, who proposed advanced model for analysis of author's experimental test results. Chapter 9 gives the summary and main conclusions.

This book provides a concise review of existing research on the behaviour and strength of FRP-strengthened RC structures, with a strong focus on the studies which based on development of new strength models and advanced design models. It grew out by a lot of published research of many researches all over the world mainly from the EMPA, the Hong Kong Polytechnic, the University of Adelaide, the University of Naples Federico II, University of Bologna, University of Padua, University of Sannio and others.

The author would like to thank personally many professors and researches, who supported this book by their valuable comments and discussions during scientific meetings, conferences and working committees. The special thanks are indebted to professors, doctors and researches: U. Meier, J.G. Teng, J.F. Chen, D. Oehlers, T. Triantafillou, K. Zilch, R. Niedermeier, W. Finckh, K. Neale, T. Ueda, R. Al-Mahaidi, R. Seracino, L. Bank, Z. Wu, A. Nanni, J. Dai, B. Täl-

## Preface

---

jsten, S. Smith, X.Z. Lu, C. Modena, C. Pellegrino, Ch. Czaderski, F. Ceroni, C. Carloni, C. Faella, , A. Bilotta, C. Mazzotti, A. Prota, I. Iovinella and companies: Sika, S&P, Mapei, Megachemie and Tyfo. Special thanks the author sends to dr. Serega for his outstanding contribution in modeling analysis.

Remarkable acknowledgements the author would like to send to the fib Committee Task Group 5.1 members (mainly to prof. S. Matthys, who accepted to use the new version of *fib* Bulletin 90, 2019, which is still under publishing process). Moreover the author renders acknowledgements to the RILEM Technical Committee for their support and acceptance for using RILEM Report 234-DUC in this book.

Last but not least thanks are expressed to dr. M. Kaszubska and J. Filipczak, who put a big effort to edit this book, moreover Phd students and laboratory technicians for their strong support in high quality research.

Finally, the author addresses unlimited thanks to the Reviewers of this book: Prof. J. Walraven and Prof. W. Radomski for their valuable comments.

Renata Kotynia  
Lodz University of Technology



## Symbols

$A_e$	– area of concrete in tension
$A_{FE}$	– area of an individual finite element
$A_p$	– axial tensile force
$A_s, A_{s1}$	– cross section area of tensile steel reinforcement
$A_{sv}$	– cross sectional area of steel stirrups
$B$	– shear span
$B_{max-p}, B_{IC}$	– maximum bond force
$B_{mod}$	– modified shear span
$C$	– coefficient of cohesion
$E_a$	– modulus of elasticity of adhesive layer
$E_c, E_{cm}$	– elasticity modulus of concrete
$E_f, E_{frp}$	– elasticity modulus of FRP
$E_m$	– elasticity modulus of matrix
$E_s$	– elasticity modulus of steel
$E_x$	– modulus of elasticity of a ply loaded at an angle $\theta$ to fibre direction
$E_1, E_2$	– elasticity modulus of composite laminate parallel and perpendicular to fibres
$\bar{E}_n, \bar{E}_t$	– secant elastic modulus in normal, tangent directions to first crack
$F_{bLRd}$	– bond resistance at idealized end anchorage body
$F_{bsm}$	– bond force per length
$F_{cr}$	– force in FRP laminate at last crack
$F_{cd}$	– concrete compressive force
$F_{fb}$	– tensile force in FRP debonding
$F_{fu}$	– ultimate tensile strength of laminate
$F_{lR}$	– anchorage resistance of strip
$F_{lR,red}$	– reduced anchorage resistance
$F_{Ld}$	– tensile force in CFRP reinforcement
$F_{LEd}$	– acting FRP force without redistribution
$F_p$	– prestressing force
$F_{s1d}, F_{s2d}$	– force in tensile, compressive reinforcement
$F_{u,exp}$	– ultimate failure load
$F_{u,0}$	– ultimate load of non-strengthened member

$F_u(\alpha_b)$	– contact pressure
$G$	– shear modulus
$G_a$	– shear modulus of adhesive layer
$G_f, G_{Fk}, G_{ft}$	– fracture energy
$G_{12}$	– in-plane shear modulus of laminate
$I_A$	– second moment of area of tooth
$I_c$	– second moment of area of beam
$I_{frp}, I_s$	– second moment of area of cracked strengthened section transformed to concrete with FRP laminate and an equivalent steel laminate
$I_{rc,c}$	– cracked second moment of area of FRP laminate section transformed to concrete
$I_{rc,frp}$	– second moment of area of cracked plated section transformed into FRP
$I_{ru,c}$	– uncracked second moment of area of plated section transformed to concrete
$K_s, K_n$	– shear stiffness, normal stiffness
$K_t$	– stiffness in tangential direction
$K_{te}$	– initial stiffness
$L_b$	– anchoring length
$L_{db}$	– unbonded FRP distance
$L_{bmax}$	– maximum anchoring length
$L$	– bond length
$L_{db-p}$	– extension of debonded region
$L_{def}$	– lengths of segment
$L_{wdg}$	– length of wedge
$L_e, L_p, L_f$	– effective FRP bond length
$M_A$	– moment at base of tooth
$M_{cr}$	– cracking moment
$M_{db,end}$	– bending moment in RC beam at plate end at its debonding
$M_{db,f}$	– flexural debonding moment
$M_{Ed}$	– acting moment
$M_{Rd}$	– load bearing capacity
$M_{u0}, M_u$	– ultimate bending moment of non-strengthened and strengthened specimen
$M_0$	– preloading bending moment

## Symbols

---

$N_f, N_p, P_p$	– force in FRP reinforcement
$V_{Ay}$	– debonding force
$V_c, V_s$	– concrete and shear steel reinforcement contribution to shear capacity of RC member
$V_{db,end}, V_{db,s}$	– critical shear force in RC beam at plate end at its debonding
$W_{c,0}$	– section modulus of uncracked concrete cross section
$P_{cc}$	– concrete compressive force
$P_{ct}$	– tensile force in concrete
$P_{IC}$	– maximum force in FRP reinforcement
$P_{pc}$	– FRP prestressing force
$P_{pp}$	– passive prestress
$P_{rc}, P_{rt}$	– tensile and compressive force in steel reinforcement
$P_I$	– ultimate normal force per unit width of FRP strip at onset of bond zone
$P_{II}$	– bond strength under pure mode II loading
$S_{frp}, S_s$	– first moment of area of FRP and steel laminate about neutral axis of cracked strengthened section transformed to concrete
$S_{pr}$	– primary crack spacing
$T_g$	– glass transition temperature
$W_f, W_m, W_c$	– weight mass of fibre, matrix and FRP composites
$a$	– distance from support to nearer end of FRP laminate
$a_A, a_P$	– midspan displacement for active and passive strengthened beam at ultimate load
$a_1, a_2$	– material constants determined empirically
$b_a$	– width of adhesive layer
$b_c$	– width of strengthened RC element
$b_f, b_F, b_{frp}$	– width of external FRP reinforcement
$b_{Lw}$	– width of transversal shear strap
$c_f$	– constant determined in linear regression analysis
$c_1, c_2$	– empirical factors
$d, h'$	– effective depth of steel tensile reinforcement
$d_{frp}$	– distance from compressive face of RC beam to centroid of FRP plate
$d_{NA}$	– depth of neutral axis
$f_{bsm}$	– mean bond stress of reinforcing steel

$f_c, f_c', f_{ck}$	– characteristic compressive concrete strength
$f_{c,cube}, f_{cu}$	– compressive strength of concrete on cubic specimens
$f_{cm}$	– mean compressive strength of concrete
$f_{ct}$	– cylinder concrete splitting tensile strength
$f_{ctm}$	– medium tensile concrete strength
$f_{ctm,surfx}$	– near-surface tensile strength
$f_f, f_{fu}$	– tensile strength of FRP reinforcement
$f_{fb}$	– maximum tensile stress
$f_{fbd}$	– design debonding strength
$f_{fbd,IC}$	– lower fractile (5%) value of bond strength
$f_{fbd,IC}$	– design value of FRP bond strength corresponding to intermediate crack debonding
$f_{fbm}$	– 5% debonding strength
$f_{fbm,IC}$	– mean value of bond strength
$f_{fbk}$	– characteristic debonding strength
$f_{fd}$	– design tensile strength of FRP
$f_{fdd}$	– maximum stress that can be carried by composite preventing end plate debonding failure
$f_m$	– tensile strength of matrix
$f_{yv}, f_y$	– steel yielding stress of steel stirrups
$f_{su}$	– ultimate tensile strength of steel
$f_t$	– concrete tensile strength
$g_t$	– post critical slope of function
$h$	– beam's depth
$h_1$	– effective depth of cross section
$i_A$	– micro-average inclination angle
$k_a$	– concrete coefficient
$k_c$	– factor accounting for concrete compaction
$k_m$	– numerical coefficient
$k_f$	– shape factor
$k_f$	– geometrical factor related to width of bonded plate
$k_f$	– width coefficient defined
$k_G$	– fracture energy coefficient
$k_r$	– roughness coefficient

## Symbols

---

$k_v$	– empirical coefficient limiting ultimate strain in FRP reinforcement
$l$	– crack spacing
$l_b$	– bond length
$l_{ba}$	– active bond length at FRP end
$l_{bL,max}$	– effective bond length
$l_{bL,lim}$	– effective bond length
$l_{e,0}$	– transfer length of reinforcing steel
$l_{se}$	– distance between end of strip and support
$l_0$	– axial span length
$n$	– coefficient governing softening branch
$n_{s,i}$	– number of steel bars with diameter $\varnothing_{s,i}$
$q$	– uniformly distributed load
$s$	– stirrup spacing
$s$	– slip
$\bar{s}$	– slip at peak
$s_f$	– slip corresponding to complete separation of interface
$s_{f,max}$	– maximum slip
$s_{Lr}$	– slip of strip
$s_{max}$	– maximum slip
$s_r$	– distance between cracks
$s_u, s_0$	– ultimate slip between FRP and concrete support
$t_a$	– thickness of adhesive layer
$t_c$	– thickness of concrete member
$t_f, t_{frp}$	– thickness of FRP reinforcement
$t_m$	– time of stress increase
$t_{max}$	– maximum traction
$t_n, t_t, t_{res,p}$	– normal traction, tangential traction, residual traction
$u$	– average bond strength of steel to concrete
$\bar{u}_n$	– relative normal displacement
$\bar{u}_t$	– relative displacement in tangential direction (concrete–laminated slip)
$\bar{u}_{t0}$	– slip associated with $t_{max}$
$v_f$	– volume fraction of fibre
$v_m$	– volume fraction of matrix
$w$	– crack width
$w_f$	– weight or mass fraction of fibre

$w_m$	– weight or mass fraction of matrix
$x$	– distance along FRP laminate from its end
$x_{tru,c}$	– neutral axis depth of this transformed section
<hr/>	
$\Delta\varepsilon_{f,max}$	– additional strain in strip due to external loads
$\Delta\sigma_f$	– stress variation in FRP between two adjacent cracks
$\Delta\sigma_R$	– maximum tensile stress increase transferred by bond stresses along crack spacing
$\Delta F_{cr}$	– force increase in FRP reinforcement due to loading
$\Delta F_{fEd}$	– change of tensile force in FRP reinforcement
$\Delta F_L$	– total change force in FRP reinforcement
$\Delta F_{L,1}$	– increase in bond force due to shear wrapping
$\Delta F_{FLk,Bf}$	– bond component from additional bond frictional
$\Delta F_{FLk,BL}$	– bond component from bilinear bond stress–slip relationship
$\Delta F_{FLk,KF}$	– bond component from curvature effect by bearable CFRP-strip stress
$\Delta F_{LEd}$	– change in FRP force in segment between cracks
$\Delta F_{LRd}$	– change in FRP force that can be accommodated by bond
$\sum Q_{bars}$	– total perimeter of tensile reinforcing bars
$\varnothing_s$	– diameter of steel reinforcement
$\alpha$	– reduction factor to account for influence of inclined cracks on bond strength
$\alpha$	– material constant that describes post critical slope of function $g_t$
$\alpha_{cc}, \alpha_{ct}$	– coefficients of long-term durability of concrete
$\alpha_{th}$	– normal expansion coefficient
$\beta$	– shear retention factor
$\beta_a$	– coefficient factor of loading angle effect
$\beta_w$	– width ratio parameter
$\gamma_{BA}, \gamma_f, \gamma_c, \gamma_{bd}$	– safety coefficients
$\delta$	– interface slip along sliding plane
$\delta_{max}$	– maximum slip
$\delta_p$	– FRP laminate slip at crack face
$\varepsilon_c, \varepsilon_{cr1}, \dots$	– compressive concrete strain
$\varepsilon_{cp}$	– concrete strain in tension

## Symbols

---

$\varepsilon_{cu}$	– ultimate concrete strain
$\varepsilon_{c0}$	– concrete strain at bottom cross section
$\varepsilon'_{c0}$	– concrete strain at top cross section
$\varepsilon_{cs}(t)$	– mean shrinkage strain evolution in time $t$ due to cement hydration and concrete drying
$\varepsilon_{f,b}$	– bond strain
$\varepsilon_{fd}, \varepsilon_{IC}$	– maximum axial strain of FRP corresponding to intermediate crack debonding
$\varepsilon_{fdb}$	– debonding FRP strain
$\varepsilon_{f,max}, \varepsilon_{fu}$	– maximum / ultimate strain in FRP reinforcement
$\varepsilon_{fp}, \varepsilon_L, \varepsilon_{Lr1}$	– strain in CFRP strip
$\varepsilon_{f,p}, \varepsilon_{L,0}, \varepsilon_{pt}$	– pretensioning strain in FRP reinforcement
$\varepsilon_{f,test}$	– maximal CFRP strain registered in test
$\varepsilon_{num}$	– numerical strains in CFRP at ultimate load
$\varepsilon_{su}$	– ultimate strain in steel
$\varepsilon_{s1}, \varepsilon_{s10}, \varepsilon_{s20}$	– strain in tensile and compressive steel reinforcement
$\varepsilon_t$	– tensile strain perpendicular to crack
$\varepsilon^0$	– mid – plane strains
$\eta_A$	– strengthening efficiency of prestressed specimens
$\eta_P$	– strengthening efficiency for non–prestressed specimen
$\eta_f$	– strengthening efficiency
$\eta\varepsilon_f$	– strain utilization of FRP reinforcement
$\eta_{ef}$	– strain efficiency
$\theta$	– angle between tensile force and fibre direction
$\kappa$	– curvature
$\kappa_{bsk}$	– bond factor
$\kappa_{vb1}, \kappa_{vb2}$	– bond coefficients
$\rho_s, \rho_f$	– longitudinal steel and FRP reinforcement ratio
$\rho_c, \rho_f, \rho_m$	– weight density of composites, fibres, matrix
$\nu_{12}$	– principal Poisson's ratio of laminate
$\sigma_A$	– stress at interface between concrete and steel plate
$\sigma_f$	– axial FRP stresses between two adjacent flexural cracks
$\sigma_{fd}$	– stress in FRP at ultimate limit state
$\sigma_{f,max}$	– maximum stress

$\sigma_{f,p}$	– prestressing stress in FRP reinforcement
$\sigma_{fp}$	– uniform load applied to ends of FRP laminate
$\sigma_m$	– tensile strength of matrix
$\sigma_{s,min}$	– minimum normal stress in soffit plate
$\sigma_u$	– ultimate uniaxial compressive stress
$\sigma_x$	– longitudinal stress
$\sigma_y$	– transverse normal stress (peeling)
$\sigma_z$	– normal stress
$\tau$	– bond shear stress
$\bar{\tau}$	– maximum shear stress
$\tau_{bl}$	– bond strength
$\tau_{f,gl,max}, \tau_{f,lim}$	– maximum global bond shear stress
$\tau_{max}$	– maximum shear stress
$\tau_{min}$	– minimum shear stress
$\varphi$	– angle of internal friction

## 1. Introduction

### 1.1. Overview

The *fibre-reinforced polymer (FRP) composites* have been used for strengthening reinforced concrete (RC) members as an alternative to steel plates bonded to the bottom surface of structures since 1984. The first experimental tests carried out on flexurally strengthened RC beams were carried out at the Swiss Federal Laboratory for Materials Testing and Research (EMPA) (Meier et al., 1993).

There have been many published studies on structural strengthening using *externally bonded (EBR) FRP composites* (Hollaway and Leeming, 1999; Teng et al., 2002; Arduini and Nanni, 1996; Bank, 2006; Wu and Eamon, 2017; Deuring, 1993; El-Hacha, 2000; Garden et al., 1998; Kaiser, 1989; Katsumata et al., 2001; Labossière et al., 1997; Meier, 1992; Meier, 1995a, 1995b; Meier, 1997; Meier et al., 1993; Nanni, 1993; Nanni, 1995; Nanni et al., 2004; Seracino et al., 2007; Täljsten, 1994). More than three decades of experience developed this technique in the field applications.

However, the design guidelines are still based on experimental simplified approaches, which gives rather conservative and uneconomical results. It seems that it is time to change the current design approaches for a new generation of models considering curvature changes along RC members dependent on the cracking pattern and preloading effect. The aim of this book is to review the existing bond models and to point out the needs in designing flexurally strengthened RC members.

### 1.2. FRP materials

A non-homogeneous structure of composite material is composed of at least two components: one is a polymer matrix, constituting a binder that guarantees cohesion, hardness, elasticity and resistance to compression, and the fibres which perform structural role due to their good mechanical and strength properties in tension. The properties of this complex composite structure are neither a sum nor an average of the properties of the composite components, but closely depend on the volume of each component in the final composite material and the orientation of fibres (unidirectional, two/or three way structure).

The main function of the matrix is to protect the fibres against abrasion or environmental corrosion, to bind the fibres together and to distribute the uniform load. The matrix is an anisotropic material, which has a strong influence on several mechanical properties of the composite, such as the transverse modulus and strength, the shear properties and the properties in compression. The most common binder matrix in the composite material is the thermosetting polymer the

second one is the thermoplastic polymer matrix. Alternatively, the cement mortars can be used. More physical and chemical characteristics of the matrix are presented in *fib* Bulletin 90, 2019; CNR-DT 200/2004, 2004; Teng et al., 2002; Wu and Eamon, 2017.

The purpose of the adhesive is to provide a shear load path between the concrete surface and the composite material, so that full composite action may develop. The science of adhesion is a multidisciplinary, demanding a consideration of concepts from such topics as surface chemistry, polymer chemistry, rheology, stress analysis and fracture mechanics (*fib* Bulletin 90, 2019).

The most common type of structural adhesive is epoxy, which is the result of mixing an epoxy resin (polymer) with a hardener. Other types of adhesives based on inorganic materials (mainly cement-based) will be discussed later. Depending on the application demands, the adhesive may contain fillers, softening inclusions, toughening additives and others. The successful application of an adhesive system requires the proper preparation (CNR-DT200/2004; *fib* Bulletin 90, 2019) of an adequate specification, which must include such provisions as adherent materials, mixing application temperature, curing temperature, surface preparation technique, thermal expansion and creep properties.

### 1.2.1. Fibres

Commercially distributed FRP fibres are made of thin continuous filaments produced in variable shapes (CNR-DT 200/ 2004):

- monofilaments (with a diameter of 10  $\mu\text{m}$ );
- tows made as untwisted bundle of continuous filaments;
- yarns consisting of twisted filaments and fibres formed as a continuous fibres used for production of weaving textile materials;
- rovings made in a form of a number of yarns or tows joined into parallel bundles with little or no twist.

Four types of fibres are commonly used in structural strengthening, namely *carbon, glass, aramid and basalt fibres*. The new steel fibres have been recently introduced to the civil engineering market but due to their higher weight and low corrosion resistance they have not been attractive. Natural fibres with their durability problems are still not recommended for practical applications. However, they are still research attractive. The physical and mechanical properties of variable fibres are very different, which is shown in Table 1.1. (*fib* Bulletin 90, 2019).

The carbon fibres exhibit the highest values of elasticity modulus when compared with other types of fibres, which makes this material more effective from a structural point of view.

The characteristics of FRP materials can be defined according to the following features:

- geometry described by a shape and dimensions of FRP material
- fibre orientation
- fibre concentration defined by the volume fraction and fibre distribution (CNR-DT 200/2004, 2004).

Table 1.1. Typical properties of fibres (*fib* Bulletin 90, 2019)

Fibre type	Fibre identification	Density	Tensile modulus	Tensile strength	Failure strain	Thermal expansion coefficient	Poisson's ratio
		kg/m <sup>3</sup>	GPa	MPa	%	×10 <sup>-6</sup> /C	-
Basalt		2691	90	2999	3.20	4.44	
Glass	E-Glass	2547	72	3447	4.80	4.99	0.20
	S-Glass	2483	87	4309	5.00	2.90	0.22
Aramid	Kevlar 49	1458	131	3620	2.80	-2.00	0.35
	Technora	1410	70	2999	4.60	-5.99	0.35
Carbon	T – 300	1762	231	3654	1.40	-0.60	0.20
	P – 100	2146	69	2413	0.32	-1.45	0.20
	As – 4	1794	248	4068	1.65	-0.60	0.20
	IM – 7	1778	300	5309	1.81	-0.75	0.20

### ***Carbon Fibres***

Carbon fibres have the highest elasticity modulus and the highest tensile strength when compared with other types of fibres. They exhibit brittle failure with quite low energy absorption. Carbon fibres indicate high creep resistance to the long-term tensile loads and fatigue loads.

Production of carbon fibres based on pitch fibres (produced by using refined petroleum or coal pitch which is passed through a thin nozzle and stabilised by heating) or PAN fibres (made of polyacrylonitrile that is carbonised by different heat treatments). A diameter of pitch-type and PAN fibres is approximately 9-18 µm and that of the PAN-type is 5-8 µm (*fib* Bulletin 90, 2019).

### ***Glass Fibres***

There are three types of glass fibres: E-glass, S-glass and alkali resistant AR-glass fibres. The E-glass fibres are susceptible to alkali. Even the S-glass fibres have higher elasticity modulus and strength than the E-glass fibres. They are not resistant to alkali either. The zircon component is added to glass fibres to improve their alkali resistance.

### ***Aramid Fibres***

Production of aramid fibres is not common. They have an anisotropic structure. Their diameter is about 12  $\mu\text{m}$ . Aramid fibres indicate non-linear and ductile behaviour under compression and good toughness, as well as fatigue resistance. Because they can absorb up to 7% of water from the ambient air humidity, they should be dried before the application. The aramid fibres are very sensitive to UV radiation, moisture and long-term loads (due to low creep behaviour), similarly to glass fibres. They can lose up to 70% of their initial tensile strength under UV exposure. Due to low compressive strength (about 1/8 of their tensile strength), the compression load evokes localized fibre yielding resulting in fibre instability and formation of kinks. However, their fatigue resistance is much better than that of glass fibres.

### ***Basalt Fibres***

Basalt fibres are produced from a volcanic mineral by melt-spinning from basalt melt. This technology is quite similar to production of glass fibres but there are fewer energy requirements. They exhibit similar mechanical properties to glass fibres but with slightly higher elasticity modulus.

### ***High strength steel fibres***

They are produced in the form of steel wires, which can be bundled into cords, typically have a protective layer of zinc or brass coating to protect them against corrosion. They have a linear elastic structural characteristics in the full range of loading.

### ***Natural fibres***

They have been used for structural applications with both organic and inorganic matrices. The main problem of natural fibres is a large variety of their mechanical and physical properties. The most often applied fibres are vegetal fibres, including hemp, flax and kenaf. The tensile strength of natural fibres can vary within the range from 500 MPa to 1500 MPa, whereas their elastic modulus varies between 30 GPa and 70 GPa.

The mechanical and physical properties of natural fibres are strongly influenced by their geographic origin as well as by the production processes. The diameter is largely variable and natural fibres are generally intertwined to form small chords that are used to prepare sheets, fabrics or grids. Due to microstructural shear-lag mechanism, their tensile strength and the elastic modulus decrease with the increase in the chord diameter. Physical and mechanical properties can be reduced in their interaction with the matrix due to their loss of bond to the matrix (*fib Bulletin* 90, 2019).

The main advantages and disadvantages of FRP fibres are summarized in Table 1.2. The benefit of FRP strengthening is high durability assurance. More common structural strengthening with FRP materials causes reduction in the cost of FRP composites and their great need for strengthening work all over the world.

Table 1.2. The comparison of advantages and disadvantage of variable fibres

Type of fibres	Advantages	Disadvantage
GFRP	low cost; high tensile strength; excellent insulating properties	low tensile modulus; relatively high specific gravity; sensitivity to abrasion from handling; sensitivity alkalies; relatively low fatigue resistance;
CFRP	high tensile strength-to-weight ratio; high tensile modulus-to-weight; very low coefficient of linear thermal expansion; high fatigue strength	high cost; high brittleness; electrical conductivity
AFRP	very low thermal conductivity; very high damping coefficient; high degree of yielding under compression	hygroscopic make absorption moisture up to about 10% of fibre weight; at high moisture content, they tend to crack internally at pre-existing microvoids and produce longitudinal splitting; low compressive strength; loss of strength and modulus at elevated temperatures; difficulty in cutting and machining; sensitive to UV lights

### 1.2.2. Matrices

The main function of a matrix is to protect the fibres against abrasion or environmental effects. Moreover, a matrix acts as a binder of fibres and distributes the uniform load. A matrix has a strong influence on several mechanical properties of a composite, such as: transverse modulus of elasticity, tensile strength, shear and compressive mechanical properties. The fabrication process is influenced by physical and chemical characteristics of the matrix, which consists of: melting, curing temperature, viscosity and reactivity with fibres. The most common matrix for composite materials used/ used for composite materials is a thermosetting polymer. A thermoplastic one is also used but it is not so common (*fib* Bulletin 90, 2019).

Thermosetting epoxy, polyester and vinylester resins are most commonly used with high-performance reinforcing fibres, which are characterised by very good chemical resistance. They have several advantages, such as low viscosity

that enables easy fibre impregnation, good adhesive properties, room temperature polymerization characteristics, good resistance to chemical agents and the absence of melting temperature. However, their disadvantages are: limited range of operating temperatures, with the upper bound limit given by the glass transition temperature, poor toughness with respect to brittle fracture and sensitivity to moisture during the field applications (CNR-DT 200/2004, 2004).

The epoxy resins have better mechanical properties (Table 1.3) than polyesters and vinylesters. From physical point of view, they have the best durability when compared with polyesters or vinylesters. However, the latter two are much cheaper than the epoxy one.

Another type of matrix, namely cement mortars, is produced on the basis of inorganic materials (cement-based, metallic or ceramic). The inorganic matrix used in the polymer-modified, cement-based mortars is most commonly applied in the form of textiles (*fib* Bulletin 90, 2019).

Table 1.3. Mechanical properties of commonly used FRP epoxies

Epoxy type	Sikadur 300 (MPa)	Tyfo S epoxy (MPa)
Tensile strength	55.16	0.07
Tensile modulus	1.72	3.18
Tensile elongation	3%	5%
Flexural strength	0.08	0.12
Flexural modulus	3.45	3.12

### 1.2.3. Adhesives

The most commonly used type of adhesive in structural applications is epoxy, which is a mixture of epoxy polymer resin with a hardener. Other types of adhesives, like cement-based ones, are made on the basis of inorganic materials. Variable adhesives may contain fillers, softening inclusions, toughening additives and others, depending on the application demands, which require a proper concrete surface preparation, adherent materials, temperature and technique control (*fib* Bulletin 90, 2019). A very important parameter influencing strengthening is the *glass transition temperature*,  $T_g$ . It is considered according to both components of an epoxy adhesive (resin and the hardener) that strongly depend on curing time and temperature. If the temperature increases above the glass transition, the mechanical properties of the adhesive drop in an abrupt manner.

The recommended epoxy adhesives in construction should be used at service temperatures below the glass transition temperature. The synthetic adhesives are used in their rubbery domain at service temperatures above glass transition temperature. The mechanical properties of polymers used in their rubbery domain show only very small temperature dependency.

The epoxy adhesive demands include two different time concepts during the application process such as: the pot life, i.e. time after mixing the resin with the hardener before it starts to harden in the mixture vessel, and the open time, i.e. time between adhesive application to the adherents and their joining. There are several advantages of the epoxy adhesives when compared to other polymers. The most important are : high surface activity, good wetting properties for different substrates, long open time formulation, high cured cohesive strength, low shrinkage, low creep and superior strength retention under sustained load (*fib* Bulletin 90, 2019). The most popular are bi-component epoxy adhesives.

The adhesive bond conditions can be identified by three types of fracture:

- cohesive - localized inside one of the materials, which means the same material remaining on the sides of the fracture surface,
- adhesive - localized at the interface between an adhesive and a substructure, which means lower adhesive strength than the substructure, which confirms improper application,
- mixed fracture – combining cohesive and adhesive fracture, which occurs when surfaces are irregular and located in both materials (adhesive and substructure).

### 1.3. FRP composites

The fibre reinforced polymer materials, made of various types of fibres embedded in a matrix of epoxy, are produced in the form of:

- thin unidirectional pultruded laminates (strips with thickness in the order of 1 mm) (Fig. 1a),
- flexible sheets or fabrics made of fibres in one or at least two different directions impregnated with resin in-situ (Fig. 1b),
- rods, with diameter in the order of a few mm, made by pultrusion (Fig. 1b, c) (*fib* Bulletin 14, 2002),
- profiles (T-shape, L-shape) – Fig. 1.d.

Composite materials are divided into two groups, based on their internal structure that include single and multi-layer materials. The first group contains laminates (prefabricated strips) with unidirectional fibres surrounded by the epoxy matrix. Depending on the saturation of fibres in the matrix, the single-layer composite laminate has different mechanical properties in the longitudinal and transverse direction.

In the second case (the multi-layer material), the structure of the composite consists of a hybrid structure. A single layer is then composed of two types of fibres (differing in type of material and strength) or consecutive layers of the same type of fibres arranged in two or three directions (Wu and Eamon, 2017).

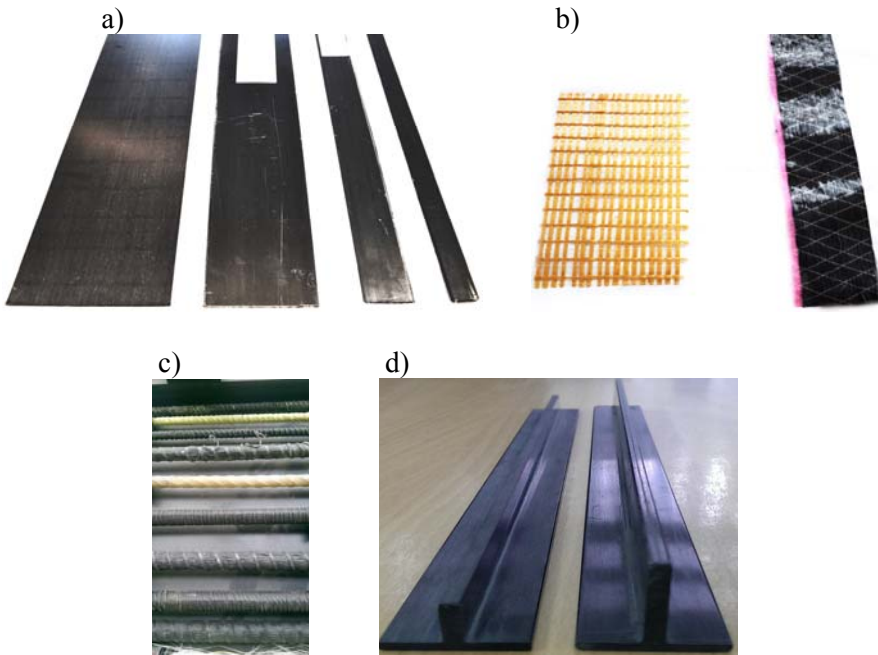


Fig. 1.1. FRP composite materials : a), b), c), d)

The mechanical properties of fibres and matrices characterised by the tensile strength and the tensile modulus of elasticity of FRP materials in the direction parallel to fibres are calculated according to the equations proposed by (Jones, 1999; Wu and Eamon, 2017):

$$\sigma_{f1} = \sigma_f v_f + \sigma_m v_m \quad (1.1)$$

$$E_{f1} = E_f v_f + E_m v_m \quad (1.2)$$

However, the tensile strength and the tensile modulus in the transverse direction is calculated according to:

$$\sigma_{f2} = \sigma_m \quad (1.3)$$

$$E_{f2} = \frac{1}{\frac{v_f}{E_f} + \frac{v_m}{E_m}} \quad (1.4)$$

where:  $\sigma_{f1}$  is the tensile strength of the cured FRP laminate;  $\sigma_f$  is the tensile strength of dry fibre;  $\sigma_m$  is the tensile strength of matrix;  $\nu_f$  is the volume fraction of fibre;  $\nu_m$  is the volume fraction of matrix;  $F_f$  is the tensile modulus;  $E_{f1}$  is elasticity modulus of FRP in fibre direction;  $E_m$  is elasticity modulus of the matrix.

$$\nu_f = w_f \frac{\rho_c}{\rho_f} \quad (1.5)$$

$$\nu_m = w_m \frac{\rho_c}{\rho_m} \quad (1.6)$$

where:  $w_f$  is the weight/or mass fraction of fibre;  $w_m$  is the weight/or mass fraction of the matrix;  $\rho_c$ ,  $\rho_f$ , and  $\rho_m$  are the weight density of composites, fibres, and matrix, respectively.

$$w_f = \frac{W_f}{W_c} \quad (1.7)$$

$$w_m = \frac{W_m}{W_c} \quad (1.8)$$

where:  $W_f$ ,  $W_m$  and  $W_c$  are the weight/mass of the fibre, matrix and FRP composites, respectively.

A density of the full FRP material containing fibres is calculated from the following equation:

$$\rho_c = \nu_f \rho_f + \nu_m \rho_m \frac{1}{\frac{w_f}{\rho_f} + \frac{w_m}{\rho_m}} \quad (1.9)$$

$$\nu_f + \nu_m = 1 \quad (1.10)$$

$$w_f + w_m = 1 \quad (1.11)$$

Typically, the volume fraction of fibres in FRP materials is about 50-70% for strips and about 25-50% for sheets or fabrics. The mechanical properties of FRP

materials are estimated on the basis of the properties of fibres and matrix and their volume fractions in the FRP material (*fib* Bulletin 90, 2019).

Prefabricated strips are the most commonly used FRP materials for structural strengthening. Their material properties based on the above mentioned calculations in comparison with the mild steel are summarized in Table 1.4. and they are shown in Fig. 1.2.

Table 1.4. Typical properties of prefabricated FRP strips in comparison with steel (*fib* Bulletin 14, 2002)

Material	Elastic modulus $E_f$ (GPa)	Tensile strength $f_f$ (MPa)	Ultimate tensile strain $\varepsilon_{fu}$ (%)
Prefabricated strips			
Low modulus CFRP strips	170	2800	1.6
Mid modulus CFRP strips	210	2800	1.6
High modulus CFRP strips	300	1300	0.5
Mild steel	200	400*/600	2*/25

\* - yielding strength

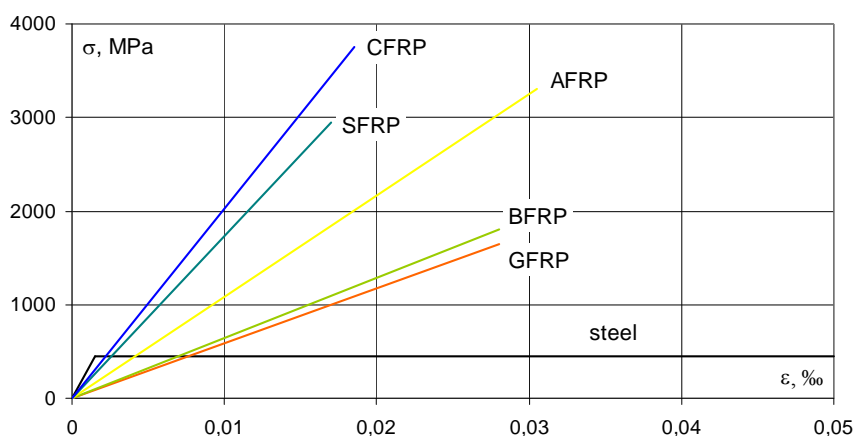


Fig. 1.2. Stress-strain diagrams for different unidirectional FRP materials: carbon fibre reinforced polymer (CFRP), glass FRP (GFRP), aramid FRP (AFRP), basalt FRP (BFRP) and steel FRP (SFRP).

The FRP laminate is fully anisotropic material with different tensile characteristic in variable directions in relation to the longitudinal one. The elasticity modulus depends on a  $\theta$  angle between tensile force and the fibre direction (Jones, 1999; Matthews and Rawlings, 1994). The modulus of elasticity  $E_x$  of a ply loaded at an angle  $\theta$  to the fibre direction is calculated on the basis of the following formula:

$$E_x = \frac{1}{E_1} \cos^4(\theta) + \left( \frac{1}{G_{12}} - \frac{2\nu_{12}}{E_1} \right) \sin^2(\theta) \cos^4(\theta) + \frac{1}{E_2} \sin^4(\theta) \quad (1.12)$$

where:  $E_1$  and  $E_2$  are the elasticity modulus of the composite laminate parallel and perpendicular to the fibres,  $\nu_{12}$  is the principal Poisson's ratio of the laminate (generally 0.3) and  $G_{12}$  is the in-plane shear modulus of the laminate (see Fig. 1.3).

The ply orientation in the FRP laminate is determined on the basis of a particular loading direction, which is known as the maximum applied load direction, which corresponds to this fibre direction, which transfers the maximum load and refers to the 0 degree direction.

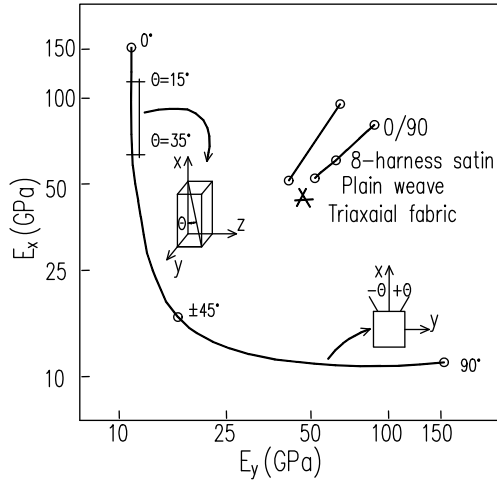


Fig. 1.3. Predicted  $E_x$  and  $E_y$  elasticity modulus in variable directions:  $\pm \theta$  angle-ply (from  $\theta = 0$  to  $\pm 45^\circ - 90^\circ$ ) (Wu and Eamon, 2017)

The balanced FRP laminate is the one in which there is an equal number of  $+\theta$  and  $-\theta$  plies. The symmetric laminate is the one in which the plies are symmetric in terms of geometry and properties with respect to the laminate mid-plane.

Balanced symmetric laminates have a simple response based on the composite structures generally designed to the strain level corresponding to the visible damage in its structure (Wu and Eamon, 2017).

Classical Laminate Theory is an extension of the theory for bending of homogeneous plates, but with an allowance for in-plane tractions in addition to bending moments, and for the varying stiffness of each ply in the analysis.

Beginning with assumption of knowledge of the tractions  $N$  and moments  $M$  applied to a plate at a position  $x, y$ :

$$N = \begin{Bmatrix} N_x \\ N_y \\ N_{xy} \end{Bmatrix} \quad (1.13)$$

$$M = \begin{Bmatrix} M_x \\ M_y \\ M_{xy} \end{Bmatrix} \quad (1.14)$$

it is possible to define stressed integrated through the laminate. The average values of the tensile stress give the in-plane loads  $N$  and the linear variation gives the couples  $M$ . The end loads and moments are shown in Fig. 1.4, where:  $N_{xx} = N_x, N_{yy} = N_y$ . Using the elasticity properties of each ply, rotated to the fibre directions, the end ultimate loads relate to the mid – plane strains  $\varepsilon^0$  and curvatures  $\kappa$  to give the laminate the stiffness properties according to the following formula:

$$\begin{bmatrix} N \\ M \end{bmatrix} = \begin{bmatrix} A & B \\ B & C \end{bmatrix} \begin{bmatrix} \varepsilon^0 \\ \kappa \end{bmatrix} \quad (1.15)$$

where:  $A, B$  and  $C$  are the stiffness propitiates: in-plane, the bending stiffness and the stiffness arises between the bending and membrane actions (shown in Fig. 1.4).

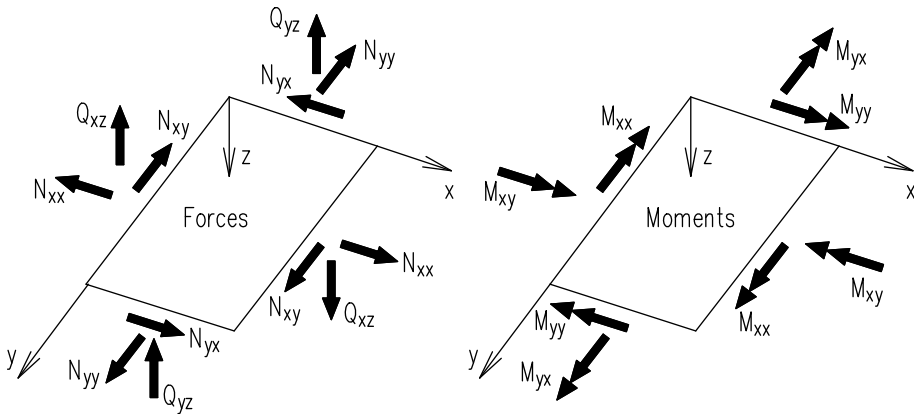


Fig. 1.4. Mid-plane forces and moments (Wu and Eamon, 2017)

The mechanical properties of the FRP materials ( $E_f$  and  $f_f$ ) are governed by the fibre properties ( $E_{fib}$  and  $f_{fib}$ ) and the cross-sectional area of the bare fibres, which have much higher stiffness and strength than the matrix ( $E_m$  and  $f_m$ ). There is a strong relation between the fibre volume fraction and the FRP properties, shown in Figure 1.5.

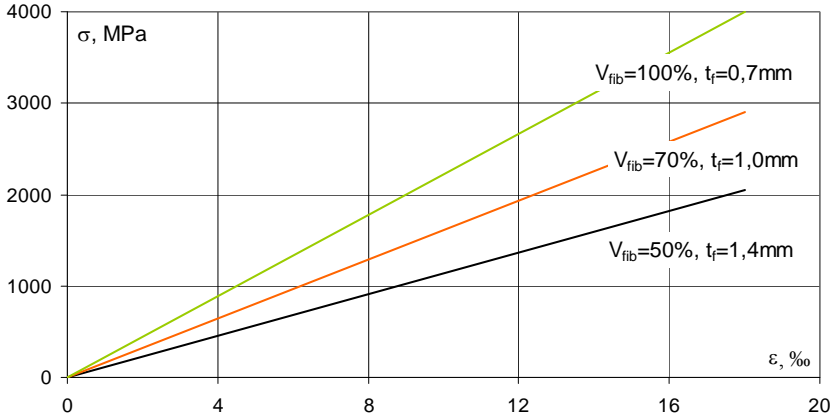


Fig. 1.5. Stress-strain relations corresponding to various fibre volume fractions of 100%. 70% and 50% (*fib* Bulletin 90, 2019).

Different properties exhibit the in-situ resin impregnated systems with variable final FRP thickness and the fibre volume fraction makes that the precise calculations of the strength properties are not possible and should be obtained from testing.

Table 1.5. Anisotropic ratios of fibre-reinforced unidirectional laminates (CNR-DT 200/2004, 2004)

Type of fibre / matrix	$E_1 / E_2$	$E_1 / G_{12}$	$\sigma_{r1} / \sigma_{r2}$	$\alpha_1 / \alpha_2$
Silicon carbide/ceramic	1.09	2.35	17.8	0.93
Boron/aluminium	1.71	5.01	11.6	0.30
Silicon carbide/aluminium	1.73	5.02	17.0	0.52
S-Glass/epoxy	2.44	5.06	28.0	0.23
E-Glass/epoxy	4.42	8.76	17.7	0.13
Boron/epoxy	9.27	37.40	24.6	0.20
Carbon/epoxy	13.60	19.10	41.4	-0.07
Aramid/epoxy	15.30	27	26.0	-0.07

$E_i$  – Young modulus of elasticity;  $G_{ij}$  : shear modulus;  $\sigma_{ri}$  – failure stress;  $\alpha_i$  - coefficient of thermal expansion; 1 or 2 – longitudinal and transversal direction, respectively

Composite materials have an anisotropic structure with entirely different physical and mechanical properties in the longitudinal and transverse directions. A degree of complexity of the composite structure is determined by the anisotropy coefficient, which expresses the ratio of physical and mechanical characteristics in two perpendicular directions. The values of anisotropic ratio in unidirectional laminates calculated as a ratio between values of the composite properties in the longitudinal and transversal fibre directions are summarized in Table 1.5.

Table 1.6. Characteristics of CFRP laminates (S&P, 2019; Sika<sup>®</sup> CarboDur<sup>®</sup>, 2016; MC-Bauchemie, 2005; Mapei, 2018; Megachemie, 2011; Tyfo<sup>®</sup> UC Composite Laminate Strip System, 2015)

Company	CFRP material	$E_f$	$f_{fu}$	Type of adhesive
		(GPa)	(MPa)	
Sika	CarboDur XS	165	2.200	Sikadur 30 Sikadur 41
	CarboDur S	165	2.800	
	CarboDur M	210	2.800	
	CarboDur UH	400	1.800	
MC-Bauchemie	MC-Dur CFK	>167	>2.950	MC-DUR 1280
Megachemie	Neoxeplate HS	>170	>2.512	Neopoxe 30 Neopoxe 41
	Neoxeplate HM	>230	>2.566	
	Neoxeplate UHS	>160	>2.571	
S&P	CFR-Lamellen 150/2000	>165	>2.500	Resine 220
	CFR-Lamellen 200/2000	>210	>2.500	
Mapei FRP	Carboplate	160 – 250	>2.000	Adesilex PG1 +PG2
Tyfo <sup>®</sup> UC	Composite Laminate Strips	155	2.790	Tyfo <sup>®</sup> Epoxy

$E_f$  – CFRP elasticity modulus;  $f_{fu}$  – CFRP tensile strength

Fibre reinforced polymer materials in the form of laminates, sheets and grids are commonly used for strengthening of existing RC members in flexure, shear (mostly existing slabs and beams) and confinement by wrapping of columns and to increase their compressive and seismic capacity. The commercially available FRP materials unidirectional and bidirectional FRP offered by Sika, S&P, Fife, and Mapei are summarized in Table 1.6.

#### 1.4. FRP strengthening systems

A division of strengthening systems came from two following technologies of application of the strengthening materials:

## Introduction

---

- bonded on the external surface of concrete, known as *externally bonded reinforcement - EBR* or externally applied reinforcement - EAR (according to a new nomenclature in *fib* Bulletin 90, 2019) containing:
  - pre-cured systems based on prefabricated elements (Fig. 1.6a., b);
  - systems cured in-situ based on flexible sheets (Fig. 1.6.c, d)
- bonded into grooves cut in the concrete cover known as *near surface mounted reinforcement* – NSMR (Fig. 1.7a, b);
- special systems: *prestressing*, *mechanically attached laminates*, *automated wrapping*, etc. (Fig. 1.8a, b, c, d);
- advanced composite systems made of *steel fibres* in combination with *polymeric matrices* (SFRP) or even fibres in the form of textiles or grids bonded to concrete surface with inorganic mortars (*textile reinforced mortars* – TRM) (Fig. 17.d, e).

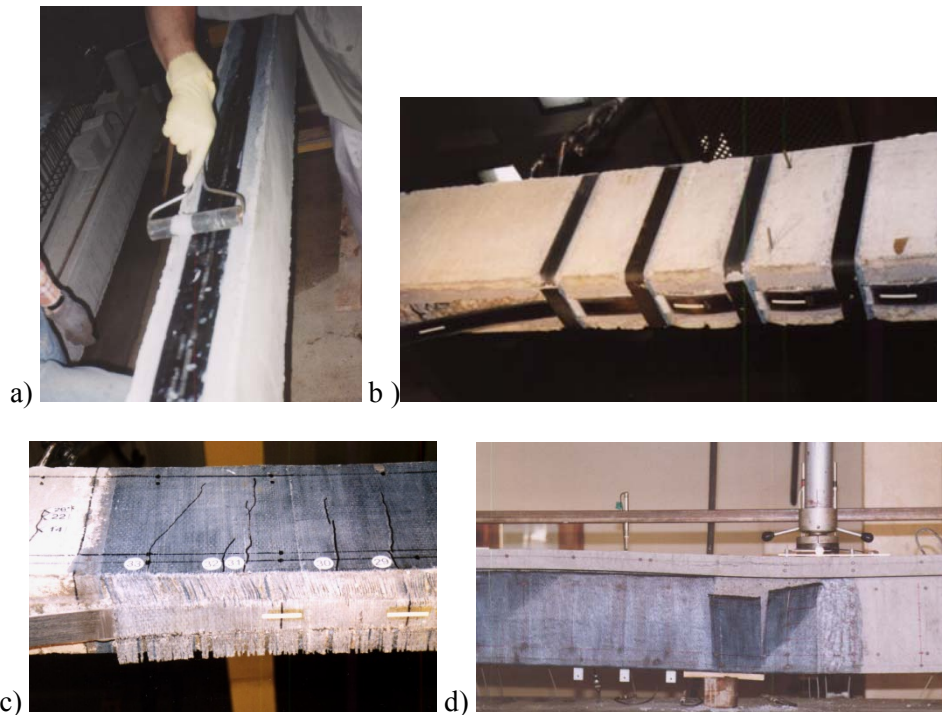


Fig. 1.6. Externally applied FRP systems for flexural strengthening with: a) laminates; b) bottom and lateral L-shape profiles; c) lateral sheets in flexural strengthening; d) lateral sheets in shear strengthening

a)



b)



c)



Fig. 1.7. Near surface mounted FRP system for flexural strengthening with strips

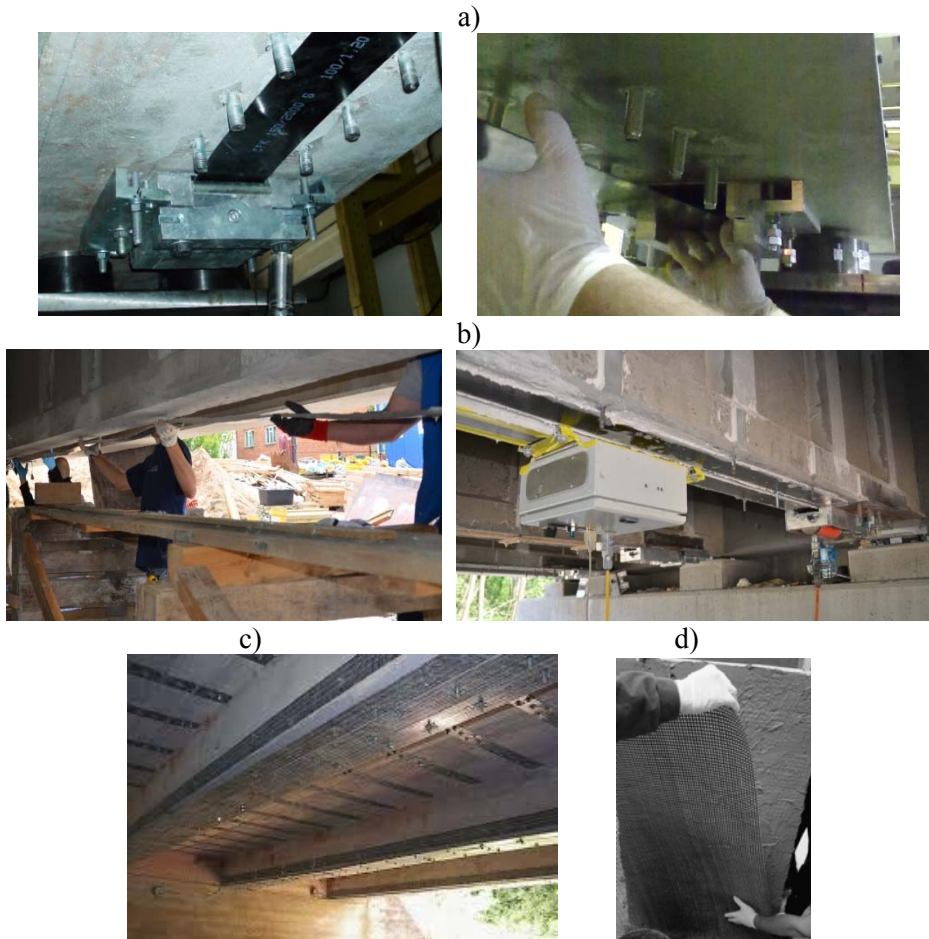


Fig. 1.8. Special FRP systems for flexural strengthening: a) prestressed with anchorages; b) non anchored prestressing system - gradient method (TULCOEMPA Project); c) mechanically fastened system (SAF-STRIP<sup>®</sup> MF-FRP on the bridge over the Meramec River in Missouri <https://www.strongwell.com/wp-content/uploads/2013/04/SAFSTRIP-Brochure.pdf>); d) Textile reinforced mortar (TRM) (Papanicolaou et al, 2007)



## 2. Flexural strengthening

### 2.1. State of the art in research

FRP application for flexural strengthening was introduced by Urs Meier in 1980s using CFRP laminates at the Swiss Federal Laboratory for Materials Testing and Research (EMPA) (Meier, 1992; Meier et al., 1993). FRP was first applied in the United States by the California Department of Transportation, Caltrans in early 1990s (Wu and Eamon, 2017).

A large amount of research was carried out all over the world (Kaiser, 1989; Ritchie et al., 1991; Saadatmanesh and Ehsani, 1991; Triantafillou and Deskovic, 1991; Triantafillou and Plevris, 1992; Uji, 1992; Jones and Swamy, 1983; Ichimasu et al., 1993; Nanni, 1993; Deuring, 1993; Deuring, 1994; Täljsten, 1994; Chajes et al., 1994; Schwegler, 1994; Sharif et al., 1994; Meier, 1995a, 1995b; Nanni, 1995; Takeda et al., 1996; Swamy et al., 1996; Shahawy et al., 1996; Arduini and Nanni, 1997; Garden et al., 1997; Meier, 1997; Labossière et al., 1997; Täljsten, 1997a; Siwowski, 1997; Siwowski and Radomski, 1998; Garden and Hollaway, 1998; Spadea et al., 1998; Garden et al., 1998; Grace et al., 1999; Kachlakev and Barnes, 1999; Kotynia, 1999; Naaman, 1999; Ross et al., 1999; Swamy and Mukhopadhyaya, 1999; Labossière et al., 2000; Nguyen et al., 2001; Teng et al., 2002; Matthys et al., 2004).

Polish experiences in structural strengthening started from bridges with the first application of CFRP laminates in 1992 on the bridge over the Wiara river (Siwowski and Radomski, 1998). One year later the second application with combined CFRP laminates and sheets was performed on the bridge over the Bystry canal (Siwowski, 2012). Other Polish CFRP applications on the RC structures were published by Furtak (1998, 2014), Radomski (2018), Siwowski and Radomski (2015), Siwowski and Żółtowski (2012). Much more effective flexural strengthening with prestressed laminates were carried out by Piątek (2017), Piątek and Siwowski (2016), Siwowski et al. (2010), Piątek and Siwowski (2017), Kotynia et al. (2014), Kotynia et al. (2015), Piątek and Siwowski (2017).

Most research and field applications on flexural strengthening of RC members were carried out on simply supported beams and slabs strengthened on the bottom surface of the RC members without additional anchorage in the support region. However, to prevent debonding at the ends of the bottom laminates, U-shape sheets (Fig. 2.1.a) and overlapping FRP materials (laminates/sheets) (Fig 2.1.b) or mechanically anchored (laminates / sheets) can be installed (Fig. 2.1.c).

The goal of this book is to introduce and describe general flexural strengthening of RC members by externally bonded laminates without additional

anchorage systems, so the only non-anchored systems will be further analysed in this book.

The best summary of variable cases of flexural strengthening configurations with EB FRP materials on the bottom, top and the lateral surfaces of RC members was published by Oehlers et al. (2007). More cases considered multiple span flexural members with possible FRP applications located in sagging and hogging regions

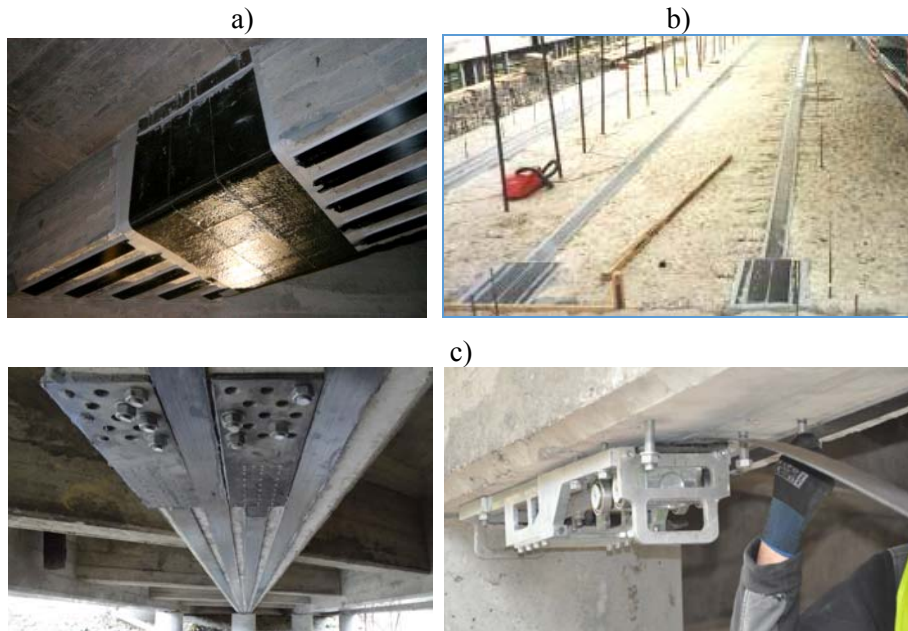


Fig. 2.1. Anchorage systems for laminates in flexurally strengthened beams and slabs: a) U-shape sheets (Euro-projekt installation, Bartosik and Kałuza, 2010); b) overlapping FRP materials laminates/sheets Bridge over Bystry Canal in Augustów (Siwowski, 2015), c) mechanically anchored laminates (Siwowski and Radomski, 2015)

## 2.2. Failure mechanisms of FRP strengthened RC members

The existing research on reinforced concrete members flexurally strengthened with FRP materials can fail in several different ways, which are completely different in comparison with original RC members. There is a wide literature referring classification of the failure modes published for last two decades (Ajdukiewicz and Hulimka, 2010; Andrä et al., 2002; Bank et al., 2004; Bartosik and Kałuza, 2010; Brandt, 1996; Casadei et al., 2003; Cichocki, 2001; Czarnecki and Emmons, 2002; Derkowski, 2005; Deuring, 1994; El-Hacha,

2000; El-Hacha et al., 2001; Garden et al., 1998; Górski et al., 2002; Grace and Sayed, 2003; Gutowski et al., 2003; Kaiser, 1989; Kałuża, 2004; Kałuża and Ajdukiewicz, 2008; Kamiński et al., 2006; Katsumata et al., 2001; Kubica et al., 2010; Lamanna et al., 2004; Lu et al., 2005; Łagoda, 2002; Łagoda, 2005; Maeda et al., 1997; Matthys et al., 2004; Meier et al., 1993; Menegotto and Monti, 2005; Michalak, 2000; Monti and Liotta, 2007; Mossakowski, 2006; Naaman, 1999; Radomski, 2005; Seracino et al., 2007; Sieńko et al., 2006; Siwowski, 1997; Siwowski and Radmoski, 1998; Taerwe et al., 1997; Täljsten, 1994; Teng et al., 2002; Triantafillou and Antonopoulos, 2000; Wan, 2002).

The most common classification based on test results of the existing research was presented in (Teng et al., 2002). Seven categories referring to material failure and interface debonding failure modes are summarized in Fig. 2.2, however the ninth mechanism was introduced by (Oehlers et al., 2007, Fig. 2.3 and Fig. 2.4).

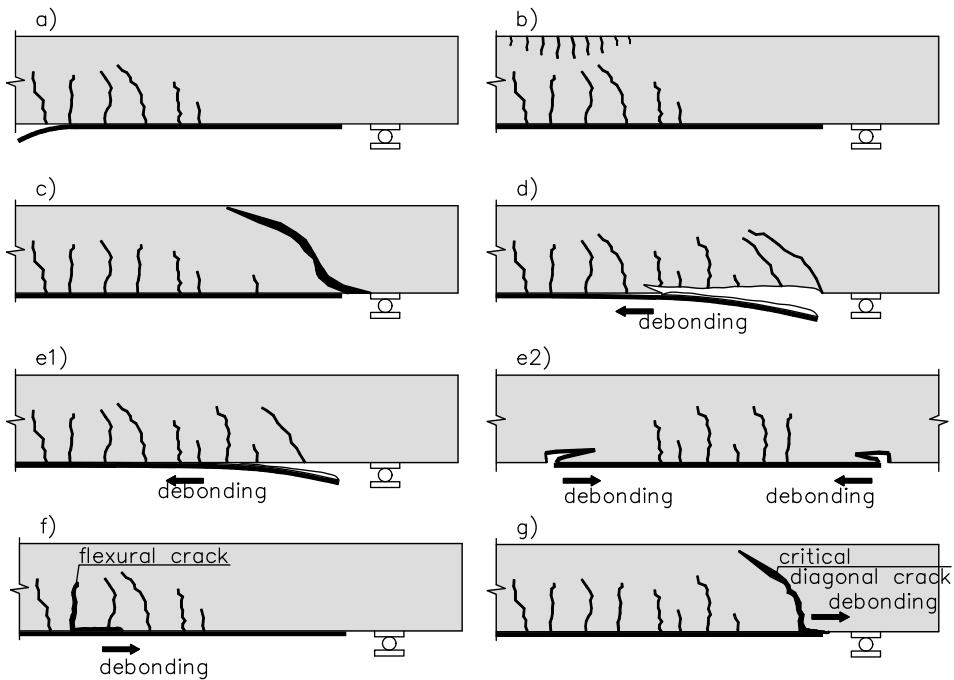


Fig. 2.2. Failure modes of FRP-plated RC beams: a) FRP rupture (R); b) concrete crushing (CC); c) shear failure; d) concrete cover separation (CCS); e) plate end interfacial debonding (PE); f) intermediate flexural/shear crack-induced interfacial debonding (IC); g) critical diagonal shear crack-induced debonding (CDC) (Smith and Teng, 2002a).

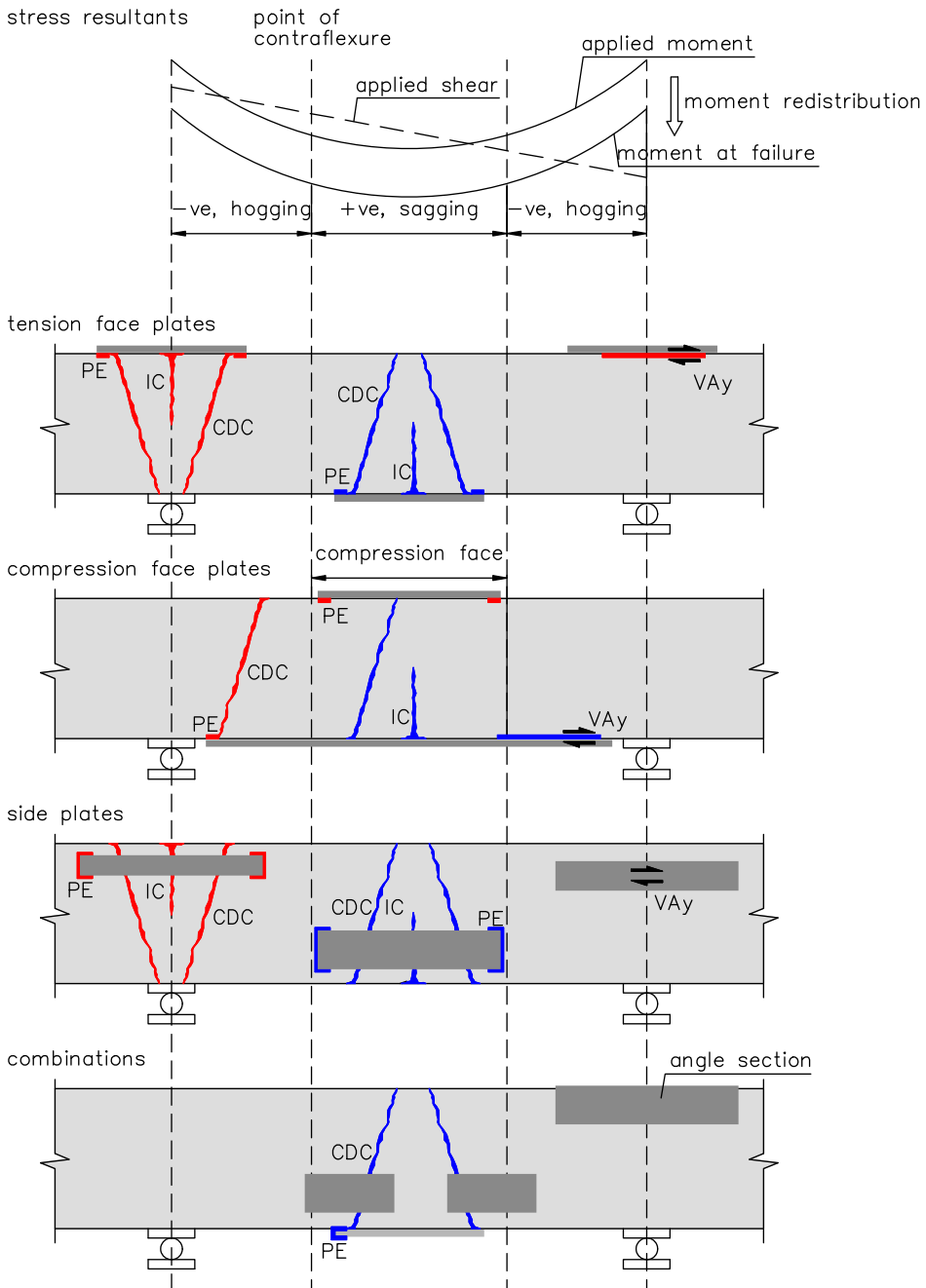


Fig. 2.3. Variable configurations of strengthening with externally boded FRP materials (Oehlers et al., 2007)

The most common failure mode is debonding of the FRP laminate from the concrete surface which may proceed as: (Fig. 2.2.f, g):

- intermediate crack induced interfacial debonding (ICD) initiates at the flexural / flexural-shear cracks in the highest bending moment region and propagates by gradual debonding of the laminate from the flexural crack to the end of the FRP end (Fig. 2.2.f. and g).

When debonding occur at or near the end of a laminate it may proceed in three different ways:

- critical diagonal crack (CDC) debonding occurs after formation of a major shear crack intersecting the plate near its end and develops from the intersection point to the plate end. This debonding develops along the laminate-concrete interface (Fig. 2.2.b)
- concrete cover separation (CCS) (Fig. 2.2.c)
- plate end interfacial debonding (PEI) (Fig. 2.2d).

There is a possible combination of CDC debonding and CCS (Fig. 2.2.e). The interface of the concrete cover separation may occur in the concrete, adjacent to the adhesive layer or at the level of the internal tensile steel reinforcement.

Two additional failure modes refer to the FRP rupture and concrete crushing, however the second one is possible only for the RC members of low concrete strength and high reinforcement ratio.

The stress concentration is the reason of three main debonding mechanisms (IC, CDC and PE, Fig. 2.3 and 2.4).

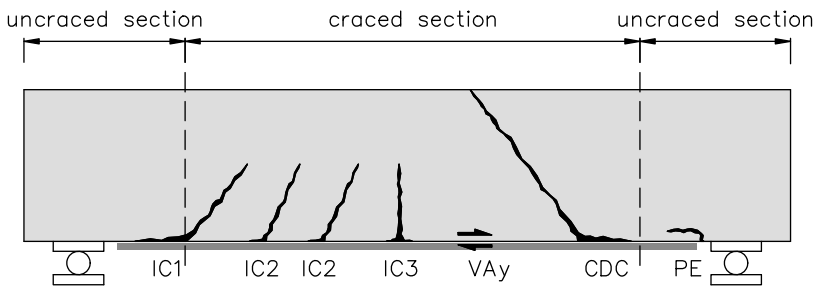


Fig. 2.4. Failure modes of FRP-plated RC beams according to (Oehlers et al., 2007)

### ***Intermediate crack debonding***

The IC debonding mechanism is induced when a flexural crack intercepts the laminate. Following the crack widening under increasing load the stress concentrations in the intercepting point cause the interface FRP debonding (Fig. 9f). It is generally located in the high bending moment region associated with

the widest flexural crack width and the highest strains of the FRP materials. The bond shear stress–slip  $\tau-s$  condition describes further crack propagation from the flexural crack to the adjacent region (Fig. 2.5). Gradual IC interface crack occurrence leads to IC debonding developing to the end of the laminate.

Table 2.1. Description of debonding mechanisms failure modes according to the existing guidelines (Oehlers et al., 2007)

Codes	FRP debonding models				
	IC1	IC2	IC3	CDC	PE
AUST	debonding	debonding	debonding	debonding	debonding
EUR	peeling off in uncracked anchorage	peeling off at flexural crack	peeling off at flexural crack	peeling off caused by shear cracks plate–end shear	concrete rip–off
BRIT	debonding	debonding	debonding, peeling	peeling off, plate end debonding	peeling
HK	induced debonding	induced debonding	induced debonding	plate end interfacial	concrete cover separation
USA	FRP peeling away from substrate			concrete cover delamination with bonded FRP reinf.	not recognised

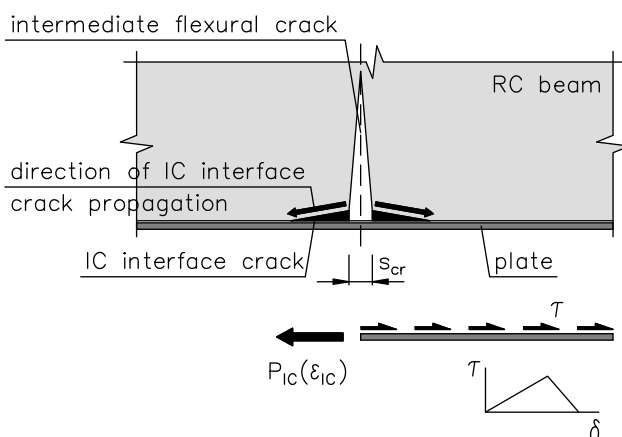


Fig. 2.5. IC debonding mechanism (Oehlers et al., 2007)

The intermediate crack debonding was observed in research by Kotynia (1999). This failure occurred in the bending region close to the flexural cracks and followed to the end of the laminate (Fig. 2.6.a, b).

## Flexural strengthening

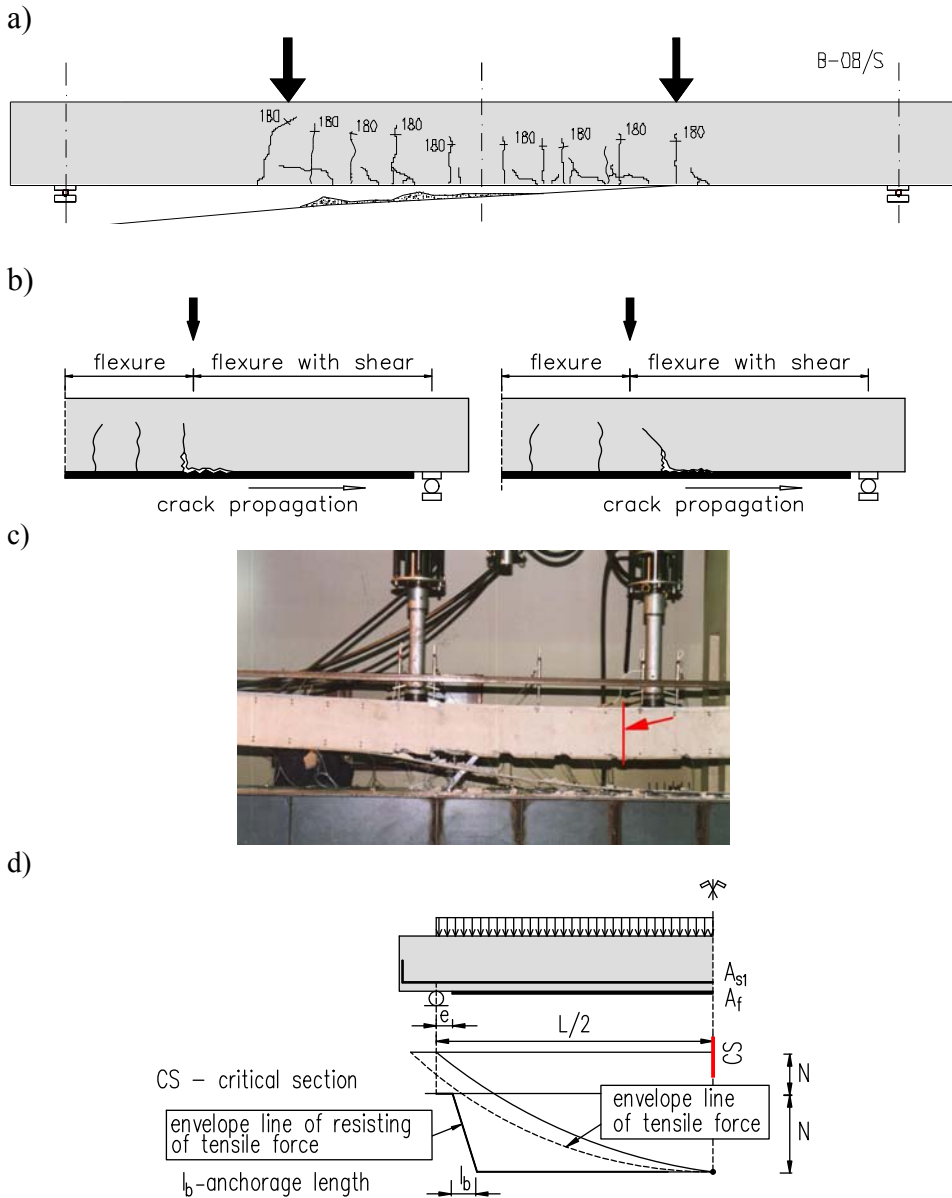


Fig. 2.6. Intermediate flexural crack debonding: a) the beam set-up, b) debonding process, c) failure mode, d) location of the critical cross-section "CS" in the bending region (Kotynia, 1999)

The plane of delamination was initiated partially in the thin adhesive layer and the concrete cover. The normal tensile forces in the cross section from the

bending moment and the shear transverse force did not cause steel yielding in the cross-section located at the end of the laminate in this section (Fig. 2.6.c).

### ***Critical diagonal crack debonding***

The second failure mode named CDC debonding occurs if a crack intercepts the laminate and the crack widening due to shear stress concentrations at the intercepting point causes abrupt debonding of the laminate (Fig. 2.7). If the concrete contribution in the shear strength  $V_c$  is exceeded, the RC beam fails under vertical shear due to the critical diagonal crack. It should be noted that the CDC mechanism is not associated with a flexural crack or a flexural-shear crack but it is caused only by a single diagonal crack that eventually slides and which governs the shear concrete capacity  $V_c$ . When the crack width  $s_{cr}$  increases, the tensile force in the laminate increases, which finally leads to the IC laminate debonding and  $V_c$  reduction (Fig. 2.7.).

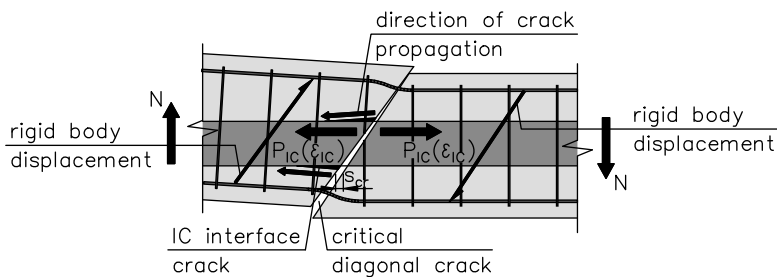


Fig. 2.7. Critical diagonal crack CDC debonding (Oehlers et al., 2007)

### ***Concrete cover separation***

The concrete cover separation induced by the inclined crack located close to the end of the laminate was described in research by (Kotynia, 1999). The FRP delamination started the moment the tensile steel reinforcement started yielding at the not strengthened cross-section of the beam (Fig. 2.8.). A sudden increase in the inclined crack width occurred close to the end of the strip caused the loss of bond between concrete and steel in the vicinity of this crack. This is why delamination occurred at the steel reinforcement level and the concrete remained joined with the laminate at this critical cross section (Fig. 2.8.).

The application of lateral laminates overlapping the bottom laminate (Fig. 2.9.) delayed delamination of the bottom laminate that lead beneficial effects for the strengthening efficiency. This failure mechanism was described in Yao (2004) and Yao et al. (2005). After forming of the inclined crack close to the end of the FRP laminate in the unstrengthened region, the crack width starts to

## Flexural strengthening

increase, which results in debonding of the bottom laminate with the adjacent concrete cover (known as the “thick composite plate”) from the tensile steel reinforcement and reduction of the flexural stiffness of the beam due to increasing beam’s curvature.

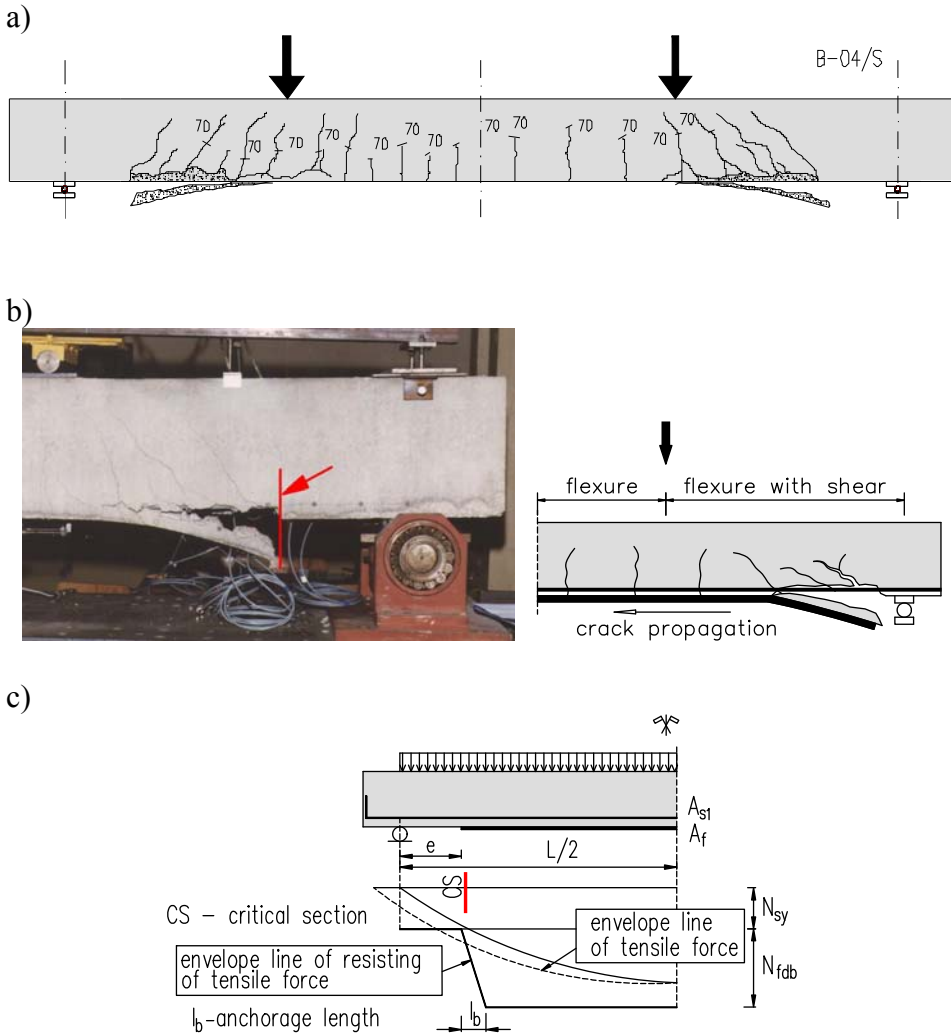


Fig. 2.8. Concrete cover separation failure (CCS): test set-up of the beam, b) failure mode, c) location of the critical cross-section “CS” at the CFRP termination

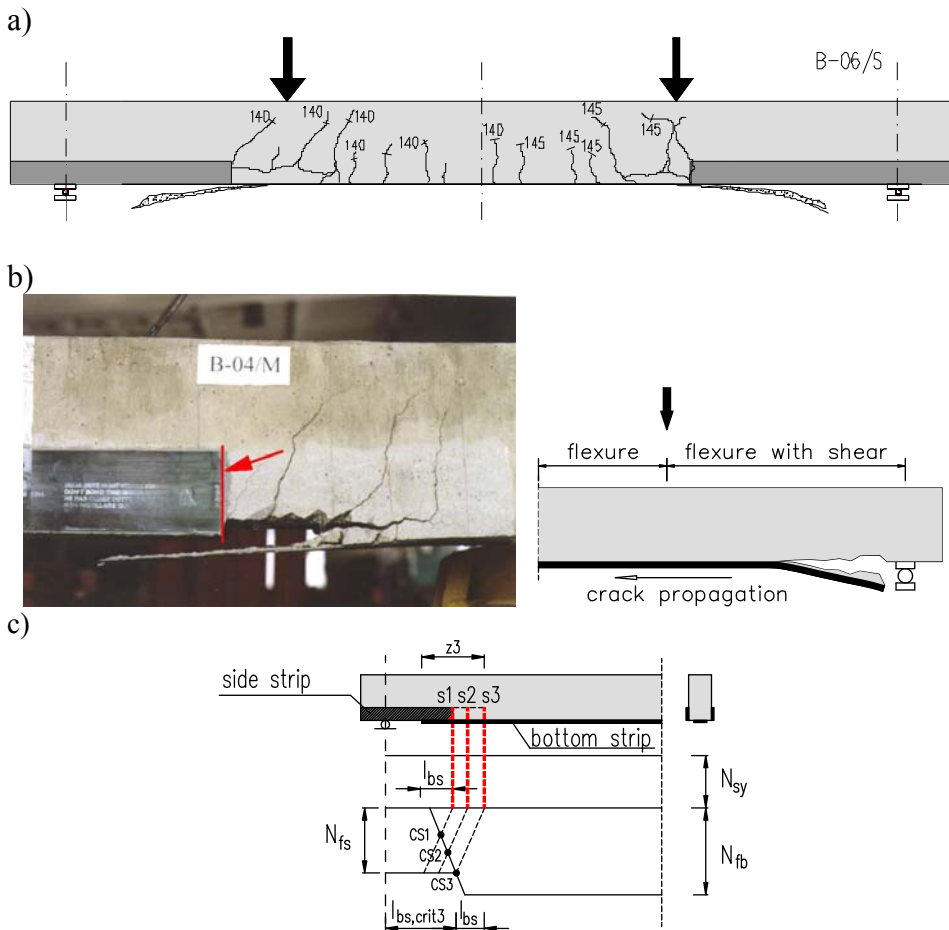


Fig. 2.9. Plate end debonding at the FRP anchorage debonding due to the predominant effect of shear stresses: a) test set-up of the beam, b) failure mode, c) location of the critical cross-section “CS” with the overlapping length of the lateral laminates on the “CS” position

The “thick composite plate” under such a large curvature increase causes high interfacial stresses between the “composite plate” and the longitudinal reinforcement. Debonding failure induces the sudden composite plate tearing off (Fig. 2.10, Yao et al., 2005).

## Flexural strengthening

---

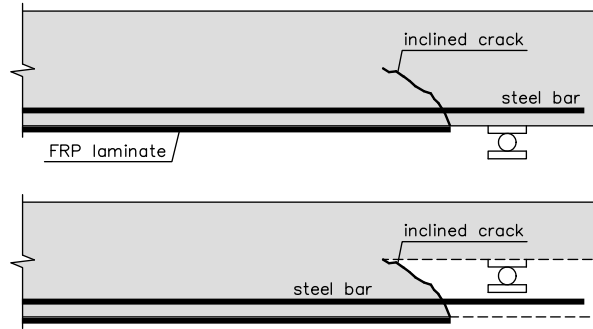


Fig. 2.10. Concrete cover separation failure mode (Yao et al., 2005)

### *Plate end debonding*

The third debonding mechanism induces the plate interfacial (PE) debonding at the FRP end due the high interfacial shear and normal stress concentration near the FRP end and the discontinuity of the laminate caused by the curvature.

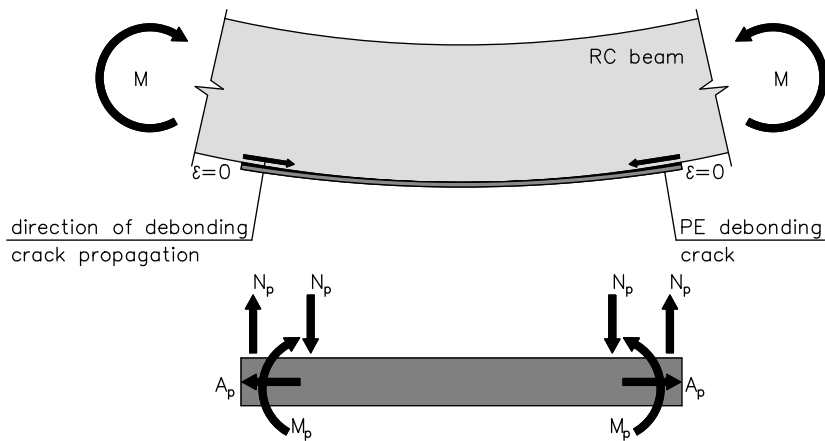


Fig. 2.11. Plate end (PE) debonding mechanism (Oehlers et al., 2007)

When curvature increases the axial tensile force,  $A_p$  in the laminate appears with the normal force  $N_p$  induced by the bending moment  $M_p$  (Fig. 2.11). The FRP end debonding starts from its end and propagates towards the maximum bending moment location. Generally, failure plane is localized in a thin concrete surface following in the interfacial adhesive layer. This failure mechanisms can be prevented by extending the laminate to the lowest bending moment position.

The fourth  $V_{Ay}$  debonding mechanism (Fig. 2.4) caused by the stress concentration due to flexural cracks (IC), neither due to critical diagonal cracks (CDC), nor due to the discontinuity of the laminate (PE) is not separately classified and it is very rarely published. The  $V_{Ay}$  debonding comes from the elementary structural mechanics referring to the shear  $\tau$  and normal stress  $\sigma_z$  (Model Björn Täljsten (Täljsten, 1997b), Fig. 2.12.).

Brittle failure observed in the PE debonding is caused by complex stress state at the anchorage distance mentioned above (Fig. 2.12.).

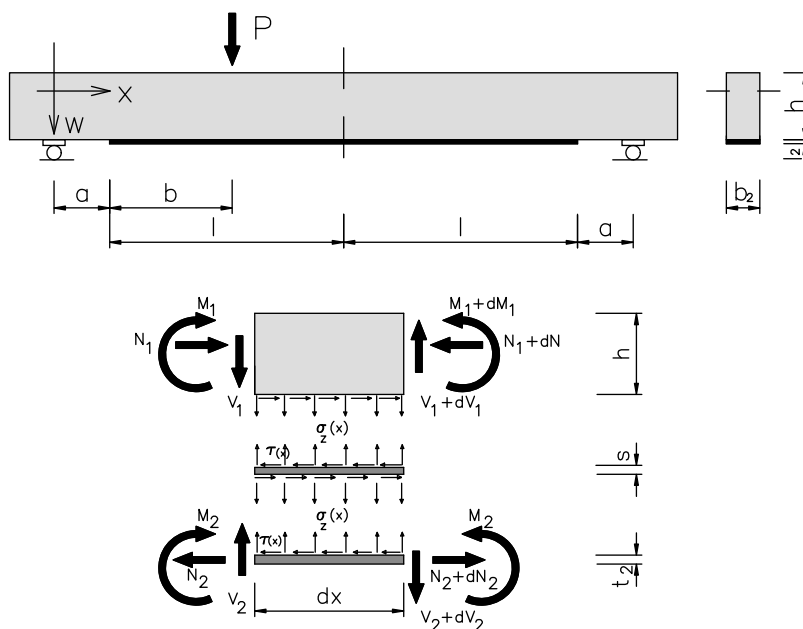


Fig. 2.12. Static scheme and complex stress state at the end of the EB FRP reinforcement (Täljsten, 1997b).

The normal stress  $\sigma_z$  (Fig. 2.13.) reached relatively much lower value in comparison with the shear stress that appeared on a very short anchorage distance (Fig. 2.14.). Hence, it is reasonable not to consider normal stress in the analysis at the end of the FRP laminate.

However, this failure mode is very probable for beams strengthened with prestressed FRP laminates. Moreover, it should be considered in the serviceability limit states as well.

Apart from the critical crack position and its width, the IC debonding depends on adjacent cracks and the curvature of the cracked RC member that is

different for slabs and beams (Nidermeier, 1997; Neubauer, 2000; Finckh, 2012; Zilch et al., 2011, 2012; Teng et al., 2006; Chen et al., 2007; Pan et al., 2009).

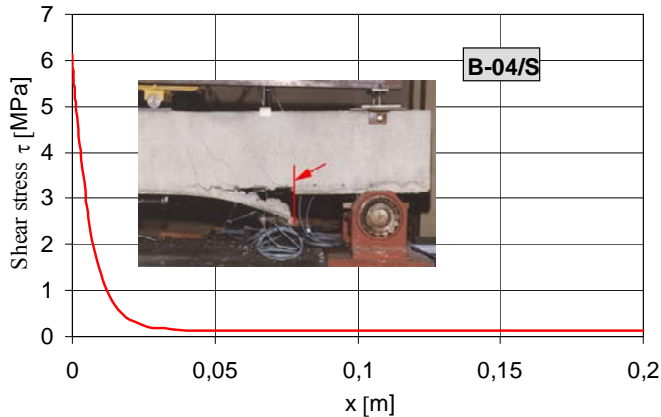


Fig. 2.13. Calculated (according to Täljsten (1996)) shear stress  $\tau$  diagram in the beam B-04/S (Kotynia, 1999).

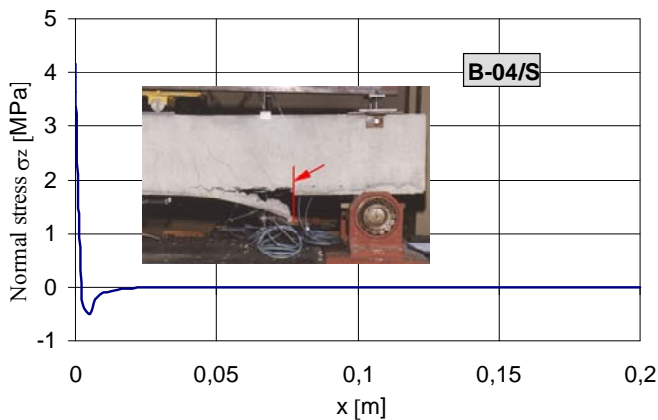


Fig. 2.14. Calculated (according to Täljsten (1996)) normal stress  $\sigma_z$  diagram in the beam B-04/S (Kotynia, 1999)

***Load distribution effect***

Flexural behaviour of EB FRP–strengthened RC members depends on the load distribution, which significantly effects the cracking pattern in the IC debonding mechanism. Most of experimental programs based on the point loaded schemes. However the uniformly distributed load is very rarely used in

scientific research. On the other hand, this scheme of loading is the most common one in the engineering practice.

The load distribution strongly effects the curvature of a member and the cracking pattern, which, in consequence govern the cracking pattern. Although IC debonding failure was investigated in a vast amount of research, few of them developed IC debonding mechanism using strong relationship based on IC debonding and the interfacial shear stress distribution (Lu et al., 2007; Rosenboom and Rizkalla, 2008). Most of the existing approaches for IC debonding used the bond strength models for FRP-to-concrete bonded joints based on the pull-out bond tests or beam-bond tests. They will be described in Chapter 4.

An effect of load distribution was investigated by Fu et al. (2018). The IC debonding was analyzed under two-point loading, four-point loading and eight-point loading schemes. The eight-point loaded beam indicated greater increase in the mid-span moment from the first appearance of local FRP debonding to the final IC debonding. More regions with local debonding were observed until the final failure of the beam. This definitely confirms a huge effect of the load distribution on the process of crack propagation, the FRP debonding and final beam failure mode.

In recent years, carbon fibre-reinforced polymer (CFRP) strips and sheets have been widely used for strengthening RC structures, by using an externally bonded (EB) technique, in which the strips and sheets are bonded to the concrete surface with epoxy resin. Many tests performed on RC members strengthened in flexure with EB FRP materials indicated low efficiency of this technique caused by premature FRP debonding. Although non-prestressed (passive) CFRP strengthening systems have shown significant increases in the ultimate strength, they have indicated slight increase in the serviceability limit state. Moreover, strain utilization of the EB CFRP laminates generally range from 30 to 35% of their tensile strength (Kotynia, 1999, Aram et al., 2008; Berset et al., 2002; Czaderski, 2012; Czaderski et al., 2012; Czaderski and Motavalli, 2007; Deuring, 1993; El-Hacha and Aly, 2013; El-Hacha et al., 2004a, 2004b; El-Hacha et al., 2001; El-Hacha et al., 2003; Garden and Hollaway, 1998; Harmanci, 2013; Kaiser, 1989; Kim et al., 2010a, 2010b; Kim et al. 2008a, 2008b; Kotynia et al. 2013a, 2013b; Kotynia et al., 2011; Lees et al., 2002; Meier, 1995; Meier et al., 1993; Meier and Stöcklin, 2005; Michels et al., 2012; Michels et al., 2011; Michels et al., 2014a, 2014b, Michels et al., 2013; Motavalli et al., 2011; Neubauer et al., 2007; Oudah and El-Hacha, 2012; Quantrill and Hollaway, 1998; Schlaich et al., 2012; Triantafillou and Deskovic, 1991; Triantafillou et al., 1992; Wight et al., 2001; Wu et al., 2003; You et al., 2012; Yu et al. 2008; Zilch et al., 2009; Gutowski et al., 2003; Kałuża and Ajdukiewicz, 2008; Siwowski et al., 2009; Stöcklin and Meier, 2003; Xue et al., 2010; Yang et al., 2009), which confirms the efficiency of this technique only in

case of RC members that have been slightly preloaded before strengthening. Such behaviour is caused premature debonding failure of the CFRP composites from the concrete surface (Seim et al., 2001; Motavalli and Czaderski, 2007; Sayed-Ahmed et al., 2009).

### **2.3. Strengthening with prestressed FRP members**

The state-of-the-art in prestressing methods were published in (El-Hacha et al., 2001; Kim et al., 2008a, 2008b; Schlaich et al., 2012). The following prestressing and anchorage commercially available systems have been developed for the last two decades:

- S&P Clever Reinforcement Company (S&P, 2019)
- “Leoba-CarboDur” system (Andrä et al., 2001)
- Polish modified “Leoba-CarboDur” system (Łagoda, 2001, 2005; Łagoda G. and Łagoda M., 2009)
- “Stresshead” system by Sika and VSL International Ltd. (Berset et al., 2002)
- “gradient – anchored” prestressing system (Meier and Stöcklin, 2005; Michels et al., 2013; Czaderski et al., 2012)
- TENROC “gradient – anchored” prestressing system (Haghani and Al-Emrani, 2014)
- Polish Neoxe Prestressing System (Siwowski et al., 2009, Piątek, 2017; Piątek and Siwowski, 2016a, 2016b; Piątek and Siwowski, 2017; Siwowski, 2012a and b; Siwowski, 2006; Siwowski et al., 2017a, 2017b; Siwowski et al., 2010; Siwowski and Radomski, 1998; Siwowski and Radomski, 2015; Siwowski and Żółtowski, 2012; Paško and Siwowski, 2106)
- Several noncommercial systems have been used in the laboratory tests:
  - multi-layer CFRP sheets technique (Wight et al., 2001),
  - (El-Hacha et al., 2003)
  - (El-Hacha and Aly, 2013)
  - mechanically anchored, CFRP anchored U-wraps sheets (Kim et al., 2008 d, e)
  - (Schlaich et al., 2012)

In order to maximize the utilization of composites, brittle failure modes caused by debonding should be prevented by prestressing the composites (Wight et al., 2001; El-Hacha et al., 2004). This solution, however, has one important drawback. The tensile force acting on the strip cannot be conveyed directly onto the concrete surface because the shear stress corresponding to it significantly exceed the tensile strength of concrete, which leads to debonding of the composite from the concrete surface. For this reason, the system of strengthening with pretensioned laminates requires mechanical anchorage of their ends in the concrete surface (Kotynia et al., 2011; You et al., 2012).

It should be emphasized that the effectiveness of the flexural strengthening depends on a number of factors including: FRP type, axial stiffness and the number of CFRP layers; distance of the CFRP end from the support; the existing longitudinal and shear steel reinforcement ratio; bending moment distribution. Although EB CFRPs increase the load-bearing capacity of an RC member, they do not significantly change the cracking load and deflections under the service loads. To gain the greatest advantage of the EB technique, CFRP prestressing has been proposed to improve the serviceability of strengthened structures, to reduce crack widths effectively, to relieve stress in the internal reinforcement, to enable control the crack distribution, limit deflection, and increase the stiffness and the load capacity of RC members.

The application of the prestressed laminates significantly increases the cracking load, the steel yielding load and finally the load carrying capacity in comparison with a reference RC member.

Since the 1990s, many researchers who investigated the efficiency of the FRP prestressing technique for RC members have proved the aforementioned advantages of this method (Triantafyllou et al., 1992; Deuring, 1993; El-Hacha et al., 2001; Wight et al., 2001; Wu et al., 2003). The application of externally bonded prestressed FRP laminates/sheets for flexural strengthening of the existing RC structures is quite a common strengthening technique. The CFRP materials (made of carbon fibres) are most recommended for prestressing due to their high strength comparison with other types of fibres. There are some historical applications with glass fibre-reinforced polymer (GFRP) sheets (Huang et al., 2005), aramid tendons (Lees and Burgoyne, 1999). However their strengthening efficiency has been quite low, because of their low elasticity modulus.

Experimental tests on RC specimens strengthened with prestressed composites indicated that prestressing levels should be at least 0.25 of the FRP ultimate strength (Meier, 1995a). For prestressing levels above 0.70 of the CFRP ultimate strength, failure attributable to the fracture of the composite was observed. However, for prestressing levels below 0.60 of the CFRP ultimate strength, strip debonding appeared as to be the most common failure mode (Meier, 1995a). To use the tensile strength of the composite effectively, a prestressing level of approximately 0.50 of the CFRP ultimate strength has been suggested (Garden and Hollaway, 1998).

A review of the available literature on strengthening of RC members with prestressed laminates was presented in (Garden and Hollaway, 1998; Teng et al., 2002; Yu et al., 2008; You et al., 2012; Kim et al., 2008a; Pellegrino and Modena, 2009; Wight et al., 2001; Kotynia and Kamińska, 2003; Meier and Stöcklin, 2005; Kotynia et al., 2011; Czaderski, 2012; Czaderski and Motavalli, 2007; El-Hacha et al., 2004; Kim et al., 2010b; Kotynia et al., 2013a, 2013b; Michels et al., 2014b; Lasek, 2015; Piątek, 2017).

Reinforced concrete beams strengthened with prestressed CFRP laminates show three groups of failure modes:

- under-reinforced RC members failed due to FRP rupture (R)
- over-reinforced RC members with composite reinforcement applied excessively, resulting in concrete crushing (CC), however this failure mode is possible only for the RC members characterised by low concrete strength and high reinforcement ratio
- intermediate crack induced by interfacial debonding (ICD), initiates at the flexural / flexural-shear cracks in the highest bending moment region and propagates by gradual debonding of the laminate from the flexural crack to the FRP end
- the group of RC members with the reinforcement not anchored sufficiently, in which leads debonding of FRP ends (plate end debonding - PE, concrete cover separation - CCS, anchorage failure - AF).

The parameters effecting strengthening efficiency with externally bonded FRP prestressed materials may be summarized as follows:

- type of FRP material (laminate, sheet)
- FRP stiffness (thickness, number of layers, elasticity modulus)
- existing flexural tensile reinforcement ratio
- existing shear reinforcement ratio
- stiffness of the strengthened RC member (slab, beam)
- size of the strengthened RC member
- type of strengthening system (mechanically anchored, fully efficient (FRP rupture) or partially efficient (FRP sliding from the anchored system))
- preloading level

The analysis of variable parameters influencing the strengthening efficiency was published by Kotynia et al. (2013a).

### **2.4. Preloading effect**

Preloading is one of the most important parameter to be taken into account in the design of strengthening of existing RC structures. This problem has been investigated in several publications (Wang and Li, 2004; Mukherjee and Rai, 2009; Gao et al., 2016; Lasek, 2015; Michels et al., 2016; Mahal et al., 2016; Correia et al., 2015; Aslam et al., 2015). The experimental tests carried out by [13, 19] revealed that the failure of beams strengthened with EB CFRP with adhesion was mainly caused by debonding of the laminate from the concrete surface. Usually, strengthening is applied to an already cracked surface or cracking appears during loading of the strengthened structure, which initiates a local slip of the laminate in the close proximity of the flexural crack. The

subsequent development of local slips of the laminate between two adjacent cracks leads to incompatibilities between the concrete and laminate strains. If the structure is cracked and deformed under initial extensive preloading, strengthening with non-prestressed composites is not effective.

Still few experimental studies considered an effect of preloading on flexural strengthening efficiency of RC members (Arduini and Nanni, 1997; Bonacci and Maalej, 2000; Shahawy et al., 2001; Yeong-soo and Chadon, 2003). Lam and Teng (2001) indicated that the effect of preloading due to self-weight and service loads is generally beneficial if a beam fails by FRP rupture. However, if the concrete strength is low and the initial preloading level is high the strengthening capacity is notably governed by the concrete crushing failure mode. This effect should be considered in the sectional design analysis of the strengthened cross section. This problem will be more developed in Chapter 5.

The research by Kotynia et al. (2013a) and Gao et al. (2016) indicated that the preloading load level had marginal effect on the flexural capacity of the strengthened beams when failure is governed by FRP rupture. However, if the FRP anchorage failure is the mode of failure, the prestressing level has the significant effect on the strengthening efficiency. Although the preloading levels exceed the serviceability limit states prior to strengthening, the application of prestressed CFRP laminates results in a significant reduction of deflections and strains due to subsequently applied loads. The prestressing technique led to partial recovery of the beam stiffness similar to specimens without preloading. Even the imposed sustained load was 40% (Gao et al., 2016) or 70% (Lasek, 2015) higher than the load of the steel yielding in the reference beam, the increase in the beam strength after strengthening was between 50-76% of the reference beam capacity.

### 3. FRP to concrete bond behaviour

#### 3.1. Debonding mechanisms

In general, the bond of externally bonded FRP reinforcement is governed by the brittle loss of adhesion between FRP and concrete that may occur in the thin adhesive layer, concrete surface or within the FRP reinforcement (it occurred in the interface between layers of the FRP sheets with different inclination of fibres bonded each other). The adhesive strength is generally much higher than the tensile concrete strength, hence debonding always takes place within the concrete in its thin surface layer or in the whole concrete cover (Fig. 3.1). Generally, the process of debonding is very rapid.

The most common FRP debonding begins in a short distance of a strengthened element and it further propagates to the end of the EB FRP reinforcement (*fib* Bulletin 90, 2019). This failure mechanism is known as the localized debonding, which is defined as a reduction of the bond performance between concrete and FRP. The bond loss proceeds along the short bond length limited to a few millimeters next to the flexural or shear crack (see Fig. 2.3., Fig. 2.4.).

On the contrary, when localized debonding propagates and the composite action is lost in such a way that the FRP reinforcement is not able to carry loads anymore, failure is called peeling-off (Fig. 2.11). If no stress redistribution from the external FRP to the internal steel reinforcement is possible, peeling-off will occur as a sudden and brittle failure.

#### *Debonding in the concrete (cohesive concrete failure; fib Bulletin 90, 2019)*

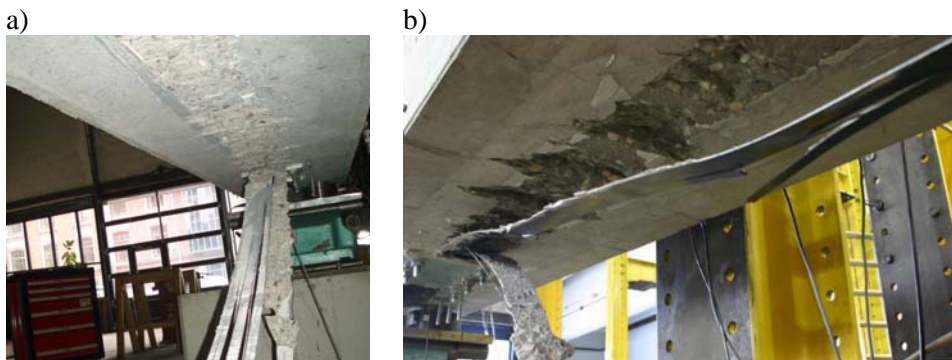


Fig. 3.1. Debonding failure: a) in a thin concrete cover; b) in a deep concrete cover (Kotynia et al., 2013; Lasek, 2015)

Due to the adhesive penetration into the concrete micro-structure, a thin layer of concrete in contact with the adhesive reaches a higher strength, resulting in debonding along a surface parallel to the FRP, a few millimeters inside the surrounding concrete (Fig. 3.1.a). Moreover, debonding may occur along a weakened layer and quite often along the internal steel reinforcement.

***Debonding in the adhesive (cohesive failure in the adhesive)***

This failure mode occurs very rarely through the adhesive layer only if its strength is lower than that of the concrete.

***Debonding at the interfaces between concrete and adhesive or adhesive and FRP reinforcement (adhesion failure)***

Bond loss along the interfaces between concrete and adhesive or adhesive and FRP reinforcement may only occur if there is an insufficient surface preparation before the strengthening application process, since the cohesion strength of epoxy resins is lower than the adhesion strength.

***Interlaminar shear failure in FRP***

Since the FRP reinforcement is a composite material, debonding may also occur through the FRP material system. This failure mechanism initiates when the maximum shear stress in the FRP reaches its shear strength. However, typical polymer matrix materials have the shear strengths that are several times higher than that of concrete, so this failure mechanism is very rare.

***FRP debonding in the concrete cover interface***

Most failure mode observed in experimental tests on RC members flexurally strengthened with FRP materials are caused by peeling-off of the external reinforcement. The weakest region in the FRP/concrete system is in the concrete layer near the surface. The debonding failure modes can be classified into two following main categories, depending on the location in which debonding occurs:

- at the anchorage end of the FRP reinforcement – ***end plate debonding*** (Oehlers and Moran, 1990; Oehlers, 1992; Garden and Hollaway, 1998; Teng and Smith, 2002a, 2002b; Oehlers et al., 2003; Yao and Teng 2007; Oehlers and Seracino, 2004)
- at the flexural-shear or flexural cracks region – ***intermediate crack debonding*** (Arduini and Nanni, 1997; Rahimi and Hutchinson, 2001; Sebastian, 2001; Smith and Teng, 2002a, 2002b; Teng et al. 2003; Teng et al.

2006; Liu et al., 2006; Chen et al., 2007; Seracino et al., 2007b; Liu et al., 2007; Czaderski, 2012) The first failure mechanism starts at the end of the FRP laminate (plate end debonding – PE), when the inclined microcracks propagate inside the concrete cover to several millimetres depth (if the concrete strength is lower than that of the adhesive) (Fig. 3.1.b).

The second failure mode is observed in the RC members subjected to the bending moment and shear deformation. Due to the curvature increase the peeling stresses increases leading to local detachment of the FRP laminate. The mixed mode of failure is possible for both mechanisms acting together.

### **3.2. Bond behaviour between FRP and concrete**

There are following five set-ups for the bond tests published in literature (Holzenkaempfer, 1994; Chajes et al., 1996; Ueda et al., 1999; Focacci et al., 2000; Chen et al., 2001; Ahmed et al., 2001; Teng et al., 2002; Smith and Teng, 2002a; Chen and Teng, 2003; Smith and Teng, 2003; Yuan et al., 2004; Yao et al., 2005; Lu et al., 2005; Ceroni et al., 2008; Olivito et al., 2009; Pellegrino and Modena, 2009b; Savoia et al., 2009; Zhou et al., 2010; Alam et al., 2012; Guadagnini et al., 2012; Serbescu et al., 2013; Mazzotti et al., 2016):

- double-shear pull test (Fig. 3.2.a)
- double-shear push test (Fig. 3.2.b)
- single-shear pull test (Fig. 3.2.c)
- single-shear push test (Fig. 3.2.d)
- beam-bond test (Fig. 3.2.e).

The test procedure depends on two main parameters:

- loading condition in the concrete block
- symmetry of the specimens that based on a single (with one side of block) or double (with two sides of blocks) tests.

In the double and single shear pull tests the tensile load is applied to the external FRP composite material and to the concrete block (Fig. 3.2.a, c). However in the next two set-ups tensile load is applied to the FRP material with the pushing force applied to the concrete block causing local compression in the pushed block (Fig. 3.2.b, d). Each set-up configuration can be symmetrical (double test, Fig. 3.2.a, b) or asymmetrical (single test, Fig. 3.2.c, d).

The pull shear test (single / double) reflects the real situation existing in RC structures flexurally strengthened with externally bonded FRP reinforcement applied on the tensile surface of the member. In this test set-up, tensile loading is applied into the steel bars embedded in the block realized by applying tension (Holzenkaempfer, 1994; Brosens and van Gemert 1997; Maeda et al. 1997; Ueda et al., 1999; Wu et al., 2001; Savoia et al., 2009; Bilotta et al., 2011, Serbescu et al., 2013). However, this test set-up is rather complicated, so more bond tests have

been realized on the single shear push tests, where the compressive force is applied into the small part of concrete block (see Fig. 3.2.d).

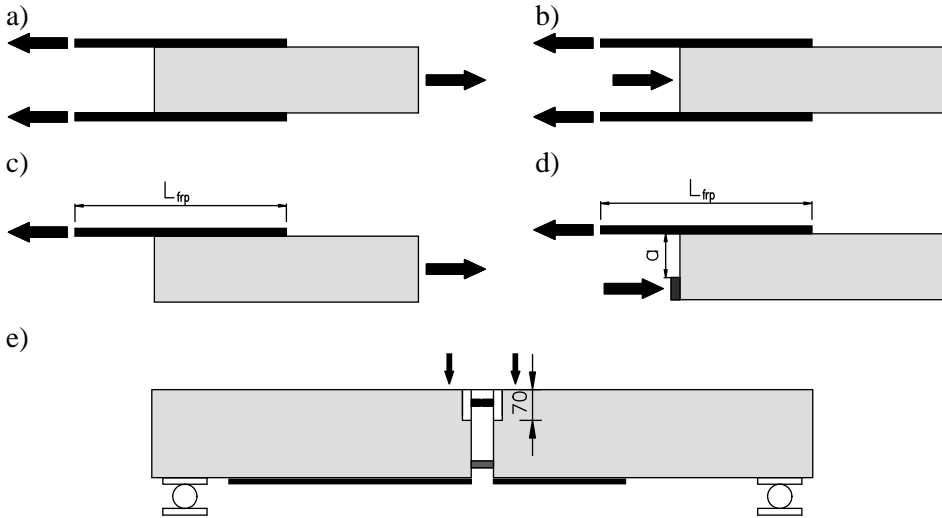


Fig. 3.2. FRP to concrete bond test set-ups: a) double-shear pull test; b) double-shear push test; c) single-shear pull test; d) single-shear push test; e) beam-bond test (Mazzotti et al., 2016)

For the RILEM standard beam-bond test set-up referring to steel bars in concrete elements was adapted with the FRP reinforcement bonded on the tensile face of the beam (Fig. 3.2.e). The beam consists of two separate concrete blocks connected at the bottom by the FRP reinforcement and on the top side by a steel hinge loaded by two vertical loads (De Lorenzis et al., 2001; Cruz and Barros, 2002; Ceroni et al., 2008; Kotynia, 2012).

The single and double shear tests reflect only pure shear test. However, in practice flexurally strengthened RC members with EB FRP reinforcement indicated under loading curvature changes that made the bond subjected to both normal and shear stresses under loading, mainly at the cracking zone (Karbhari et al., 1997; Mukhtar and Faysal, 2018). This problem can be successfully simulated in the beam-bond tests and other mixed-mode tests. However, the FRP in the bending test is not directly loaded but somehow subjected to tensile stresses due to bending action (Mazotti et al., 2016). In general, the specimens subjected to the mixed-mode type of test set-ups are reported to have less bonding strength compared to other test set-ups (Ghorbani et al., 2017). If the FRP material is bonded to the bottom surface of the beam under flexure, the orthogonal compressive state appears to FRP bonded length leading to increase in the bond strength (Miller and Nanni, 1999; Ghorbani et al., 2017). The reason

of the higher bond strength is the orthogonal compressive stress, which makes anti-peeling effect in the FRP-to-concrete bond behaviour.

Most of the existing FRP-concrete bond tests based on the direct tension pull-off test. It should be noted that the direct tensile test is difficult to perform in real tests.

If debonding is induced by a flexural-shear crack the vertical displacement between the two sides of this crack appears (Fig. 3.3). Then the FRP reinforcement starts to be loaded by the positive inclination angle to the longitudinal axis on one side and at the same but negative angle on the other side of the crack (Yao et al., 2005).

Due to acting flexure and shear, curvature deformation causes displacement of two sides of the crack, which generates relative vertical displacement across the crack. The flexure and shear lead to the mixed-mode loading, resulting in plate end debonding and intermediate crack-induced debonding, followed by crack opening and vertical shearing of the two faces of the crack interface (Fig. 3.4).

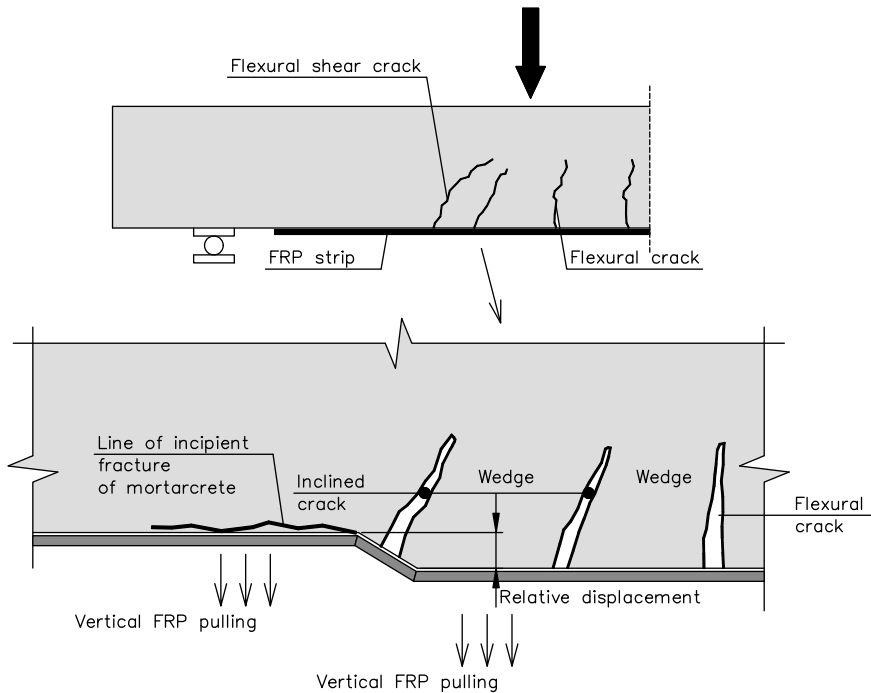


Fig. 3.3. Initiation of FRP peeling by vertical displacement between two sides of a flexural-shear crack (Sebastian, 2001; Yao et al., 2005).

When the normal tensile stress acts the FRP-to-concrete interface is under positive eccentricity that makes the positive angle between FRP and concrete interface. However if the FRP-to-concrete interface is exposed to the normal compressive stresses the negative eccentricity appears with the negative angle

(Triantafyllou and Plevris, 1992; Yao et al., 2005; Ghorbani et al., 2017). In this case the tensile stresses is more dominant contribution to the interface fracture than the axial tensile debonding load in the pure loading in the common single lap-shear bond test.

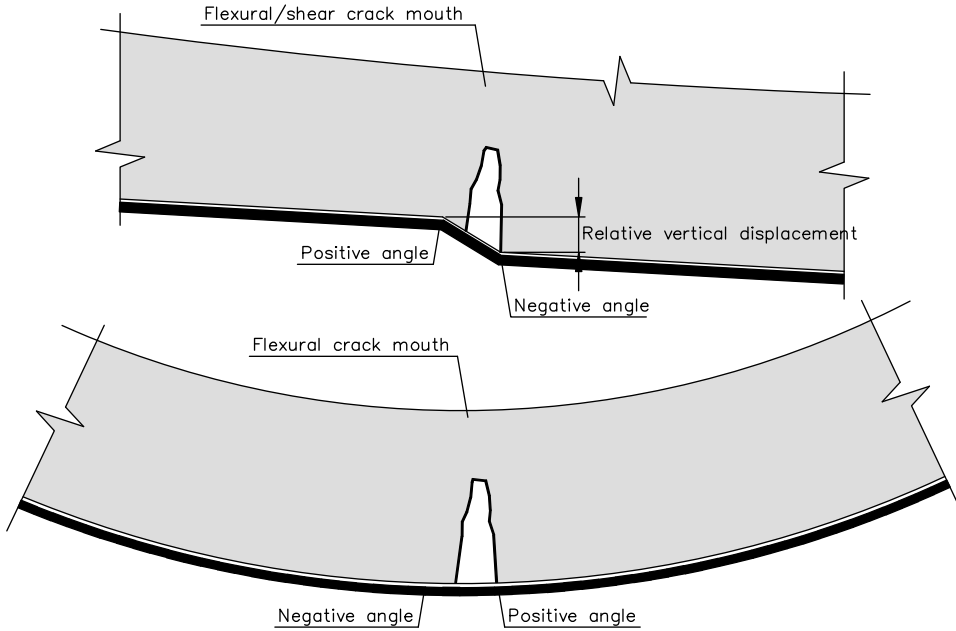


Fig. 3.4. State of FRP sheet at the location of: (a) flexural/shear crack (Yao et al., 2005); and (b) pure flexural crack (Ghorbani et al., 2017).

To find an effect of the load inclination on the FRP-to-concrete interface 31 experimental single bond tests with variable bond length, loading angle and positive or negative angle inclination were performed by Ghorbani et al. (2017), Fig. 3.5.

Ghorbani et al. (2017) proposed the formula to predict the mixed-mode loading:

$$P_{II,\alpha} = \beta_a P_{II} \quad (3.1)$$

where:  $P_{II}$  is the bond strength under pure mode II loading;  $\beta_a$  is a coefficient factor accounting for the effect of loading angle and is determined by:

$$\beta_a = \left( \frac{0.08L_f - 61}{1000} \right) \alpha + \frac{855 + 1.1L_f}{1000} \quad (3.2)$$

where:  $\alpha [^\circ]$  is the loading angle in degrees;  $L_f$  is the FRP bond length [mm]. If  $\alpha < 0$ , the coefficient  $\beta_a$  (3.2) is greater than that in pure mode II loading, resulting in a higher debonding load obtained from (3.1). However, if  $\alpha > 0$ , a lower  $\beta_a$  is obtained from (3.1).

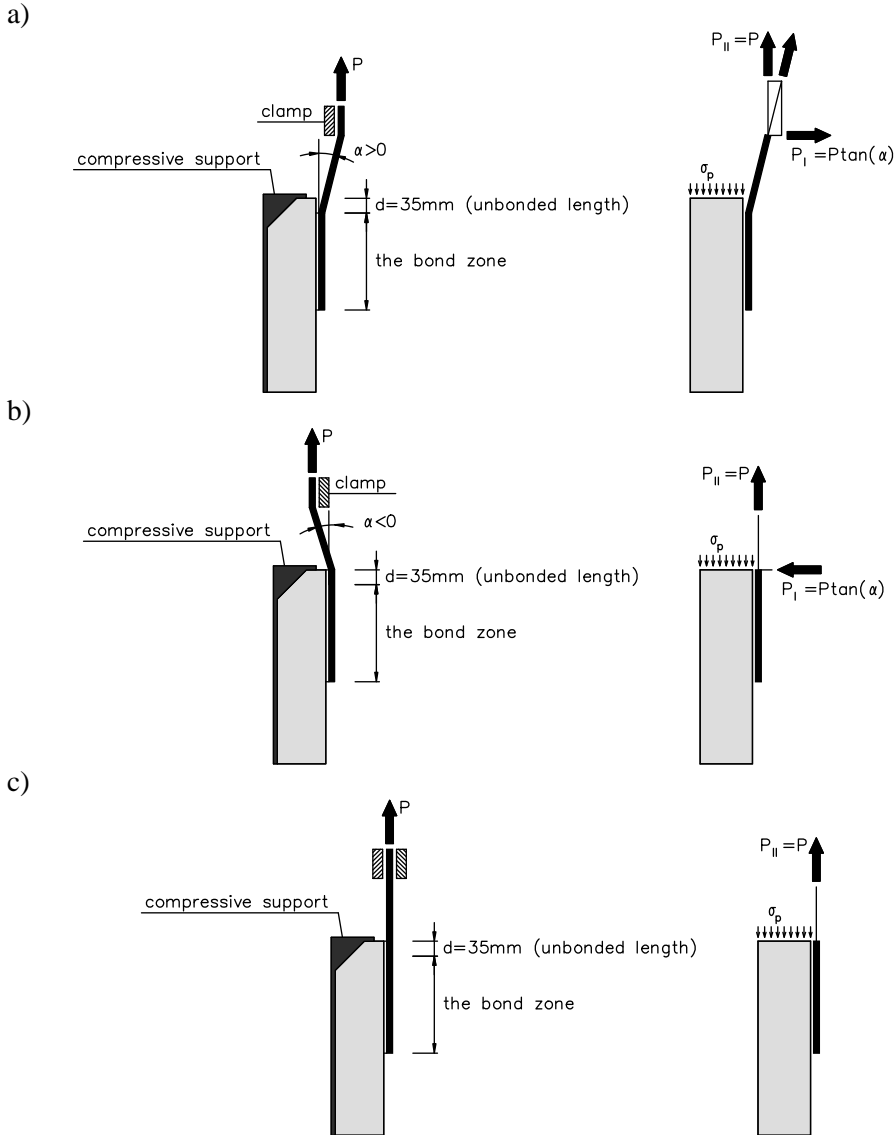


Fig. 3.5. Single lap-shear test under: a) positive angle; b) negative angle; c) pure (zero angle) loading (Ghorbani et al., 2017).

The relationship between ultimate axial force,  $P_{II}$ , and the ultimate normal force,  $P_I$ , was proposed in by Ghorbani at al. (2017) as:

$$P_{II} = \begin{cases} -0.061P_I^2 - 3.695P_I + 228.7 & L_f = 100mm \\ 0.011P_I^2 - 2.414P_I + 223.2 & L_f = 150mm \end{cases} \quad (3.3)$$

where:  $P_I$  [N/mm] is the ultimate normal force per unit width of FRP strip at the onset of bond zone;  $P_{II}$  [N/mm] is the ultimate axial force developed in the unit width of FRP sheet.

Ghorbani at al. (2017) indicated that the load-slip curves of all tested specimens under compressive mode I loading confirmed 4 distinct regions, with linear-nonlinear and hardening-softening branches. Moreover, specimens experiencing compressive mode I loading showed a stiffer bond between FRP and the concrete substrate, in a way that the debonding crack opens at a higher load in comparison with the control specimen. It strongly emphasized that the effect of normal compressive stresses on the strength specifications of FRP-to-concrete joints should be considered. The proposed model confirmed compatibility of predicted and test results.

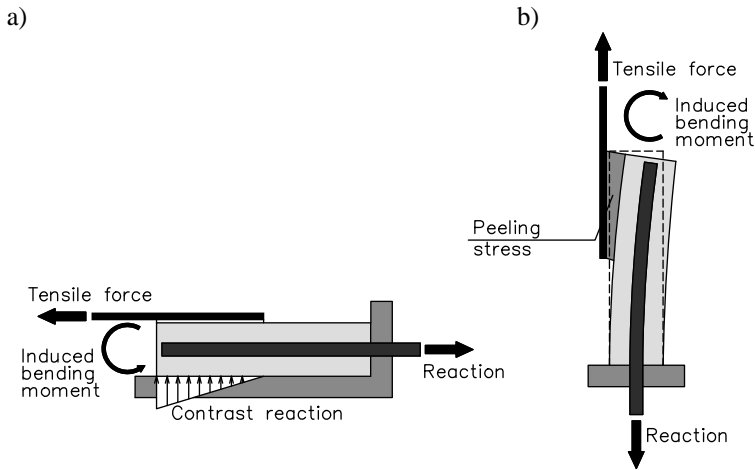


Fig. 3.6. Single-shear push bond test set-ups: a) horizontal; b) vertical (Mazotti et al., 2016)

Another parameter investigated in the bond tests refers to position of the concrete block, that makes differences referring to debonding load effecting by

the different restraint conditions of the concrete blocks. The difference is caused by the tensile force applied to the FRP reinforcement:

- in the horizontal set-up the FRP is axially tensioned without any restrains from the tensile plane (Fig. 3.6.a)
- in the vertical set-up the FRP material is loaded with a small eccentricity that makes a misalignment to the FRP (Fig. 3.6.b).

### 3.3. Effective bond length

The effective bond length  $L_e$  is the minimum bonded length of the FRP reinforcement that ensures the maximum tensile force transfer between the concrete element and the external FRP reinforcement. Variable guidelines give empirical equations based on the experimental tests. The following existing guidelines propose the effective bond length (without any safety coefficient  $\gamma_f$ ,  $\gamma_c$  and  $\gamma_{bd}$ ).

#### 3.3.1. *fib* Bulletin 14, 2001

The formulation suggested by *fib* (2001) and CNR (2004) for the effective bond is:

$$L_e = \sqrt{\frac{E_f t_f}{2 f_{ctm}}} \quad (3.4)$$

where:  $E_f$ ,  $t_f$  are the elasticity modulus and thickness of FRP reinforcement, respectively,  $f_{ctm}$  is the medium tensile concrete strength.

#### 3.3.2. CNR-DT 200 R1, 2013

A new version of CNR\_DT200 R1 (2013) proposes the following formula for the effective bond length:

$$L_e = \frac{1}{f_{bd}} \sqrt{\frac{\pi^2 E_f t_f G_{Fd}}{2}} \leq 200mm \quad (3.5)$$

$$f_{bd} = \frac{2G_{Fd}}{s_u} \quad (3.6)$$

$$G_{Fd} = \frac{k_b k_G}{FC} \sqrt{f_{cm} f_{ctm}} \quad (3.7)$$

$$k_f = \sqrt{\frac{2 - b_f/b_c}{1 + b_f/b_c}} \geq 1 \quad (3.8)$$

$$s_u = 0.25mm \quad (3.9)$$

where:  $k_G = 0.023$  in case of pre-impregnated laminates, and  $k_G = 0.037$  in case of post-impregnated sheets;  $k_f$  is the shape factor;  $b_f$  and  $b_c$  are the width of external FRP reinforcement and the width of the strengthened element, respectively. FC is an additional safety factor (only for design value).

### 3.3.3. *fib* Bulletin 90, 2019

A generic  $\tau_b - s$  bond law is characterized by a softening branch leading to an ultimate slip  $s_0$ . An accurate analysis of the bond–slip law is presented in Chapter 4 (Fig 4.3, Table 4.2, with  $s_0 = s_f$ ,  $\tau_{b1} = \tau_{max}$ ). The effective bond length is the length necessary to attain the slip  $s_0$  at the loaded section of the FRP reinforcement, defined as:

$$L_e = \frac{\pi}{2} \sqrt{\frac{E_f t_f s_0}{\tau_{b1}}} \quad (3.10)$$

or

$$L_e = \pi s_0 \sqrt{\frac{E_f t_f}{8G_f}} \quad (3.11)$$

where:  $G_f$  is the fracture energy, defined as:

$$G_f = \frac{\tau_{b1} s_0}{2} \quad (3.12)$$

where:  $\tau_{b1}$  is the bond strength ( $\tau_{max}$ ).

In general, for any relationship  $\tau_b - s$ , the fracture energy depends on the strength properties of concrete and adhesive and on the characteristics of the concrete surface. In particular, if the FRP reinforcement is correctly applied, debonding occurs in the concrete and the fracture energy can be expressed as a function of the bond strength,  $\tau_{b1}$ . Since  $\tau_{b1}$  the bond depends on the concrete tensile strength, the fracture energy can be directly expressed as a function of the mean tensile,  $f_{ctm}$  or mean compressive,  $f_{cm}$ , strength of concrete:

The fracture energy is calculated from the formula:

$$G_f = k^2 k_f^2 f_{cm}^{2/3} \quad (3.13)$$

$$k_f = \sqrt{\frac{2 - b_f/b_c}{1 + b_f/b_c}} \quad (3.14)$$

Thus, the effective bond length  $L_e$  may be estimated from the following general expression:

$$L_e = \frac{\pi s_0}{k_b k} \sqrt{\frac{E_f t_f}{8 f_{cm}^{2/3}}} \quad (3.15)$$

The coefficient  $k$  is calibrated by a statistical procedure;  $s_0 = 0.25\text{mm}$ , the values of the coefficient  $k_G$  can be assumed as 0.25 for the mean value or 0.17 for characteristic value (5%) of the compressive concrete strength. Thus, the effective bond length  $L_e$  may be expressed as:

$$L_e = \frac{\pi}{k_b} \sqrt{\frac{E_f t_f}{8 f_{cm}^{2/3}}} \quad \text{for mean value} \quad (3.16)$$

$$L_e = \frac{0.25\pi}{0.17k_b} \sqrt{\frac{E_f t_f}{8 f_{cm}^{2/3}}} \approx 1.5 \frac{\pi}{k_b} \sqrt{\frac{E_f t_f}{8 f_{cm}^{2/3}}} \quad \text{for 5\% characteristic value} \quad (3.17)$$

### 3.3.4. ACI 440.2R-08, 2008

$$L_e = \frac{23300}{(E_f t_f n_f)^{0.58}} \quad (3.18)$$

where:  $n_f$  is a number of FRP layers with  $t_f$  thickness of the layer.

### 3.3.5. Other approaches to the effective bond length

The following approaches were proposed in chosen research on FRP-to-concrete bond:

$$\text{Holzenkampfer, 1994} \quad L_e = \sqrt{\frac{E_f t_f}{2E_{cm}}} \quad (3.19)$$

where:  $E_{cm}$  is the elasticity modulus of concrete.

$$\text{Chen and Teng, 2001} \quad L_e = \sqrt{\frac{E_f t_f}{\sqrt{f'_c}}} \quad (3.20)$$

$$\text{Faella et al., 2002} \quad L_e = s_u \sqrt{\frac{\pi^2 E_f t_f}{8G_f}} \quad (3.21)$$

$$s_u = 0.41 \frac{k_f}{\sqrt{f_{cm}}} \quad (3.22)$$

$$G_f = 0.03k_f \sqrt{f_{ck} f_{cm}} \quad (3.23)$$

$$\text{Pellegrino et al., 2008} \quad L_e = \sqrt{\frac{E_f t_f}{c_2 f_{cm}}} \leq 140\text{mm} \quad (3.24)$$

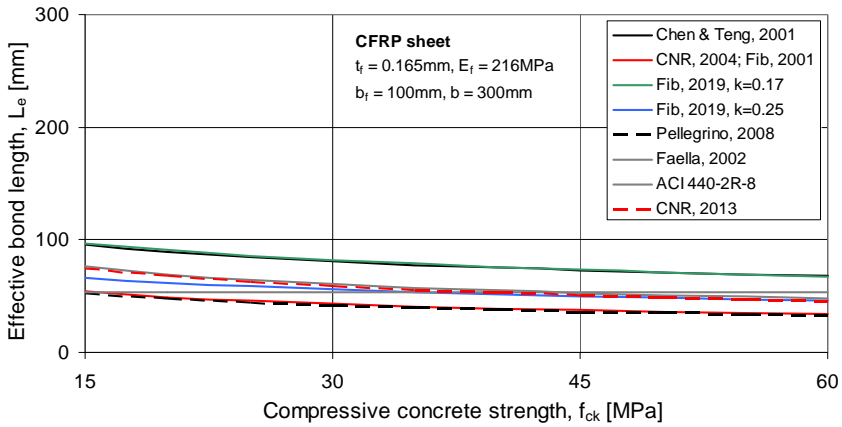
$$c_2 = 2.15 \quad (3.25)$$

The comparison of the effective bond  $h$  in the function of the compressive concrete strength, according to the above presented formulas is shown in Fig. 3.4 for separate four cases referring to: a) cured in-situ one layer of CFRP sheets ( $t_f = 0.165\text{mm}$ ,  $E_f = 216\text{GPa}$ ), b) cured in-situ three layers of CFRP sheets ( $t_f = 0.495\text{mm}$ ,  $E_f = 216\text{GPa}$ ), c) pre-cured CFRP laminate ( $t_f = 1.4\text{mm}$ ,  $E_f = 210\text{GPa}$ ), d) pre-cured CFRP laminate ( $t_f = 1.2\text{mm}$ ,  $E_f = 165\text{GPa}$ ).

It is visible that flexible cured in-situ sheets require the shortest bond length in comparison with the rigid CFRP pre-cured laminates. It is a well known rule, on the basis of the axial stiffness ( $E_f t_f$ ) of the FRP externally-bonded reinforcement, which indicates that with the increase in the FRP thickness and its modulus of

elasticity  $E_f$ , the bond strain  $\varepsilon_{f,b}$  decreases. For one type of FRP reinforcement (e.g. CFRP materials), the elasticity modulus varies from 165GPa to 220GPa, However, the thickness varies from 0.165mm to 1.4mm, which gives 8.5 times higher difference). This is why the main effect on the bond properties comes from the CFRP thickness. This phenomenon is described in details in Chapter 5.7.

a)



b)

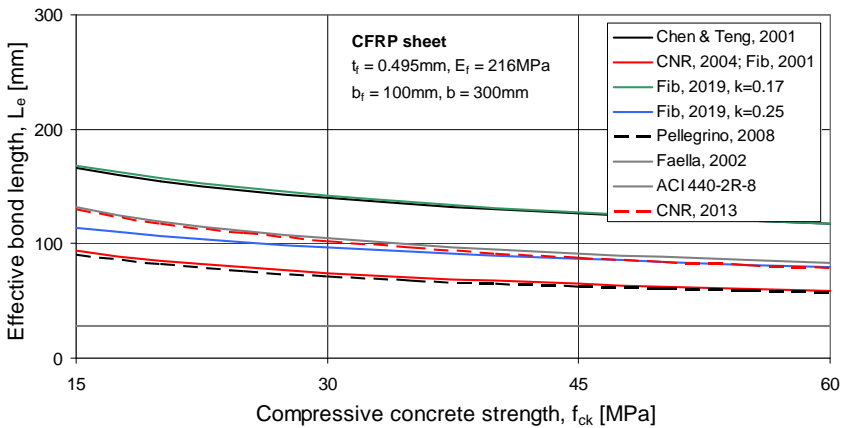


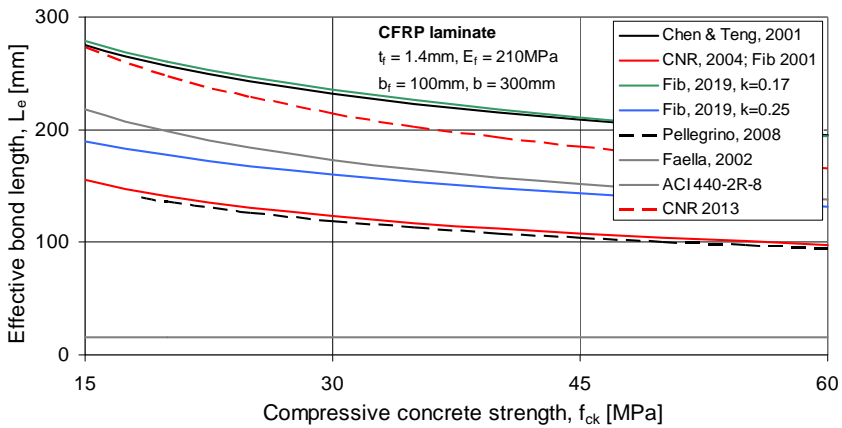
Fig. 3.7. The comparison of the effective bond length according to variable formulations for: a) one layer,  $t_f = 0.165\text{mm}$ ,  $E_f = 216\text{GPa}$ , b) three layers,  $t_f = 3 \times 0.165\text{mm}$ ,  $E_f = 216\text{GPa}$ )

A consequence of the stiffness effect ( $E_f t_f$ ) the bond length of pre-cured laminates is much higher than the FRP cured in-situ sheets. The effective bond

length by Chen and Teng (2001) and by ACI 440-2R-8 is the most conservative one, when compared to other codes and formulas. The new *fib* Bulletin 90 (2019) gives effective length similar to the new version of CNR-DT200 (2013). However, the previous version of CNR-DT200 (2004) follows the formula by Pellegrino (2008).

The CFRP sheets are not sensitive to the concrete strength (mainly if one 0.165 mm-thick layer is considered). However, 3 layers of CFRP sheets require almost 2 times higher effective bond length  $L_e$  when compared to one sheet ( $t_f = 0.165\text{mm}$ ). The CFRP laminates with much higher thickness than CFRP sheets require almost twice higher effective bond length when compared to sheets.

c)



d)

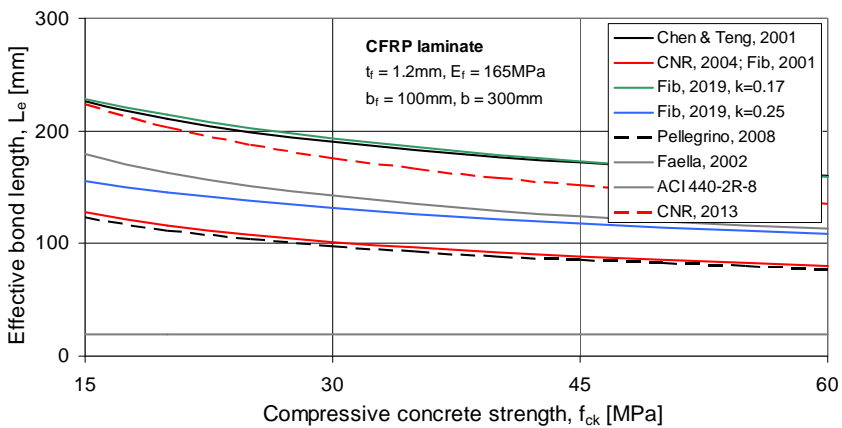


Fig. 3.7. cont. c)  $t_f = 1.4\text{mm}$ ,  $E_f = 210\text{GPa}$ , d)  $t_f = 1.2\text{mm}$ ,  $E_f = 165\text{GPa}$

### 3.4. Theoretical bond models

The model on the basis of the general debonding failure mode due to the concrete cover separation with the attached soffit FRP laminate bonded to the separated concrete cover (described in Chapter 3.1) has several different names: *end-of-plate failure through the concrete*, *concrete rip-off failure*, *debonding at rebar layer*, *concrete cover delamination* and *plate end interfacial debonding*.

The published debonding strength models were classified into following four categories (Smith and Teng, 2001, 2002a, 2002b):

- shear capacity models – on the basis of debonding failure strength related to the shear strength of the concrete with none or partial contribution of the steel shear reinforcement (Oehlers, 1992; Ahmed and van Gemert, 1999; Jansze, 1997)
- concrete tooth models (Wang and Ling, 1998; Raof and Hassanen, 2000; Raof and Zhang, 1997)
- interfacial stress based models (models I and II of Ziraba et al., 1994; Varastehpour and Hamelin, 1997; Saadatmanesh and Malek, 1998; Tumialan et al., 1999)
- bending-shear interaction model (Oehlers, 1992)

#### 3.4.1. Shear capacity based models

##### *Oehlers' model (Oehlers and Moran, 1990; Oehlers, 1992)*

This strength model considers two positions of the bottom FRP laminate termination:

- a) in the constant moment region
- b) in the FRP laminate terminated closed to the support.

For the first flexural debonding moment  $M_{db,f}$  at the end of the laminate is defined on the basis of the formula calibrated for the steel plates on the bottom surface of a beam:

$$M_{db,f} = \frac{E_c I_{trc,c} f_{ct}}{0.901 E_{frp} t_{frp}} \quad (3.26)$$

where:  $E_c$  and  $E_{frp}$  are the elasticity modulus of concrete and FRP, respectively;  $I_{trc,c}$  is the cracked second moment of area of the FRP laminate section transformed to the concrete;  $f_{ct}$  is the cylinder concrete splitting tensile

strength (if not experimentally determined,  $f_{ct} = 0.5(f'_c)^{0.5}$ );  $t_{frp}$  is the thickness of FRP laminate. This bending moment should be taken as the additional moment applied to the beam at the FRP end. For the second model at the plate FRP terminated close to the support, it is assumed that debonding occurs, when the shear force at the plate end  $V_{db,s}$  reaches the shear concrete capacity, without the steel shear reinforcement contribution defined by formula (according to the Australian Concrete Standards; AS 3600, 1988):

$$V_{db,s} = V_c = \left(1.4 - \frac{d}{2000}\right) b_c d (\rho_s f'_c)^{2/3} \quad (3.27)$$

where:  $\rho_s \frac{A_s}{b_c d}$  is the tensile steel reinforcement ratio;  $A_s$  is the cross section area of the tensile steel reinforcement;  $b_c$  is the concrete cross section width;  $d$  is the effective depth of the section and  $1.4 - (d/2000) \geq 1.1$ .

$$\frac{M_{db,end}}{M_{db,f}} + \frac{V_{db,end}}{V_{db,s}} \leq 1.17 \quad (3.28)$$

$$M_{db,end} \leq M_{db,f}, \quad V_{db,end} \leq V_{db,s} \quad (3.29)$$

$$V_{db,end} = \frac{1.17}{\frac{a}{M_{db,f}} + \frac{1}{V_{db,s}}} \quad (3.30)$$

$$V_{db,end} a \leq M_{db,f}, \quad V_{db,end} \leq V_{db,s} \quad (3.31)$$

where:  $a$  is a distance from the support to the nearer end of the FRP laminate;  $M_{db,f}$  is the flexural debonding moment;  $V_{db,s}$  is the shear concrete capacity in the beam without steel shear reinforcement;  $M_{db,end}$  and  $V_{db,end}$  are the bending moment and critical shear force in the RC beam at the plate end at its debonding.

**Jansze's model (Jansze, 1997)**

This model is based on the initiation of shear cracking in the RC beam without contribution of the shear reinforcement. The critical shear force in the RC beam at the FRP end causing its debonding  $V_{db,end}$  is calculated from:

$$V_{db,end} = \tau_{PES} b_c d \quad (3.32)$$

$$\tau_{PES} = 0.18^3 \sqrt{3 \frac{d}{B_{mod}} \left( 1 + \sqrt{\frac{200}{d}} \right)^3} \sqrt{100 \rho_s f'_c} \quad (3.33)$$

$$B_{mod} = 4 \sqrt{\frac{(1 - \sqrt{\rho_s})^2}{\rho_s}} da^3 \quad (3.34)$$

where:  $B$  is the shear span,  $B_{mod}$  is a modified shear span. If  $B_{mod}$  is greater than the actual shear span  $B$  of the beam, the modified shear span should be given by  $\frac{B_{mod} + B}{2}$ .

Jansze's model (Jansze, 1997) is not valid for the bottom FRP laminates terminated at the support, where  $B_{mod} = 0$ .

**Ahmed and van Gemert's model (Ahmed and Gemert, 1999)**

This model is the modified Jansze's model

$$V_{db,end} = (\tau_{PES} + \Delta\tau_{mod}) b_c d \quad (3.35)$$

$$\Delta\tau_{mod} = \tau_{PES} b_c d \left( \frac{S_s}{I_s b_{frp}} + \frac{S_{frp}}{I_{frp} b_a} \right) + 6188.5 \frac{\tau - 4.121}{b_c d} \quad (3.36)$$

$$\tau = 0.15776 \sqrt{f'_c} + \frac{17.2366 \rho_s d}{B} + 0.9 \frac{A_{sv} f_{yv}}{b_c s} \quad (3.37)$$

where:  $\tau_{PES}$  is the same as in Jansze's model;  $S_{frp}$  and  $S_s$  are the first moment of area of the FRP laminate and steel reinforcement, respectively, concerning the neutral axis of the cracked strengthened section transformed to concrete. The

equivalent steel laminate is one that has the same total tensile capacity and width as that of the FRP laminate, but with an equivalent thickness determined assuming that the yield stress of steel is 550 MPa;  $I_{frp}$  and  $I_s$  are the second moments of area of the cracked strengthened section transformed to concrete with an FRP laminate and an equivalent steel laminate, respectively;  $b_{frp}$  and  $b_a$  are the widths of the FRP and adhesive, respectively;  $s$  is the stirrup spacing;  $A_{sv}$  and  $f_{yv}$  are the cross sectional area and steel yielding stress of the steel stirrups, respectively;  $b_a = b_{frp}$ .

### 3.4.2. Concrete tooth models

The fundamental assumption of these models based on a cantilever formed between two adjacent cracks under the action of horizontal shear stress at the base of the beam (Fig. 3.4.b). If the shear stresses exceeds the tensile strength of concrete at the root of this tooth, FRP debonding occurs (Fig. 3.4.).

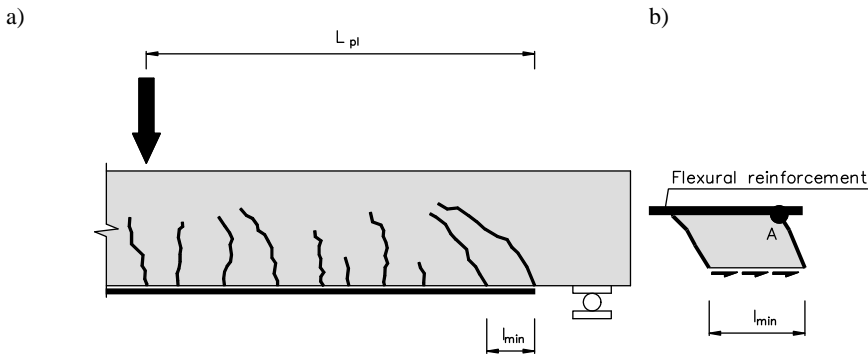


Fig. 3.8. Concrete tooth model: a) cracked beam, b) concrete tooth between two adjacent flexural cracks (Zhang et al., 1995)

#### *Raouf and Zhang's model*

First approach to externally bonded steel plates was proposed by Raouf and Zhang (Raouf and Zhang, 1997; Zhang et al., 1995). Then the model was developed for the concrete cover separation failure in FRP-strengthened beams. The minimum crack spacing is the boundary condition for the FRP debonding determined by the minimum crack spacing defined as:

$$l_{min} = \frac{A_e f_{ct}}{u \sum Q_{bars} + b_{frp}} \quad (3.38)$$

where:  $A_e$  is the area of concrete in tension;  $u$  is the average bond strength of steel to concrete,  $\sum Q_{bars}$  is the total perimeter of the tensile reinforcing bars; it is assumed that  $u = 0.28\sqrt{f_{cu}}$  and  $f_{ct} = 0.36\sqrt{f_{cu}}$ ;  $f_{cu}$  is the compressive cubic concrete strength.

The tooth failure occurs when the stress at point A (Fig. 3.4.) exceeds tensile concrete strength. The tensile stress at point A can be determined on the basis of the formula:

$$\sigma_A = \frac{l}{2} \frac{M_A}{I_A} \quad (3.39)$$

where:  $M_A = \tau l b_{frp} h'$  and  $I_A = b_{frp} l^3 / 12$ ;  $l$  is the crack spacing,  $h'$  is the effective depth of steel tensile reinforcement;  $\tau$  is the shear stress at the interface between the concrete and the soffit plate;  $I_A$  is the second moment of area of the tooth;  $M_A$  is the moment at the base of the tooth;  $\sigma_A = f_{ct}$  is the stress at the interface between the concrete and the steel plate.

The minimum shear stress  $\tau_{min}$  is calculated from the formula:

$$\tau_{min} = \frac{f_{ct} l_{min}}{6h'} \frac{b_c}{b_{frp}} \quad (3.40)$$

The minimum normal stress in the soffit plate  $\sigma_{s,min}$  corresponding to the flexural cracking and failure of a tooth covering the minimum stabilized crack spacing is calculated on the basis of the formula:

$$\sigma_{s(min)} = 0.154 \frac{L_p h_1 b_c^2 \sqrt{f_{cu}}}{h' b_{frp} t_{frp} (\sum Q_{bars} + b_{frp})} \quad (3.41)$$

where:  $L_p$  is an effective length of the FRP plate for end anchorage;  $h_1$  is the effective depth of the cross section;  $f_{cu}$  is the compressive concrete strength. On the basis of the Raof and Zhang model (Raof and Zhang, 1997) the effective length for end anchorage is the minimum FRP length from  $L_{p1}$  and  $L_{p2}$ :

$$L_{p2} = l_{min} (21 - 0.25 L_{min}), \quad l_{min} \leq 72mm \quad (3.42a)$$

$$L_{p2} = 3l_{min}, \quad l_{min} > 72mm \quad (3.42b)$$


---

**Wang and Ling's model (Wang and Ling, 1998)**

A modification to the Zhang et al.'s tooth model originally dedicated to steel plates (Zhang et al., 1995) was proposed by Wang and Ling (1998) for the FRP plate debonding. This approach considers bond strength between the concrete and the FRP laminate, leading to the following formula for the minimum crack spacing:

$$l_{min} = \frac{A_e f_{ct}}{u_s \sum Q_{bars} + u_{frp} b_{frp}} \tag{3.43}$$

where:  $u_s = 0.313\sqrt{f'_c}$  is the average bond strength between the steel tension reinforcement and concrete assumed as  $f_c = 0.8f_{cu}$ ,  $u_{frp}$  is the average FRP to concrete bond shear strength,  $u_{frp} = 1.96MPa$ .

**3.4.3. Interfacial stress based models**

On the basis of the existing knowledge, failure due to concrete cover separation or plate end interfacial debonding occurs at the end of the laminate, where the shear stress  $\tau$ , transverse normal stress  $\sigma_y$  (peeling) and longitudinal stress  $\sigma_x$  exceed the limit values (Fig. 3.5.) (Ziraba et al., 1994; Varastehpour and Hamelin, 1997; Saadatmanesh and Malek, 1998; Tumialan et al., 1999).

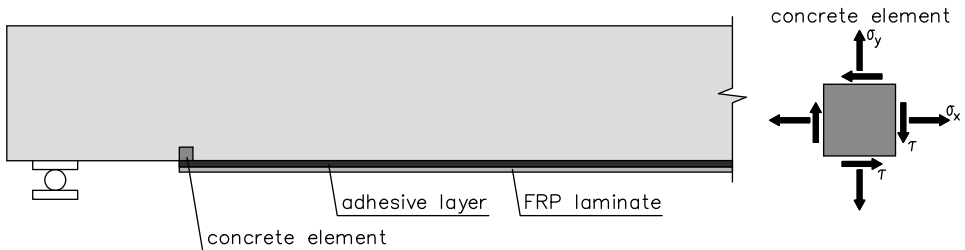


Fig. 3.9. Interfacial stress based model at the end of the FRP laminate (Saadatmanesh and Malek, 1998)

**Ziraba et al.'s models**

Ziraba et al. (1994) proposed two debonding models dedicated to RC beams reinforced with steel plates: the first one (Ziraba et al.'s model I) considers interfacial debonding of the steel plate end, and the second one (Ziraba et al.'s model II) refers to the concrete cover separation.

**Ziraba et al.'s model I – is called plate end interfacial debonding**

Based on the Mohr–Coulomb approach the critical stress state at the plate end interfacial debonding is defined:

$$\tau + \sigma_y \tan(\varphi) \leq C \quad (3.44)$$

where:  $\tau$  and  $\sigma_y$  are the maximum interfacial shear and normal stresses at the plate end;  $C$  is the coefficient of cohesion;  $\varphi$  is an angle of internal friction. All these parameters are given by:

$$\sigma_y = \alpha_2 C_{R2} \tau \quad (3.45)$$

$$C_{R1} = \left[ 1 + \left( \frac{K_s}{E_{frp} b_{frp} t_{frp}} \right)^{1/2} \frac{M_0}{V_0} \right] \frac{b_{frp} t_{frp}}{I_{irc,frp} b_a} (d_{frp} - x_{irc,frp}) \quad (3.46)$$

$$C_{R2} = t_{frp} \left( \frac{K_n}{4E_{frp} I_{frp}} \right)^{1/4} \quad (3.47)$$

where:  $C_{R1}$  and  $C_{R2}$  are obtained from analytical solution by Roberts (1989) for internal shear and normal stresses, while  $\alpha_1$  and  $\alpha_2$  are empirical multipliers calibrated from numerical studies (Ziraba et al., 1994) for RC beams retrofitted with steel plates. The shear stiffness  $K_s$  and the normal stiffness  $K_n$  of the adhesive layer are given by:

$$K_s = \frac{G_a b_a}{t_a} \quad (3.48)$$

$$K_n = \frac{E_a b_a}{t_a} \quad (3.49)$$

where:  $E_a$ ,  $G_a$ ,  $b_a$  and  $t_a$  are the modulus of elasticity, shear modulus, width and thickness of the adhesive layer, respectively;  $I_{irc,frp}$  is the second moment of area of the cracked plated section transformed into FRP;  $x_{irc,frp}$  is the neutral axis depth of this transformed cracked section;

$I_{frp}$  the second moment of area of the FRP plate alone;  $d_{frp}$  the distance from the compressive face of the RC beam to the centroid of the FRP plate;  $M_0$  and  $V_0$  are the bending moment and shear force at the plate end, respectively.

The shear force at the plate end causing the plate end interfacial debonding is calculated from the equation:

$$V_{db,end} = \frac{f'_c}{C_{R1}} \left[ \frac{C}{\alpha_1 f_{ct} (1 + \alpha_2 C_{R2} \tan(\varphi))} \right]^{4/5} \quad (3.50)$$

where:  $h$  is the beam's depth and  $\frac{a}{h} \leq 3$ . Ziraba et al. specifies:  $\alpha_1 = 35$ ,  $\alpha_2 = 1.1$ ,  $\varphi = 28^\circ$  and two values of  $C$  equal to: 2.68 MPa and 5.36 MPa.

#### ***Ziraba et al.'s model II - concrete cover separation***

Ziraba et al. (1994) modified the ACI code (ACI 318-95, 1999) prediction of the shear capacity of an RC beam into the following equation, where  $k$  is the efficiency factor of steel shear reinforcement:

$$V_{db,end} = V_c + kV_s \quad (3.51)$$

where:  $V_c$  and  $V_s$  are the contributions of concrete and steel shear reinforcement to the shear capacity of an RC beam, respectively and are given by:

$$V_c = \frac{1}{6} \left( \sqrt{f'_c} + 100\rho_s \right) b_c d \quad (3.52)$$

$$V_s = \frac{A_{sy} f_{yv} d}{s} \quad (3.53)$$

where:  $\rho_s$  is longitudinal steel reinforcement ratio

$$k = 2.4e^n \quad \text{and} \quad n = -0.08C_{R1}C_{R2} \times 10^6 \quad (3.54)$$

***Saadatmanesh and Malek's model (Saadatmanesh and Malek, 1998)***

This model predicts concrete cover separation in the FRP strengthened RC beams. The shear stress  $\tau$  and the normal stress  $\sigma_y$  at the end of the FRP laminate are derived from Malek et al.'s (1998) approach, while the longitudinal stress  $\sigma_x$  is calculated from the bending analysis on the basis of an uncracked section. This closed-form solution was derived assuming the following quadratic distribution for the bending moment, which can accommodate both point and uniformly-distributed loads:

$$M = a_1(x+a)^2 + a_2(x+a) + a_3 \quad (3.55)$$

where:  $x$  is the distance along the FRP laminate from its end. For a simply supported beam subjected to three or four point bending, the bending moment at the plate end  $M_0$ , for FRP laminate terminated in the shear span, is given by  $M_0 = a_2a + a_3$ . The interfacial shear stress  $\tau$  at the end of the FRP laminate is given as:

$$\tau = t_{frp} (b_3 \sqrt{A} + b_2) \quad (3.56)$$

where:

$$A = \frac{G_a}{t_a t_{frp} E_{frp}} \quad (3.57)$$

$$b_2 = \frac{E_{frp}}{I_{tru,c} E_c} (d_{frp} - x_{tru,c}) (2a_1a + a_2) \quad (3.58)$$

$$b_3 = E_{frp} \left[ \frac{1}{I_{tru,c} E_c} (d_{frp} - x_{tru,c}) (a_1a^2 + a_2a + a_3) + 2 \frac{a_1 E_{frp}}{I_{tru,c} E_c} (d_{frp} - x_{tru,c}) \frac{t_a t_{frp}}{G_a} \right] \quad (3.59)$$

where:  $I_{tru,c}$  is the uncracked second moment of area of the plated section transformed to concrete, and  $x_{tru,c}$  is the neutral axis depth of this transformed section. The normal stress  $\sigma_y$  at the plate end is (Malek et al., 1998)

$$\sigma_y = \frac{K_n}{2b_a\beta^{*3}} \left( \frac{V_{frp}}{E_{frp}I_{frp}} - \frac{V_0^* + \beta^* M_0}{E_c I_c} \right) + \frac{qE_{frp}I_{frp}}{b_{frp}E_c I_c} \quad (3.60)$$

where:

$$V_0^* = V_0 - 0.5hb_{frp}t_{frp} \left( b_3\sqrt{A} + b_2 \right) \quad (3.61)$$

$$V_{frp} = -0.5b_{frp}t_{frp}^2 \left( b_3\sqrt{A} + b_2 \right) \quad (3.62)$$

and

$$\beta^* = \left( \frac{K_n b_{frp}}{4b_a E_{frp} I_{frp}} \right)^{1/4} \quad (3.63)$$

where:  $I_c$  is the second moment of area of the beam and  $q$  is a uniformly distributed load if such a load exists.

The longitudinal stress  $\sigma_x$  at the base of the RC beam, at the end of the soffit laminate, due to a bending moment  $M_0$  can be determined from a bending analysis of an uncracked section. The bending moment in the concrete beam at the end of the FRP laminate is increased by the bending moment  $M_m$ :

$$M_m = 0.5hab_{frp}\tau \quad (3.64)$$

The maximum principal stress can be calculated from:

$$\sigma_1 = \frac{\sigma_x + \sigma_y}{2} + \sqrt{\left( \frac{\sigma_x - \sigma_y}{2} \right)^2 + \tau^2} \quad (3.65)$$

At the plate end, the concrete is generally subjected to biaxial tension. Concrete cover separation occurs, when the maximum principal stress reaches the concrete splitting tensile strength:

$$\sigma_1 = f_{ct} = 0.295(f'_c)^{2/3} \quad (3.66)$$

$$\tau = \bar{C}_{R1} = \frac{E_{frp}}{E_c} V_0 \quad (3.67)$$

$$\sigma_y = C_{R2} \tau \quad (3.68)$$

where:  $\bar{C}_{R1}$  is given by

$$\bar{C}_{R1} = \left[ 1 + \left( \frac{K_s}{E_{frp} b_{frp} t_{frp}} \right)^{1/2} \frac{M_0}{V_0} \frac{b_{frp} t_{frp}}{I_{tru,c} b_a} (d_{frp} - x_{tru,c}) \right] \quad (3.69)$$



## 4. Bond strength models

The existing shear anchorage strength models published in literature contains variable approaches. On the basis of experimental results and general division of the existing approaches proposed by Faella et. al. (2004). They consisted of:

- models determining the maximum axial strain of FRP materials  $\varepsilon_{fd}$  corresponding to intermediate crack debonding,
- models determining the maximum gradient of axial FRP stresses  $\sigma_f$  between two adjacent flexural cracks,
- models defining a maximum shear stress  $\tau_{max}$ , corresponding to the intermediate debonding. (Bilotta et al., 2013; Pellegrino et al., 2008).

The intermediate crack debonding model has been studied by limited number of research. Simple shear tests describe the most common debonding behaviour corresponding to debonding due to flexural cracks. Hence, the simple strength models for FRP plate-concrete joints can be used to predict the intermediate flexural crack debonding failure. Many available studies about the intermediate crack debonding are based on the bond-slip model derived from direct shear bond tests (Fig. 4.1). In this approach there is a stress concentration near the crack. The interfacial slips occur on both sides of the flexural crack and the total amount of interfacial slip is equal to the width of the flexural crack.

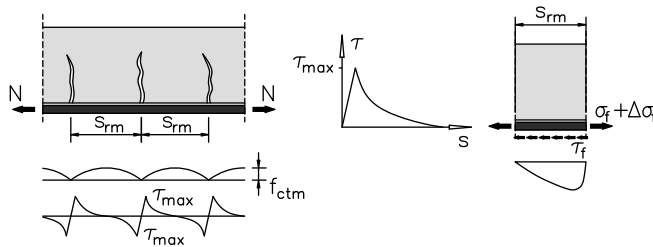


Fig. 4.1. The bond-slip model for the flexural intermediate crack debonding

A review of existing models with a division into models that consider or not consider the effective bond length in calculation of the anchored load is provided in the following subchapters.

### 4.1. Empirical models

On the basis of various experimental shear tests described in Chapter 3.1, a considerable amount of models were published by: Bizindavyi and Neale (1999); Brosens and Van Gemert (1997); De Lorenzis et al. (2001); Maeda et al. (1997); Miller et al. (1999); Nakaba et al. (2001); Neubauer and Rostasy (1999); Pellegrino et al. (2008); Täljsten (1997); Yao et al. (2005); Chen and Teng (2001); Maeda et al. (1997); Nakaba et al. (2001); Neubauer and Rostasy (1999);

Khalifa et al. (1998); Horiguchi and Saeki (1997); Chen and Teng (2003); Chen and Teng (2001); Yao et al. (2005); Ceroni and Pecce (2002); Blontrock et al. (2002); Brosen and van Gemert (1997); Guadagnini et al. (2012); McSweeney and Lopez (2005); Ceroni et al. (2008), Mazzotti et al. (2005); Matana et al. (2005); Ceroni et al. (2014); Guo et al. (2005); Dai et al. (2003).

Table 4.1. Empirical bond models

Authors	Ultimate load $N_f$
van Gemert (1980)	$N_f = 0.5b_f L_b f_{ctm}$
Tanaka (1996)	$N_f = b_f L_b (6.13 - \ln(L_b))$
Hiroiyuki and Wu (1997)	$N_f = b_f L_b 5.88 L_b^{-0.669}$
Maeda et al. (1997)	$N_f = b_f L_e 110.2 E_f t_f \times 10^{-6}$ $L_e = e^{6.13 - 0.580 \ln(E_f t_f)}$ (mm), $E_f t_f$ [GPa-mm]
Brosens and van Gemert (1997)	$N_f = 0.5b_f L_e f_{ctm}$
Adhikary and Mutsuyoshi (2001)	$N_f = b_f L_e 0.25 f_{ck}^{2/3}$
Khalifa at al. (1998)	$N_f = b_f L_e \left[ \frac{110.2}{10^6} \left( \frac{f'_c}{42} \right)^{2/3} \right] E_f t_f$
Izumo's (JCI, 2003)	$N_f = (3.8 f_c'^{2/3} + 15.2) b_f L_b E_f t_f \times 10^{-3}$ for CFRP $N_f = (3.4 f_c'^{2/3} + 69) b_f L_b E_f t_f \times 10^{-3}$ for AFRP
Chen and Teng (2001)	$N_{f,max} = \alpha \beta_p \beta_L b_f L_e \sqrt{f'_c}$ , $L_e = \sqrt{\frac{E_f t_f}{\sqrt{f'_c}}}$ $\beta_p = \sqrt{\frac{2 - b_f/b_c}{1 + b_f/b_c}}$ $\beta_L = \sin\left(\frac{\pi L_b}{2L_e}\right)$ if $L_b \leq L_e$ , $\beta_L = 1$
$N_f$ – ultimate load [N]; $b_c$ – width of the beam [mm]; $b_f$ – composite width [mm]; $L_e$ – effective bond length [mm]; $t_f$ – thickness of FRP material [mm]; $E_f$ – elasticity modulus of the FRP material [MPa]; $f_{ctm}$ – surface tensile strength of concrete [MPa]; $f'_c$ – compressive strength of concrete [MPa]	

The existing knowledge of the FRP-to-concrete bond behaviour confirms the main difference between the anchorage design of the externally bonded FRP materials in comparison with internal steel reinforcement which fulfils a sufficiently long anchorage length in a concrete member. This fundamental principle in the EB FRP-to-concrete and internal steel-to concrete bond behaviour leads the difference in exhaustion of the tensile strength of both materials.

The aim of the flexural strengthening is to use the thin CFRP laminates with the highest level of exhaustion of the tensile strength. However, the most common failure mode is debonding of the externally bonded FRP materials from concrete due to shear failure. This failure mode occurs in the thin concrete cover few millimeters above the bottom of the adhesive layer. This failure mode significantly depends on:

- the concrete strength,
- the bond width of the FRP material to comparison with to the concrete width ( $b_f/b_c$ ),
- an effective bond length.

Another investigated parameter governing the bond strength is the bond length. On the basis of the bond test data published in Chen and Teng (2001), the effective bond length is the length beyond which any increase in the bond length does not cause any increase in the bond strength. The effective bond length issue is presented in Chapter 3.3.

### 4.2. Shear bond slip models

There are two ways to determine the local bond–slip characteristics on the basis of the pull tests (Lu et al., 2005a):

- on the basis of the axial strain measurements from the strain gauges bonded on the externally bonded FRP laminate/sheet
- on the basis of the load–slip curves at the loaded end.

The first simple method is not precise and it gives not accurate local bond–slip characteristics., because the strain measurement is local and does not reflect the real FRP strain. The shear stress calculated from the strain is thus not reliable, even though the slip is less sensitive to variations of crack pattern.

The second method is an indirect method and on the basis of the local bond–slip curve from the load–slip curve. It was indicated that even different local bond–slip curves may lead to similar load–displacement curves (Lu et al., 2005a).

To describe the FRP-to-concrete bond phenomenon (Fig. 4.2) the fracture plane (marked with a dotted line) shows debonding plane that is wider than the

width of the FRP laminate and extend more on the free zone at the concrete prism edge, where the FRP laminate is not bonded.

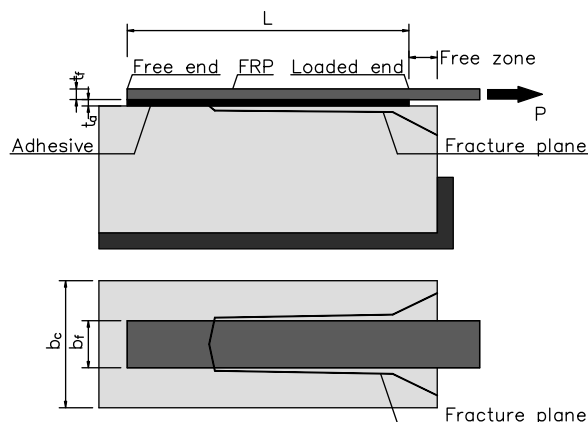


Fig. 4.2. The scheme of the FRP to concrete pull-out test (Lu et al., 2005a)

There are several parameters effecting the local FRP-to-concrete bond-slip behaviour:

- the concrete strength,  $f_c$
- the bond length,  $L$
- the FRP laminate axial stiffness,  $E_f t_f$
- the FRP-to-concrete width ratio,
- the adhesive stiffness,
- the adhesive strength.

It should be pointed out that the main difference between the internal reinforcement and externally bonded reinforcement is the effective bond length  $L_e$  beyond, which an extension of the bond length  $L$  cannot increase the ultimate load. This justifies the opinion that the full tensile strength of the EB FRP reinforcement cannot be achieved (without any anchorage system).

#### 4.2.1. Fracture mechanics models

Fracture energy  $G_f$  is the parameter directly characterising the FRP-to-concrete bond behaviour, which is used for determining the ultimate bond load  $F_{max}$  taken from the pull-out test. However, the only fracture energy parameter  $G_f$  is not sufficient to obtain the full range behaviour of the FRP-to-concrete interface in the intermediate debonding in the FRP strengthened RC members. This phenomenon was described in the publication by Faella et al. (2008a). The

## Bond strength models

---

accurate local bond–slip model is the most important one in modeling EB FRP RC members.

The interfacial fracture energy  $G_f$  is the energy required to create and fully break the elementary unit area of the cohesive crack (Mazzotti et al., 2016). The physical meaning of the fracture energy  $G_f$  is determined by the area under the shear stress-slip ( $\tau_{zy} - s$ ) curve of Bazant and Planas (1997):

$$G_f = \int_0^{s_f} \tau_{zy}(s) ds \quad (4.1)$$

where:  $s_f$  is the slip corresponding to complete separation of the interface. The mean values of  $G_f$  Rabinovitch (2004) developed fracture energy of the concrete model to study the end plate debonding on the basis of the fracture mechanics concept of energy release rate.

On the basis of the direct shear tests Täljsten (1996) proposed the relationship between the fracture energy and the load-carrying capacity determined by the formula:

$$N_f = b_f \sqrt{2G_f E_f t_f} \quad (4.2)$$

One of the first bond strength models between steel and concrete on the basis of nonlinear fracture mechanics (NLFM) was investigated by Holzenkämpfer (1994). It was modified by Niedermeier (1996) as follows

$$N_f = \begin{cases} 0.78b_f \sqrt{2G_f E_f t_f} & \text{if } L \geq L_e \\ 0.78b_f \sqrt{2G_f E_f t_f} \frac{L}{L_e} \left(2 - \frac{L}{L_e}\right) & \text{if } L < L_e \end{cases} \quad (4.3)$$

where:  $N_f$  is the bond strength [N],  $E_f t_f$  [MPa-mm],  $L_e$  is the effective bond length [mm] and  $G_f$  is the fracture energy given by

$$L_e = \sqrt{\frac{E_f t_f}{4f_{ctm}}} \quad (4.4)$$

$$G_f = c_f k_f^2 f_{ctm} \quad (4.5)$$

where:  $f_{ctm}$  is the average surface tensile strength of the concrete determined in the pull-off test [MPa],  $c_f$  is a constant determined in linear regression analysis using the results of double shear or similar tests,  $k_f$  is a geometrical factor related to the width of the bonded plate  $b_f$  [mm] and the width of the concrete member  $b_c$  [mm]

$$k_f = \sqrt{1.125 \frac{2-b_f/b_c}{1+b_f/400}} \quad (4.6)$$

Neubauer and Rostasy (1997) modified Holzenkämpfer's bond strength model for the FRP strengthened concrete

$$N_f = \begin{cases} 0.64k_f b_f \sqrt{E_f t_f f_{ctm}} & \text{if } L \geq L_e \\ 0.64k_f b_f \sqrt{E_f t_f f_{ctm}} \frac{L}{L_e} \left(2 - \frac{L}{L_e}\right) & \text{if } L < L_e \end{cases} \quad (4.7)$$

where:

$$L_e = \sqrt{\frac{E_f t_f}{2f_{ctm}}} \quad (4.8)$$

The nonlinear fracture mechanics analysis by Täljsten (1996) used to developed the bond strength formula

$$N_f = \sqrt{\frac{2E_f t_f G_f}{1 + \alpha_T}} b_f, \quad \alpha_T = \frac{E_f t_f}{E_c t_c} \quad (4.9)$$

where:  $E_c$  and  $t_c$  are the elastic modulus and thickness of the concrete member.

Yuan and Wu (1999) developed the bond strength between FRP and concrete on the basis of linear elastic fracture mechanics (LEFM) and NLFM given by

$$N_f = \sqrt{\frac{2E_f t_f G_f}{1 + \alpha_Y}} b_f, \quad \alpha_Y = \frac{b_f E_f t_f}{b_c E_c t_c} \quad (4.10)$$

## Bond strength models

---

On the basis of the results of different shear tests Yuan and Wu (1999) performed the most real linearly ascending and then descending response shown in Fig. 4.4 (with  $s_0 = s_e$  and  $s_f = s_u$ ). For this shear-slip model the bond strength was given by Yuan et al. (2004)

$$N_f = \beta_l b_f \sqrt{2E_f t_f G_f} \quad (4.11)$$

where:

$$\beta_l = \begin{cases} 1 & \text{if } L > L_e \\ \frac{L}{L_e} \left( 2 - \frac{L}{L_e} \right) & \text{if } L < L_e \end{cases}, \quad G_f = 0.308 \beta_w^2 \sqrt{f_{ct}} \quad (4.12)$$

$$\beta_w = \sqrt{\frac{2.25 - b_f / b_c}{1.25 + b_f / 400}} \quad (4.13)$$

$$L_e = a + \frac{1}{\lambda_2} \ln \frac{\lambda_1 + \lambda_2 \tan(\lambda_2 a)}{\lambda_1 - \lambda_2 \tan(\lambda_2 a)} \quad (4.14)$$

$$\lambda_1 = \sqrt{\frac{\tau_{max}}{s_0 E_f t_f}}, \quad \lambda_2 = \sqrt{\frac{\tau_{max}}{(s_f - s_0) E_f t_f}} \quad (4.15)$$

$$a = \frac{1}{\lambda_2} \sin^{-1} \left[ 0.99 \sqrt{\frac{s_f - s_0}{s_f}} \right]; \quad \tau_{max} = 1.5 \beta_w f_{ct}; \quad s_0 = 0.0195 \beta_w f_{ct}, \quad s_f = \frac{2G_f}{\tau_{max}} \quad (4.16)$$

where  $f_{ct}$  is the concrete splitting tensile strength.

Yang et al.'s model (2001) considers the tensile strength of concrete and the constant value of the effective length  $L_e = 100 \text{ mm}$ .

$$N_f = \left( 0.5 + 0.08 \sqrt{\frac{E_f t_f}{100 f_{ct}}} \right) L_e b_f (0.5 f_{ct}) \quad (4.17)$$

where:

$$\beta_l = \begin{cases} 1 & \text{if } L > L_e \\ \frac{L}{L_e} \left( 2 - \frac{L}{L_e} \right) & \text{if } L < L_e \end{cases}, \quad G_f = 0.308 \beta_w^2 \sqrt{f_{ct}} \quad (4.18)$$

Teng et al. (2002, 2003) based their model on the NLFM analysis developed by Yuan and Wu (1999). Chen and Teng's model predicts the bond strength and the effective bond length given by

$$N_f = 0.427 \beta_f \beta_L \sqrt{f'_c} b_f L_e, \quad [N] \quad (4.19)$$

$$\beta_f = \sqrt{\frac{2 - b_f/b_c}{1 + b_f/b_c}}; \quad \beta_L = \begin{cases} 1 & \text{for } L \geq L_e \\ \sin \frac{\pi L}{2L_e} & \text{for } L < L_e \end{cases}; \quad L_e = \sqrt{\frac{E_f t_f}{\sqrt{f'_c}}} \quad (4.20)$$

Chen and Teng (2003) modified their expression above to the ultimate strength design to the form given by

$$N_f = 0.315 \beta_f \beta_L \sqrt{f'_c} b_f L_e, \quad [N] \quad (4.21)$$

Teng et al. (2004) presented a smeared crack approach for a finite element simulation of intermediate crack-induced debonding. A design model, on the basis of interfacial stress distributions defines the limiting FRP strain,  $\varepsilon_{fub}$  given by

$$\varepsilon_{fub} = 0.171 k_f (4.32 - \alpha) \frac{f_{ct}}{\sqrt{E_f t_f}} \quad (4.22)$$

where  $\beta_p$ ,  $\alpha$  and  $G_f$  are given as follows

$$\beta_p = \sqrt{\frac{2.25 - b_f/b_c}{1.25 + b_f/b_c}}; \quad \alpha = \frac{1}{\frac{G_f}{\tau_{max} s_o} - \frac{2}{3}}; \quad G_f = 0.308 \beta_w^2 \sqrt{f_{ct}} \quad (4.23)$$

The comparison of four chosen bond-slip models for normal-adhesive interfaces is shown in Fig. 4.3 and in Table 4.2 (Lu et al., 2005a). The following

## Bond strength models

parameters were used for the comparison:  $f'_c = 32\text{MPa}$ ,  $f_t = 3.0\text{MPa}$ ,  $b_f = 50\text{mm}$ ,  $b_c = 100\text{mm}$ ,  $E_f t_f = 16.2\text{GPa} \cdot \text{mm}$ ,  $b_f / b_c = 0.5$

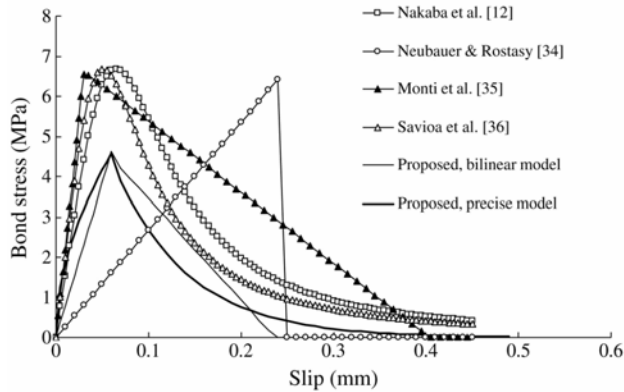


Fig. 4.3. Comparison of curves on the basis of existing bond-slip models by Lu et al. (2005a)

The linear-brittle model of Neubauer and Rostasy (1999) stands out of other three models. Several published bond tests indicated that the bond-slip curve have an ascending branch and a descending branch, similar to the curve from Nakaba et al.'s (2001) model or Savioa et al.'s (2003) model. From comparison shown in Fig. 4.3 seems that the linear-brittle model by Neubauer and Rostasy (1999) is rather unrealistic. However, other models confirm reasonably close agreement both in ascending branch and a descending branch.

The summary of existing bond-slip models is shown in Table 4.2 with determination of the local bond shear stress,  $\tau$ ; the local slip  $s$ , the local bond strength,  $\tau_{max}$ ; the slip for the maximum bond stress  $\tau_{max}$ ;  $s_0$  the slip for the bond stress reduced to zero,  $s_f$ ; the width ratio factor,  $\beta_w$  and the compressive concrete strength,  $f'_c$ .

### 4.2.2. Meso-scale finite element model

Lu et al. (2005a) proposed three bond-slip models of different sophistication levels on the basis of meso-scale finite element model. These bond-slip models on the basis of a combination of finite element results and the test results predict both the bond strength and strain distribution in the FRP plate.

These models can be recommended for the numerical modelling of FRP strengthened RC structures. However, these modes are limited to the joints with the adhesive layer shear stiffness no less than 2.5 GPa/mm.

Table 4.2 Existing bond-slip models (Lu et al., 2005a)

Bond-slip model	Ascending branch $s \leq s_0$	Descending branch $s > s_0$	$\tau_{max}$	$s_0$	$s_f$	$\beta_w$
Neubauer and Rostasy (1999)	$\tau_{max}(s/s_0)$	0	$1.8\beta_w f_t$	$0.202\beta_w$		$\sqrt{\frac{1.125}{1+b_f/b_c} \frac{2-b_f/b_c}{1+b_f/400}}$
Nakeba et al. (2001)	$\tau_{max}(s/s_0) \left[ \frac{\beta}{2 + (s/s_0)^3} \right]$		$3.5(f_c')^{0.19}$	0.065		
Monti et al. (2003)	$\tau_{max}(s/s_0)$	$\tau_{max} \left[ (s_f - s) / (s_f - s_0) \right]$	$1.8\beta_w f_t$	$2.5\tau_{max}(t_a/E_a + 50/E_t)$	$0.33\beta_w$	$\sqrt{\frac{1.5}{1+b_f/100} \frac{2-b_f/b_c}{1+b_f/100}}$
Savio et al. (2003)	$\tau_{max}(s/s_0) \left[ 2.86 / (1.86 + (s/s_0)^{2.86}) \right]$		$3.5(f_c')^{0.19}$	0.051	$\alpha = 0.028(E_f t_f / 1000)^{0.254}$	
Dai and Ueda (2003)	$\tau_{max}(s/s_0)^{0.575}$	$\tau_{max} e^{-\beta(s-s_0)}$	$\frac{-1.575\alpha K_a + \sqrt{2.48\alpha^2 K_a^2 + 6.3\alpha\beta^2 K_a G_f}}{2\beta}$		$\beta = 0.0035 K_a (E_f t_f / 1000)^{0.34}$ $K_a = G_a / t_a$ $G_f = 7.554 K_a^{-0.449} (f_c')^{0.343}$	
Lu et al. (2005)	$\tau_{max} \sqrt{s/s_0}$	$\tau_{max} e^{-\alpha[(s-s_0)-1]}$	$1.5\beta_w f_{cm}$	$0.0195 K_{w,cm}$	$\frac{2G_f/\tau_{max}}{G_f = 0.308\beta_w^2 \sqrt{f_f}}$ $\alpha = \frac{G_f/\tau_{max} s_0 - 2/3}{1}$	$\sqrt{\frac{2.25 - b_f/b_c}{1.25 + b_f/b_c}}$
De Lorenzis et al. (2001)	$\tau_{max} 3.1 (t_f t_f E_f)^{0.32}$		$3.1 (t_f t_f E_f)^{0.32}$	$0.075 (t_f t_f E_f)^{0.2}$	$10.5 (t_f t_f E_f)^{0.6}$	

## Bond strength models

---

The simplified bilinear bond–slip model on the basis of the simple explicit design equation for the bond strength. This bilinear model has the same local bond strength and total interfacial fracture energy, so the bond strength is unaffected by this simplification if the bond length is longer than the effective bond length. This bilinear model is described by the following bond equations (Lu et al., 2005a):

$$\begin{aligned}\tau &= \tau_{max} \frac{s}{s_0} \quad \text{if } s \leq s_0 \\ \tau &= \tau_{max} \frac{s_f - s}{s_f - s_0} \quad \text{if } s_0 < s \leq s_f \\ \tau &= 0 \quad \text{if } s > s_f\end{aligned}\tag{4.24}$$

where:

$$s_f = 2G_f / \tau_{max}\tag{4.25}$$

Regardless of the bond–slip model, the bond strength of the FRP-to-concrete bonded joint in terms of the interfacial fracture energy is given by equation:

$$P_u = \beta_l b_f \sqrt{2E_f t_f G_f}\tag{4.26}$$

where  $\beta_l$  is the bond length factor. When  $L > L_e$ ,  $\beta_l = 1$ , but when  $L < L_e$   $\beta_l < 1$ . The analytical solution for  $L_e$  with a bilinear bond–slip model is given by Yuan et al. (2004):

$$L_e = a + \frac{1}{2\lambda_1} \ln \left( \frac{\lambda_1 + \lambda_2 \tan(\lambda_2 a)}{\lambda_1 - \lambda_2 \tan(\lambda_2 a)} \right)\tag{4.27}$$

where

$$\lambda_1 = \sqrt{\frac{\tau_{max}}{s_0 E_f t_f}}\tag{4.28}$$

$$\lambda_2 = \sqrt{\frac{\tau_{max}}{(s_f - s_0) E_f t_f}}\tag{4.29}$$

$$a = \frac{1}{\lambda_2} \arcsin \left( 0.99 \sqrt{\frac{s_f - s_0}{s_f}} \right) \quad (4.30)$$

According to Chen and Teng (2001), the effective bond length factor  $\beta_l$  is defined as:

$$\beta_l = \sin \left( \frac{\pi L}{2L_e} \right) \quad \text{if } L \leq L_e \quad (4.31)$$

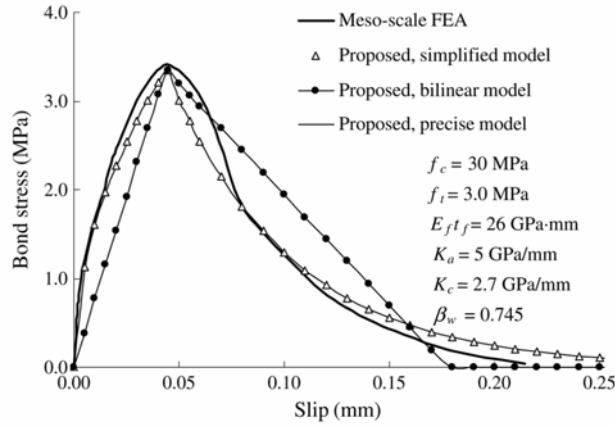


Fig. 4.4. Bond-slip curves from meso-scale finite element simulation and proposed bond-slip models (Lu et al., 2005a)

Among the three models proposed by Lu et al. (2005a) (Fig. 4.4), two of them are precised and the third simplified one is a bilinear, identified by the following relationships for determining the three parameters:  $\tau_{max}$ ,  $s_e$  and  $s_u$  (Fig. 4.5, Bilotta et al., 2012):

$$\begin{aligned} \tau_{max} &= 1.5\beta_w f_t \\ s_e &= 0.015\beta_w f_t \\ s_u &= \frac{2G_f}{\tau_{max}} = \frac{2 \times 0.308\beta_w^2 \sqrt{f_t}}{1.5\beta_w f_t} = \frac{0.41\beta_w}{\sqrt{f_t}} \end{aligned} \quad (4.32)$$

A simplified curve was achieved by using the experimental results of bond tests performed on wet-lay-up sheets with thickness between 0.133 and 0.5 mm

for one or three layers. The model by Lu et al. (2005a) proposed the approach for assessing the interface relationship and, consequently, the fracture energy value, considering only the strength of the concrete, but neglecting the influence of the axial stiffness of the FRP reinforcement, in particular the FRP thickness. However, it is known that the reinforcement thickness is one of the main parameter affecting debonding behaviour. With the increase of the FRP thickness, the normal and shear stresses in FRP-to-concrete interface increases leading to the probability of premature FRP debonding.

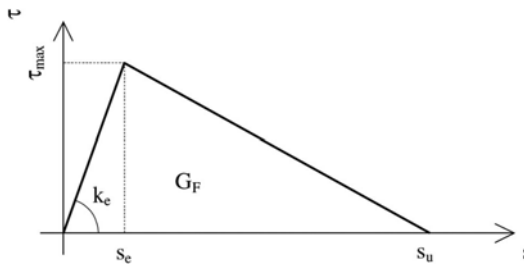


Fig. 4.5. Bilinear (elastic-softening) law at the FRP-to-concrete interface (Bilotta et al., 2012)

This problem was developed by Bilotta et al. (2011b) using the statistical analysis of the variable experimental bond tests, containing both wet lay-up sheets and laminates. They indicated limited application of the Lu et al.'s (2005a) model (limited only to the FRP sheets). Regardless of  $\beta_w$  value, the same values of maximum shear stress were calculated for the FRP laminates and sheets bonded to concrete.

The indirect identification method (IndIM) procedure of the bilinear curve published by Bilotta et al. (2012) indicated reliability of this method regardless of a type of FRP reinforcement (sheet or laminate).

### 4.3. Parameters effecting the FRP to concrete bond behaviour

The most important factor effecting the proper bond between FRP and concrete is the concrete strength, its surface roughness, FRP and concrete cleanliness.

There are several surface preparation methods, which affects the bond properties: brushing, bush-hammering, sandblasting, grinding and steel shotblasting. One of the most common techniques in the experimental tests is sandblasting, while other techniques have been described to a very small extent (Mazzotti et al., 2007).

A wide analysis of over 200 pull-off tests carried out on different types of the concrete surface roughness was published by Iovinella et al. (2013). The

roughness index  $I_R$  determined by (4.28), was used to provide precise information concerning the magnitude of the roughness and the type of discontinuity.

$$I_R = Ri_A \quad (4.33)$$

where:  $R$  is the average of all individually measured peak to valley heights (Fig. 4.6);  $i_A$  is the micro-average inclination angle which is the average of the pixel to pixel angles of the stripe profile.

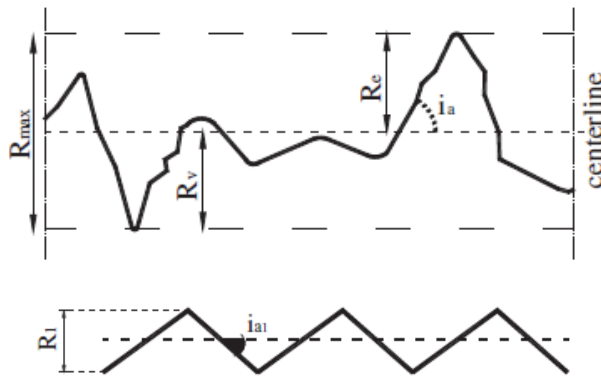


Fig. 4.6. Roughness parameters (Iovinella et al., 2013)

On the basis of two values of concrete strength and variable surface preparation (grinding, brushing, bush-hammering and sandblasting) dependency of the roughness index  $I_R$  on the bond strength was determined. The bush-hammering and sandblasting were the most effective techniques, increasing the bond strength by more than 30 and 50% of the reference strength, respectively. Irrespectively of the type of surface preparation the correlation between the bond strength and the roughness index  $I_R$  for both types of concrete was observed. This relationship was proposed in the following expression:

$$aI_R + b \quad (4.34)$$

where:  $a$  is the effectiveness of the roughness increasing for a specific concrete and  $b$  is the limit strength if the theoretical roughness value is zero (referring to the case of no roughness surface). Two curves were proposed for two values of concrete strength: 15 MPa and 20 MPa (Fig. 4.7).

## Bond strength models

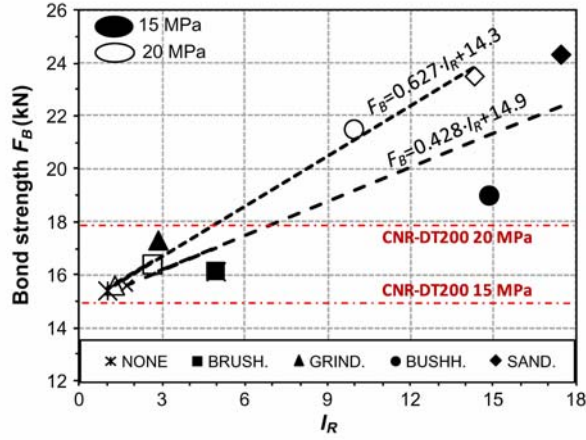


Fig. 4.7. Roughness index-bond strength relationship (Iovinella et al., 2013)

The calculated curves of the bond strength dash-dot lines according to the Italian Guidelines DT-200 concerning these two values of concrete strength (15 and 20 MPa) on the basis of the following expressions:

$$F_B = b_f \sqrt{2E_f t_f G_f} \quad (4.35)$$

where:  $G_f$  is the interface fracture energy defined as:

$$G_f = k_G k_f \sqrt{f_{cm} f_{ctm}} \quad (4.36)$$

and  $k_G$  is the fracture energy coefficient  $k_G = 0.77$ ,  $k_f$  is the width coefficient defined as:

$$k_f = \sqrt{\frac{2 - b_f/b_c}{1 + b_f/b_c}} \geq 1 \quad (4.37)$$

$f_{cm}$  and  $f_{ctm}$  are the mean values of compressive and tensile concrete strength.

On the basis of the collected test data the new formula of the bond strength by introduction of new roughness coefficient  $k_r$  for CNR DT200 guideline was proposed by Iovinella et al. (2013):

$$k_r = \frac{0.059 + 0.0062I_R}{0.077} = 0.766 + 0.08I_R \quad (4.38)$$

which gives the final form shown in Fig. 4.8:

$$G_f = k_G k_f k_r \sqrt{f_{cm} f_{ctm}} \quad (4.39)$$

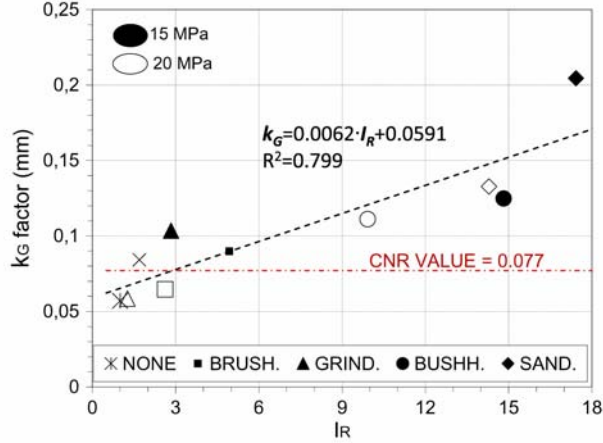


Fig. 4.8. Relationship  $k_G$  factor vs  $I_R$  parameter (Iovinella et al., 2013)

In order to compare interface laws obtained from specimens subject to surface treatments, the following new non-linear interface law was proposed by Lu et al. (2005a) and Ferracuti et al. (2007):

$$\tau = \bar{\tau} \frac{s_p}{\bar{s}} \frac{n}{n-1 + \left(\frac{s_p}{\bar{s}}\right)^n} \quad (4.40)$$

where:  $\bar{\tau}$  is the maximum shear stress,  $\bar{s}$  is the slip at the peak,  $n$  coefficient governing the softening branch, calibrated for each surface condition by a mean square fitting procedure according to Table 4.3.

Very good compatibility of the proposed model with the test results is shown in Figure 4.9.

## Bond strength models

---

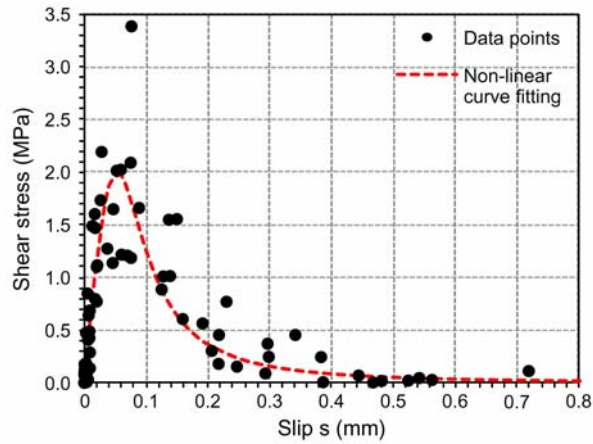


Fig. 4.9. The comparison of the predicted shear stress-slip model with the test results (Iovinella et al., 2013)

Table 4.3. Parameters used in the proposed shear stress–slip calibrated curves

Surface preparation	$n$	$s_{max}$ , (mm)	$\tau_{max}$ , MPa
None	4.20	0.070	2.35
Gringing	3.50	0.090	2.17
Brushing	3.11	0.053	2.00
Bush Hamm.	3.22	0.100	1.94
Sandblasting	3.20	0.120	3.20

One of the main conclusions from Iovinella et al. (2013) research is that **the effect of concrete surface roughness should be included in the design formulas** (codes, guidelines) by introduction of the roughness coefficient  $k_r$ .



## 5. Design guidelines and code formulations

### 5.1. ACI 440.2R-08

In order to avoid the intermediate crack debonding failure of the RC members strengthened with EBR FRP, the ACI 440.2R-08 (2008) propose to limit strain in FRP to

$$\varepsilon_{fd} = 0.41 \sqrt{\frac{f'_c}{nE_f t_f}} \leq 0.9\varepsilon_{fu}, \quad f_{fe} = E_f \varepsilon_{fe} \quad (5.1)$$

where:  $\varepsilon_{fu}$  is the FRP design rupture strain.

The ACI 440.2R recommendations indicate that if the stiffness of the laminate increases, the strain limitation becomes more severe. It is important to recognize that ACI does not include the effect of existing internal longitudinal or transverse steel, concrete strength, the properties of the adhesive layer bonding the FRP to the concrete or the width of the FRP laminate relative to the concrete width.

In case of shear or pure axial strengthening, the maximum bond strength is calculated according to the following formula:

$$\varepsilon_{fe} = k_v \varepsilon_{fu} \leq 0.004, \quad k_v = \frac{k_1 k_2 l_e}{11900 \varepsilon_{fu}} \leq 0.75 \quad (5.2)$$

where:  $k_v$  is an empirical coefficient limiting the ultimate strain in the FRP reinforcement.

### 5.2. *fib* Bulletin 14

The *fib* Bulletin 14 (2001) takes a design approach, recommending a direct use of a shear stress-slip relationship to predict the debonding failure. In the *fib* model the critical bond stress and slip parameters are determined from experimental analysis of the FRP system and substrate condition. The Bulletin 14 presents three approaches to assessing the potential for debonding modes.

### **Approach 1 – FRP Tensile Force**

The maximum axial force in the FRP that may be anchored  $N_{f\ max}$  and the corresponding required anchorage length  $L_{b\ max}$ , are given by

$$N_{f\ max} = \alpha c_1 k_c k_b b_f \sqrt{E_f t_f f_{ctm}} \quad (5.3)$$

$$L_{b\ max} = \sqrt{\frac{E_f t_f}{c_2 f_{ctm}}}, \quad [mm] \quad (5.4)$$

where:  $\alpha$  is a reduction factor to account for influence of inclined cracks on bond strength, typically  $\alpha = 0.9$ , whereas  $\alpha = 1.0$  should be taken for beams having sufficient internal or external shear reinforcement and for slabs,  $k_c$  is a factor accounting for concrete compaction,  $k_c = 1.0$  for FRP bonded to concrete faces cast against formwork,  $k_c = 0.67$  for FRP bonded to concrete faces not cast against formwork,  $b$  is the width of a beam soffit,  $f_{ctm}$  is the tensile strength of concrete,  $c_1$  and  $c_2$  are empirical factors determined for CFRP to be 0.64 and 2.0, respectively.

$$k_b = 1.06 \sqrt{\left(2 - \frac{b_f}{b}\right) / \left(1 + \frac{b_f}{400}\right)} \geq 1.0, \quad b, b_f \text{ in } [mm] \quad (5.5)$$

where:  $b_f$  is the FRP width. The maximum axial force in FRP and the debonding FRP strain  $\varepsilon_{fdb}$  are given by

$$N_f = E_f \varepsilon_f t_f b_f \quad (5.6)$$

$$\varepsilon_{fdb} = \alpha c_1 k_c k_b \sqrt{\frac{f_{ctm}}{E_f t_f}} \quad (5.7)$$

### **Approach 2 – FRP bond stress**

The second *fib* approach involves determining the critical increase in tensile stress in the bonded FRP, transferred by bond stress, between adjacent concrete flexural cracks. This model requires determination of a critical crack pattern and the corresponding bond stresses transferred to the FRP. This aspect of analysis is

beyond the scope of the present discussion. However, the maximum stress  $\sigma_{f\ max}$  and strain  $\varepsilon_{fdb}$  that may be transferred are given by

$$\sigma_{f\ max} = c_1 \sqrt{\frac{E_f \sqrt{f_{ctm} f'_c}}{t_f}}, \quad \varepsilon_{fdb} = c_1 \sqrt{\frac{\sqrt{f_{ctm} f'_c}}{E_f t_f}} \quad (5.8)$$

$$L_{b\ max} = c_2 \sqrt{\frac{E_f t_f}{\sqrt{f_{ctm} f'_c}}} \quad (5.9)$$

where:  $f'_c$  is the compressive strength of concrete,  $c_1 = 0.23$  and  $c_2 = 1.44$  for CFRP.

In both 1 and 2 *fib* approaches, the FRP capacity is reduced if the available bonded development length,  $L_b < L_{b\ max}$ . In cases where  $L_b$  is less than  $L_{b\ max}$  (Fig. 5.1), the FRP capacity  $\sigma_{f\ max}$  and the FRP strain limit  $\varepsilon_{fdb}$  are reduced by the following factor

$$\frac{L_b}{L_{b\ max}} \left( 2 - \frac{L_b}{L_{b\ max}} \right) \quad (5.10)$$

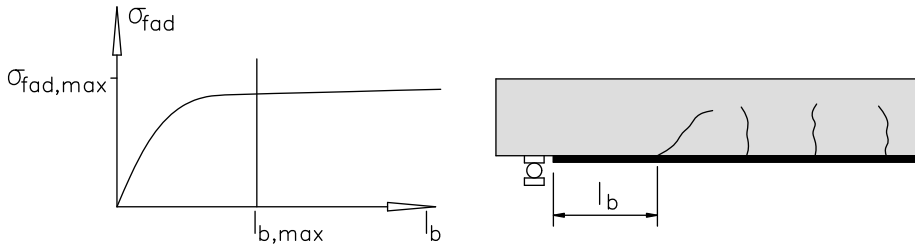


Fig. 5.1. Anchorable tensile stress related to anchoring (*fib* Bulletin 14, 2001)

### Approach 3 – Concrete bond strength

The third *fib* approach comprises two steps. The first step involves verification of the end anchorage as in Approach 1. The second step involves verifying that the substrate concrete can transfer the expected shear stress developed across the FRP-concrete interface. The main assumption of this approach is that if shear stress is maintained below the concrete bond shear strength, flexural cracks will not lead to debonding.

### 5.3. *fib* Bulletin 90

The simplified method presented in the new version of *fib* Bulletin 90 is based on the analysis of two main approaches corresponding to debonding at:

- the end of anchorage zone,
- intermediate crack debonding based on the ultimate FRP strain.

The second approach is more conservative than that predicted by the more accurate method, which is further presented in Chapter 6.

#### *Approach 1 - Ultimate strength for debonding at the end anchorage zone*

The main assumption of this approach is the predominant effect of the interfacial shear stress, which indicates that normal stress can be neglected.

The maximum tensile stress  $f_{fb}$  and corresponding tensile force in the FRP debonding  $F_{fb}$  are determined from:

$$f_{fb}(l_b) = \beta_1(l_b) \sqrt{\frac{2E_f G_f}{t_f}} \quad (5.11)$$

$$F_{fb}(l_b) = \beta_1(l_b) b_f \sqrt{2E_f t_f G_f} \quad (5.12)$$

where:  $\beta_1$  is a factor that depends on the bond length according to the following equation:

$$\beta_1 = \begin{cases} \frac{l_b}{l_e} \left( 2 - \frac{l_b}{l_e} \right) < 1 & \text{if } l_b < l_e \\ 1 & \text{if } l_b \geq l_e \end{cases} \quad (5.13)$$

#### *Solution with the bilinear bond stress-slip relationship*

If bilinear bond law model presented in Fig. 4.1 is assumed, the fracture energy can be expressed by

$$G_f = \frac{\tau_{b1} s_0}{2} \quad (5.14)$$

and the maximum stress in the FRP at debonding can be calculated from:

$$f_{fb}(l_b) = \beta_1(l_b) \sqrt{\frac{2E_f s_0 \tau_{b1}}{t_f}} \quad (5.15)$$

***The solution based on the “design by testing” approach***

For debonding at the end of anchorage zone approach, the mean, the 5% characteristics and the design debonding strength,  $f_{fbm}$ ,  $f_{fbk}$  and  $f_{fbd}$ , in the FRP reinforcement can be calculated as:

$$f_{fbm} = k_m k_f \beta_1 \sqrt{\frac{2E_f}{t_f} f_{cm}^{2/3}} \quad (5.16)$$

$$f_{fbk} = k_k k_f \beta_1 \sqrt{\frac{2E_f}{t_f} f_{cm}^{2/3}} \quad (5.17)$$

$$f_{fbd} = \frac{k_k}{\gamma_{fb}} k_f \beta_1 \sqrt{\frac{2E_f}{t_f} f_{cm}^{2/3}} \quad (5.18)$$

where: forces in [N], lengths in [mm] and the partial factor  $\gamma_{fb} = 1.5$ .

The numerical coefficient  $k_m$  can be calibrated by a statistical procedure as  $k_m = 0.25$  (Bilotta et al., 2011), or it can be obtained considering the 5% characteristic value of the parameter  $k$  as  $k_k = k_{0.05} = 0.17$  (presented in Chapter 3).

Thus the tensile FRP force can be calculated as:

$$F_{fbm} = b_f k_m k_f \beta_1 \sqrt{2E_f t_f} f_{cm}^{2/3} \quad (5.19)$$

***Approach 2 - Ultimate strength for debonding at intermediate cracks***

FRP debonding at intermediate cracks is analysed in four main approaches:

- a) a simplified approach based on the maximum strain in the FRP
- b) a more accurate approach based on the bond force transfer at the concrete elements between cracks
- c) the one based on bending–shear interaction
- d) the approach based on the shear transfer between the concrete and external FRP reinforcement.

---

***Simplified approach based on maximum strain in the FRP reinforcement***

At the ultimate limit state, the maximum the tensile stress does not exceed the lower fractile value (5%) of the bond strength  $f_{fbd,IC}$ , obtained by the corresponding mean value  $f_{fbm,IC}$ , by applying the following equations:

$$f_{fbm,IC} = k_{cr,m} f_{fbm} \quad (5.20)$$

$$f_{fbk,IC} = k_{cr,k} f_{fbk} \quad (5.21)$$

$$f_{fbd,IC} = \frac{f_{fbk,IC}}{\gamma_{fb}} \quad (5.22)$$

where:  $k_{cr,m} = 2.1$  and  $k_{cr,k} = 1.8$ .

The maximum values of interfacial shear stress are significantly lower when compared to the stress developed close to the end of the FRP itself. This implies that the value of the maximum FRP strain related to the intermediate crack debonding can be assumed higher than that pertaining to end debonding. The tensile stress at the intermediate crack ( $f_{fbm,IC}$ ,  $f_{fbk,IC}$ ,  $f_{fbd,IC}$ ) has to be calculated. The safety factor  $\gamma_{fb}$  can be assumed 1.5.

The corresponding value of the design strain in the FRP reinforcement,  $\varepsilon_{fbd,IC}$ , is:

$$\varepsilon_{fbd,IC} = \frac{f_{fbd,IC}}{E_f} \quad (5.23)$$

This limiting value of strain in the FRP reinforcement should be adopted in the critical sections of the strengthened element, i.e. in the sections where the bending moment is maximum and where it is assumed that a flexural or shear/flexural crack will form.

***Bond force transfer at the concrete elements between cracks approach***

In this approach, the stress variation,  $\Delta\sigma_f$ , in the FRP between two adjacent cracks should not exceed a suitable limiting value  $\Delta\sigma_R$ , which corresponds to the maximum increase in tensile stress that can be transferred by means of bond stresses along the crack spacing. The value of  $\Delta\sigma_R$  depends, in general, on the

bond constitutive law, on the distance between cracks,  $s_r$ , and on the stress level,  $\sigma_f$ , in the FRP reinforcement under the ultimate load condition.

The formulation given in DAFStb (2014) is based on the definition of the shear strength and includes the effect of the bond of the external reinforcement, the bond friction and the curvature of the element. Both simplified and detailed approaches are suggested in DAFStb (2012) and are presented in Chapter 6.1.

The analysis of flexural strengthening for non-prestressed members may be simplified as the analysis of flexural load-bearing capacity, using general stress of the FRP. In this approach, an analysis of the bond force transmission at an element between cracks is not necessary.

The stress in the FRP at the ultimate limit state can be calculated as

$$\sigma_{fd} = \min\{f_{fbd,IC}, f_{fd}\} \quad (5.24)$$

where:  $f_{fbd,IC}$  is design value of the FRP bond strength corresponding to intermediate crack debonding Eq. (5.22) (with  $\beta_1 = 1$ ) or (5.24), and  $f_{fd}$  is design tensile strength of FRP.

$$f_{fbd,IC} = \frac{k_{cr,k} k_k k_f \sqrt{\frac{2E_f}{t_f} f_{cm}^{2/3}}}{\gamma_{fb}} \quad (5.25)$$

where:  $k_{cr,k} = 1.8$ ,  $k_k = 0.17$ ,  $k_b = \sqrt{\frac{2-b_f/b}{1+b_f/b}} \geq 1$ .

### ***More accurate method***

The more accurate method comprises the verification of bond strength transmission at the elements between cracks. For this verification, it must be checked whether the change of the tensile force of the FRP,  $\Delta F_{fEd}$ , is lower than the resistance,  $\Delta F_{fRd}$ , at each concrete element between cracks:

$$\Delta F_{fEd} \leq \Delta F_{fRd} \quad (5.26)$$

The increment of FRP tensile force at the element between cracks can be calculated from the difference of the FRP tensile forces at both cracks:

$$\Delta F_{fEd} = \Delta F_{fEd}(x + s_r) - F_{fEd}(x) \quad (5.27)$$

where:  $s_r$  is the crack spacing. Then, either a *detailed analysis* of bond strength transmission at the elements between cracks or a *simplified analysis* may be performed, as given next (DAfStb 2012).

***Determining the crack spacing for reinforced concrete members***

The crack spacing  $s_r$  may be determined as

$$s_r = 1.5l_{e,0} \quad (5.28)$$

where:  $l_{e,0}$  is transfer length of the reinforcing steel, equal to

$$l_{e,0} = \frac{M_{cr}}{z_s F_{bsm}} \quad (5.29)$$

where:  $M_{cr}$  is cracking moment,  $z_s \approx 0.85h$  ( $h$  is total member height) and  $F_{bsm}$  is bond force per length. In reinforced concrete members, the cracking moment may be approximated as

$$M_{cr} = \kappa_{f1} f_{ctm} W_{c,0} \quad (5.30)$$

where:  $\kappa_{f1} = 1.6 - \frac{h}{1000} \geq 1$ ,  $h$  in mm and  $W_{c,0}$  is section modulus of the uncracked concrete cross section (moment of inertia divided by the distance of the extreme tensile fibre from the neutral axis). When determining  $M_{cr}$  for T-beams, the effective flange width shall be taken into account. The bond force per length may be calculated as

$$F_{bsm} = \sum_{i=1}^n n_{s,i} \pi \varnothing_{s,i} f_{bsm} \quad (5.31)$$

where:  $f_{bsm}$  is mean bond stress of the reinforcing steel,  $n_{s,i}$  is the number of steel rebars with diameter  $\varnothing_{s,i}$ .

The mean bond stress  $f_{bsm}$  may be obtained as follows:

$$f_{bsm} = \begin{cases} 0.43 \kappa_{vb1} f_{cm}^{2/3} & \text{for ribbed bars} \\ 0.28 \kappa_{vb2} \sqrt{f_{cm}} & \text{for smooth bars} \end{cases} \quad (5.32)$$

where:  $\kappa_{vb1}$  and  $\kappa_{vb2}$  depend on the bond conditions and may be taken as  $\kappa_{vb1} = \kappa_{vb2} = 1.0$  for good bond conditions and  $\kappa_{vb1} = 0.7$  and  $\kappa_{vb2} = 0.5$  for medium bond conditions.

#### 5.4. JSCE Recommendations

The Japanese Society of Civil Engineers Recommendations for Upgrading of Concrete Structures with use of Continuous Fibre Sheets (JSCE, 2001) notes that the important contribution of the interfacial fracture energy between the bonded FRP and substrate concrete in determining the maximum stress and the FRP strain, prior to debonding are given by

$$\sigma_{f \max} \leq \sqrt{\frac{2G_f E_f}{t_f}}, \quad \varepsilon_{fdb} = \sqrt{\frac{2G_f}{E_f t_f}} \quad (5.33)$$

where: the reported values of total interfacial fracture energy  $G_f$  for CFRP strips bonded to the clean concrete substrate range from 0.44 to 0.55 N/mm.

#### 5.5. Concrete Society TR55

The Concrete Society Technical Report 55 (2000) takes essentially the same approach to avoid FRP debonding as it is in the *fib* Bulletin 14 (2001) Approach 1. The tensile bond capacity and corresponding FRP debonding strain are given by

$$N_{f \max} = 0.5k_f b_f \sqrt{E_f t_f f_{ct}}, \quad \varepsilon_{fdb} = 0.5k_f \sqrt{\frac{f_{ct}}{E_f t_f}} \quad (5.34)$$

where:  $k_f$  term is given by Equation (5.5).

#### 5.6. CNR DT200

##### 5.6.1. CNR DT200/2004

##### *Approach 1 – Ultimate design strength for laminate / sheet end debonding*

For laminate / sheet end debonding, assuming that the provided bond length is equal to or larger than the optimal bonded length, the ultimate design strength,  $f_{fdd}$ , can be calculated as follows:

$$f_{fdd} = \frac{1}{\gamma_{f,d} \sqrt{\gamma_c}} \sqrt{\frac{2E_f G_{Fk}}{t_f}} \quad (5.35)$$

where:  $\gamma_{f,d}$  is partial safety factor;  $\gamma_{f,d} = 1.2$  for precured FRP laminates and  $\gamma_{f,d} = 1.5$  for cured in-site sheets,  $\gamma_c = 1.5$ .

For bond lengths  $l_b < l_e$ , the ultimate design strength shall be reduced according to the following equation:

$$f_{fdd,rid} = f_{fdd} \frac{l_b}{l_e} \left( 2 - \frac{l_b}{l_e} \right) \quad (5.36)$$

When the special anchoring devices (FRP transverse bars, U-wrap with FRP sheets, etc.) are used, the maximum design strength must be evaluated directly with ad-hoc experimental tests.

### ***Approach 2 – Ultimate design strength for intermediate debonding***

To prevent failure from IC mechanism, the stress variation  $\Delta\sigma_f$  in the FRP system between two subsequent cracks should not exceed the limit  $\Delta\sigma_R$ . The later value typically depends on the characteristics of bond between concrete and FRP, the distance between cracks in the concrete, and the level of stress  $\sigma_f$  in the FRP reinforcement.

Alternatively, a simplified procedure may be used. The maximum strength fold shall be less than  $f_{fdd,2}$ :

$$f_{fdd,2} = k_{cr} f_{fdd} = \frac{k_{cr}}{\gamma_{f,d} \sqrt{\gamma_c}} \sqrt{\frac{2E_f G_{Fk}}{t_f}} \quad (5.37)$$

where:  $k_{cr} = 3.0$  if specific data is not available.

The corresponding value of the design strain,  $\varepsilon_{fdd}$ , in the FRP system can be calculated as follows:

$$\varepsilon_{fdd} = \frac{f_{fdd,2}}{E_f} \quad (5.38)$$

### 5.6.2. CNR DT200/2013

A new version of the Italian guidelines, CNR–DT 200 R1/2013, has been recently published. It provides new equations that can improve the model accuracy. Among the others, a new equation for computing the fracture energy, which has different values, depending on the material used, the effective bond length, and the FRP–concrete strength is provided. The maximum stress  $f_{fdd}$  that can be carried by the composite preventing the end plate debonding failure is calculated as:

$$f_{fdd} = \frac{k_{cr}}{\gamma_{f,d}} \sqrt{\frac{2E_f G_{Fk}}{t_f}} \quad (5.39)$$

$$f_{fdd,rid} = f_{fdd} \frac{l_b}{l_e} \left( 2 - \frac{l_b}{l_e} \right) \quad \text{for } l_b < l_e \quad (5.40)$$

The fracture energy  $G_{Fk}$  is calculated as:

$$G_{fd} = \frac{k_b k_G}{FC} \sqrt{f_{cm} f_{ctm}} \quad (5.41)$$

$$k_b = \sqrt{\frac{2 - b_f/b}{1 + b_f/b}} \geq 1 \quad (5.42)$$

where:  $k_G = 0.023$  in case of pre–impregnated laminate, and  $k_G = 0.037$  in case of post–impregnated sheet.  $FC$  is an additional safety factor. In order to avoid the intermediate crack–induced debonding failure, the maximum FRP stress must be less or equal to  $f_{fdd,2}$ :

$$f_{fdd,2} = \frac{k_q}{\gamma_{f,d}} \sqrt{\frac{E_f}{t_f} \frac{2k_f k_{G,2}}{FC} \sqrt{f_{cm} f_{ctm}}} \quad (5.43)$$

where:  $k_{G,2}$  is an empirical coefficient equal to 0.10, and  $k_q = 1.25$  for distributed load, and  $k_q = 1.0$  in all other cases. The CNR–DT 200 R1/2013 computes the effective bond length, named optimum bond length, as:

$$l_e = \min \left\{ \frac{1}{\gamma_{Rd} f_{bd}} \sqrt{\frac{\pi^2 E_f t_f G_{Fd}}{2}}, 200 \right\} \quad (5.44)$$

$$f_{bd} = \frac{2G_{Fd}}{s_u} \quad (5.45)$$

where:  $s_u = 0.25$  is the ultimate slip between the FRP and the concrete support, and  $\gamma_{Rd} = 1.25$  is a modification factor.

## 5.7. Swiss guide SIA166 2004

### 5.7.1. Strengthening with non-prestressed FRP laminates

SIA166 2004 proposes the following three steps design concept for flexural strengthening of RC beams with EB FRP reinforcement:

1. Strip end failure (Approach 1)
2. Tensile force change (Approach 2)
3. Local debonding at flexural cracks (Approach 3)

The first design level considers the strain pattern in the FRP laminate along the structure for the assumed load according to in Fig. 5.2. The strain pattern corresponds to the ordinary cross-section analysis at the regular distance (length) along the member.

There are three main locations to be considered in the design analysis (Fig. 5.2):

1. location of the last crack (the closest to the support),
2. location of internal steel yielding reinforcement,
3. maximum FRP strain.

The most popular research based on the 4-point bending beam, hence the selected points are easy to define. For the distributed load the situation is more complex and then the lengths of  $l_{cr}$ ,  $l_y$  and  $\Delta x$  can be determined from the locations of the characteristic points. Based on the above mentioned information, the following design procedure should be performed:

#### ***Approach 1 - Ultimate design strength for laminate end debonding***

To save the end FRP debonding, the SIA166 2004 code requires to limit the force in FRP laminate at the last crack  $F_{cr}$  to the anchorage resistance of this strip  $F_{IR}$ :  $F_{cr} = \varepsilon_{f,cr} E_{fr} b_f t_f$

---

Design guidelines and code formulations

---

$$F_{cr} \leq F_{lR} \quad l_b > l_{ba} \quad (5.46)$$

$$F_{cr} \leq F_{lR,s} \quad l_b \leq l_{ba} \quad (5.47)$$

$$F_{lR} = b_f \sqrt{2G_f E_f t_f} \quad (5.48)$$

$$F_{lR,s} = l_b b_f \tau_{f,mean} \quad (5.49)$$

The effective bond length  $l_b$  and the active bond length  $l_{ba}$  at the FRP end can be calculated as:

$$l_b = l_{cr} - l_{se} \quad (5.50)$$

$$l_{ba} = \frac{F_{lR}}{\tau_{f,mean} b_f} \quad (5.51)$$

$$\tau_{f,mean} = \frac{G_f}{s_{f,max}} \quad (5.52)$$

where:  $l_{se}$  is the distance between the end of the strip and the support (Fig. 5.2);  $s_{f,max}$  is the maximum slip  $s_{f,max} = 0.2mm$  for the CFRP strip ( $E_f = 150GPa$ ,  $t_f = 1.2mm$ ,  $25MPa < f_{ck} < 50MPa$ ).

The fracture energy  $G_f$  for pull-off tests on CFRP laminates depending on the maximum aggregate size  $d_{max}$  was proposed by Czaderski (2012):

$$G_f = 0.018 f_{ck}^{2/3} d_{max}^{1/4} \quad (5.53)$$

### ***Approach 2 - Ultimate design strength for tensile force change***

The maximum global bond shear stress should be limited to:

$$\tau_{f,gl,max} \leq \tau_{f,lim} = 2.5\tau_c \quad (5.54)$$

$$\tau_c = 0.3\sqrt{f_{ck}} \quad (5.55)$$

The maximum global bond shear stress occurs in the cross-section of the internal reinforcement yielding (Fig. 5.2), while the global bond shear stress is limited to:

$$\tau_{f,lim} = 0.75\sqrt{f_{ck}} \quad (5.56)$$

However, according to research by Aram et al. (2008), the global bond shear stress should be limited to a more conservative value:

$$\tau_{f,lim} = f_{ctm} \quad (5.57)$$

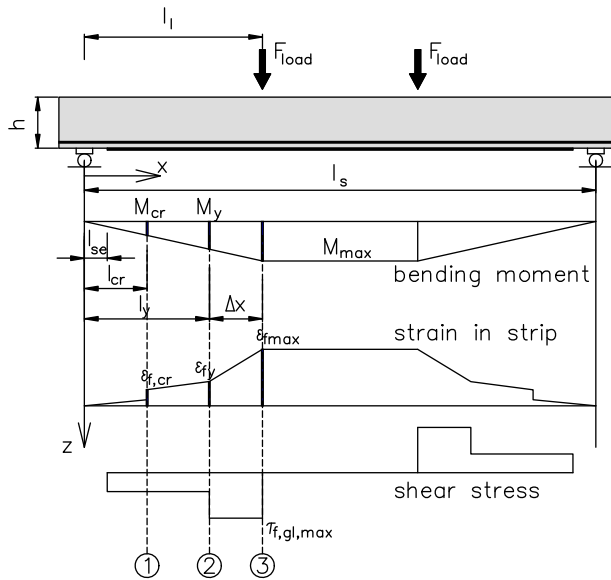


Fig. 5.2. Bending moment envelope, FRP strain and bond shear stress distribution in a point loaded beam strengthened with EBR laminates (Czaderski, 2012)

As it is shown in Fig. 5.2., the maximum global bond shear stress can be obtained from:

$$\tau_{f,gl,max} = \frac{(\varepsilon_{f,max} - \varepsilon_{fy})E_f t_f}{\Delta x} \quad (5.58)$$

**Approach 3 - Ultimate design strength for local intermediate crack debonding**

This approach gives the strain limitation of the EBR FRP laminate according to:

$$\varepsilon_{f,max} \leq \varepsilon_{f,lim} = 8\% \text{ and } \varepsilon_{f,max} \leq \varepsilon_{fu} \quad (5.59)$$

**5.7.2. Strengthening with prestressed FRP laminates (Gradient method)**

An RC member flexurally strengthened with the linear force gradient is presented in Fig. 5.3. The design procedure based on the full bonded FRP length published in Michels et al. (2012b).

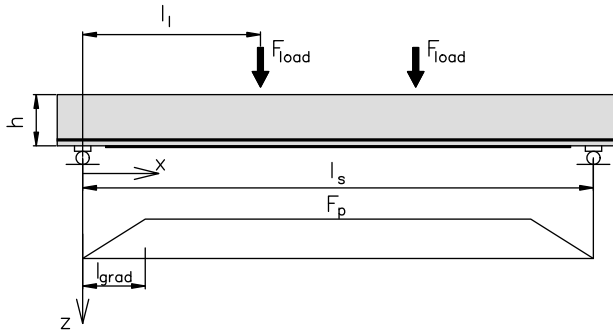


Fig. 5.3. Prestressing force  $F_p$  distribution in the gradient prestressing method (Czaderski, 2012)

The same procedure based on the cross-section analysis for the first crack position is assumed as presented in 5.2.

**Approach 1a - Ultimate strength for laminate end debonding - last crack outside of gradient anchorage**

In this approach the force increase in the strip due to loading  $\Delta F_{cr}$  at the last crack is smaller than the anchorage resistance of the strip  $F_{IR}$ .

$$F_p + \Delta F_{cr} \leq F_p + F_{IR} \rightarrow \Delta F_{cr} \leq F_{IR} \quad (5.60)$$

$$\Delta F_{cr} \leq F_{IR} \quad l_b > l_{ba} \quad (5.61)$$

$$\Delta F_{cr} \leq F_{IR,s} \quad l_b \leq l_{ba} \quad (5.62)$$

**Approach 1b - Ultimate strength for laminate end debonding - last crack inside the gradient anchorage**

This design approach is shown in Fig. 5.4.

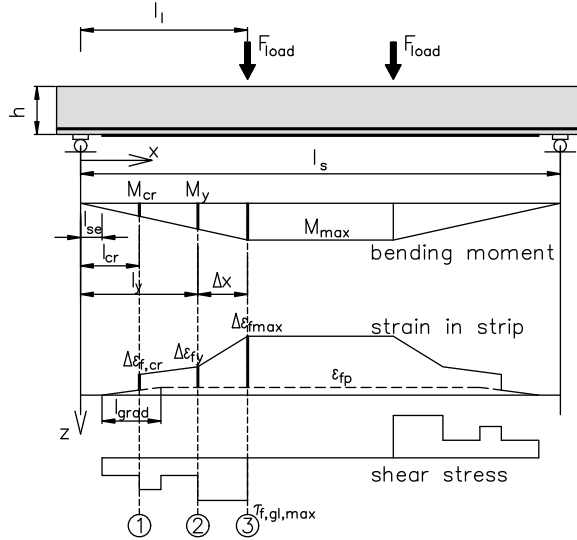


Fig. 5.4. Design concept for prestressed externally bonded FRP strip anchored with the gradient method.

The force increase in the strip due to external loads  $\Delta F_{cr}$  at the last crack cross-section should be smaller than the reduced anchorage resistance at this location:

$$\Delta F_{cr} \leq F_{IR,red} \quad l_b \leq l_{ba} \quad (5.63)$$

$$\Delta F_{cr} \leq F_{IR,s,red} \quad l_b \leq l_{ba} \quad (5.64)$$

The reduced anchorage resistance  $F_{IR,red}$  is calculated from:

$$F_{IR,red} = \sqrt{b_f^2 l_{ba}^2 \tau_{f,mean}^2 - \left( \frac{l_{ba}}{l_{grad}} F_p \right)^2}, \quad l_b \geq l_{ba} \quad (5.65)$$

$$F_{IR,s,red} = \sqrt{b_f^2 l_{ba}^2 \tau_{f,mean}^2 - \left( \frac{l_{ba,s}}{l_{grad}} F_p \right)^2}, \quad l_b = l_{ba,s} \leq l_{ba} \quad (5.66)$$

***Approach 2 - Ultimate design strength for tensile force change***

In most cases the anchorage gradient is located outside the region where the internal steel reinforcement is yielding, hence the design procedure should be followed according to the *Approach 2* in Chapter 5.7.1.

However, if the anchorage gradient is located in the steel yielding, the bond shear stress should be limited to:

$$\tau_{f,lim} = 0.75\sqrt{f_{ck}} - \frac{F_p}{b_f l_{grad}} \quad (5.67)$$

and

$$\tau_{f,lim} = f_{ctm} - \frac{F_p}{b_f l_{grad}} \quad (5.68)$$

***Approach 3 - Ultimate design strength for local intermediate crack debonding***

To avoid local debonding of the prestressed PEFR at flexural cracks, the additional strain in the strip due to the external loads should be limited to:

$$\Delta\varepsilon_{f,max} \leq \varepsilon_{f,lim} = 8\text{‰} \quad (5.69)$$

or

$$\Delta\varepsilon_{f,max} \leq \varepsilon_{fu} - \varepsilon_{fp} \quad (5.70)$$

**5.8. German simplified method DAFStb (2014)**

The CFRP strain approach has to meet the condition of the end anchorage at the final element between cracks analysis:

$$\varepsilon_{Ld,max} = \max \left\{ \begin{array}{l} 0.5\text{mm}/m + 0.1\text{mm}/m \frac{l_0}{h} - 0.04\text{mm}/m \varnothing_s + 0.06\text{mm}/m f_{cm} \\ 3.0\text{mm}/m \frac{l_0}{9700\text{mm}} \left( 2 - \frac{l_0}{9700\text{mm}} \right) \quad \text{for } l_0 \leq 9700\text{mm} \\ 3.0\text{mm}/m \quad \text{for } l_0 > 9700\text{mm} \end{array} \right. \quad (5.71)$$

where:  $l_0$  is the axial span length;  $\varnothing_s$  is a diameter of the steel reinforcement.

The parametric study needs to meet certain boundary conditions:

1. the CFRP strip should be located not farther than 50mm from the front edge of the support,
2. the ribbed internal reinforcing steel is needed,
3. the internal reinforcing steel is not curtailed,
4. the tensile concrete strength correlates with the compressive strength,
5. only reinforced members are considered, whereas prestressed structures are excluded from the analysis,
6. the strengthening is provided for positive moments (span moments).

With uniformly distributed loads it can be assumed that if the conditions from 1 to 3 are not fulfilled, the simplified analysis also lies on the safe side, with an additional check of the end anchorage and the associated checking of the initial increase in the strip tensile force envelope.

The correlation between the tensile and compressive strength of the concrete mentioned (4th condition) is achieved by adapting the concrete compressive strength according to (5.71) equation to the near-surface tensile strength determined as:

$$f_{ctm,surfx} \geq 0.26 f_{cm}^{2/3} \quad (5.72)$$

The simplified method cannot be applied for the prestressed members because in some circumstances prestressing can significantly change the distribution of the strains over the cross-section.

The strengthening in hogging moment regions, in the continuous RC members cannot be designed with this method because there is an unfavourable relationship between moment and shear force. In addition, this method assumes that a member is cracked at the ultimate limit state.

## 5.9. The comparison of design approaches

The comparison of FRP axial stiffness-strain relationship for simplified chosen theoretical models corresponding to IC debonding approach (Fig. 5.5) confirms similar tendency of the reduction in the bond FRP strain with the increase in the stiffness of the EB FRP reinforcement. The following assumptions were taken for analysis:  $b_f = 50mm$ ,  $b_c = 150mm$ ,  $f'_c = 40MPa$ ,  $f_{ctm} = 2.5MPa$ . It should be emphasized that FRP stiffness is much more effected by FRP thickness  $t_f$  than the elasticity modulus  $E_f$ . This problem was analysed in Chapter 3 (Fig. 3.4) in the aspect of effective bond length  $l_e$ . It is visible that flexible cured in-situ sheets indicate much higher bond strain in

comparison with rigid CFRP pre-cured laminates. It is a well known rule, based on the axial stiffness ( $E_f t_f$ ) of the FRP externally bonded reinforcement, that with the increase in the FRP thickness and its modulus of elasticity  $E_f$  the bond strain decreases. For one type of FRP reinforcement, e.g. CFRP materials, the elasticity modulus varies from 165GPa to 220GPa, whereas the thickness varies from 0.165mm to 1.4mm, which gives 8.5 times higher difference. This is why the main effect on the bond properties comes from CFRP thickness.

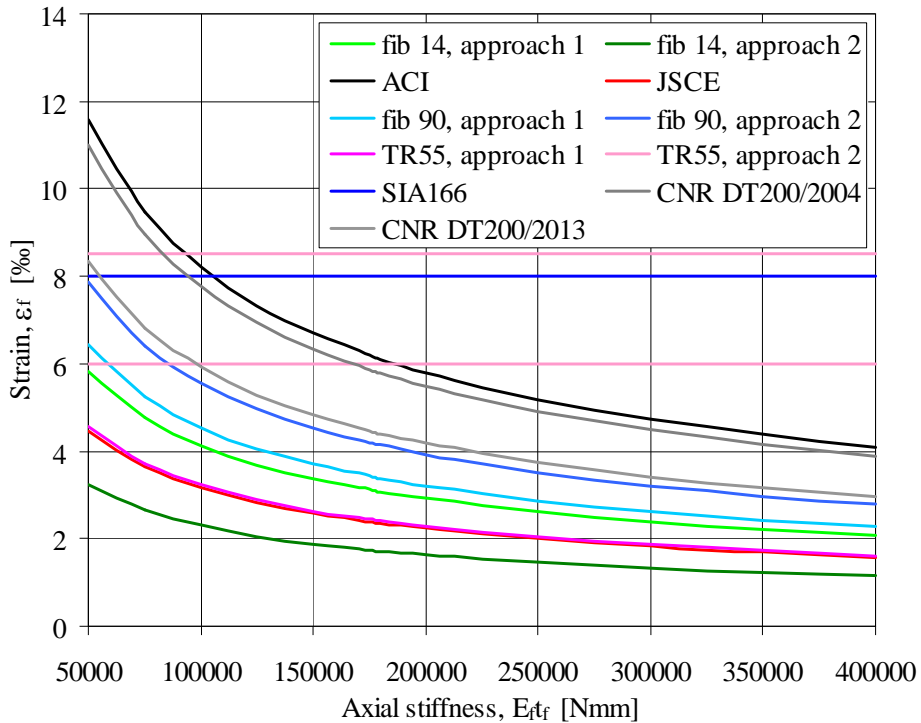


Fig. 5.5. The comparison of theoretical models recommendation for predicting IC FRP debonding strain

A similar comparison of design FRP axial stiffness-strain relationship, according to the design guidelines described in this Chapter, is shown in Fig. 5.6.

The ACI 440-2R-08 gives the highest bond strain mainly for lower values of  $E_f t_f$ , whereas and Swiss SIA166, German DAFStb (2014) and British TR55 standards propose stable strain bond limits in the range  $6.0‰ \leq \varepsilon_{fdb} \leq 8.5‰$ . It

seems tendency to increase the FRP bond strain limits in the new versions of *fib* Bulletin 90 (2019) and CNR DT200/2013 in comparison with the corresponding previous versions *fib* Bulletin 14 (2002) and CNR DT200/2004. However, to avoid the intermediate crack debonding, the unconservative FRP limit debonding strain in the range of  $6.0\text{‰} \leq \varepsilon_{fdb} \leq 8.5\text{‰}$  is proposed by Swiss SIA166, German DAFStb (2014) and British TR55 standards.

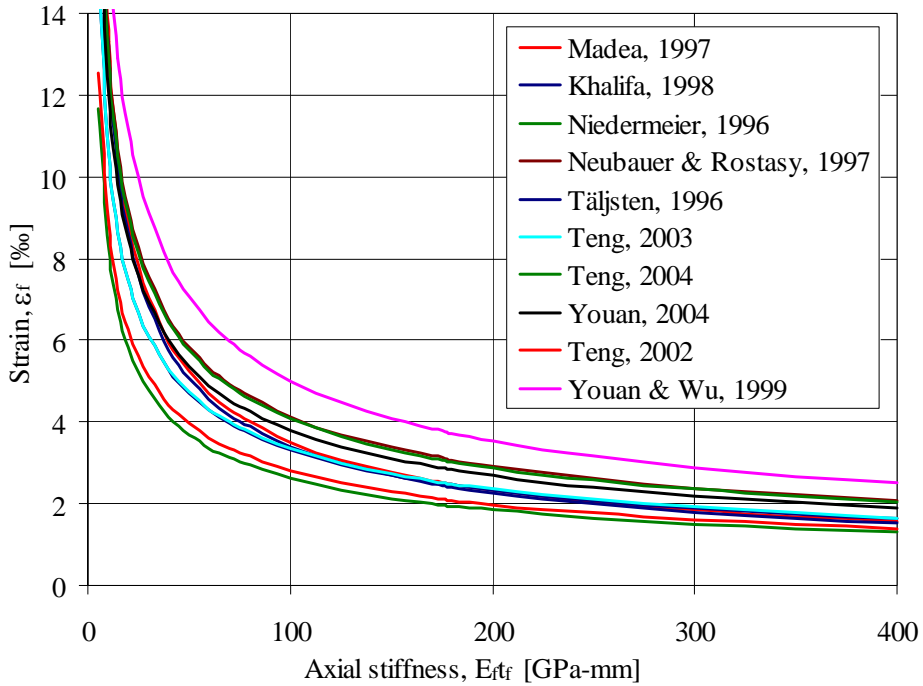


Fig. 5.6. The comparison of design models recommendations for predicting IC FRP debonding strain

## 6. Advanced design models

### 6.1. Accurate analysis of bond strength according to DAFStb

The design methods presented in DAFStb (2014) and Zilch et al. (2014) for flexural strengthening with externally bonded FRP materials can be performed in two ways:

- a simple analysis based on basic approaches regarding only the ultimate strain in externally bonded reinforcement in addition to performing the end anchorage analysis is not recommended by DafStb (2014) for designing EB FRP strengthening but only for accuracy or economic purpose,
- the accurate method based on the analysis of bond strength transmission at the segments of the RC member between cracks so-called *intermediate crack element method (ICE)* is recommended by DAFStb (2014).

The simplified methods are described in Chapter 5 according to several existing design codes. The accurate method referring only to CFRP (carbon fibre reinforced polymer) strengthening materials is presented in this Chapter .

A scheme for the analysis of flexurally strengthened RC members with EB CFRP materials is described in details in Chapter 3. This concept is based on the major flexural analysis of conventional failure modes:

- in the concrete compression (due to concrete crushing),
- in the internal steel reinforcement (due to steel yielding or rupture),
- general shear failure mode if the load bearing capacity of an existing member is high.

Then variable bond failure modes of externally bonded reinforcement to concrete should be analysed very carefully, considering the following aspects:

- steel yielding of the internal reinforcement followed by failure of EB laminates,
- concrete cover separation failure, referring to the end of the FRP debonding due to additional, vertical, offset between the shear FRP–concrete links, when tensile stress from the laminate cannot be transferred to the RC beam,
- horizontal shear failure in the interface between the EB FRP reinforcement and the internal reinforcement,
- bond failure between the adhesive and concrete, when the concrete layers near the concrete–adhesive interface exceed the tensile concrete strength,
- due to variable tensile strength of concrete layers near the adhesive, following the local CFRP debonding, bond between the CFRP reinforcement and concrete cannot be transferred by any remaining areas of intact bonding (called *the unzipping effect*).

### 6.1.1. Curvature effect on the bond behaviour

The analysis of bond should be considered in several stages referring to the accuracy requirements. However, the CFRP end anchorage analysis is required at every stage. CFRP-to-concrete bond behaviour is under special consideration. When it comes to EB CFRP strengthened RC members, in which the tensile force in the FRP reinforcement can not be anchored, the increase in the bond is rather impossible. The research on flexurally strengthened RC members indicates that much higher laminate forces can be reached at the maximum bending moment region that at the end anchorage. As far as CFRP laminates are concerned, only the end anchorage analysis gives uneconomic strengthening solutions. However, the transfer of the bond force should be considered at the point at which the changes in tensile force occur (Fig. 6.1).

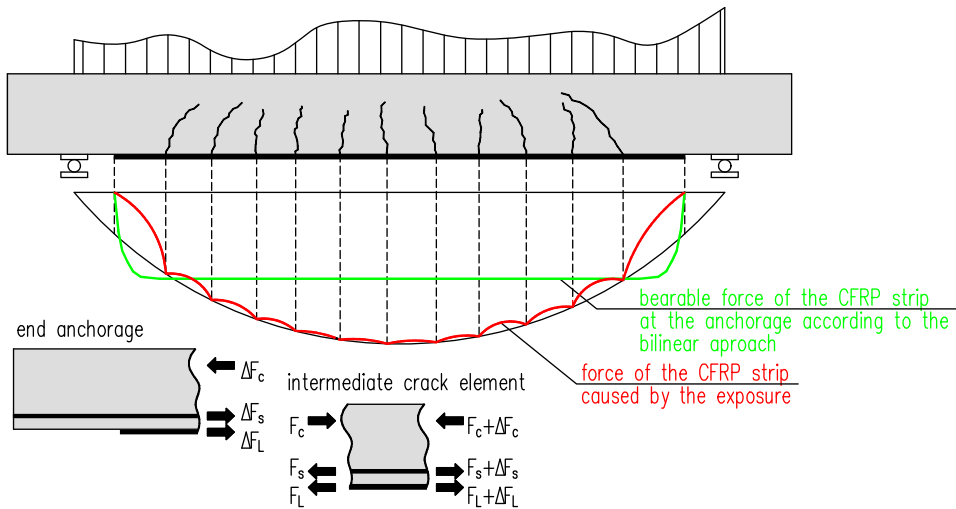


Fig. 6.1. Bond force transfer with externally bonded CFRP reinforcement (Zilch et al., 2014)

For this reason two approaches must be analysed:

- the end anchorage region
- the rest part of the member.

The laminate forces at the flexural crack nearest the point of contraflexure must be anchored at the end of the anchorage point. The bond forces at the end of the anchorage zone of the CFRP reinforcement can be determined from the pull-out anchorage bond tests.

The curvature effect investigated by Zilch et al. (2012) and Finckh and Zilch (2012) enabled testing different parts of the beam, while on the remainder a bond break-up was prevented by actively pressing onto the strip (Fig. 6.2).

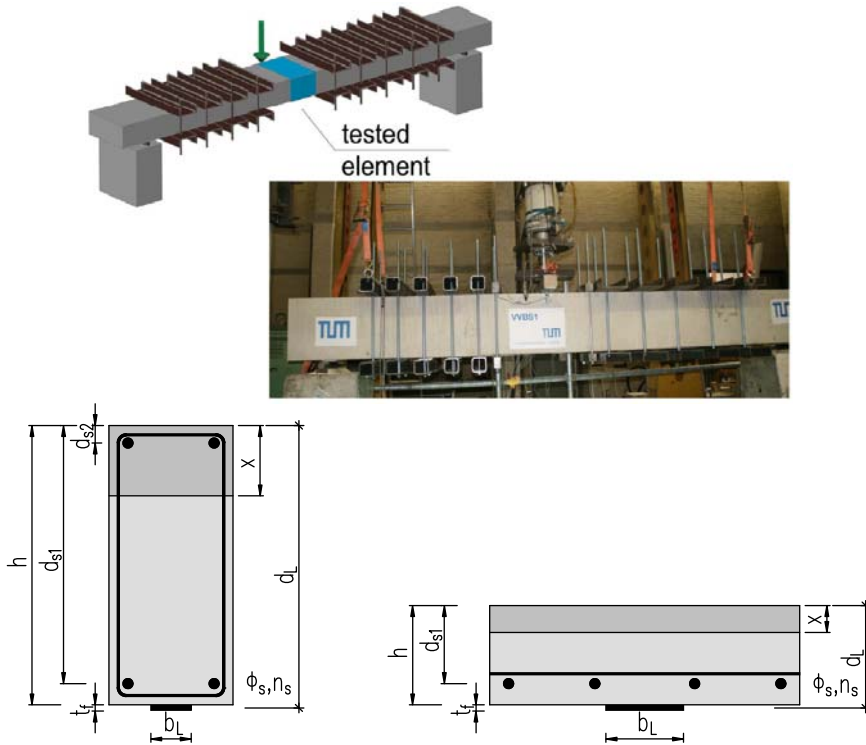


Fig. 6.2. Test set-up for IC debonding of beams and slabs strengthened with VFRP laminates (Finckh and Zilch, 2012)

Through measurements of the CFRP strain the uncoupling of the bond was accurately registered. Another advantage of this test set-up was that several investigated parts of the beam varying in ratios of shear and bending were performed in a single beam. The beginning of the CFRP laminate uncoupling was possible due to the observation of the difference of the CFRP strains at both sides of the investigated concrete segment between the cracks turned from increasing to dropping. The uncoupling process was then observed through an increase in the sway between the strip and concrete, which in the tests was determined by optical deformation measurements (Fig. 6.3).

Tests performed on the beams and slabs indicated the positive effect of the curvature of the structural RC elements (beams and slabs) on the EB FRP bond behaviour to concrete (Fig. 6.4). RC slabs act more favourably than beams. This confirms detrimental effect of the larger deflection curvature in the slabs than that in the beams. Moreover, this positive curvature effect creates a self-induced contact pressure in comparison with the contact pressure investigated by Husemann and Budelmann (2009), when bracing the CFRP strips by gluing stirrups around them.

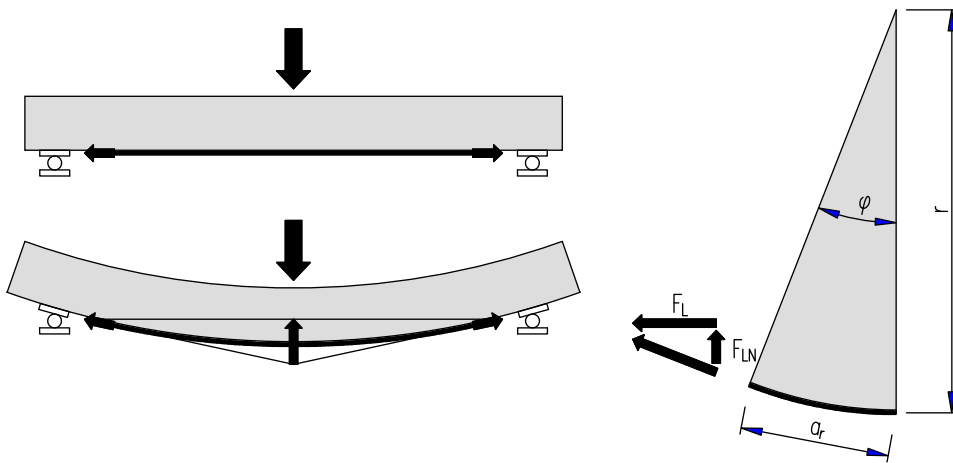


Fig. 6.3. The effect of the self induced contact pressure on the CFRP-strip stress at the IC debonding (Finckh and Zilch, 2012)

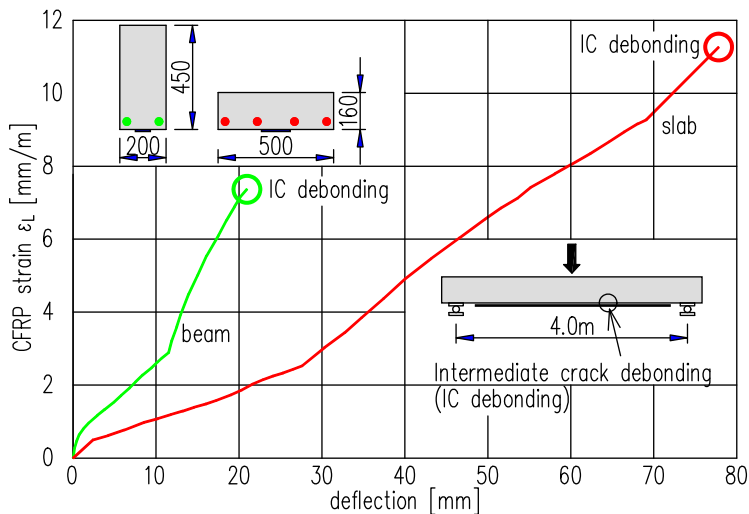


Fig. 6.4. The comparison of CFRP strain-deflection responses for EB CFRP beam and slab (Finckh and Zilch, 2012)

### 6.1.2. Flexural strength analysis

The flexural strength analysis can be carried out similarly to an RC member with assumption of the cracked cross-section.

Firstly, the equilibrium of the internal and external forces should be considered:

$$\sum M = 0, \quad M_{Rd} = M_{Ed} \quad (6.1)$$

$$\sum N = 0, \quad N_{Rd} = N_{Ed} \quad (6.2)$$

The general equations used for conventional RC members should be extended with the CFRP reinforcement according to Fig. 6.5. Then the equations 1 and 2 can be expressed by:

$$N_{Rd} = F_{cd} + F_{Ld} + F_{s1d} + F_{s2d} \quad (6.3)$$

$$M_{Rd} = -F_{cd}(z - z_L) + F_{Ld}z_L + F_{s1d}z_{s1} + F_{s2d}z_{s2} \quad (6.4)$$

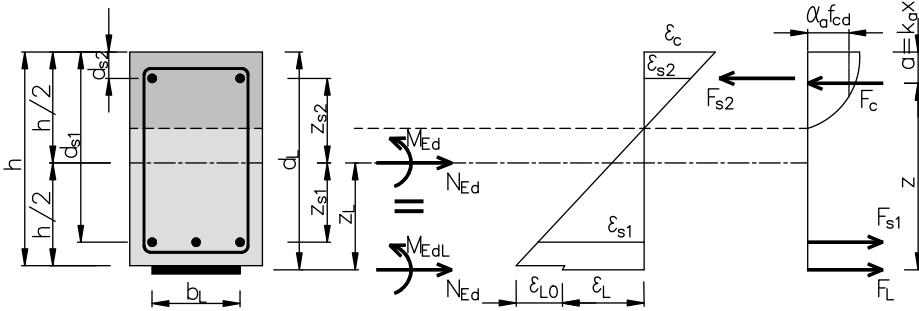


Fig. 6.5. Geometry, strain and stress distribution, and internal forces of a strengthened and preloaded RC cross-section (all measurements used in equations are in mm) (Zilch et al., 2014)

The moment resistance of the cross-section converted to the axis of the CFRP reinforcement and to the axis of the compressive concrete force can be calculated in the following way:

$$M_{RdL} = M_{Rd} - N_{Rd}z_L = -F_{cd}z - F_{s1d}(d_L - d_{s1}) + F_{s2d}(d_L - d_{s2}) \quad (6.5)$$

$$M_{Rdc} = M_{Rd} + N_{Rd}(z - z_L) = F_{Ld}(d_L - k_a x) + F_{s1d}(d_{s1} - k_a x) + F_{s2d}(k_a x - d_{s2}) \quad (6.6)$$

where:  $F_{cd}$ ,  $F_{Ld}$ ,  $F_{s1d}$ ,  $F_{s2d}$  are: the concrete compressive force, tensile force in CFRP reinforcement, force in tensile and compressive reinforcement, respectively;  $k_a$  is the concrete coefficient (referring to the magnitude of the compressive force in concrete) calculated from:

$$k_a = \begin{cases} \frac{8 + \varepsilon_c}{24 + 4\varepsilon_c} & \text{for } \varepsilon_c \geq -2\text{mm}/m \\ \frac{3\varepsilon_c^2 + 4\varepsilon_c + 2}{6\varepsilon_c^2 + 4\varepsilon_c} & \text{for } -2\text{mm}/m > \varepsilon_c \geq -3,5\text{mm}/m \end{cases} \quad (6.7)$$

$$F_{cd} = b x f_{cd} \alpha_R \quad (6.8)$$

$$\alpha_R = \begin{cases} \frac{-\varepsilon_c}{2} - \frac{\varepsilon_c^2}{12} & \text{for } \varepsilon_c \geq -2\text{mm}/m \\ 1 + \frac{2}{3\varepsilon_c} & \text{for } -2\text{mm}/m > \varepsilon_c \geq -3,5\text{mm}/m \end{cases} \quad (6.9)$$

The compression zone depth can be determined on the basis of the CFRP strain  $\varepsilon_L$  and the compressive concrete strain  $\varepsilon_c$  considering the prestrain of the cross-section before its strengthening  $\varepsilon_{L,0}$ :

$$x = \frac{-\varepsilon_c}{-\varepsilon_c + \varepsilon_{L,0} + \varepsilon_L} d_L \quad (6.10)$$

$$F_{Ld} = A_L E_L \varepsilon_L \leq A_L f_{Lud} \quad (6.11)$$

$$F_{s1d} = A_{s1} E_s \varepsilon_{s1} \leq A_{s1} f_{yd} \quad (6.12)$$

$$F_{s2d} = A_{s2} E_s \varepsilon_{s2} \leq A_{s2} f_{yd} \quad (6.13)$$

$$\varepsilon_{s1} = -\varepsilon_c \frac{d_{s1} - x}{x} \quad (6.14)$$

$$\varepsilon_{s2} = -\varepsilon_c \frac{d_{s2} - x}{x} \quad (6.15)$$

Geometry parameters are presented in Fig. 6.5.

Based on the iteration process of the CFRP strain:  $\varepsilon_L \leq \varepsilon_{Lud} \leq \varepsilon_{sud}$ , the compressive concrete strain:  $\varepsilon_c \leq \varepsilon_{cud}$  and the steel strain:  $\varepsilon_{s1}$  and  $\varepsilon_{s1u} \leq \varepsilon_{syd}$  may be calculated.

### 6.1.3. Accurate method for IC FRP debonding

The more accurate method is fully adapted from DafStb (2014). This approach is based on the transfer of the bond force at the concrete element between cracks (Fig. 6.1).

The source of this model was proposed in the fundamental bond-slip approach proposed by Niedermeier (1997), then the ideas was continued by Neubauer (2000), who proposed a solution for the bond force transfer at the element between cracks. The transfer of the bond force across the elements between cracks is determined by subdivision of the RC member into several elements by means of flexural cracks position.

Two main regions are considered in this analysis:

- the end of CFRP anchorage region,
- the rest of the RC member.

The laminate forces at the flexural crack closest to the support must be anchored at the end anchorage point. The bond forces that can be accommodated at the end anchorage zone are determined by so-called idealized end anchorage tests, in which the externally bonded reinforcement is peeled off in the longitudinal direction. According to Fig. 6.1, the bond forces can be transferred to concrete elements separated by flexural cracks. The forces in the concrete segment divided by the cracks consist of the basic CFRP force at the less heavily stressed crack edge and the additional force at the more highly stressed crack edge. This additional laminate force must be transferred into a member via bond.

On the basis of the mechanics derivation (Niedermeier, 1997; Neubauer, 2000; Finckh, 2012) the expressions for the bond analyses given in the guideline dependent on the bond coefficients of the extended bilinear bond stress-slip relationship are shown in Fig. 6.6.

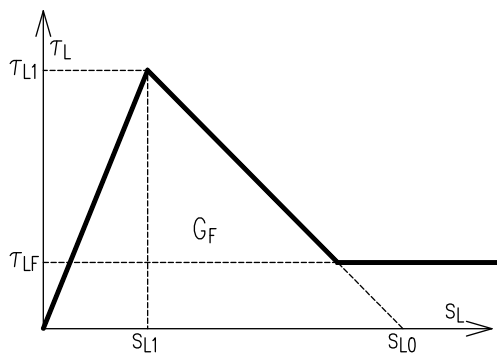


Fig. 6.6. Extended bilinear bond stress-slip relationship (Zilch et al., 2012)

The extended bilinear bond stress–slip model for externally bonded CFRP laminates is specified by the following equations:

$$\tau_{Llk} = 0,366\sqrt{\alpha_{cc}f_{cm}\alpha_{ct}f_{ctm,surf}} \quad (6.16)$$

$$s_{L0k} = 0,201mm \quad (6.17)$$

$$\tau_{Llk} = 10,8\alpha_{cc}f_{cm}^{-0,89} \quad (6.18)$$

The bond characteristics (Fig. 6.6) considers the influence of the long-term durability of concrete by the coefficients  $\alpha_{cc}$  and  $\alpha_{ct}$  (according to DIN EN 1992-1-1 and National Annex DIN EN 1992-1-1/NA).

### **Crack spacing analysis**

The crack spacing is the one of the most important parameters taking the *more accurate bond analysis or intermediate crack element (ICE) analysis* into account. A simplified way of calculating the mean crack spacing  $s_r$  for a stabilized crack pattern is based on the following assumption:

$$s_r = 1,5l_{e,0} \quad (6.19)$$

where:  $l_{e,0}$  is the transmission length of the reinforcing steel, which is determined by Noakowski (1988) approach:

$$l_{e,0} = \frac{M_{cr}}{z_s F_{bsm}} \quad (6.20)$$

where:  $M_{cr}$  is the cracking moment;  $F_{bsm}$  is the mean bond force;  $z_s \approx 0.85h$

$$M_{cr} = \kappa_{fl} f_{ctm,surf} W_{c,0} \quad (6.21)$$

$$\kappa_{fl} = \left( 1,6 - \frac{h}{1000} \right) \geq 1,0 \quad (6.22)$$

$W_{c,0}$  is the section modulus of uncracked concrete cross–section (moment of inertia divided by the distance of the extreme tensile fibre from the neutral axis).

The mean bond force is determined as:

$$F_{bsm} = \sum_{i=1}^n n_{s,i} \phi_i \pi f_{bsm} \quad (6.23)$$

where:  $n_{s,i}$  and  $\phi_i$  are the number and diameter of the steel bars;  $f_{bSm}$  is the mean bond stress of steel reinforcement calculated as:

$$f_{bSm} = \begin{cases} \kappa_{vb1} 0,43 f_{cm}^{2/3} & \text{for ribbed rebars} \\ \kappa_{vb2} 0,28 \sqrt{f_{cm}} & \text{for plain rebars} \end{cases} \quad (6.24)$$

where: the bond coefficients for internal reinforcement for the end anchorage analysis at the flexural crack nearest to the point of contraflexure can be taken from Table 6.1.

Table 6.1. Bond coefficients for internal reinforcement referring to the end anchorage analysis

Internal reinforcement	Ribbed	Plain
$\kappa_{b1k}$	2.545	1.292
$\kappa_{b2}$	1.0	1.3
$\kappa_{b3}$	0.8	1.0
$\kappa_{b4}$	0.2	0.3

***The accurate analysis of a concrete element between cracks***

The accurate analysis (called *detailed analysis*) of a concrete element between cracks requires calculating the change in CFRP force  $\Delta F_{LEd}$  in the segment between cracks that must be smaller than the change in force that can be accommodated by bond:

$$\Delta F_{LEd} \leq \Delta F_{LRd} \quad (6.25)$$

$$\Delta F_{LEd} = F_{LEd}(x + s_r) - F_{LEd}(x) \quad (6.26)$$

The force in the segment between cracks  $\Delta F_{LEd}$  depends on the laminate force at the less heavily-stressed crack edge  $F_{LEd}(x)$ , which depends on the bending moment in this section. The total change in the CFRP laminate force  $\Delta F_{LRd}$  consists of three effects:

- the component from the *bilinear bond stress-slip relationship*  $\Delta F_{FLk,BL}$  (Fig. 6.7),
- the component from the *additional frictional bond* that occurs when CFRP started  $\Delta F_{FLk,Bf}$  (Fig. 6.8),
- the component of the *curvature effect* by bearable CFRP-strip stress  $\Delta F_{FLk,KF}$  (see Fig. 6.3).

$$\Delta F_{LRd} = \frac{\Delta F_{Lk,BL} + \Delta F_{Lk,BF} + \Delta F_{Lk,KF}}{\gamma_{BA}} \quad (6.27)$$

where:  $\gamma_{BA}$  is a safety coefficient.

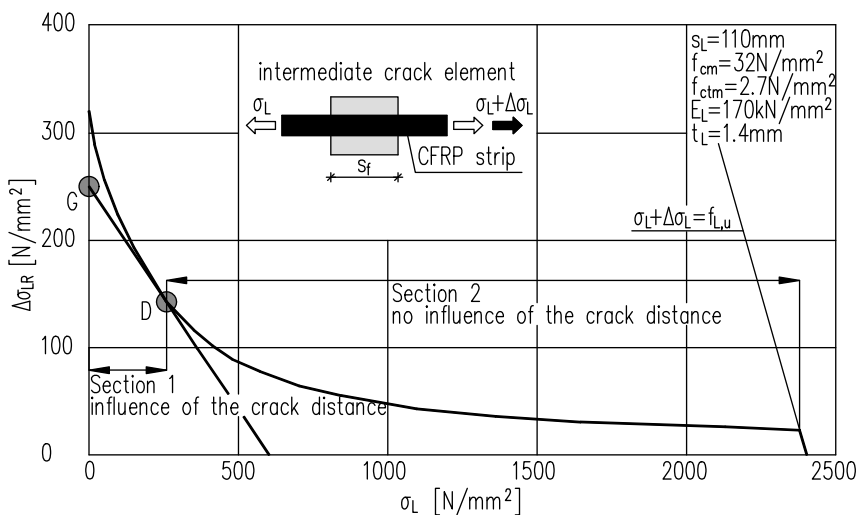


Fig. 6.7. Bond force transfer at ICes for CFRP laminates  $\Delta F_{FLk,BL}$ , (Finckh and Zilch, 2012)

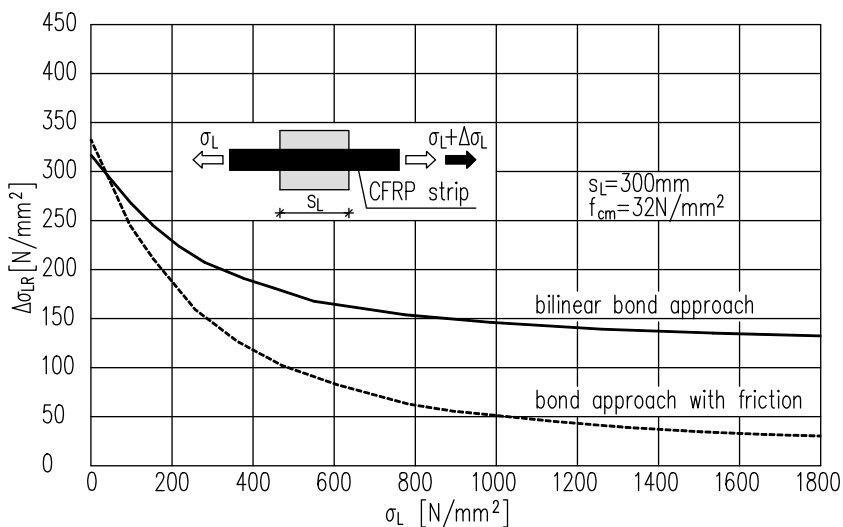


Fig. 6.8. The relationship of the bearable and frictional components of CFRP strip-stresses at the ICE  $\Delta F_{FLk,BF}$ , (Finckh and Zilch, 2012)

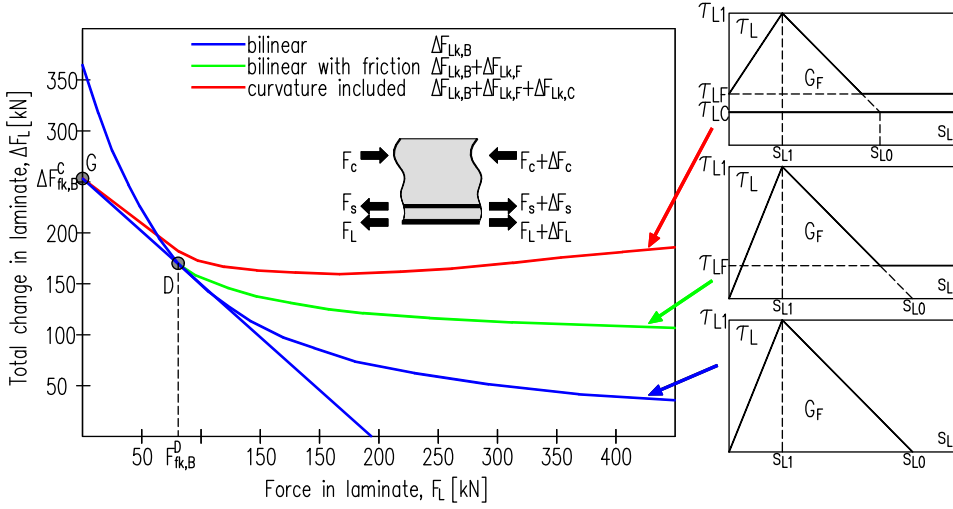


Fig. 6.9. The total change force in CFRP  $\Delta F_L$  in the function of the force in the laminate at less heavily stressed crack edge (Zilch et al., 2012)

The first component  $\Delta F_{FLk,BL}$  of the the bond strength from the bilinear bond stress–slip curve is divided into two parts by point D (Fig. 6.7). The first part of the curve from point G to point D is the linear function corresponding to the range over which the required transfer length of the bilinear bond stress–slip model is greater than the length of the element between cracks  $s_r$ . The bond forces corresponding to points G and D can be determined as:

$$\Delta F_{Lk,BL} = \begin{cases} \Delta F_{Lk,BL}^G - \frac{\Delta F_{Lk,BL}^G - \Delta F_{Lk,BL}^D}{\Delta F_{Lk,BL}^D} F_{LEd} & \text{for } F_{LEd} \leq \Delta F_{Lk,BL}^D \\ \sqrt{b_L^2 \tau_{L1k} s_{L0k} E_{Lm} t_L + F_{LEd}^2} - F_{LEd} & \text{for } F_{Lk,BL}^D < F_{LEd} \leq F_{Lud} \end{cases} \quad (6.28)$$

$$\Delta F_{Lk,BL}^G = \begin{cases} b_L \sqrt{\tau_{L1k} s_{L0k} E_{Lm}} \frac{s_r}{l_{bL,max}} \left( 2 - \frac{s_r}{l_{bL,max}} \right) & s_r < l_{bL,max} \\ b_L \sqrt{\tau_{L1k} s_{L0k} E_{Lm}} & s_r \geq l_{bL,max} \end{cases} \quad (6.29)$$

$$F_{Lk,BL}^D = \frac{b_L t_L s_{L0k} E_{Lm}}{s_r} - \tau_{L1k} \frac{s_r b_L}{4} \quad (6.30)$$

$$\Delta F_{Lk,BL}^D = \sqrt{b_L^2 \tau_{Llk} s_{L0k} E_{Lm} t_L + F_{Lk,BL}^D}^2 - F_{Lk,BL}^D \quad (6.31)$$

The effective bond length  $l_{bL,max}$  required for this can be determined via the bond parameters of the bilinear bond stress–slip relationship and the empirical calibration coefficient  $\kappa_{Lb} = 1.128$  from the following equation:

$$l_{bL,max} = \frac{2}{\kappa_{Lb}} \sqrt{\frac{s_{L0k} E_{Lm} t_L}{\tau_{Llk}}} \quad (6.32)$$

The second component of frictional bond between the debonded laminate and the concrete surface, which can only occur after point D is  $\Delta F_{FLk,BF}$  force is determined as:

$$\Delta F_{Lk,BF} = \begin{cases} 0 & \text{for } F_{LEd} \leq F_{Lk,BL}^D \\ \tau_{LFk} b_L \left[ s_r - \frac{2t_L E_{Lm}}{\tau_{Llk}} \right] \times \\ \times \left( \sqrt{\frac{\tau_{Llk} s_{L0k}}{t_L E_{Lm}} + \frac{F_{LEd}^2}{b_L^2 t_L^2 E_L^2}} - \frac{F_{LEd}}{b_L t_L E_{Lm}} \right) & \text{for } F_{Lk,BL}^D < F_{LEd} \leq F_{Lud} \end{cases} \quad (6.33)$$

The third component  $\Delta F_{FLk,KF}$  depending on the curvature of the RC member proposed by Zilch et al. (2010) was the first to investigate and quantify this effect. A convex curvature deflection causes a change in direction at each concrete element between cracks, which therefore leads to a self–induced contact pressure. This contact pressure on the EB FRP reinforcement brings about an increase in the bond strength.

The component  $\Delta F_{FLk,KF}$  can be determined as:

$$\Delta F_{Lk,KF} = s_r \kappa_k \frac{\varepsilon_{Lr1} - \varepsilon_{cr1}}{h} b_L \quad (6.34)$$

where:  $\varepsilon_{cr1}$  and  $\varepsilon_{Lr1}$  are the concrete and CFRP laminate strains, respectively;  $\kappa_k = 24.3 \times 10^3 \text{ N/mm}$  is the empirical coefficient as the curvature effect on the bond.

The accurate analysis of the concrete element between cracks is not suitable for manual calculations because the critical cross-section is not easy to define for the design purpose. However, this complex analysis is relatively well-suited to computer calculations because case distinction is hardly necessary.

**The simplified analysis of an element between cracks**

A simpler approach for the bond analysis proposed in the DAfStb (2014) is to limit the change in the FRP force according to Fig. 6.10.

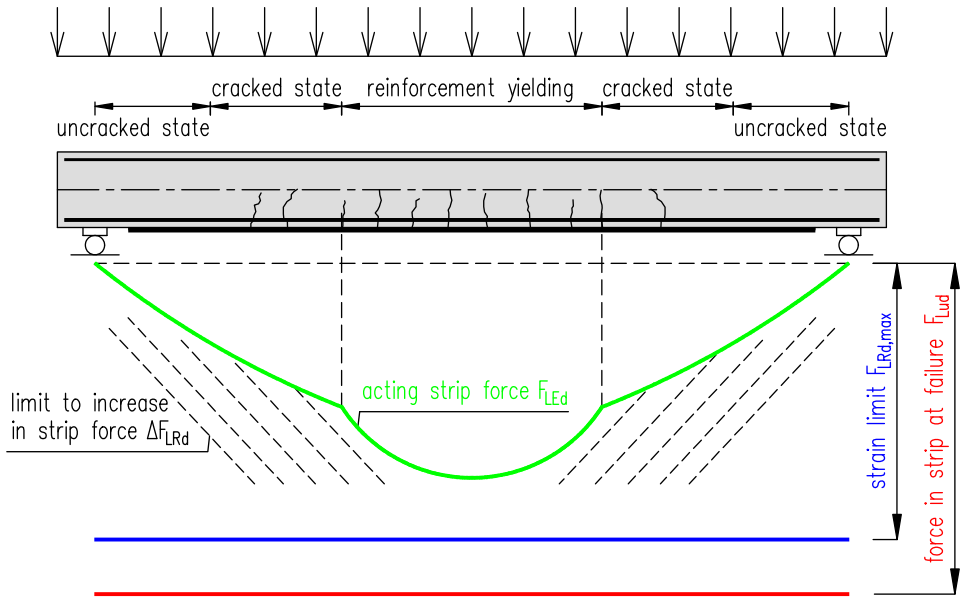


Fig. 6.10. The scheme for simplified analysis of ultimate FRP strain and change in the FRP force in concrete segment between cracks (Zilch et al., 2012)

The strain in the FRP must not exceed the minimum of 0.01 and  $f_{bd}/E_f$  at any point. The elements between cracks appear at the maximum moment and extend to the last crack which is closest to the point of zero bending moment.

The simplified analysis requires to verifying if the change in the strip force does not exceed a constant resistance value at any point in the member. This resistance value, limited by the dotted line corresponding to the limit of the FRP force increase, can be determined in the numerical approach to the more accurate method. Because of this complexity disadvantage, the principle of superposition is no longer valid. But the model can also be simplified by using

the following equation for the bond resistance to FRP force difference in the concrete segment between cracks:

$$\Delta F_{LRd} = s_r \kappa_k \frac{2,3\tau_{L1k} \sqrt{s_r} + 0,098\tau_{LFk} s_r^{4/3} + \frac{\kappa_h}{h} s_r^{1/3}}{\gamma_{BA}} b_L \quad (6.35)$$

were: factor  $\kappa_h = 2000$  for RC members and  $\kappa_h = 0$  for prestressed concrete members, which has the influence the curvature.

### 6.1.4. End anchorage analysis

The analysis of the end anchorage is the second required condition after the analysis of bond at the concrete segment between cracks. The end anchorage analysis can be performed in three different ways:

1. End anchorage analysis at flexural crack nearest to the point of contraflexure
2. Anchorage analysis at the arbitrary concrete element between cracks
3. End anchorage analysis with the shear wrapping

#### *End anchorage analysis at flexural crack nearest to the point of contraflexure*

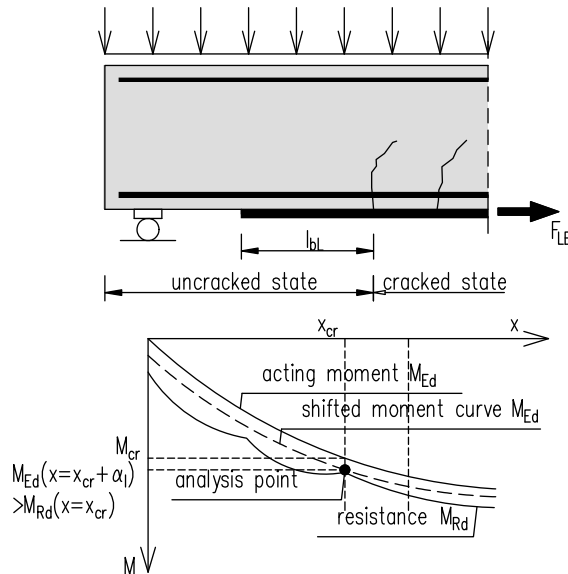


Fig. 6.11. Scheme for analysis of the end anchorage of EB CFRP reinforcement at flexural crack nearest to the point of contraflexure (Zilch et al., 2012)

The analysis at the flexural crack closest to the point of contraflexure represents the standard case shown in Fig. 6.11. In this case, the moment acting at this flexural crack must be lower than the resistance of the cross-section taking the “shifted curves” into account.

The resistance of the cross-section is determined on the basis of the bond conditions, which consider redistribution between the EB FRP reinforcement and the internal reinforcement. Considering the different bond behaviour and depending on the strain state of the EB FRP reinforcement, a different distribution of the forces between various lines of reinforcement occurs, which is presented in Figures 6.11, 6.12 and 6.13.

The analysis is carried out at the position of the flexural crack nearest to the point of contraflexure. As the analysis considers the interaction of the lines of reinforcement, it includes the acting moment and the moment that can be accommodated by the crosssection according to the formula:

$$M_{Ed} \leq M_{Rd}(l_{bL}) \quad (6.36)$$

The admissible moment is determined depending on the strains in the lines of reinforcement using the formula:

$$M_{Rd}(l_{bL}) = \varepsilon_{LRk}^a(l_{bL})E_{lm}A_Lz_L^a \frac{1}{\gamma_{BA}} + \varepsilon_{sRk}^a(l_{bL})E_sA_s z_s^a \frac{1}{\gamma_s} \quad (6.37)$$

This sufficiently extends anchorage length for the steel reinforcement.

The strain in the strengthening element depending on the bond length available beyond the flexural crack closest to the point of contraflexure should be calculated as:

$$\varepsilon_{LRk}^a(l_{bL}) = \begin{cases} \sin\left(\frac{\pi}{2} \frac{l_{bL}}{l_{bL,lim}}\right) \varepsilon_{LRk,lim}^a & \text{for } 0 < l_{bL} < l_{bL,lim} \\ \varepsilon_{LRk,lim}^a & \text{for } l_{bL,lim} \leq l_{bL} \end{cases} \quad (6.38)$$

where: the effective bond length  $l_{bL,lim}$  and the maximum strain  $\varepsilon_{LRk,lim}^a$  can be calculated on the basis of the bilinear bond stress–slip relationship (Fig. 6.6) as:

$$\varepsilon_{LRk,lim}^a = 0.985 \frac{f_{bLk,max}}{E_{Lm}} \quad (6.39)$$

$$l_{bL,lim} = 0.86l_{bL,max} \quad (6.40)$$

$$f_{bLk,max} = \sqrt{\frac{E_{Lm} s_{L0k} \tau_{L1k}}{t_L}} \quad (6.41)$$

$$l_{bL,max} = \frac{2}{\kappa_{Lb}} \sqrt{\frac{E_{Lm} t_L s_{L0k}}{\tau_{L1k}}} \quad (6.42)$$

The strain in the reinforcing steel is calculated depending on the slip of the strip  $s_{Lr}$ , the bond factor  $\kappa_{bsk}$  and the weighting of the different lever arms.

$$\varepsilon_{sRk}^a(l_{bL}) = \kappa_{VB} \kappa_{bsk} [s_{Lr}^a(l_{bL})]^{(\alpha_n+1)/2} \left( \frac{d^a - x^a}{d_L^a - x^a} \right)^{(\alpha_n+1)/2} \leq \frac{f_{byk}}{E_s} \quad (6.43)$$

where:  $\alpha_N = 0.25$  for ribbed reinforcement and  $\alpha_N = 0$  for plain reinforcement;  $\kappa_{VB} = 1$  for good bond conditions and  $\kappa_{VB} = 0.7$  for moderate conditions; other coefficients are taken from Table 6.1.

The bond factor  $\kappa_{bsk}$  is calculated as:

$$s_{Lr}^a(l_{bL}) = \begin{cases} 0.213mm \left[ 1 - \cos\left(\frac{\pi}{2} \frac{l_{bL}}{l_{bL,lim}}\right) \right] & \text{for } 0 < l_{bL} \leq l_{bL,lim} \\ 0.213mm + (l_{bL} - l_{bL,lim}) \varepsilon_{LRk,lim}^a & \text{for } l_{bL,lim} \leq l_{bL} \end{cases} \quad (6.44)$$

$$\kappa_{bsk} = \kappa_{b1k} \sqrt{\frac{f_{cm}^{\kappa_{b2}}}{E_s \phi^{\kappa_{b3}} (E_{Lm} t_L)^{\kappa_{b4}}}} \quad (6.45)$$

### ***Anchorage analysis at an arbitrary concrete element between cracks***

In the second way of carrying out the end anchorage analysis at the segment between cracks in RC members with the low tensile concrete strength, the flexural crack closest to the point of contraflexure is located very close to the support. In this analysis, externally bonded reinforcement has to be anchored at an arbitrary element between cracks similarly to the analysis for the concrete segment between cracks shown in Fig. 6.12.

Besides considering shifting of the curves, the cross-section between the support and the element between cracks must have sufficient load carrying capacity even without externally bonded reinforcement. It is clear that the last element between cracks must be checked to ensure that the acting FRP force without redistribution  $F_{LEd}$  is less than the bond resistance at the idealized end anchorage body  $F_{bLRd}$ :

$$F_{LEd} \leq F_{bLRd} \quad (6.46)$$

In this analysis, the last concrete segment between cracks may be positioned at the end of the strip and may have a length corresponding to the crack spacing:

$$s_r = 1,5l_{e,0} \quad (6.47)$$

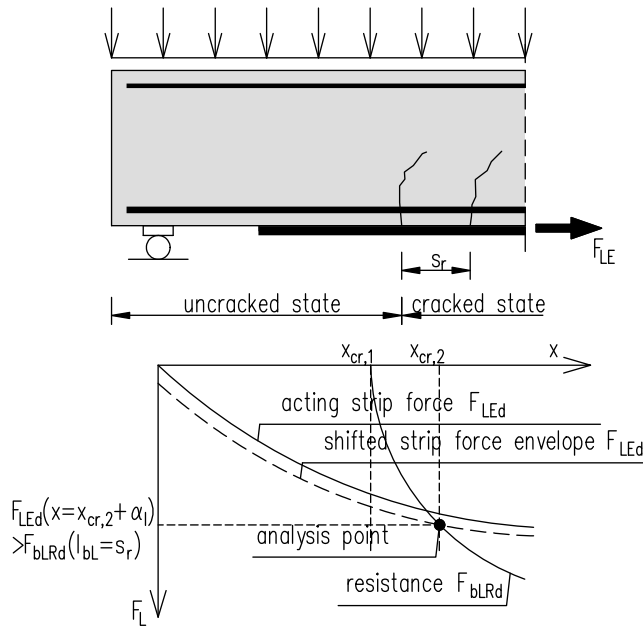


Fig. 6.12. Scheme for analysis of the end anchorage of EB CFRP reinforcement at an arbitrary concrete element between cracks (Zilch et al., 2012)

The resistance to debonding at the last segment between cracks is similar to that tested on the idealized end anchorage body and evaluated on the basis of the bilinear bond stress–slip relationship. Therefore, the bond resistance can be calculates as:

$$F_{bLRd} = b_L t_L f_{bLd}(s_r) \quad (6.48)$$

$$f_{bLd}(s_r) = \frac{f_{bLk}(s_r)}{\gamma_{BA}} \quad (6.49)$$

$$f_{bLk}(s_r) = \begin{cases} f_{bLk,max} \frac{s_r}{l_{bL,max}} \left( 2 - \frac{s_r}{l_{bL,max}} \right) & s_r < l_{bL,max} \\ f_{bLk,max} & s_r \geq l_{bL,max} \end{cases} \quad (6.50)$$

$$f_{bLk,max} = \sqrt{\frac{E_{Lm} s_{L0k} \tau_{Llk}}{t_L}} \quad (6.51)$$

$$f_{bL,max} = \frac{2}{\kappa_{Lb}} \sqrt{\frac{E_{Lm} s_{L0k} t_L}{\tau_{Llk}}} \quad (6.52)$$

**End anchorage analysis with shear wrapping**

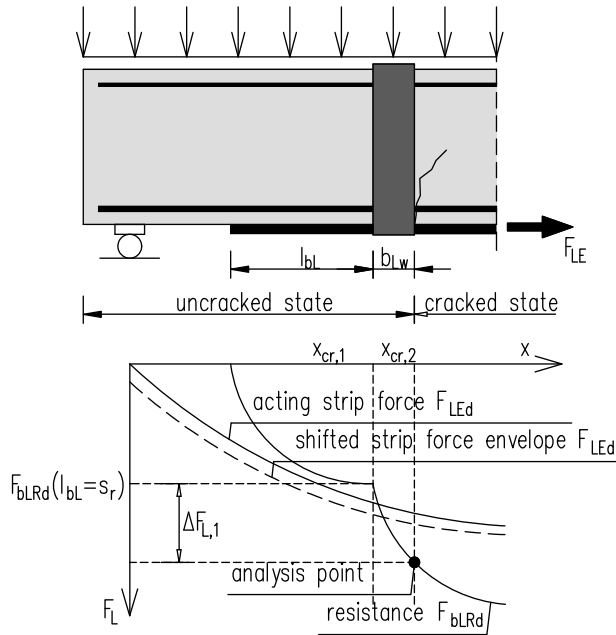


Fig. 6.13. The scheme for the analysis of the end anchorage of EB CFRP reinforcement with shear wrapping (Zilch et al., 2012)

The third way of end anchorage analysis with the shear wrapping is needed to design the shear strengthening or to avoid a concrete cover separation failure, and to increase the bond force (Fig. 6.13). The concept of increasing the bond

force as a consequence of shear wrapping was proposed by Husemann (2002). The resistance at the end of the shear wrapping is compared with the shifted strip force envelope. The increase in the bond force due to the shear wrapping  $\Delta F_{L,1}$  is added to the end anchorage force of the CFRP segment beyond the shear wrapping. The resistance at the end of the shear wrapping is calculated as:

$$F_{bLRd} = b_L t_L f_{bLd}(l_{bL}) + \frac{\Delta F_{L,1}}{\gamma_{BA}} \quad (6.53)$$

$$\Delta F_{L,1} = \frac{t_L b_L b_{Lw}}{120} \sqrt{\frac{f_{ctm,surf}}{1,33}} \left[ 230 \kappa_I \frac{F_u(\alpha_b)}{b_L b_{Lw}} - 23 \left( \kappa_I \frac{F_u(\alpha_b)}{b_L b_{Lw}} \right)^2 \right] \quad (6.54)$$

where:  $b_{Lw}$  is the width of the transversal shear strap; the contact pressure  $F_u(\alpha_b)$  and the factor  $\kappa_I$  to take into account the form of the wrapped strip cross-section can be calculated as:

$$F_u(\alpha_b) = F_{u,2} \frac{0,8 - \alpha_b}{0,4} + F_{u,4} \frac{\alpha_b - 0,4}{0,4} \quad (6.55)$$

To calculate the contact pressure, a distinction is made between the contact pressures  $F_{u,2}$  and  $F_{u,4}$ , which are always formed by the two geometric limit cases shown in Fig. 6.14.

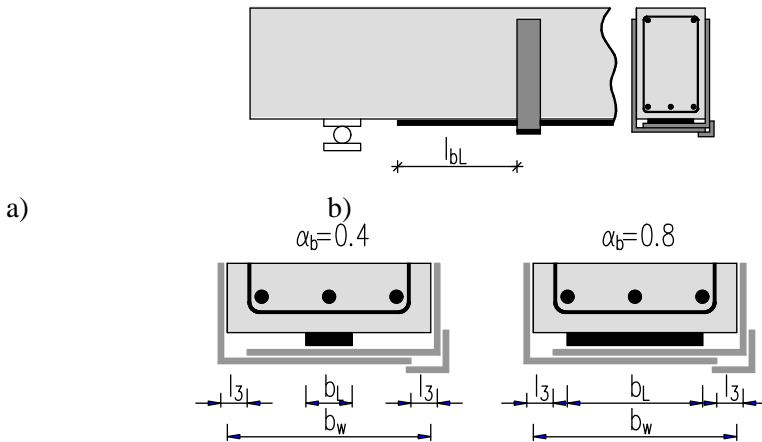


Fig. 6.14. RC cross section beam with EB CFRP strip and shear wrapping (Zilch et al., 2012): a) detail A, b) detail B

Interpolation between two limit cases (according to formula 6.55) is possible depending on the geometry factor  $0.4 \leq \alpha_b = b_L/b_W \leq 0.8$ .

The contact pressures depend on the stiffness of the shear wrapping in all cases. It is therefore necessary to calculate the stiffness of the shear wrapping first, which is generally made up of two L–straps and one closure piece bonded with adhesive (Fig. 6.14) corresponding in further analysis of two cases: Detail A and Detail B.

#### **Detail A**

This case consists of two bonded L–straps (Fig. 6.14.a)  
Stiffness analysis should be determined as:

$$EI_{S,A} = 2E_S \left( I_S + A_S z_{S,A}^2 \right) \quad (6.56)$$

$$z_{S,A} = \frac{1}{2} t_{Lw} + 0.5 \quad (6.57)$$

#### **Detail B**

This case consists of two bonded L–straps and one closure piece (Fig. 6.14.b)

$$EI_{S,B} = 2E_S \left( I_S + A_S z_{S,B}^2 \right) + E_S I_S \quad (6.58)$$

$$z_{S,B} = t_{Lw} + 1.0 \quad (6.59)$$

Using these variables it is now possible to determine the contact pressures for the two limit cases corresponding to coefficient:  $\alpha_b = 0.4$  and  $0.8$ .

The contact pressure for limit case  $\alpha_b = 0.4$  can be calculated as:

$$F_{u,2} = \frac{48EI_{s,g,\alpha_b=0.4}}{\left(3\alpha - 4\alpha^3\right)_2^3} w_1 + \frac{26400EI_{s,g,\alpha_b=0.4}}{11000l_1^3 + 2,4EI_{s,g,\alpha_b=0.4}} \quad (6.60)$$

$$l_1 = 0.3b_w - 20 \text{ and } l_2 = b_w - 40.$$

The crack width for CFRP strips is then  $w = 0.35$ .

$$w_1 = w - 0.1 \left( 1 - \frac{2EI_{s,g,\alpha_b=0.4}}{4583l_1^3 + EI_{s,g,\alpha_b=0.4}} \right) \quad (6.61)$$

$$\alpha = \frac{0.3b_w - 20}{b_w - 40} \quad (6.62)$$

$$EI_{s,g,\alpha_b=0.4} = 2 \frac{EI_{S,A}EI_{S,B}}{EI_{S,A} + EI_{S,B}} \quad (6.63)$$

Consequently, the contact pressure for limit case  $\alpha_b = 0.8$  is given by:

$$F_{u,4} = \frac{48EI_{s,g,\alpha_b=0.8}}{l_4^3} w_2 + \frac{26400EI_{s,g,\alpha_b=0.8}}{11000l_3^3 + 2.4EI_{s,g,\alpha_b=0.8}} \quad (6.64)$$

$$w_2 = w - 0.1 \left( 1 - \frac{2EI_{s,g,\alpha_b=0.8}}{4583l_3^3 + EI_{s,g,\alpha_b=0.8}} \right) \quad (6.65)$$

$$EI_{s,g,\alpha_b=0.8} = 2 \frac{EI_{S,A}E_S I_S}{EI_{S,A} + E_S I_S} \quad (6.66)$$

This results in the lengths:  $l_3 = 20 + t_{LW}$  and  $l_4 = 2l_3$ .

The crack width for CFRP strips is then  $w = 0.35$ .

## 6.2. Fundamental mechanics model

The mechanics of a displacement based on *three-dimensional partial-interaction moment-rotation model* was proposed by Oehlers et al. (2015) to determine two distinct but interacting forms of flexural IC debonding. According to possible failure modes (described in details in Chapter 3), two of them are considered in this analysis:

- plate end debonding – PED,
- intermediate crack debonding – ICD.

The IC debonding initiates at the maximum bending moment region in the vicinity of the flexural crack in the interface shear between the FRP laminate and the concrete. This mode of debonding is strongly affected by the interface shear stress  $\tau$  and the normal stress  $\sigma$  in the interface of the FRP and concrete and it depends on the vertical shear force as well.

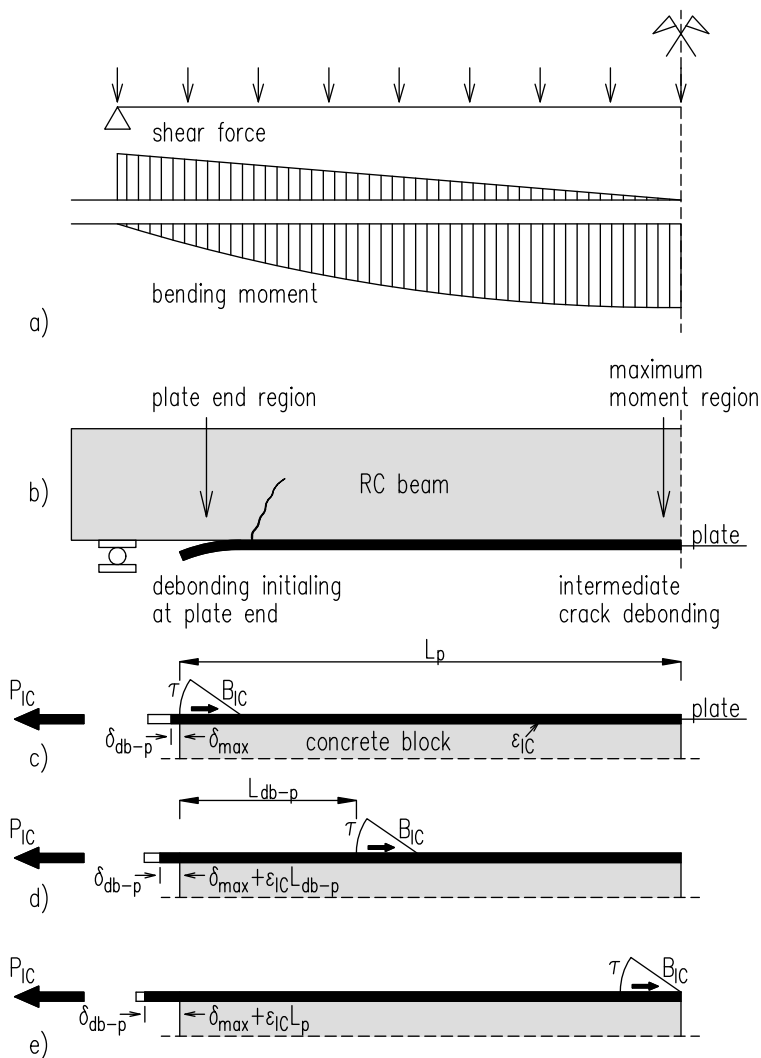


Fig. 6.15. Types of debonding mechanisms (Oehlers et al., 2015)

There are two approaches to be considered in the analysis of the flexural IC debonding.

1. **Local segmental IC debonding** at concentrations of the beam rotation. The maximum force in the FRP reinforcement  $P_{IC}$  and, consequently, the maximum strain  $\epsilon_{IC}$  are limited by the bond-slip properties between the FRP reinforcement and adjacent concrete, which depend on the beam geometry and material properties.

2. **Global member IC debonding** is based on the progressive IC debonding along the beam after local segmental debonding. The deboned FRP in the central region acts as an FRP prestressing tendon (attached at its ends to the concrete substrate), in contrast to the FRP reinforcement, with a prestressing force  $P_{IC}$ .

For general cases the example based on the single span beam is analyzed. For this approach the half span of the RC beam strengthened with externally bonded laminate bonded on the length of  $L_p$  is considered. The beam loaded with distributed load is subjected to the bending moment shown in Fig. 6.15.

There are several possible IC debonding mechanisms shown in Fig 6.15 a–e. The first one (a) starts at maximum bending moment and then propagates towards the support. The IC debonding mechanism is similar to the pull-out test with the FRP laminate bonded to a concrete block over the long distance (Fig. 6.15.c). If the tensile force  $P$  in the FRP laminate exceeds the bond force  $B_{IC}$ , the slip of the FRP reaches the maximum slip capacity  $\delta_{max}$ . Then the force at the FRP end leads the IC debonding, corresponding to  $P_{IC}$  and the FRP strain reaches  $\varepsilon_{IC}$  with the extension  $\delta_{db-p} = \delta_{max}$ .

If the FRP is pulled further, the bond force remains at  $B_{IC}$ . Hence the force in the FRP remains as  $P_{IC}$  and the extension is then a sum the extension of the debonded region  $L_{db-p}$  (with the FRP strain  $\varepsilon_{IC}$ ) and that of  $\delta_{db-p}$ . If the FRP debonding reaches the full its length (Fig. 6.15.e), the extension of the FRP is  $\delta = \delta_{max} + \varepsilon_{IC}L_p$ .

The *mechanics based generic model* can be used for designing flexurally strengthened RC members with EB FRP laminates directly or to improve the existing design techniques. This general model can be adopted for new techniques such as for new FRP reinforcement with new bond characteristics.

**Segmental debonding mechanisms**

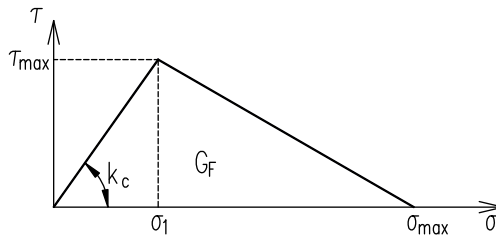


Fig. 6.16. Bilinear (elastic-softening) law at the FRP-to-concrete interface (Oehlers et al., 2015)

The shear stress-slip  $\tau - \delta$  FRP-to-concrete bond characteristics depends on the interface slip along the sliding plane  $\delta$  (Fig. 6.16). This debonding affects the behaviour of FRP strengthened RC beams but generally not in a detrimental way, as will be further explained.

**Multiple crack segment debonding**

The analysis considers a segment of a beam limited by two adjacent flexural cracks at spacing “S” and within a constant moment region (Fig. 6.17).

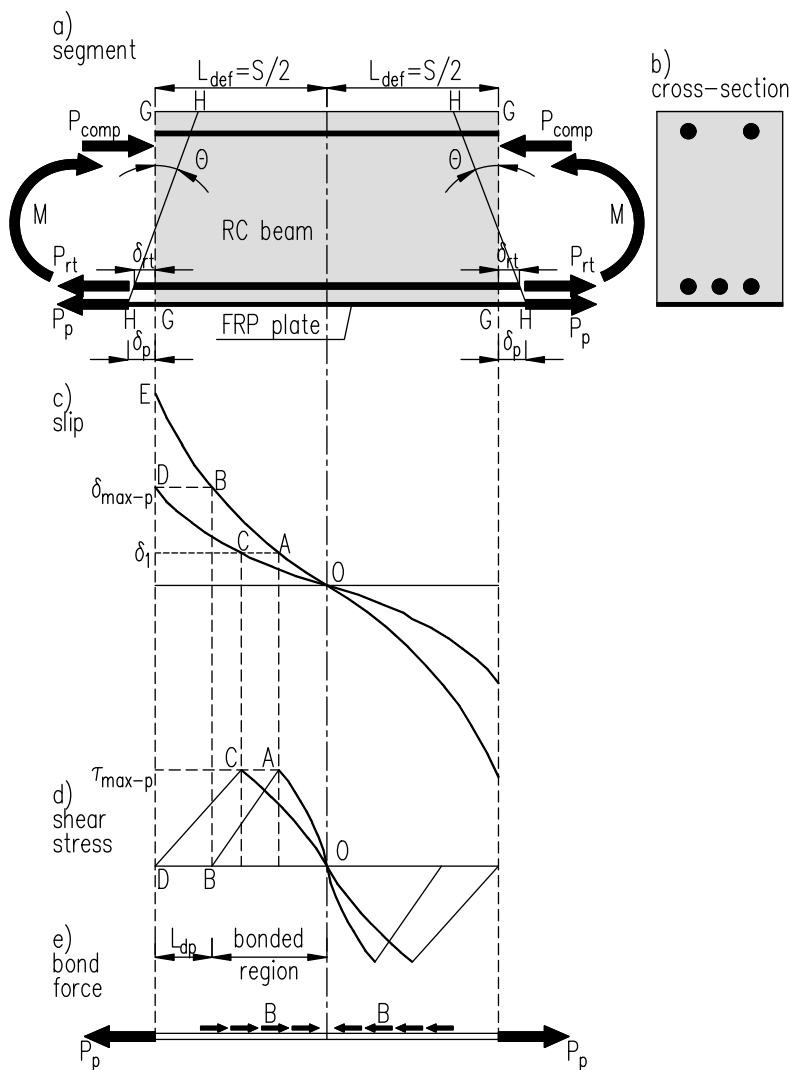


Fig. 6.17. Segmental multiple crack debonding (Oehlers et al., 2015)

The Euler-Bernoulli displacement is applied to the sides of the segment whose each side rotates from G-G to H-H to cause a rotation  $\theta$  (Fig. 6.17). This induces a tensile force in the steel reinforcement  $P_{rt}$  and in the FRP plate, which causes the reinforcement slip in relation to the crack face by  $\delta_{rt}$  and  $\delta_p$ . The crack width  $w$  at the level of the steel reinforcement is  $2\delta_{rt}$  and that at the plate  $2\delta_p$ . As the segment is symmetrically loaded, the behaviour on both sides of the segment has the identical values. With gradual increase in  $\theta$  rotation angle, the gradual slip along the FRP laminate increases along the segment length until it reaches D-C-O position, which corresponds to the slip at the crack face  $\delta_p$  at point D that is the maximum bond slip to transfer shear for the slip  $\delta_{max-p}$ , that is  $\delta_{max}$  in Fig. 6.17.c for the FRP-to-concrete bond-slip characteristics. When  $\delta_{max-p}$  is achieved at point D (Fig. 6.17.c), the shear stress distribution shown as D-C-O in Fig. 6.17.d is fully developed so that the integration of the shear stress distribution D-C-O over the surface of the half length of segment  $S/2$  gives the maximum bond force  $B_{max-p}$ .

If the slip increases to E-B-A-O, the region where the slip is greater than  $\delta_{max-p}$  (that is E-B), the shear stress goes to zero. Then the region is debonded, as it is shown as  $L_{db}$  in Fig. 6.17.d. The shear stresses B-A-O are then concentrated over a smaller length, so that the bond force  $B$  is reduced from  $B_{max-p}$ . Further increase in slip causes the bond force  $B$  and the bonded region in Fig. 6.17.e tends to zero. However, it can be seen that this form of debonding does not limit the force in the reinforcement  $P_p$ , irrespectively of a type of reinforcement. This form of debonding is important in terms of tension stiffening but not as far as the ultimate strength is concerned.

### ***Single crack segment debonding***

If the single crack is considered in a constant moment region (Fig. 6.18.a), the Euler-Bernoulli displacements H-H cause a crack width at the level of the steel reinforcement and FRP reinforcement of  $2\delta_{rt}$  and  $2\delta_p$  respectively, where  $\delta_{rt}$  and  $\delta_p$  are the slips of the reinforcement relative to the crack faces, which occur at forces  $P_{rt}$  and  $P_p$ , respectively, as it is shown in Fig. 6.18.

If the rotation angle  $\theta$  increases (Fig. 6.18.a), the FRP laminate slip at the crack face  $\delta_p$  increases to  $\delta_{max-p}$  (Fig. 6.18.b), which allows the bond stresses increase (Fig. 6.18.c).

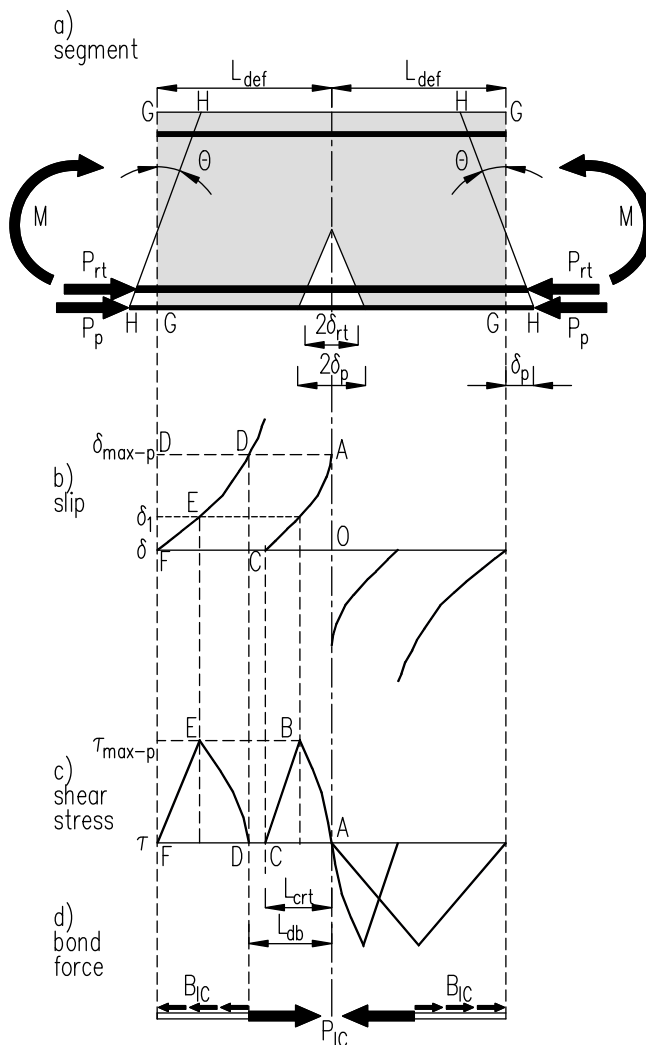


Fig. 6.18. Segmental single crack debonding

The integration of this fully developed bond stress distribution over the bonded surface area gives the maximum bond force  $B_{IC}$ . Consequently, the maximum force the reinforcement can resist at the IC debonding  $P_{IC}$  corresponds to the strain in the reinforcement equal to  $\epsilon_{IC}$ . The minimum length of the FRP reinforcement required to develop  $P_{IC}$  is referred to the critical length  $L_{crit}$  (Fig. 6.18.c), which is the minimum crack spacing. Any increase in  $\delta_p$  above  $\delta_{max-p}$  causes a rigid body movement of the stress block from A-B-C to

D-E-F position (Fig. 6.18.c) that results in FRP debonding length  $L_{db}$ , whilst the reinforcement force remains constant at  $P_{IC}$ . This is a stable form of debonding, which leads to stable rotation and ductility.

On the basis of the analysis of two segmental debonding mechanisms described in this section (named as *multiple and single crack segment debonding*) the IC debonding strain  $\varepsilon_{IC}$  is very sensitive to the crack position and the bending moment distributions.

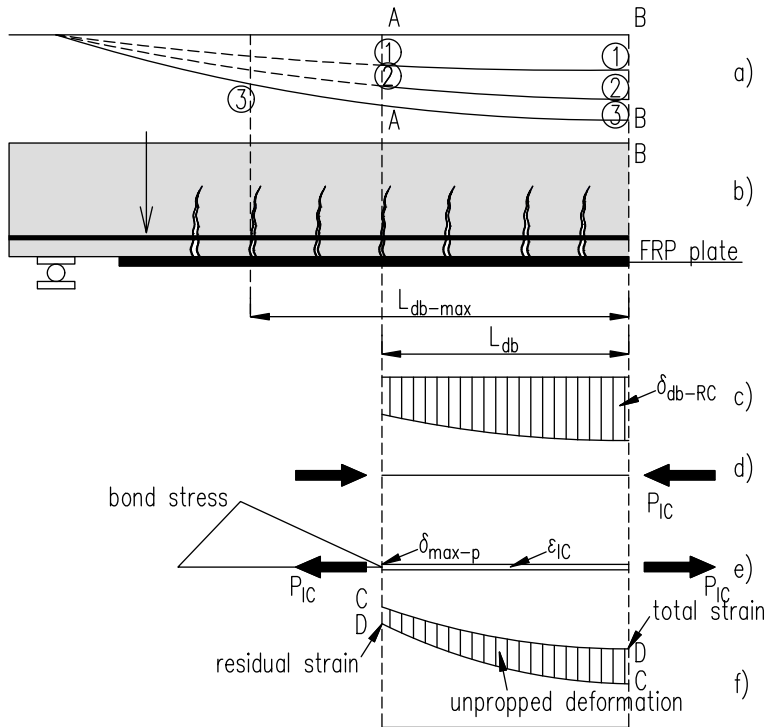


Fig. 6.19. Member passive prestress debonding mechanism

$$\delta_{db-p} = \delta_{max-p} + \varepsilon_{IC} L_{db} \text{ (Oehlers et al., 2015)}$$

For practical purposes, stable behaviour of the cracking pattern and stable ductility of the RC beams is assumed with the limit of the FRP strain to the safe value corresponding to the IC debonding.

The applied bending moment along the beam's length causes deformations associated with a single crack (presented in Fig. 6.19.a). If the tensile force in the FRP laminate reaches  $P_{IC}$ , the IC debonding occurs.

When the FRP laminate starts to debond, the distance  $L_{db}$  between sections A-A and B-B is completely detached from the RC member so that the FRP laminate does not act as the external reinforcement. However, it acts in transfer of the tensile force  $P_{IC}$  as an unbonded prestressing external tendon along the line of the FRP laminate (Fig. 6.19.d).

This prestressing force (called passive prestressing  $P_{pp}$ ), in the absence of mechanical anchorage equals to  $P_{IC}$  value. The aim is to find the moment distribution that causes FRP debonding on the length  $L_{db}$ . The force  $P_{IC}$  in the IC FRP debonding occurs at the FRP tendon strain  $\varepsilon_{IC}$ . Hence the material extension of the tendon within  $L_{db}$  is equal to  $\varepsilon_{IC}L_{db}$  and the total extension between sections A-A and B-B, due to the FRP material extension and bond slip, is calculated as:

$$\delta_{db-p} = \delta_{max-p} + \varepsilon_{IC}L_{db} \quad (6.67)$$

If the concrete strain in the bottom surface of the beam is  $\varepsilon_{RC}$ , then the total strain over length  $L_{db}$  gives the deformation of the RC beam at the level of the FRP plate  $\delta_{db-RC}$  that can be calculated as:

$$\delta_{db-RC} = \int_0^{L_{db}} \varepsilon_{RC} \quad (6.68)$$

A segment between adjacent cracks of length  $2L_{def}$  is similar to that of the *multiple crack segment* (Fig. 6.20) except the FRP laminate that is replaced by a prestressing force of  $P_{IC}$ .

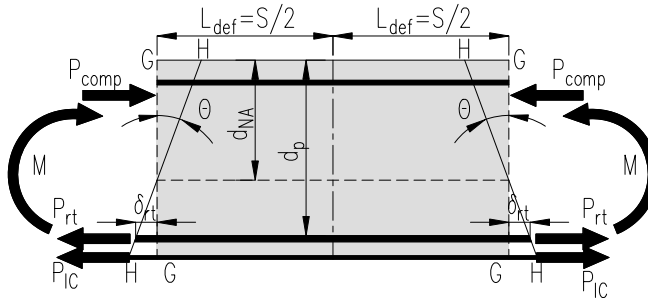


Fig. 6.20. Passively prestressed RC segment (Oehlers et al., 2015)

The results from the moment-rotation ( $M - \theta$ ) analysis of a *passively prestressed* segment are shown in Fig. 6.21.a, where  $M_{u-pp}$  is the ultimate moment of the passively prestressed segment. Based on the curvature  $\chi = \theta/L_{def}$ , the required bottom concrete strain  $\varepsilon_{RC}$  can be calculated as:

$$\varepsilon_{RC} = \chi(d_p - d_{NA}) \quad (6.69)$$

The calculations are repeated by extending  $L_{db}$  until the maximum moment capacity of the passively prestressed RC beam according to the moment distribution 3-3 until the moment  $M_{u-pp}$  (Fig. 6.18.a), which corresponds to the length of the debonded distance equal to  $L_{db-max}$ . Then the extent of the FRP bonding is a sum of  $L_{db-max}$  and the anchorage length  $L_{crit}$  (defined in Fig. 6.21).

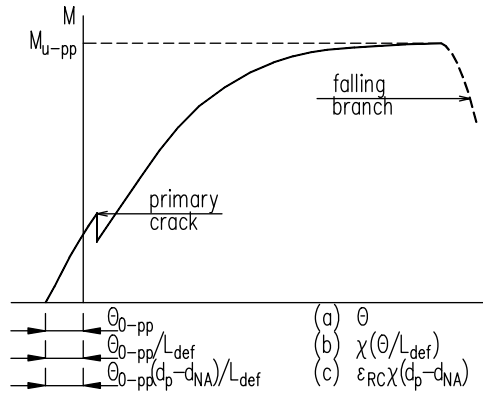


Fig. 6.21. Behaviour from passively prestressed segment (Oehlers et al., 2015)

This ensures that the full strength of the FRP passively prestressed member is achieved. In theory, the falling branch can be taken into account in a collapse analysis (Fig. 6.21).

### Segmental solutions for debonding

Considering the case of beam strengthened with FRP laminate subjected to serviceability loads, two approaches should be considered:

- 1) the beam subjected to the serviceability loads prior to strengthening, does need considering the residual stresses or deformations in the beam prior its retrofitting, however closed flexural cracks are present;
- 2) the beam is subjected to loads over its self weight prior to strengthening.

---

**IC debonding segmental analysis**

Beginning with the single crack analysis of the unloaded RC member by strengthening, only one crack can be considered (Fig. 6.17.a). The concrete softening can be achieved  $L_{def} > L_{wdg}$ , ( $L_{def}$  and  $L_{wdg}$  are lengths of the segment and the length of the wedge), which depends on the depth of the neutral axis  $d_{NA}$ . Based on the approach by Visintin et al. (2015) with the angle of the wedge  $\alpha = 26^\circ$  the length of the segment  $L_{def}$  needs to meet the following conditions:

- for the steel reinforcement:  $L_{def} > L_{crit-rt}$
- for the FRP laminate:  $L_{def} > L_{crit-p}$

to allow the shear stress distributions and, consequently, IC debonding.

Using the Euler-Bernoulli displacement principle with the rotation angle  $\theta$ , prior to flexural cracking and concrete softening due to the formation of the concrete wedge, based on a linear strain profile A-B-C, the curvature is calculated as  $\chi = \theta/L_{def}$ . From the strain distribution, the stress profile can be derived and then the force distribution along the beam's height can be calculated with the concrete compressive force  $P_{cc}$ ; the compressive force in the steel reinforcement  $P_{rc}$ ; the tensile force in concrete  $P_{ct}$  (can be omitted in practice); the tensile steel and FRP reinforcement  $P_{rt}$  and  $P_p$ ; respectively. For a fixed rotation  $\theta$ , the neutral axis depth  $d_{NA}$  can be calculated on the basis of the equilibrium of the internal forces and the applied bending moment  $M$  (Fig. 6.22.e).

The flexural cracking occurs when the moment reaches  $M_{cr-FI}$ .

After cracking and prior to the formation of the softening wedge, only the strain profile A-B can be applied and then the internal forces distribution with the neutral axis location (Fig. 6.22.b) can be determined. In the cracked zone (B-C), the force in the steel reinforcement and the FRP laminate depends on the slip  $\delta_{rt-SC}$  and  $\delta_{p-SC}$  consequently the  $R_{rt-SC}/\delta_{rt-SC}$  and  $P_{p-SC}/\delta_{p-SC}$ , on the basis of the tension stiffening analysis.

The rotation can be increased until IC debonding in the FRP or in the steel reinforcement. If the IC debonding occurs first, the force in FRP laminate reaches  $P_{IC-p}$  value, which can be determined from the tension-stiffening principle. This force occurs when the half crack width at the FRP  $\delta_{p-SC} = \delta_{max-p}$  for the FRP bond-slip properties (Fig. 6.22.a), achieves IC FRP debonding moment  $M_{IC-p}$ .

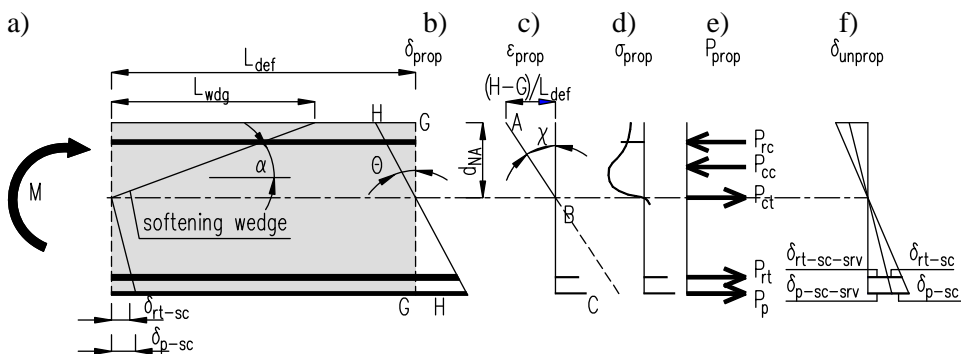


Fig. 6.22. IC debonding mechanism

Before the strengthening that is performed in the beam under serviceability moment, the half crack width at the steel reinforcement and at the FRP levels equals to  $\delta_{rt-sc-srv}$  and  $\delta_{p-sc-srv}$ , respectively. After strengthening and growth of the bending moment, the crack width increases by  $\delta_{rt-sc}$  and  $\delta_{p-sc}$  in the steel and FRP levels, respectively (Fig. 6.22.f). Hence the development of the forces in the laminates is delayed behind this one in the steel reinforcement. The same refers to the moment at the beginning of the FRP IC debonding that is larger than that for the propped construction. It seems that unpropped construction is more efficient than a propped one but in the case of ductility it is not approved.

### *Passive prestressed segmental analysis*

Half a segment with the FRP unbonded RC beam along the unbonded FRP distance  $L_{db}$  is presented in Fig. 6.23.a. The half length of the segment  $L_{def}$  needs to be as small as possible to confine all of the wedge length  $L_{wdg}$ . This segment is subjected to a prestressing force equal to the IC debonding resistance of the FRP laminate  $P_{IC-p}$  (Fig. 6.23.a). If the prestressing force is first applied without applied moment  $M$  (such a case never occurs in practice) as this is a passive prestress, this causes a deformation such as A-A (Fig. 6.23.b). Then deformation A-A causing the forces in tensile and compressive reinforcement equal to  $P_{RC}$  and  $P_{rt}$  can be determined; in the tensile and compressive concrete equal to  $P_{cc}$ ,  $P_{ct}$  and  $P_{pc}$  in the FRP prestressing force (Fig. 6.23.c). This analysis gives the prestressing rotation  $\theta_{0-pp}$  shown in Figs. 6.23.

After prestressing, the moment is applied by rotating the displacement profile from A-A to B-B. When the concrete first goes into tension at the soffit of the beam, this gives the moment causing or initiating flexural cracking in this pas-

sively prestressed member  $M_{cr-FI-pp}$ . This is a full-interaction analysis, always applicable in the regions of the beam where a full-interaction is obtained from a standard moment–curvature analysis.

When the initial flexural crack crosses the bottom reinforcement level, then the force in the bottom reinforcement is no longer dependent on the strain but on the deformation analysis.

When  $P_{rt-sc}$  is the force causing the primary cracks  $P_{rt-sc-pr}$ , then the moment at which this occurs  $M_{cr-PI-pr}$  is the moment of multiple primary cracking from a partial–interaction analysis of a partially prestressed beam. Primary cracks occur at the boundary of the partial-interaction region, where there is the full interaction. Hence primary cracking occurs at a moment which is at least of  $M_{cr-FI}$  and  $M_{cr-PI-PP-pr}$ .

When multiple cracks occur with the primary crack spacing equal to  $S_{pr}$ , then the tension stiffening analysis controls this behaviour. The total deformation along the line of the reinforcement  $n\delta_{i-rt}$  is the total deformation at all the crack faces, so for the specific crack distribution in Fig. 6.23.a  $n = 5.0$ . The total rotation is  $n\theta_i$ , where  $\theta_i$  is the rotation of an individual crack face. On further application of displacement, the reinforcement force should cause the secondary cracks, then the crack spacing is equal to  $S_{pr}/2$ , as shown in Fig. 6.23.a. Then the deformation B-B should be determined as the result of the forces in the RC beam (Fig. 6.23.d) that is equal to the prestressing force  $P_{IC}$ .

This state corresponds to a rotation angle  $\theta_{imp} = n\theta_i$  and the depth of the neutral axis  $d_{NA}$  until the force reaches  $P_{IC}$ . Then the moment of these forces about the level of the passive prestress  $P_{IC}$  is the moment  $M$  causing the imposed rotation  $\theta_{imp}$ .

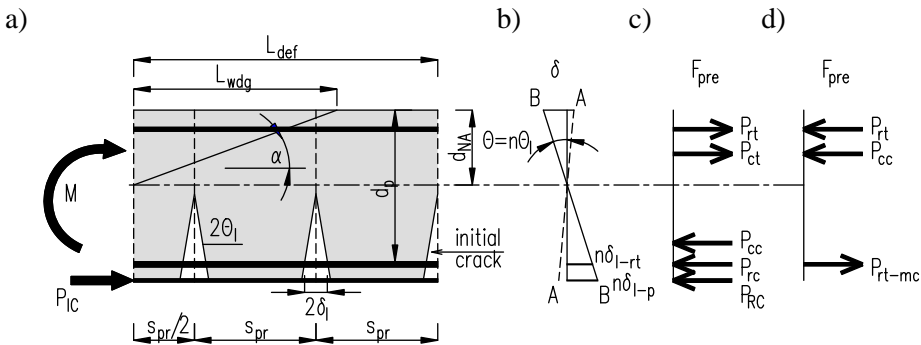


Fig. 6.23. Passive prestressed segmental analysis (Oehlers et al., 2015)

This analysis can be used to plot the moment-rotation response, the moment–curvature response and the strain variation in the RC beam at the level of the FRP laminate (as shown in Fig. 6.21.c), where  $d_p$  is defined as the distance from the line of action of the prestressing force from the extreme compressive fibre.



## 7. Author's approach to flexural strengthening

### 7.1. Description of the model

For the computational analysis of load–deformation of RC elements strengthened with the non–pretensioned and pretensioned FRP materials, the nonlinear model of RC members by Kaminska and Czkwianianc was used (Czkwianianc and Kamińska 1993). This is the cross–sectional analysis referring to the pure bending based on the following assumptions:

- Bernoulli's plain section principle (Fig. 7.1),
- only normal stress in the section is considered,
- full adhesion between materials (good bond behaviour of steel-concrete and EB FRP-concrete)
- tension stiffening principle with the assumption that cracks perpendicular to the axis of a bar are smeared on the pure bending distance,
- non-linear strength characteristics  $\sigma - \varepsilon$  for the concrete in compression and tension (Fig. 7.2),
- experimental strength characteristics  $\sigma - \varepsilon$  for the internal steel reinforcement and composite (Fig. 7.3).

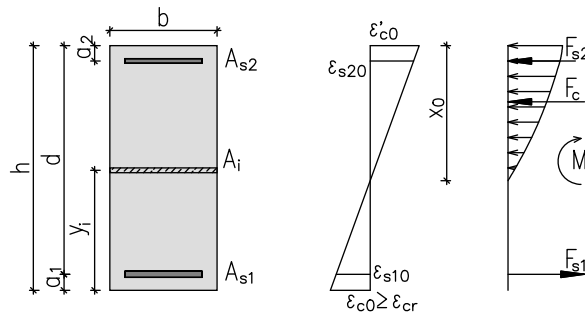


Fig. 7.1. Strain, stress and forces in the unstrengthened RC member

The external load is determined on the basis of the criteria for the forces and moments balance equilibrium in a section, for subsequent strain pattern with the following assumptions:

$$\sum_{i=1}^n F_i = N \quad (7.1)$$

$$\sum_{i=1}^n F_i y_i = M \quad (7.2)$$

**Strength characteristics of concrete**

The strain-stress relationship for concrete is defined in Fig. 7.2 and presented by several equations (7.3 – 7.10):

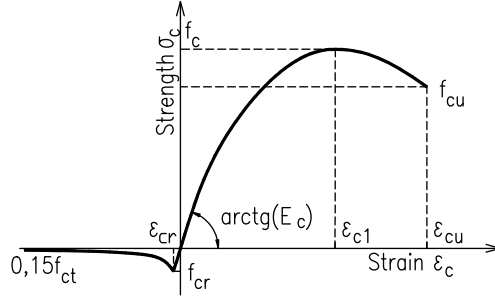


Fig. 7.2. Stress-strain response of concrete

$$\sigma_c = f_c \frac{\beta \frac{\varepsilon_c}{\varepsilon_{c1}}}{\beta - 1 + \left(\frac{\varepsilon_c}{\varepsilon_{c1}}\right)^\beta} \quad (7.3)$$

$$\beta = \frac{1}{1 - \frac{f_c}{\varepsilon_{c1} E_c}} \quad (7.4)$$

$$E_c = E_{c0} [0.99 - 0.0158 \ln(t_m) - 0.0013 f_{c,cube}] \quad (7.5)$$

$$E_{c0} = 4.03 \times (2300 + 3.17 f_{c,cube}) f_{c,cube}^{1/3} \quad (7.6)$$

$$\varepsilon_{c1} = [0.0075 f_{c,cube} + 0.125 \ln(t_m) + 1.655] \times 10^{-3} \quad (7.7)$$

$$\varepsilon_{cu} = [4.51 - 0.1244 f_{c,cube} + 0.000948 f_{c,cube}^2 t_m^{0.14} + 2.20] \times 10^{-3} \quad (7.8)$$

$$f_c = [0.83 - 0.01 \ln(t_m)] f_{c,cube} \quad (7.9)$$

$$f_{cu} = (0.0051 f_{c,cube} + 0.38) f_{c,cube} \quad (7.10)$$

where:

$E_c$  is the elasticity modulus of concrete,  
 $f_c$  is the compressive strength of concrete,  
 $f_{cu}$  is the ultimate compressive strength of concrete,  
 $f_{c,cube}$  is the compressive strength of concrete on cubic specimens,  
 $t_m$  is the time of stress increase

Strength characteristics of steel and FRP reinforcement is shown in Fig. 7.3.

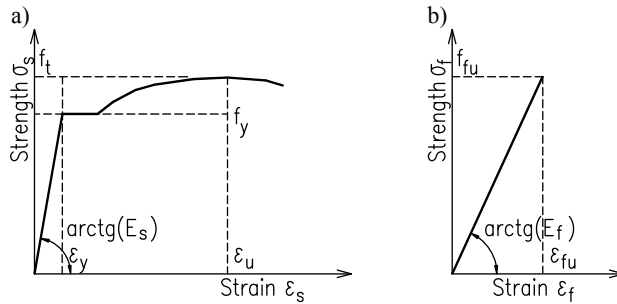


Fig. 7.3. Stress-strain response of: a) steel and b) FRP reinforcement

The load bearing capacity of the non-strengthened element (Fig. 7.1) is the bending moment corresponding to the strain pattern, for which the ultimate strain in one of materials (concrete or steel) is reached ( $\epsilon_{cu} = 3.5\%$  in concrete or  $\epsilon_{su}$  in steel).

In a flexurally strengthened member, intermediate crack debonding of the FRP reinforcement, initiated by flexural cracking in the pure bending distance, is considered to be the most common failure mode (Fig. 7.4). Therefore, the load bearing capacity of a strengthened element is determined for the state of strain of the section in which limit strain in one of the materials is reached ( $\epsilon_{cu}$  in concrete,  $\epsilon_{su}$  in steel or  $\epsilon_{f,b}$  in the FRP strip, corresponding to its debonding or rupture  $\epsilon_{fu}$ ).

It is a common practice in design to consider the state of preloading of elements before their strengthening. The greater preloading of an element before strengthening, the smaller increase of load and possibility of using load bearing capacity of a CFRP laminate after its application.

The preloading state is considered in the current analytical model by the concrete strain at the top  $\epsilon'_{c0}$  and the bottom  $\epsilon_{c0}$  edge of a section, as well as the strain in the tensile and compressive steel reinforcement  $\epsilon_{s10}$ ,  $\epsilon_{s20}$  (Fig. 7.4). This analytical model has been verified in a large number of tests on

RC beams, both non-strengthened and strengthened with CFRP laminates (Kotynia, 1999; Kotynia and Kaminska, 2003; Kotynia et al., 2014; Kotynia and Lasek, 2018) with a very good compatibility of the results.

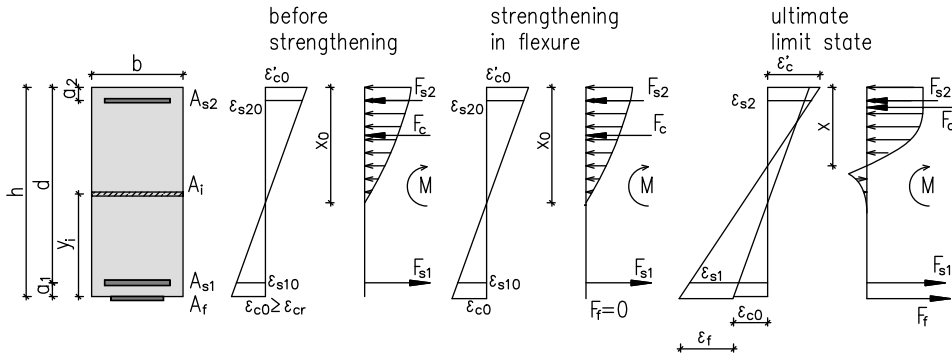


Fig. 7.4. Strain, stress and forces pattern in RC member strengthened with non-prestressed FRP material

Pretensioning of the CFRP laminate is introduced in the model by the corresponding concrete strain in compression and tension ( $\epsilon'_{cp}$  and  $\epsilon_{cp}$ , respectively), and the strain in the CFRP strip  $\epsilon_{fp}$  (Fig. 7.5).

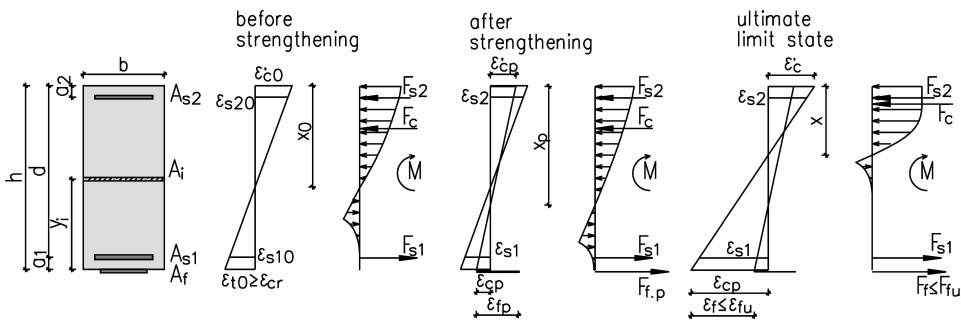


Fig. 7.5. Strain, stress and forces pattern in RC member strengthened with prestressed FRP material

The analytical model was used to build the software used to predict flexural behaviour of non-strengthened and strengthened RC members, with variable FRP materials externally bonded to the concrete surface. The software was developed with the part referring to the preloaded state. The software can be used for variable shapes (rectangular, T and double T-cross sections, with variable accurate concrete, steel and FRP characteristics). Fig. 7.6. shows “step

## Author's approach to flexural strengthening

by step” procedure of the calculated analysis with the description of variable parameters introduced in the computer software:

- geometry of the RC cross section; concrete strength characteristics; preloading bending moment  $M_0$  [kNm]; prestressing FRP strain  $\varepsilon_{pt}$  [%] (Fig. 7.6a),
- location of the internal reinforcement in compression and tension zone with their accurate stress-strain characteristics (Fig. 7.6b),
- location, dimensions of the EB FRP reinforcement with its stress-strain characteristics (Fig. 7.6c),
- details of the procedure step density, introduced by a number of horizontal layers (Fig. 7.6c),

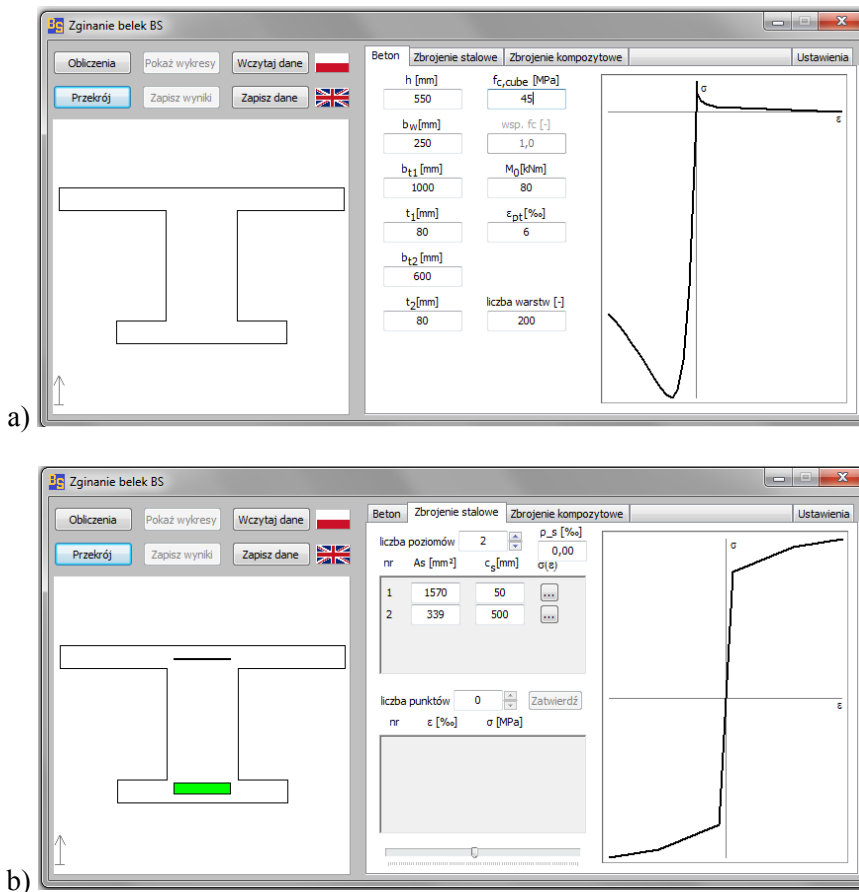


Fig. 7.6. “Step by step” software procedure .

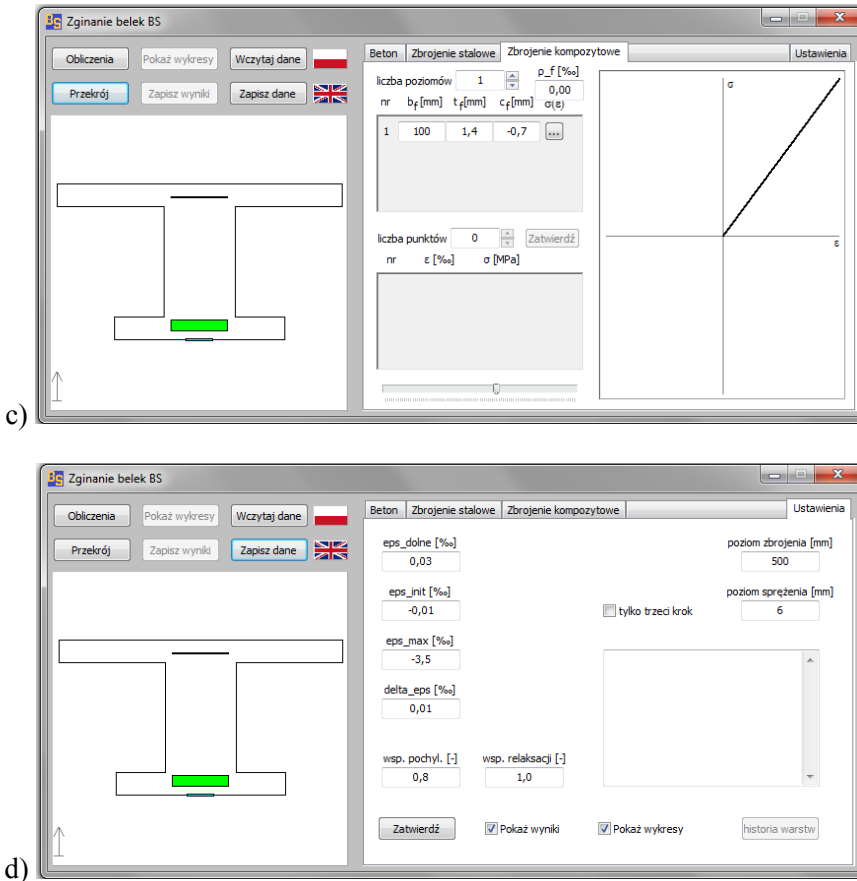


Fig. 7.6. cont "Step by step" software procedure

## 7.2. Comparative analysis of the tested members

The analytical model has been used for calculated analysis of the RC beams tested at the Laboratory of the Department of Concrete Structures in Lodz University of Technology (Kotynia and Lasek, 2018). The experimental programme composed of four rectangular RC beams with 500×220 mm cross-section. The shear reinforcement consisted of 8-mm-diameter steel stirrups with 150-mm spacing. The beams were casted from commercially-supplied concrete of class C30/37. CFRP laminates with dimensions of 100 mm × 1.2 mm were bonded to the bottom surface of the beams with two epoxy adhesive components. The average tensile strength in bending and the compressive strength of the adhesive were experimentally determined standard prisms to be equal to 23.2 MPa and 57.9 MPa, respectively.

## Author's approach to flexural strengthening

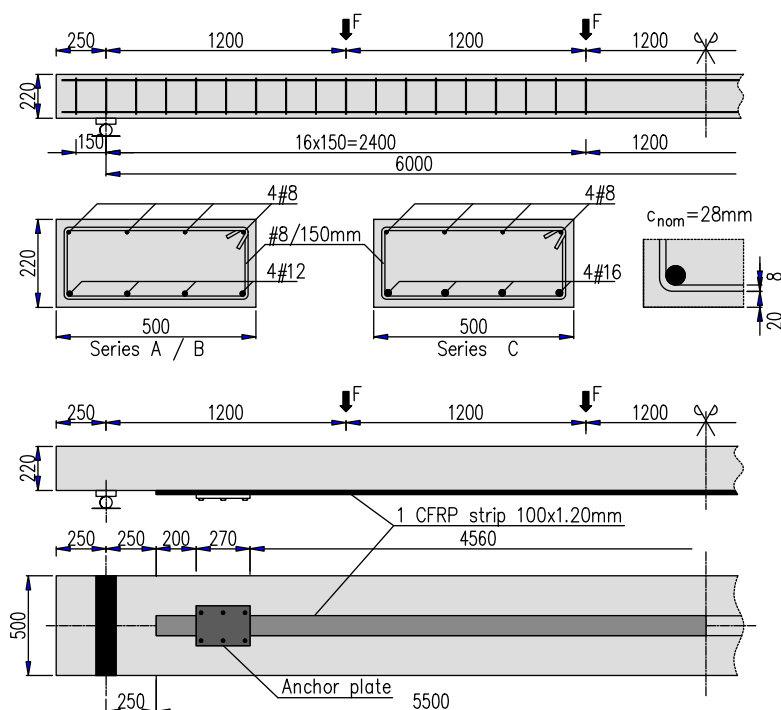


Fig. 7.7. Steel reinforcement, strengthening configuration and test set-up

Table 7.1. List of the tested members and essential test results

Beam	Tensile reinforcement	Initial preloading; $2F_p/2F_{u0} \times 100\%$ , [%]	$f_{ck}$ [MPa]	$2F_u$ [kN]	$\varepsilon_{f,p}$ [‰]	$\sigma_{f,p}$	$\varepsilon_{f,test}$ [‰]	$\eta\varepsilon_f$ [%]
B12-asp	4#12	Self-weight; (25)	32.2	53.0	5.20	$0.32 f_{fu}$	9.30	86
B12-asp-e	4#12	Self-weight + external preloading; (76)	41.6	49.0	4.75	$0.29 f_{fu}$	6.85	69
B16-asp	4#16	Self-weight; (14)	49.0	74.4	4.80	$0.29 f_{fu}$	8.00	76
B16-asp-e	4#16	Self-weight + external preloading; (76)	51.0	72.0	4.85	$0.29 f_{fu}$	7.15	71

$2F_p$  – initial preloading;  $2F_u$  – failure load;  $2F_p/2F_{u0} \times 100\%$  – initial preloading level in comparison to the yield strength of non-strengthened beam;  $\varepsilon_{f,p}$ ,  $\sigma_{f,p}$  – pretensioning strain and stress in the CFRP laminate during strengthening;  $\varepsilon_{f,test}$  – maximal CFRP strain registered in the test;  $\varepsilon_{f,tot}$  – total CFRP strain,  $\varepsilon_{f,tot} = \varepsilon_{fp} + \varepsilon_{f,test}$ ;  $\varepsilon_{fu}$  – rupture strain of CFRP laminate;  $\eta\varepsilon_f$  – utilisation of the tensile CFRP strain,  $\eta\varepsilon_f = \varepsilon_{f,tot}/\varepsilon_{fu} \times 100\%$ ;  $F_{fu}$  – tensile strength of the laminate;  $f_{ck}$  – cylinder compressive concrete strength

The geometry, steel reinforcement, strengthening configurations and test set-up are shown in Fig. 7.7. The main test results are summarised in Table 7.1.

A comparison of experimental and calculated curvature-load curves for the beams strengthened in flexure with the CFRP laminates, is presented in Fig. 7.8. On the calculated graphs, points corresponding to the strain of the strip  $\varepsilon_{f,test}$  equal to 5.0 and 8.0% have been marked to indicate the CFRP strain range at which IC debonding of the CFRP strip from the concrete surface is expected. The initial CFRP prestressing strain  $\varepsilon_{fp}$  equals to 5%, corresponding to 30% of the CFRP tensile strength. The simply supported RC beams were investigated in a 6-point bending test set-up.

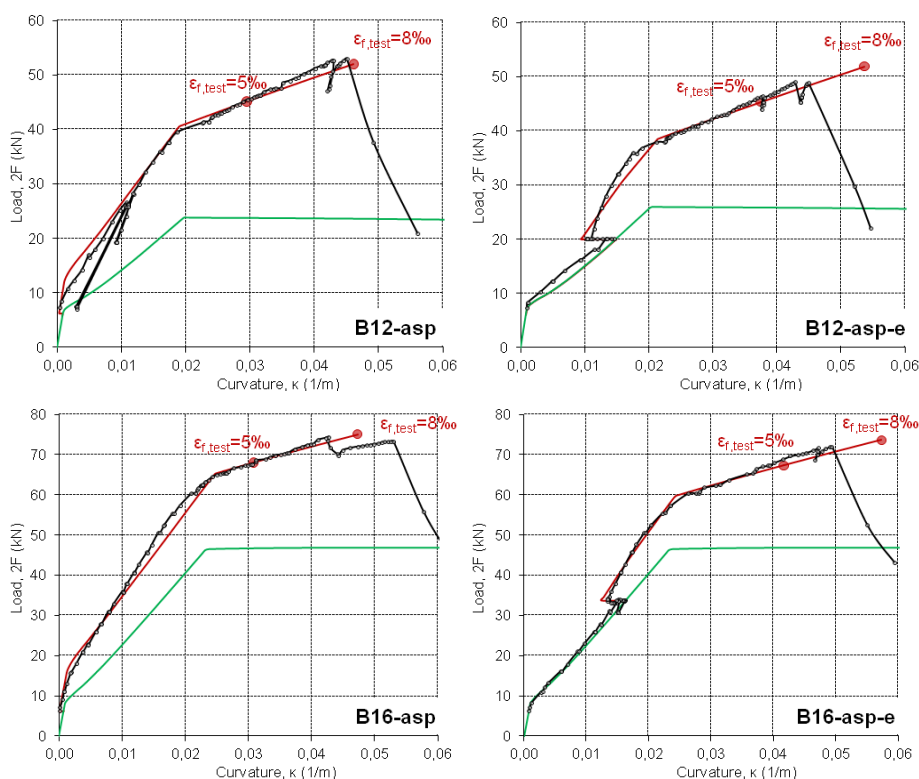


Fig. 7.8. The comparison of the calculated and test curvature-load graphs for the RC beams strengthened with prestressed FRP laminates (Kotynia and Lasek, 2018)

The calculated green line corresponds to the non-strengthened beam.

Slight differences between the calculated and test results may come from inaccuracy of the real geometry of the beams in reference to the calculated

assumptions (due to different location of the steel reinforcement and inaccuracies in the geometry of the elements).

The calculated graphs prove compatibility with the real test results in the full range of loads. Such a good match of the model enables prediction of the flexural behaviour of the strengthened RC member under loading on the safe site, even in case of highly preloaded RC members before strengthening.

### **7.3. Parametric analysis**

The comparative analysis described in Chapter 7.2 confirms very good compatibility of the calculated model in the full range of loading that could be useful for prediction of the load bearing capacity of RC members strengthened with non-prestressed as well as prestressed FRP materials. Moreover, the model has a unique feature based on consideration of the preloading effect.

The main goal of this section is a parametric analysis of the strengthening efficiency of concrete members strengthened with CFRP laminates with consideration of the following effects:

- stiffness of the member (slabs with the cross section 1000×200 mm and beams with different dimensions: 250×500 mm and 500×1000 mm are considered),
- concrete strength (concrete class C30 / 37 and C50 / 60),
- variable utilisation of the CFRP ultimate stress (6‰ as the bond strain in IC debonding of non-prestressed laminates; 8‰ as a sum of the CFRP strain corresponding to 2‰ of prestressing strain and 6‰ as the bond strain; 11‰ as a sum of 5‰ prestressing strain and 6‰ the bond strain),
- variable internal steel reinforcement in the range between 0.135% and 3.0%,
- variable CFRP reinforcement ratio up to 0.7%.

To prepare monograms of strengthening efficiency  $\eta_f$  in the function of the CFRP reinforcement ratio  $\rho_f$ , plenty of calculated examples have been performed. Each case corresponds to one cross section of a member and one reinforcement ratio of steel and CFRP reinforcement. The calculated procedure performed for the slab with the cross section of 1000 x 200mm, the concrete C30/37 and only for six chosen cases corresponding to  $\rho_s = 0.135\%$ , 0.4%, 0.8%, 1.0%, 1.4% and 2.0% are shown as  $\eta_f - \rho_f$  responses in Fig. 7.9. The red line corresponds to the capacity of the member strengthened with the non-prestressed CFRP laminates that failed due to IC debonding with the strain limited to  $\varepsilon_{fb} = 6\text{‰}$ . The green line corresponds to the member strengthened with CFRP laminates prestressed to  $\varepsilon_{fp} = 2\text{‰}$ , which failed due to IC debonding with the strain limited to  $\varepsilon_{fb} = 6\text{‰}$ . The purple line corresponds to the capacity of the member strengthened with CFRP laminates prestressed to  $\varepsilon_{fp} = 5\text{‰}$  that failed

due to IC debonding with the strain limited to  $\varepsilon_{fb} = 6\text{‰}$ . However, the blue line follows the concrete crushing cases for variable cases of  $\rho_f$  and  $\rho_s$ .

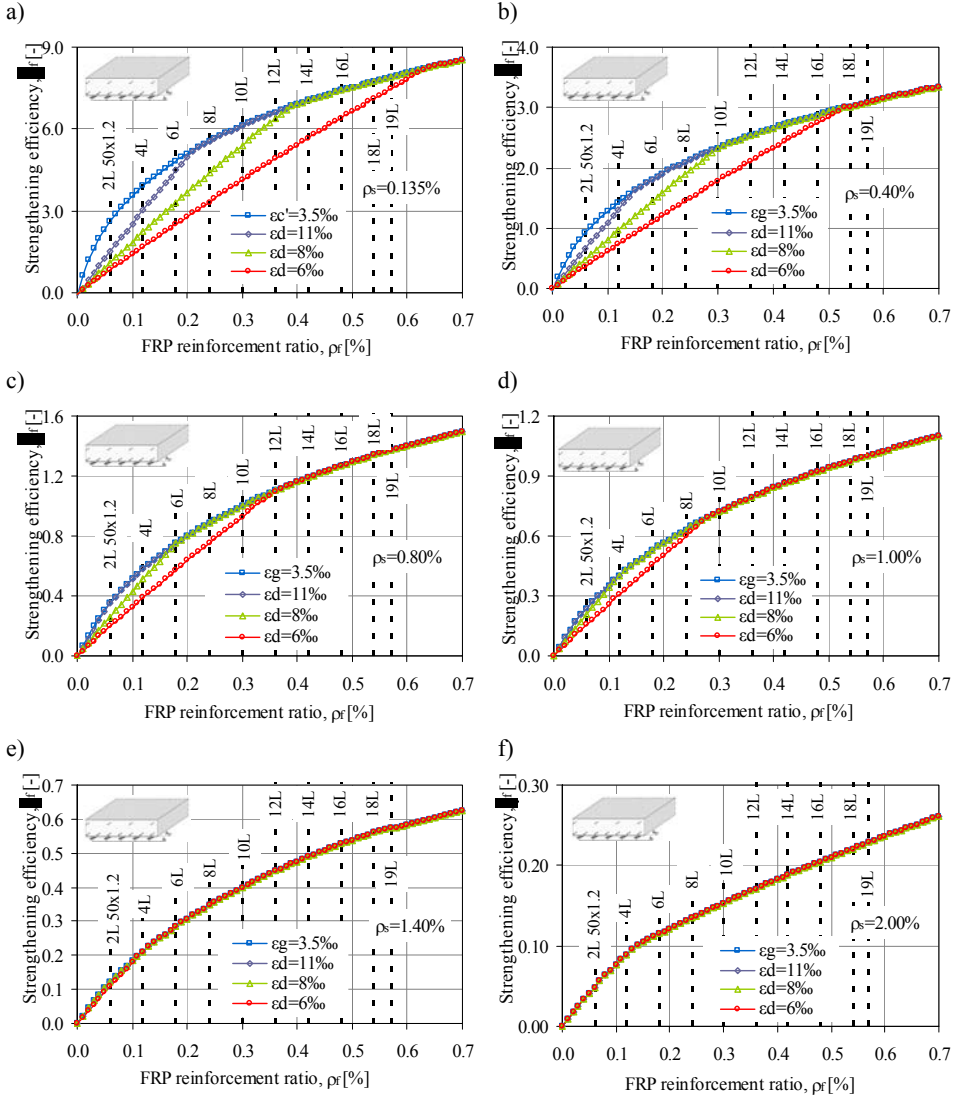


Fig. 7.9. Strengthening efficiency  $\eta_f$  in the function of variable EB CFRP reinforcement ratio  $\rho_f$ , for the 1000×200 mm slab made of concrete C30/37 for chosen cases of variable steel reinforcement ratio  $\rho_s$ : a) 0.135%; b) 0.4%; c) 0.8%; d) 1.0%; e) 1.4% and f) 2.0%.

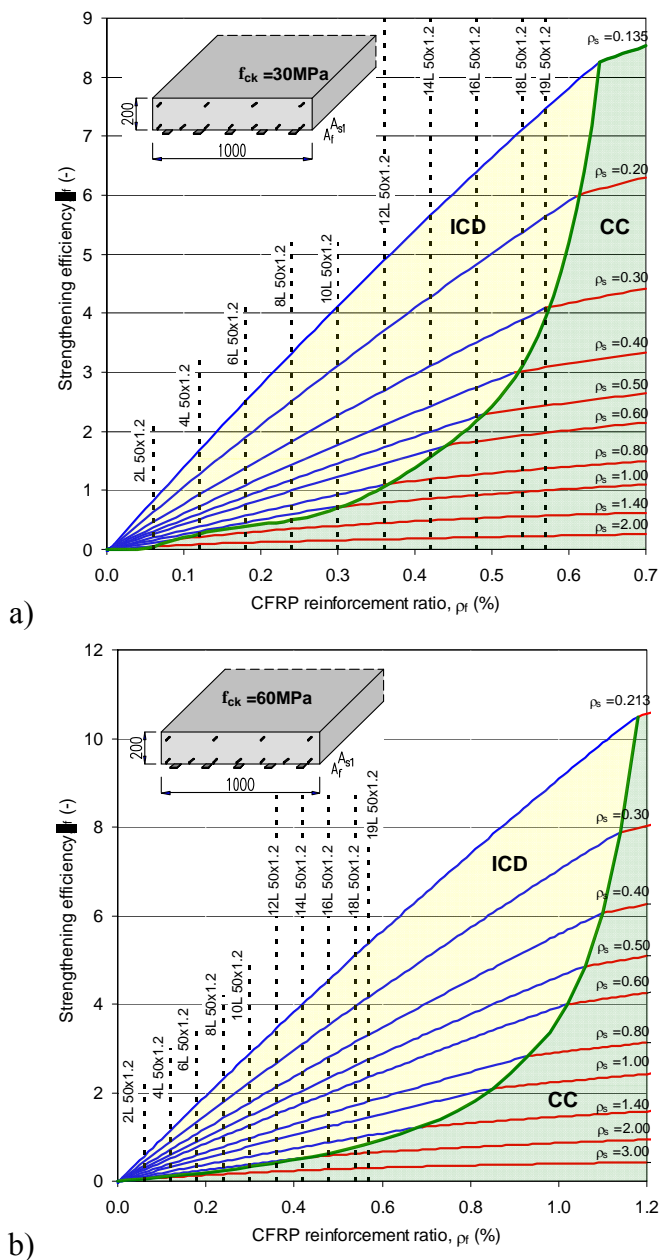


Fig. 7.10. Strengthening efficiency  $\eta_f$  in the function of variable EB CFRP reinforcement ratio  $\rho_f$ , variable steel reinforcement ratio  $\rho_s$  and concrete: a) C30/37, b) C50/60 for slab 1000×200 mm.

It is clearly visible that the limit state is governed mainly by the IC debonding of the CFRP laminates. The concrete crushing for the real cases is rather impossible (see the vertical black dashed lines corresponding to application of 2, 4, 6, 8, 10, 12, 14, 16, 18 and 19 CFRP laminates with the cross section of 50×1.2 mm).

Compositions of  $\eta_f - \rho_f$  curves corresponding to the 1000×200 mm RC slab for variable steel and CFRP reinforcement ratios and two values of concrete strength, C30/37 and C50/60, are shown in Fig. 7.10.a and 7.10.b, respectively.

The area under the curves is divided into two parts: yellow and green, corresponding to IC debonding (ICD) and concrete crushing (CC), respectively. It is confirmed that strengthening efficiency  $\eta_f$  increases with the decrease in the internal steel reinforcement ratio, irrespectively of a member type (slab or beam) and the concrete strength.

The concrete strength governs failure mode (ICD or CC) only for slabs. That means possibility of the concrete crushing (CC) failure mode only for slabs made of concrete C30/37 with the steel reinforcement  $\rho_s < 0.3\%$  (see Fig. 7.10.a). However, in the real RC slab made of concrete C50/60 with the common steel reinforcement ratio  $\rho_s < 1.4\%$ , the concrete crushing (CC) failure is not possible (Fig. 7.10.b). It is clearly visible that in most cases the slab made of concrete C50/60 fails due to CFRP IC debonding (Fig.7.11.b).

For the lowest internal steel reinforcement  $\rho_s = 0.135\%$  in the slab concrete of class C30/37, irrespectively of a number of laminates, failure is governed by IC debonding. If the steel ratio  $\rho_s$  increases, concrete crushing failure is possible for  $\rho_s = 0.40\%$  and 17 CFRP laminates 50×1.2mm.

Further increase in a number of CFRP laminates combined with the increase in the internal steel reinforcement ratio  $\rho_s$  makes the strengthened slab more sensitive to concrete crushing (the red line corresponding to  $\rho_d = 6\%$  shifts to the blue line that is concrete crushing). Both curves have the same line from the internal steel reinforcement ratio equal to  $\rho_s = 1.40\%$ .

Considering strengthening slab with CFRP prestressing to 5‰ and CFRP debonding with CFRP bond strain equal to 6‰ (the purple line), the IC debonding governs the slab failure for the number of CFRP laminates  $n_f \leq 5$  and internal steel reinforcement ratio  $\rho_s = 0.40\%$ .

Composition of separate cases of variable steel and CFRP reinforcement ratios for the 1000 x 200mm slab and two values of concrete strength, C30/37 and C50/60, are shown in Fig. 7.10 and 7.11, respectively.

---

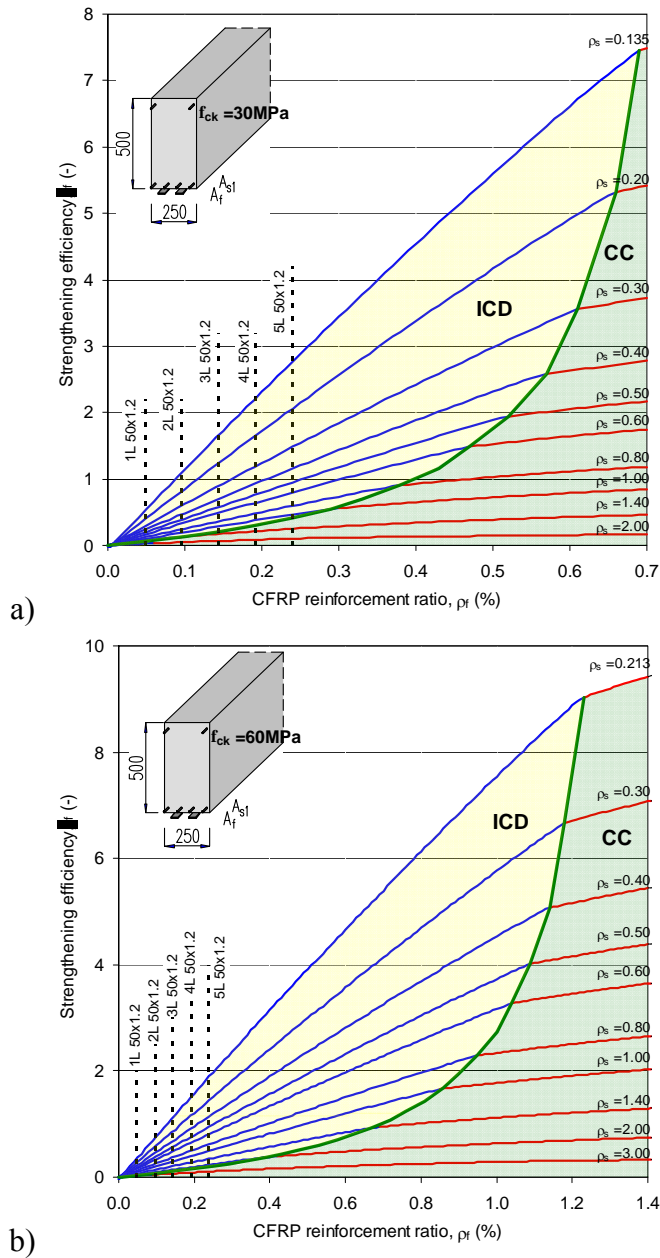


Fig. 7.11. Strengthening efficiency  $\eta_f$  in the function of variable EB CFRP reinforcement ratio  $\rho_f$ , variable steel reinforcement ratio  $\rho_s$  and concrete: a) C30/37, b) C50/60 for the 250 x 500 mm beam

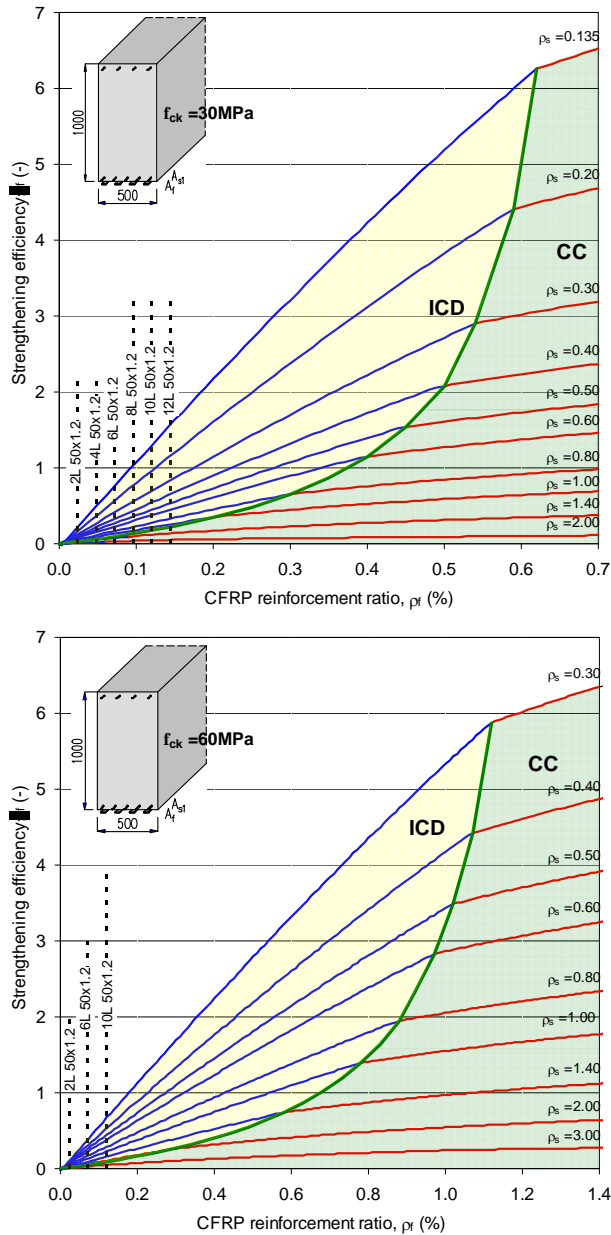


Fig. 7.12. Strengthening efficiency  $\eta_f$  in the function of variable EB CFRP reinforcement ratio  $\rho_f$ , variable steel reinforcement ratio  $\rho_s$  and concrete: a) C30/37, b) C50/60 for the 500 × 1000 mm beam

---

### **Author's approach to flexural strengthening**

---

The area under the curves is divided into yellow and green parts corresponding to IC debonding (ICD) and concrete crushing (CC), respectively. It is clearly visible that the slab made of concrete C50/60 fails in most cases due to CFRP IC debonding (Fig.7.11).

Figures 7.12 and 7.13 confirm a strong effect of the beam stiffness on the strengthening efficiency. Irrespectively of a number of CFRP laminates and the concrete strength C30/37 and C50/60, the beams fail due to IC debonding.

The concrete strength does not affect failure mode of the RC beams, mainly due to IC debonding of the CFRP laminates (compare Fig. 7.12 - 7.15).



## **8. Chosen nonlinear finite element models**

One of the first analytical works on the behaviour of FRP-strengthened beams was presented by Ehsani and Saadatmanesh (1990). This was based on a linear-elastic analysis and was thus limited to the interfacial behaviour before cracking. A more advanced approach, the layer-by-layer numerical model, was subsequently adopted by other researchers to account for the material nonlinearities of the concrete before and after cracking (Takahashi et al. 1997; Nitereka and Neale 1999), or to include the effect of tension stiffening (Ebead and Marzouk 2005). These analyses were intended for the prediction of the load-deflection behaviour and the ultimate load carrying capacities; they did not model the debonding failure modes as such. Ebead et al. (2004) and Yuan et al. (2001) in their finite element analyses modelled the adhesive layer as a linear-elastic material, rather than adopting the commonly used full-bond assumption between the FRP and concrete.

Interface elements were used to represent the interfacial behaviour between the FRP and concrete in the studies of Sand and Remlo (2001), Wong and Vecchio (2003), Teng et al. (2004), and Abdel Baky et al. (2004). An accurate concrete cracking model at the interface is generally required to properly determine the strain distributions in the concrete due to crack formation. The nonlinear fracture mechanics approach used by Rabinovitch and Frostig (2001) was introduced to analyze the interfacial stresses in the vicinity of the crack. The interfacial shear stress was addressed before and after concrete cracking for a plane stress analysis of FRP-strengthened reinforced concrete beams (Abdel Baky et al., 2004) and a 3-D analysis of FRP-strengthened concrete slabs (Neale et al., 2005).

### **8.1. Nonlinear finite element analysis by R. Kotynia, H. Abdel Baky, K. Neale and U. A. Ebead (2009)**

As far as numerical modelling is concerned, Ebead and Neale presented a nonlinear finite element modelling of the interfacial behaviour of FRP/concrete joints (Ebead and Neale 2006). This numerical analysis has been performed for experimental results of two series of ten RC concrete beams externally strengthened with CFRPs (Kotynia et al., 2009). The RC beams with the rectangular cross-section of 150x300 mm and a span of 4200 mm were strengthened with externally bonded CFRP strips or sheets. Continuous and spaced L-shaped CFRP reinforcement was used to delay the debonding of the bottom longitudinal CFRP laminates (Kotynia and Kamińska 2003). The

experimental program (Table 8.1) addresses the efficiency of using different configurations for the CFRP strengthening by altering the U-shaped systems.

A displacement-controlled nonlinear finite element analysis of FRP-strengthened concrete beams was carried out using the finite element package ADINA (ADINA, 2004a).

Table 8.1. Summary of test specimens

	Beam ID	CFRP configuration		$\rho_s$	$\rho_f$	$f'_c$	$f_t$
		Bottom CFRP*	U-shaped CFRP	(%)	(MPa)		
Series I	B-08S	Type S	-	0.84	0.15	32.3	2.8
	B-08M	Type M	-		0.41	37.3	3.5
	B-08Sm	Type S	U-wrap, fibres perpendicular to the beam axis (1 layer)		0.15	33.5	3.4
	B-08Mm	Type M			0.41	38.2	3.3
	B-08Sk	Type S	L-shaped plates (spacing 200 mm)		0.15	33.8	3.2
	B-08Mk	Type M			0.41	32.0	3.1
Series II	B-083m	Sheet (width 150 mm, 3 layers)	-	0.14	34.4	2.9	
	B-083mb	Sheet (width 150 mm, 2 layers)	U-wrap, fibres parallel to the beam axis (1 layer)	0.14	25.8	2.7	
	B-08Smb	Type S		0.20	25.7	2.4	
	B0-08Smb	Type S		0.20	27.4	2.7	

\* distance between the bottom plate end and the beam support is 75 mm  
 $\rho_s$  – longitudinal steel reinforcement ratio,  $\rho_s = A_s/bd$   
 $\rho_f$  – total longitudinal CFRP reinforcement ratio,  $\rho_f = A_f/bd$

### 8.1.1. Material modelling for concrete, steel, and FRP

The constitutive law used for modelling the behaviour of the concrete is based on the following assumptions:

- a nonlinear stress–strain relation that allows for the weakening of the material under increasing compressive stresses,
- tension and crushing failure envelopes,
- a strategy for modelling of fixed smeared crack model, the post-cracking and post-crushing behaviour of concrete.

The general multiaxial stress–strain relations are derived from a nonlinear uniaxial stress–strain relation. The cracked concrete is assumed orthotropic, with the directions of orthotropy being defined by the principal stress directions. Failure envelopes are utilized to establish the uniaxial stress–strain law

accounting for multiaxial stress conditions, and to identify whether tensile or crushing failure of the concrete has occurred.

The post failure material behaviour considers:

- post-tensile cracking,
- post-compression crushing,
- strain-softening principle.

The hypoelastic concrete model is used for description of the nonlinear stress-strain relationship (Fig. 8.1). The ultimate uniaxial compressive stress  $\sigma_u = 0.85 f'_c$  and the ultimate uniaxial compressive strain  $\epsilon_u = 0.0035$ . The concrete tensile strength  $f_t$  and the initial modulus of elasticity  $E_c$  are determined experimentally and Poisson's ratio  $\nu = 0.18$  (Table 8.1).

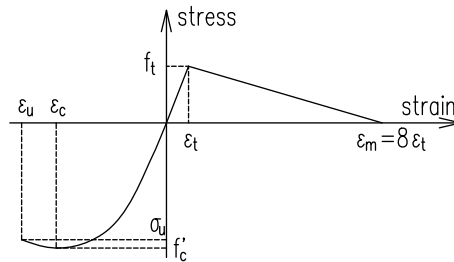


Fig. 8.1. Concrete stress–strain constitutive model

Failure envelopes are utilized to establish the uniaxial stress-strain law accounting for multiaxial stress conditions and to identify whether tensile or crushing failures of the concrete have occurred. A uniaxial elastic-pure plastic constitutive law is employed for the steel reinforcement (Table 8.2), while for the FRP composites, an orthotropic 3D linear elastic relation up to failure is assumed. The orthotropic parameters of the FRP composites are considered using the mechanical properties of FRP s and epoxy.

The behaviour of the cracked concrete is described assuming a system of orthogonal cracks. Once a crack occurs in any direction  $i$  the material is considered orthotropic with the directions of orthotropy being defined by the principal stress directions. Cracking of the concrete occurs when the principal tensile stress lies outside the tensile failure envelope. The elastic modulus of the concrete is reduced to zero in the direction parallel to the principal tensile stress direction and then a redistribution of stresses takes place. Once cracking occurs, the shear reduction factor decreases linearly from 1.0 for the uncracked section to 0.5 for cracked sections, at a strain level of eight times the cracking strain  $\epsilon_m$  (Fig. 8.1), and then remains constant.

The steel reinforcement has a bilinear elastic-plastic stress-strain relationship with the strength characteristics shown in Table 8.2.

A linear elastic relationship until rupture is assumed for the CFRP composites (Table 8.3). For the analysis, the elastic modulus in the direction perpendicular to the fibres  $E_t$  is assumed to be one-tenth of that in the direction of the fibres  $E_f$ .

Table 8.2. Steel reinforcement characteristics

Diameter (mm)		$E_s$ (GPa)	$f_{su}$ (MPa)	$f_y$ (MPa)
6		207	501	437
10		209	647	524
12	Series I	195	692	490
	Series II	220	662	436

Table 8.3. Mechanical properties of one layer of CFRP reinforcement

Parameters	Strips		Continuous sheets**	Spaced laminates
	Type S	Type M		
Thickness (mm)	1.2	1.4	0.13	1.4
Width (mm)	50	120	150*	40
$f_u$ (MPa)	2915	2743	3500	2295
$E_{frp}$ (GPa)	172	220	230	132
$\epsilon_u$ (%)	1.7	1.24	1.5	1.73
* when used as longitudinal strengthening reinforcement				
** data supplied by the manufacturer				

### 8.1.2. FRP to concrete interface bond model

The mechanical behaviour of the FRP-to-concrete interface is modelled by the local shear stress-slip  $\tau - S$  curve proposed by Lu et al. (2005) presented in details in Chapter 4 and shown in Fig. 8.2.

$$\tau = \tau_{max} \sqrt{\frac{S}{S_0}} \quad \text{if } S \leq S_0 \quad (8.1)$$

$$\tau = \tau_{max} e^{-\alpha(S/S_0-1)} \quad \text{if } S \geq S_0 \quad (8.2)$$

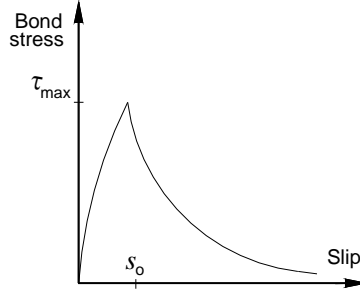


Fig. 8.2. FRP-to-concrete constitutive bond model (Lu et al., 2005)

The maximum bond strength,  $\tau_{max}$ , and the corresponding slip,  $S_0$ , are governed by the tensile strength of the concrete,  $f_t$ , and a width ratio parameter,  $\beta_w$ , as follows:

$$\tau_{max} = 1.5\beta_w f_t \quad (8.3)$$

$$S_0 = 0.0195\beta_w f_t \quad (8.4)$$

The parameter  $\beta_w$  is defined in terms of the laminate width,  $b_f$ , and the width of the beam,  $b_c$ , as follows:

$$\beta_w = \sqrt{\frac{2.25 - \frac{b_f}{b_c}}{1.25 + \frac{b_f}{b_c}}} \quad (8.5)$$

The interfacial fracture energy,  $G_f$  is the area under the  $\tau - S$  curve, which corresponds to the energy per unit bond area required for complete debonding, calculated as follows:

$$G_f = 0.308\beta_w^2 \sqrt{f_t} \quad (8.6)$$

The factor  $\alpha$  is related to  $G_f$  according to the following equation:

$$\alpha = \frac{1}{\frac{G_f}{\tau_{max} S_0} - \frac{2}{3}} \quad (8.7)$$

Values of  $\tau_{max}$  and corresponding slip  $S_0$  are listed for each beam specimen in Table 8.4.

Table 8.4. Comparison between the experimental and numerical results

Beam series	Beam ID	$\tau_{max}$ (MPa)	$S_0$ (mm)	$P_{num}$ (kN)	$P_{num}/P_{exp}$	$\varepsilon_{num}$ (‰)	$\varepsilon_{num}/\varepsilon_{exp}$
Series I	B-08S	4.62	0.060	93.7	0.98	6.65	1.08
	B-08M	4.42	0.057	139.5	1.00	5.68	1.12
	B-08Sm	5.61	0.073	105.4	1.03	7.03	1.07
	B-08Mm	4.16	0.054	153.2	1.00	6.31	1.15
	B-08Sk	5.28	0.069	100.3	0.98	8.09	0.94
	B-08Mk	3.91	0.051	157.2	1.05	7.90	1.40
Series II	B-083m	3.24	0.042	89.9	0.98	6.65	0.98
	B-083mb	3.02	0.094	119.3	0.97	7.84	0.93
	B-08Smb	3.96	0.051	113.8	1.00	7.88	1.03
	B0-08Smb	4.46	0.058	106.0	0.96	7.92	1.26

$P_{num}$  is the numerical ultimate load and  $\varepsilon_{num}$  is the numerical strains in CFRP at ultimate load

### 8.1.3. Geometrical modelling

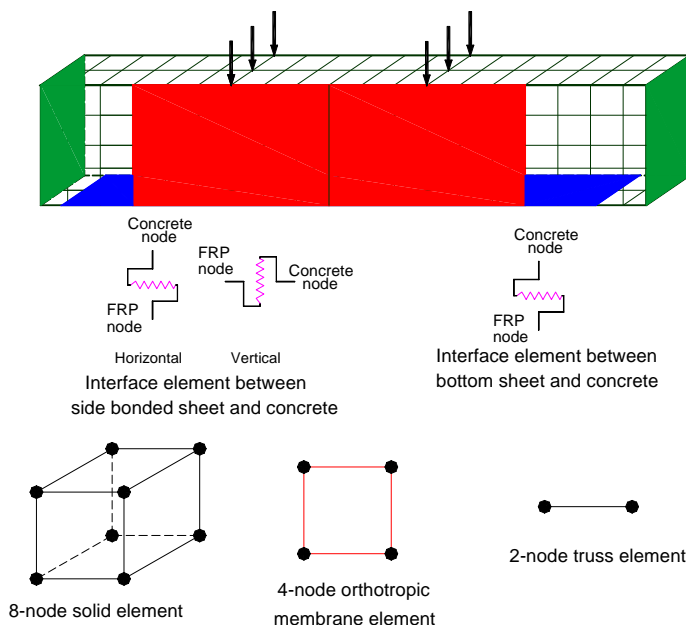


Fig. 8.3. Finite element model

## Chosen nonlinear finite element models

In the current finite element simulations, only one quarter of the beam is modeled due to the geometrical, material and loading symmetries. The concrete is modelled using 8-node 3D solid elements with three transitional degrees of freedom per node in three perpendicular directions. The steel reinforcement is modelled using 2-node truss elements with three transitional degrees of freedom per node.

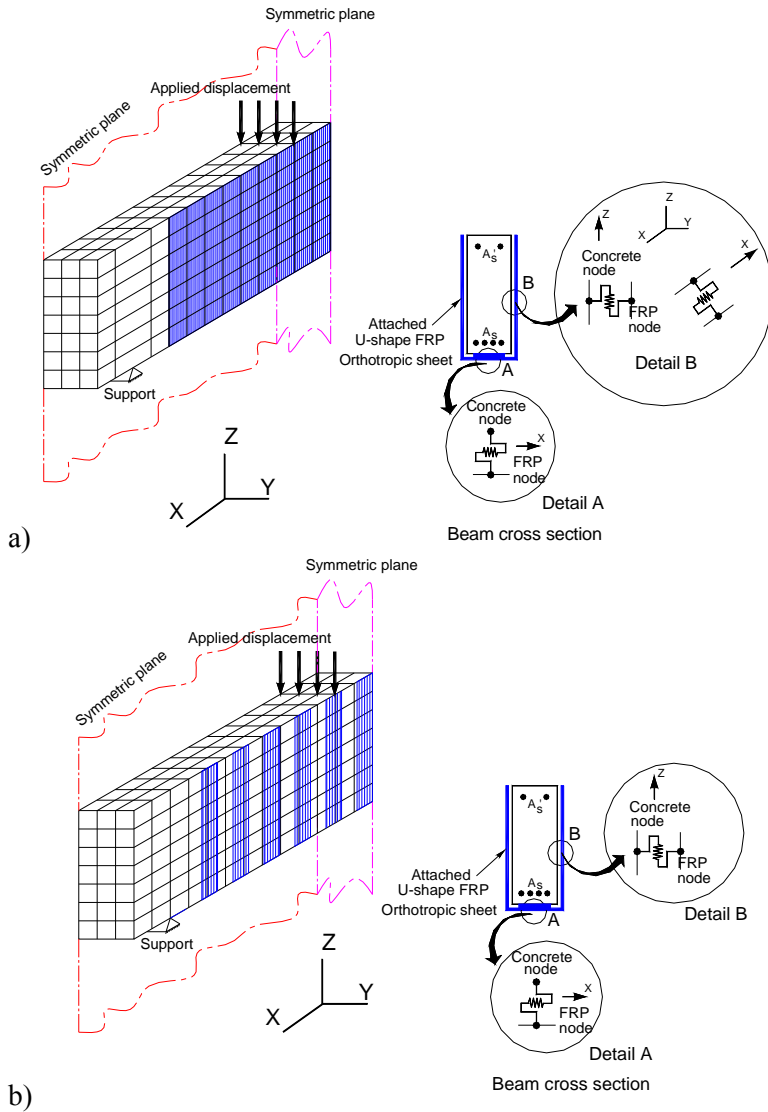


Fig. 8.4. Finite element mesh for (a) beam B-08/Sm and (b) B-08/Sk

The FRP laminates is modelled using 4-node membrane element with three translational degrees of freedom per node. These elements are aligned in the direction of the unidirectional fibres, and in both directions for the case of longitudinal and transverse oriented fibres (Fig. 8.3). The constitutive relationship for the interface truss elements was based on the above bond-slip model. Due to the geometrical and loading symmetries, only one quarter of the beam was analyzed.

Fig. 8.4 shows the finite element meshes and the interface elements in two specific beams, B-08/Sm and B-08/Sk, respectively.

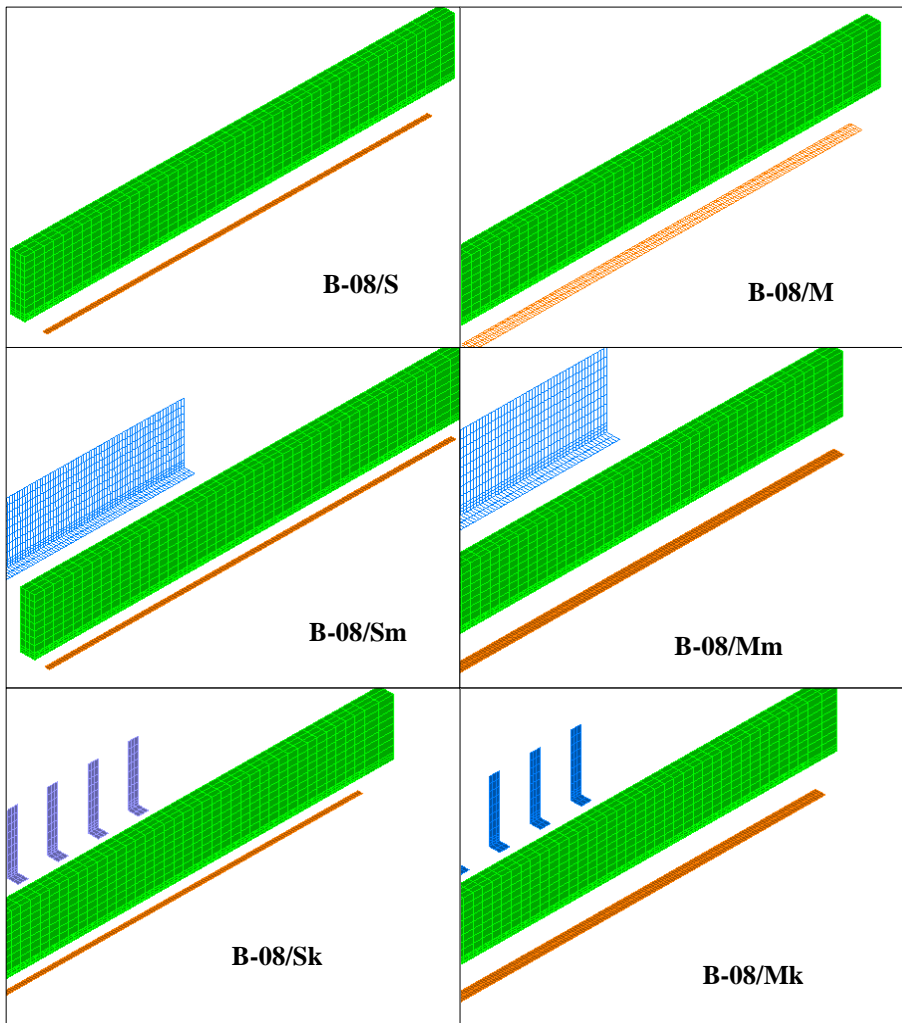


Fig. 8.5. Finite element models of I Series beams

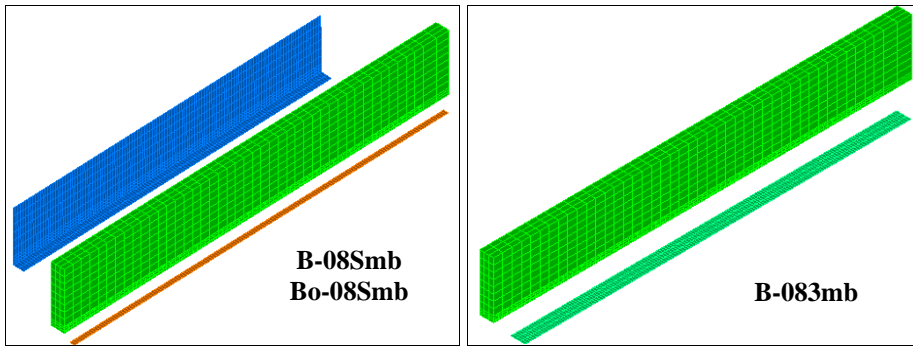


Fig. 8.6 Finite element models of II Series beams

#### 8.1.4. Numerical results and discussion

The comparisons between the results of our numerical predictions and that of the experimental results for all the specimens, in terms of the ultimate load carrying capacities and modes of failure, are summarized in Table 8.4. with the ratio of the numerical-to-experimental load capacity is given for each beam.

There is a very good agreement between the numerically predicted load capacities and the experimental results for all the test specimens.

#### *Deformation characteristics*

The average numerical-to-experimental load ratios are 1.00 with a  $5e^{-6}$  standard deviation. The proposed models are able to simulate the entire load-deflection relationships, including the descending and post failure profiles, in view of the displacement-controlled solution adopted in these analyses. The numerical results shown in Figure 8.7 are for the numerical versus experimental comparisons in terms of the load-deflection relationships for tested beam specimens of I Series. Debonding of the FRP laminates off the concrete surface caused the failures that were observed experimentally.

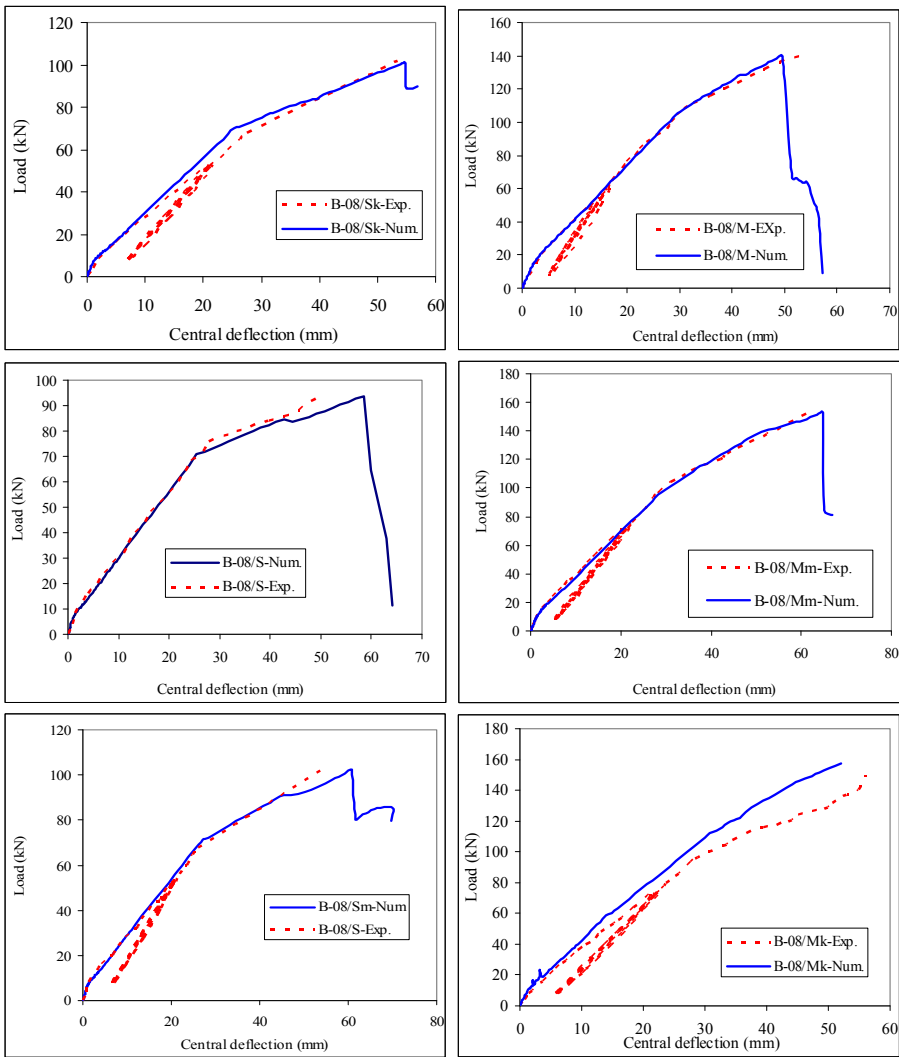


Fig. 8.7. Load–deflection relationships for the beam specimens in I Series

### *Axial strains in tension steel bars and FRP sheets*

The numerical results shown in Figure 8.8 and 8.9 are for the numerical versus experimental comparisons in terms of the load–strain relationships in tension steel bars and bottom FRP sheet, respectively for tested beam specimens of I Series. There is a very good agreement between the prediction and the response observed experimentally.

## Chosen nonlinear finite element models

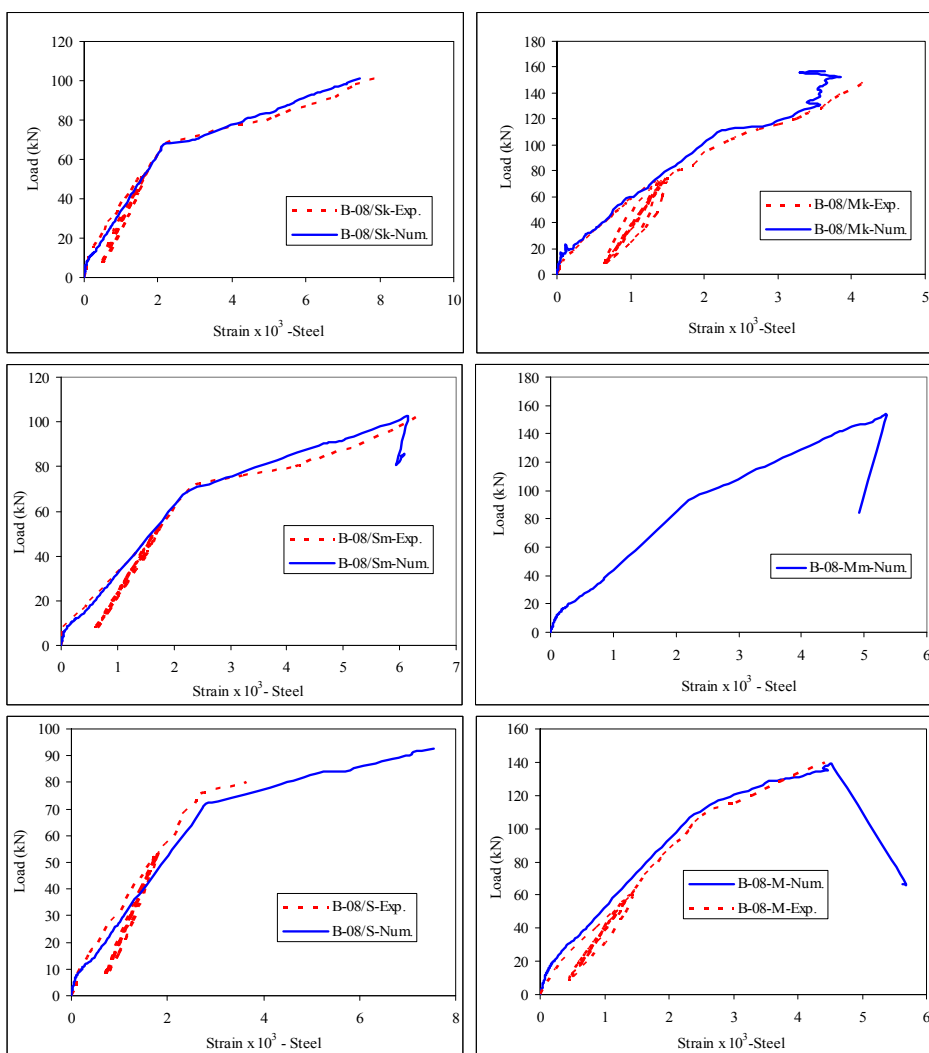


Fig. 8.8. Load–strain curves in tension steel bars of I Series beams

The experimental measurements of the strain in steel bars around failure are quite difficult and generally not very accurate. This explains the discrepancy in beam B-08/Mk, while for beam B-08/S, the experimental reading did not capture the strain in steel bars after yielding.

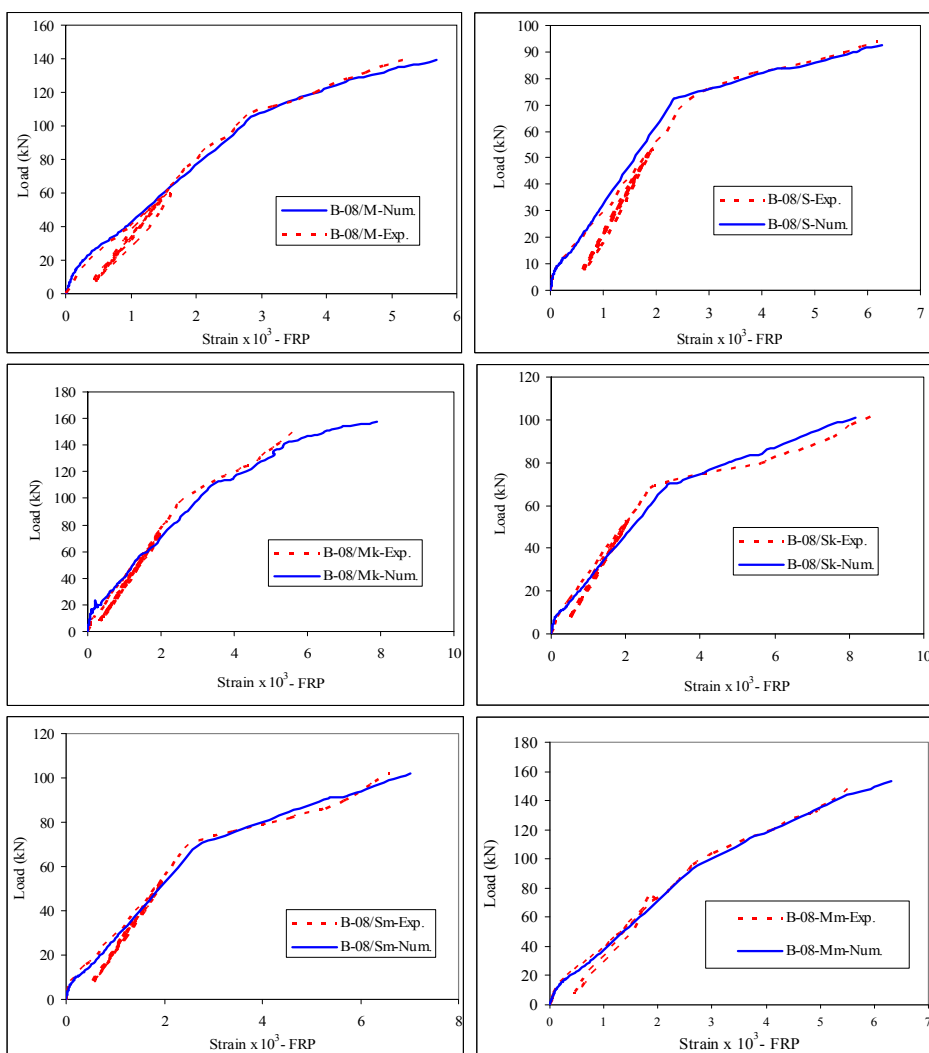


Fig. 8.9. Load–strain curves in tension steel bars of II Series beams

### 8.1.5. Interfacial shear slip profile

The interfacial shear slip in the subsequent sections is presented for three beams. The first beam, B-08/S, represents the case of unanchored FRP system. The second beam, B-08/Sm, represents the case of using continuous U-shape FRP anchored system. The third beam, B-08/Sk, represents the case of using separated U-shape FRP anchored system.

**Beam B-08/S**

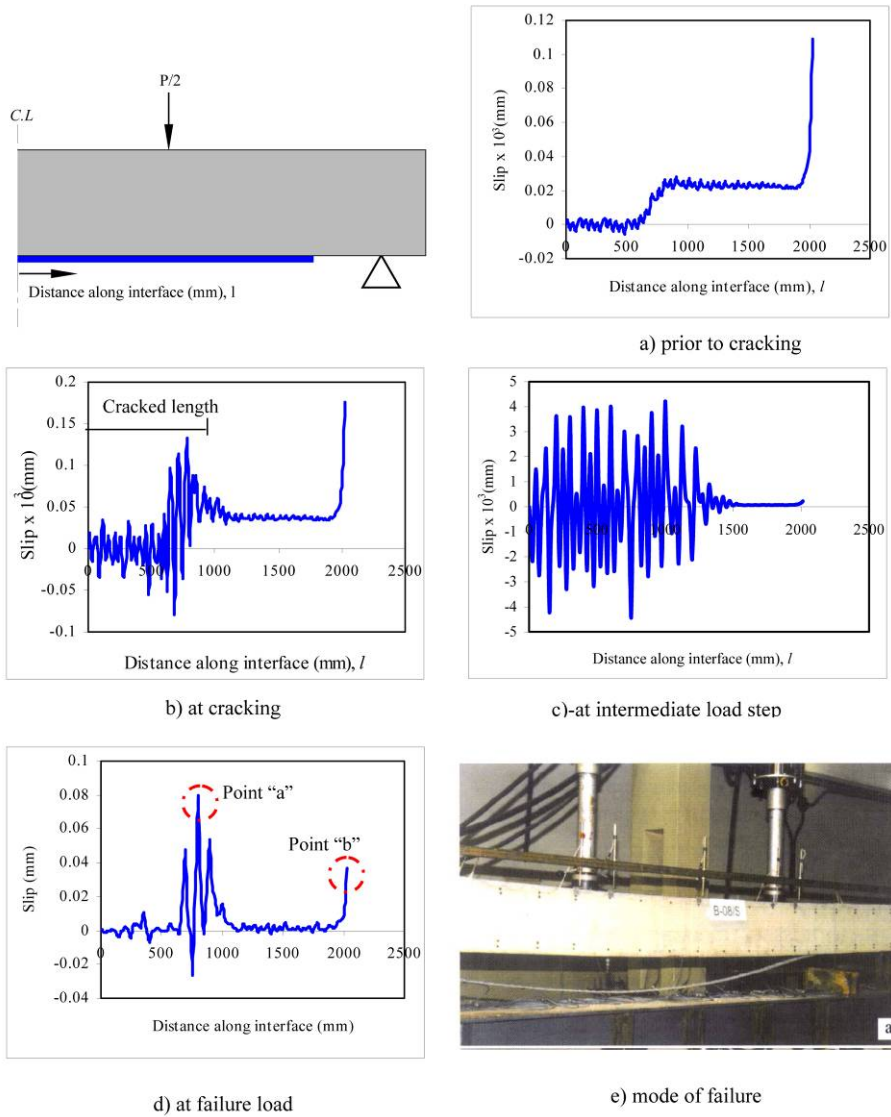


Fig. 8.10. Interfacial slip profile for the Beam B-08/S

Figures 8.10a to 8.10d present interfacial shear slip distributions along the interface for load levels prior to and at cracking, at intermediate load step and at failure load.

With an increase of the applied load up to the cracking load, the interfacial shear slip increases progressively along the bonded plate, with an abrupt

increase at the plate end. At this stage of loading (prior to cracking) the interfacial shear slip distribution is similar to that derived from the direct shear tests (Ebead et al., 2004). At the cracking load, higher fluctuating interfacial slip values are observed at the cracked sections. However these values are still less than that at the plate end. As shown in Figure 8.10c, with an increase of the applied load up to the yield load, the flexural cracks tend to open causing a shift of the maximum values of the bond slip from the plate end to the mid-span.

Figure 8.10d shows the interfacial shear slip distributions along the interface for the level of load around the failure load. For this specific beam, the interfacial shear slip increases dramatically at the mid-span causing an intermediate crack debonding. Moreover, the interfacial slip increases simultaneously at the plate end with a significant value of 0.04 mm. The interfacial slip profile explains the debonding failure mode that has been observed experimentally as shown in Figure 8.10. The debonding mode of failure initiates at the intermediate crack around the concentrated load, corresponding to point “a” in Figure 8.10d, then suddenly propagates toward the plate end, corresponding to point “b”.

#### ***Beam B-08/Sk***

The effect of using anchored strengthening on the interfacial slip distribution is depicted Fig. 8.11a to 11d. It is obvious that the slip distribution is decreased at the anchored zone, slip equals  $.005 \times 10^{-3}$  mm, compared to that for the unanchored beam B-08/S, slip equals  $.02 \times 10^{-3}$  mm in Fig. 8.11a. At the cracking load, higher fluctuating interfacial slip values are observed at the cracked sections, yet these are still lower than those at the plate end, as shown in Figure 11b. Both at the intermediate load level; and at failure, the interfacial slip values concentrate at the end of the anchored sheet. At failure, as shown in Fig. 8.11d, the maximum interfacial shear slip occurs at the beginning of the anchoring sheet, causing debonding to initiate and to propagate towards the end plate, where the interfacial slip has a maximum value. This slip profiles could explain the mechanism of the experimentally observed debonding failure mode as presented in Fig. 8.11e, where the observed debonding failure initiated at the mid span and propagated toward the plate end.

#### ***Beam B-08/Sm***

This beam specimen addresses the effect of using transverse sheet for anchoring bottom FRP sheets. When using intermediate transverse sheets for anchoring the laminates, the slip distributions along the interface become those shown in Fig. 12a to 12d. In the predicted interfacial shear slip profiles, we observe zones where the interfacial slips decrease relative to those in the

adjacent zones, as can be seen clearly in Fig. 12c and 12d. This result suggests that, in general, the addition of transverse anchorage strips is quite effective for mitigating debonding failures in these regions. At failure load as shown in Fig. 11d, the interfacial slip value increases significantly between the transverse sheets and this explains the local debonding failure mode that has been observed experimentally and shown in Fig. 12e.

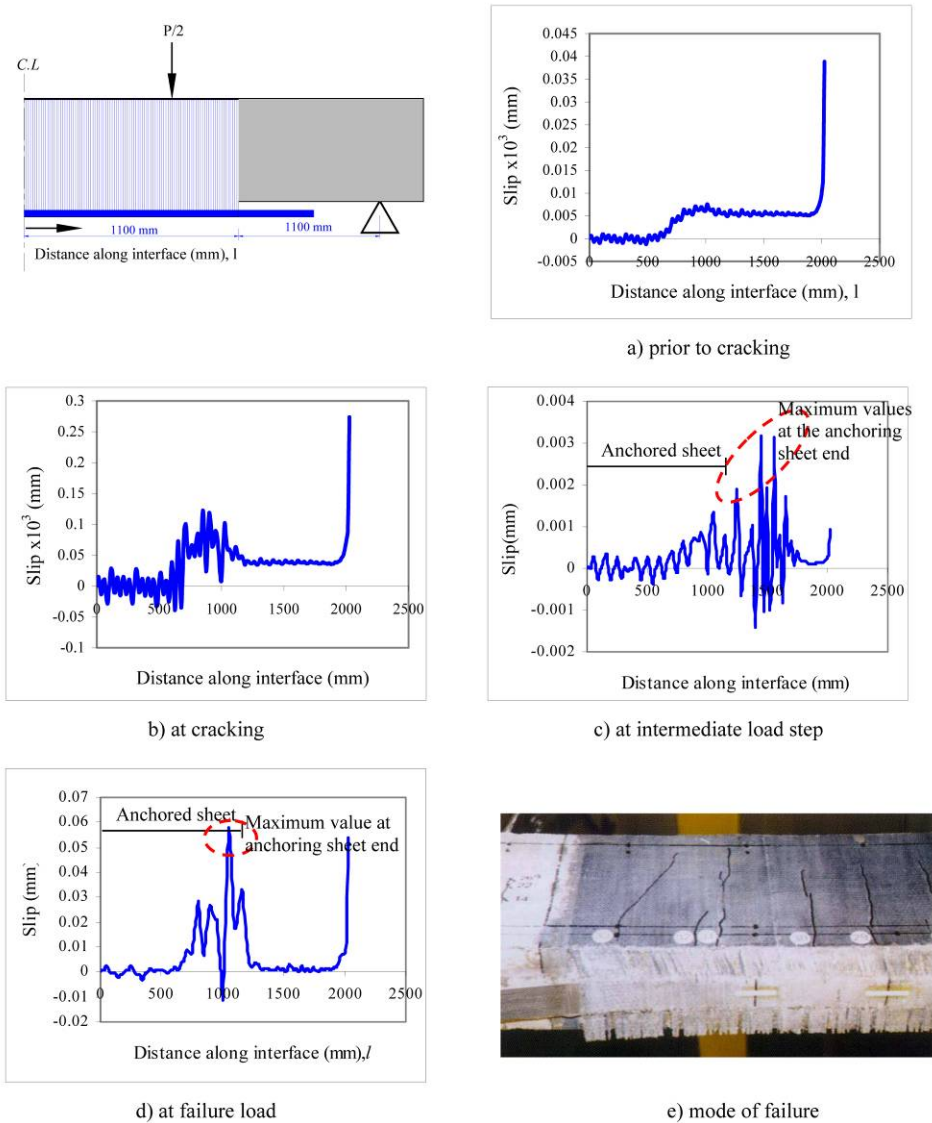


Fig. 8.11. Interfacial slip profiles for the beam B-08/Sk

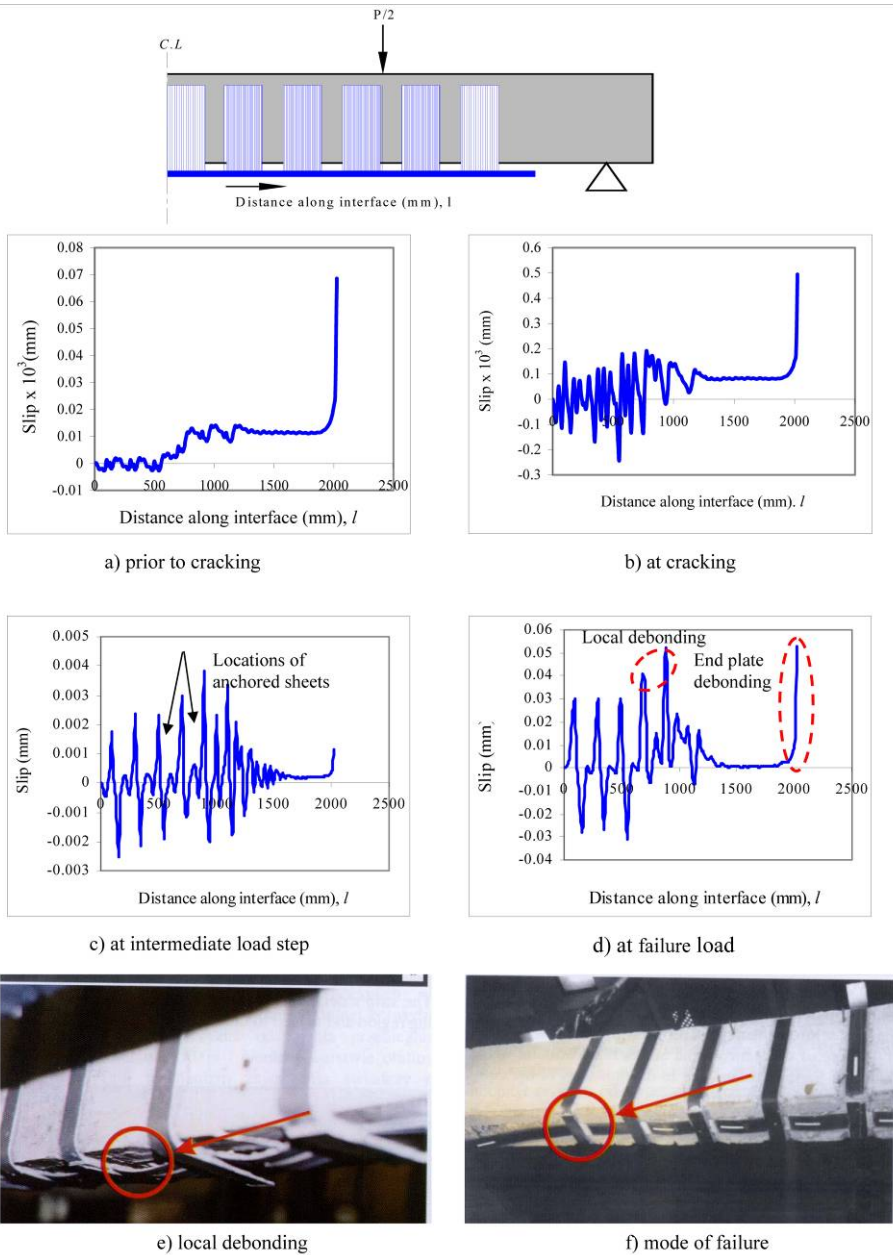


Fig. 8.12. Interfacial slip profiles for the beam B-08/Sm

At failure, the slip increased dramatically at the plate end with a value similar to that at the end of anchoring sheet causing the mode of failure that have been

observed experimentally and represented in Fig. 12f. The debonding mode of failure initiated at the plate end and propagated toward the mid span. Simultaneously, a local debonding failure occurred between the transverse sheets.

### 8.1.6 Conclusion

The nonlinear numerical analysis using a displacement-controlled 3-D finite element model indicated that the following conclusions may be drawn:

- For all of the tested specimens, the mode of failure was characterized by intermediate crack debonding of the bottom FRP flexural strengthening reinforcement.
- There was a significant effect of the width of the flexural CFRP laminates on the debonding mechanism. In the case of the narrow laminates, the debonding plane occurred a few millimetres inside the thin concrete cover. However, when using wide laminates, the debonding plane was observed inside the concrete cover, along the steel reinforcement.
- Using an additional transverse FRP continuous U-wrap system with the fibre direction parallel to the beam axis increased the ultimate load carrying capacity, mainly because of the flexural contribution of the additional CFRP reinforcement.
- Not extending the length of the U-shaped distance to cover the ends of the laminates limited the effectiveness of the anchorage technique as far as the ultimate load capacities were concerned.
- Initial loading of a strengthened beam to a level of 50% of the corresponding capacity of an unstrengthened beam had very little influence on the ultimate load capacity.
- The finite element model predicted the ultimate load carrying capacities of the various FRP-strengthened beams with an average numerical-to-experimental ratio and standard deviation of 0.998 and 0.0276, respectively. As far as the CFRP strains at the ultimate loads were concerned, the average numerical-to-experimental ratio and its corresponding standard deviation were 1.096 and 0.147, respectively.
- For all of the specimens, the finite element analysis was capable of predicting the experimentally observed CFRP debonding mode of failure (intermediate crack debonding).

## 8.2. Nonlinear finite element analysis by Sz. Serega, R. Kotynia and K. Lasek (2018)

### 8.2.1. Finite element model of preloaded RC beams strengthened with prestressed CFRP laminates

The geometry of the tested beams and the loading configuration indicate that the structure can be modelled in a plane stress state (2D). The finite element mesh topology adopted for calculations is presented in Fig. 8.13. Only half-span with proper boundary conditions was modelled as the structure is symmetrical. The finite element mesh of the concrete matrix and the CFRP laminate consists of quadrilateral eight-node isoparametric plane stress elements. The maximum dimension of each finite element does not exceed 15 mm. The thickness of these elements is equal to 500mm and 100mm for concrete and CFRP, respectively. Six-node interface elements with zero thickness in the normal direction were used in order to model the bond-slip behaviour between the composite laminate and the concrete surface. The thickness of the interface elements in the direction perpendicular to the plane of the structure is 100 mm. Similarly, the CFRP anchorage area, i.e. the set of steel plate and bolts, was modelled using the interface elements but with a different bond-slip behaviour.

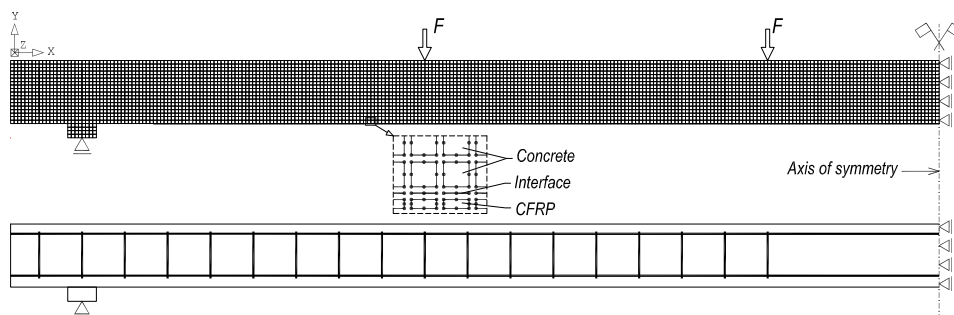


Fig. 8.13. Finite element model for RC beams; a) mesh topology, b) configuration of steel reinforcement

The upper bars and stirrups were modelled using the concept of embedded reinforcement. This means that the reinforcement does not have its own degrees of freedom. The uniaxial strain in the reinforcement element is compatible with the so-called mother element, i.e. an element in which reinforcement is embedded. The embedded reinforcement changes the stiffness of the mother element. The strain and stress in the embedded reinforcement are calculated from the mother element strains fields.

In the case of the bottom reinforcement, local slips in the vicinity of the flexural cracks affect crack spacing, which should be reflected by the numerical model. For this reason, the bottom reinforcement was modelled using three-node truss elements connected with the concrete matrix by special interface elements. This type of connection is able to model relative displacements (slips) between the concrete matrix and reinforcing bars in the direction tangential to the reinforcement. The displacements of the concrete matrix along the bar are calculated by interpolation of the nodes displacements of the 2D element. Therefore, similarly to the concept of embedded reinforcement, slipping reinforcement can be modelled independently of the connectivity of the concrete matrix elements. The configuration of steel reinforcement is presented in Fig. 4b. Each line represents four  $\varnothing 8$  bars for the upper reinforcement, two  $\varnothing 8$  bars for the stirrups and four  $\varnothing 12$  or  $\varnothing 16$  bars for the bottom reinforcement.

### 8.2.2. Constitutive material models

#### *Concrete model*

The constitutive model for concrete adopted in the current analysis is based on the concept of smeared cracks and formulated in total strains, following the propositions in (Vecchio, 1989; Vecchio, 1990; TNO DIANA). The fixed crack approach is used in this study. Before cracking, the stress-strain relationships (secant stiffness) are evaluated in the directions of principal strains. After cracking, the local directions are fixed and the stress-strain relationship are evaluated in the coordinate system determined by the first crack. Additionally, the shear stiffness is reduced in the direction tangential to the crack (shear modulus is multiplied by a shear retention factor  $\beta < 1.0$ ). A secondary crack may appear only in the direction perpendicular to the first crack.

The constitutive relationship in the plane stress conditions (2D) based on the secant stiffness matrix is described by the following formula (Vecchio, 1989; Vecchio, 1990):

$$\sigma = D_{sec} \varepsilon \quad (8.8)$$

where:  $\sigma = [\sigma_n \ \sigma_t \ \tau_{nt}]^T$  is the vector of stresses,  $\varepsilon = [\varepsilon_n \ \varepsilon_t \ \gamma_{nt}]^T$  is the vector of mechanical strains,  $n$  and  $t$  are the directions perpendicular and tangent to the first crack, respectively. Strains  $\varepsilon$  are decomposed from the total strains (total means here mechanical strains and the ones induced by shrinkage and temperature) in the following way:

$$\varepsilon = \varepsilon_{tot} - \varepsilon_{sh} - \varepsilon_{th}, \quad \varepsilon_{sh} = -|\varepsilon_{cs}(t)| [1 \ 1 \ 0]^T, \quad \varepsilon_{th} = \alpha_{th} \Delta T [1 \ 1 \ 0]^T \quad (8.9)$$

where  $\varepsilon_{cs}(t)$  is mean shrinkage strain evolution in time  $t$  due to cement hydration and concrete drying,  $\alpha_{th}$  is the thermal expansion coefficient,  $\Delta T$  is the increase of temperature from the initial temperature. In the present study, the temperature in the beams was uniform, the thermal expansions of all materials were similar and the structure was not restrained in any direction. Thus, the thermal effects can be omitted in calculations.

The secant stiffness matrix can be determined as:

$$D_{sec} = \begin{bmatrix} \bar{E}_n & 0 & 0 \\ 0 & \bar{E}_t & 0 \\ 0 & 0 & \beta G \end{bmatrix} \quad (8.10)$$

where  $\bar{E}_n$  and  $\bar{E}_t$  are secant elastic modulus in the normal and tangent directions to the first crack, respectively,  $G$  is a shear modulus,  $\beta$  – a shear retention factor. The secant values of the stiffness matrix are calculated from the uniaxial stress-strain relationships. In tension this relationship is assumed as in (Cornelissen et al., 1986; Hordijk, 1991) – see Fig. 8.14:

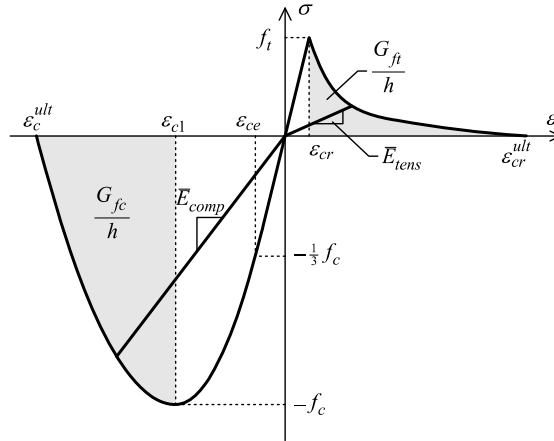


Fig. 8.14. Uniaxial stress-strain relationships for concrete

$$\sigma_t = \begin{cases} E_c \varepsilon & 0 \leq \varepsilon \leq \varepsilon_{cr} \\ f_t \left\{ \left[ 1 + \left( c_1 \frac{\varepsilon - \varepsilon_{cr}}{\varepsilon_{cr}^{ult}} \right)^3 \right] e^{-c_2 \frac{\varepsilon - \varepsilon_{cr}}{\varepsilon_{cr}^{ult}}} - \frac{\varepsilon - \varepsilon_{cr}}{\varepsilon_{cr}^{ult}} (1 + c_1^3) e^{-c_2} \right\} & \varepsilon_{cr} < \varepsilon \leq \varepsilon_{cr}^{ult} \\ 0 & \varepsilon > \varepsilon_{cr}^{ult} \end{cases} \quad (8.11)$$

where  $E_c$  is mean concrete elastic modulus,  $f_t$  is concrete tensile strength,  $\varepsilon_{cr} = f_t/E_c$  and constants  $c_1 = 3.0$ ,  $c_2 = 6.93$  are taken from (Hordijk, 1991).

The mesh objectivity of the numerical solution is provided by keeping constant fracture energy  $G_{ft}$  for a given area of a cracked element (“fracture energy trick” (de Borst, 1987)). Thus, the ultimate strain  $\varepsilon_{cr}^{ult}$  is calculated from:

$$\varepsilon_{cr}^{ult} = \varepsilon_{cr} + 5.136 \frac{G_{ft}}{hf_t} \quad (8.12)$$

where  $h$  is the crack bandwidth. For the applied type of finite element,  $h = \sqrt{A_{FE}}$  (Rots, 1988), where  $A_{FE}$  is the area of an individual finite element.

Tensile strength  $f_t$  and fracture energy  $G_{ft}$  were not directly measured in the experimental tests (Kotynia et al., 2013a). These material parameters were fitted in such a way that the simulated cracking load and load-displacement behaviour of the considered beams followed the experimental ones prior to strengthening. The adopted values of material parameters are shown in Table 8.5.

The uniaxial stress-strain curve for concrete in compression is shown in Fig. 8.14. The formula is defined in compliance with (Feenstra and De Borst, 1993) as:

$$\sigma_c = \begin{cases} -\frac{1}{3} f_c \frac{\varepsilon}{\varepsilon_{ce}} & \varepsilon_{ce} < \varepsilon \leq 0 \\ -\frac{1}{3} f_c \left[ 1 + 4 \frac{\varepsilon - \varepsilon_{ce}}{\varepsilon_{c1} - \varepsilon_{ce}} - 2 \left( \frac{\varepsilon - \varepsilon_{ce}}{\varepsilon_{c1} - \varepsilon_{ce}} \right)^2 \right] & \varepsilon_{c1} < \varepsilon \leq \varepsilon_{ce} \\ -f_c \left[ 1 - \left( \frac{\varepsilon - \varepsilon_{c1}}{\varepsilon_c^{ult} - \varepsilon_{c1}} \right)^2 \right] & \varepsilon_c^{ult} < \varepsilon \leq \varepsilon_{c1} \end{cases} \quad (8.13)$$

where:  $\varepsilon_{ce} = -\frac{1}{3} \frac{f_c}{E_c}$ ,  $\varepsilon_{c1} = 5\varepsilon_{ce}$ ,  $f_c$  is concrete compressive strength. The values of compressive strength and elastic modulus of concrete were taken directly from experimental tests (Kotynia et al., 2013a).

Table 8.5. Mechanical properties of concrete adopted in calculations

Element	$E_c$	$E_c$	$f_c$	$f_t$	$G_{ft}$	$G_{fc}$	$\beta$
	[GPa]	[-]	[MPa]	[MPa]	[N/m]	[N/m]	[-]
B12-a	23.7	0.2	32.2	1.9	90	$1.0 \cdot 10^4$	0.2
B12-a-e	24.7	0.2	41.6	3.2	90	$1.0 \cdot 10^4$	0.2
B16-a	25.4	0.2	49.0	2.5	90	$1.0 \cdot 10^4$	0.2
B16-a-e	26.4	0.2	51.0	4.1	90	$1.0 \cdot 10^4$	0.2

Similarly to the post-peak behaviour of concrete in tension, compression deformations after peak stress show a tendency to localization to a certain zone (Jansen and Shah, 1997; Markeset and Hillerborg, 1995; van Mier et al., 1997). This means that the descending part of the stress-strain relationship is size dependent, and stress-displacement description is more suitable in this case than stress-strain relationship. However, it is very convenient in FEM to have the constitutive material model defined by stress-strain relationship (or by their increments). In order to gain the objectivity of the post-peak behaviour of concrete in compression independently of FE mesh, the ultimate compressive strain can be introduced in the form (Feenstra and De Borst, 1993):

$$\varepsilon_c^{ult} = \varepsilon_{c1} - \frac{3 G_{fc}}{2 h f_c} \quad (8.14)$$

where  $G_{fc}$  is compressive fracture energy,  $h$  is the characteristic length of a finite element, assumed the same as for tension. The  $G_{fc}$  value is an additional material property and can be calculated from the post-peak stress-displacement diagram. The values for this quantity available in literature range from  $1.0 \cdot 10^4$  to  $2.5 \cdot 10^4$  N/m (Jansen and Shah, 1997; Vonk, 1992). The compression fracture energy is also expressed as the multiple of fracture energy – for example  $G_{fc} = 250G_{ft}$  (Nakamura and Higai, 2001). The values of  $G_{fc}$  adopted in the calculations are shown in Tab. 8.5. (note that the lower limit of  $G_{fc}$  values reported in (Jansen and Shah, 1997; Vonk, 1992; Nakamura and Higai, 2001) was assumed in the calculations).

If tensile strain exists in the direction perpendicular to compression, the compressive strength is substantially reduced (Belarbi and Hsu, 1995; Vecchio and Collins, 1993). The uniaxial compressive strength is multiplied by factor  $\beta_\sigma$  to take this effect into account (Vecchio and Collins, 1993):

$$\beta_{\sigma} = \min \left[ \left( 1 + 0.27 \left( \frac{\varepsilon_t}{\varepsilon_{cr}} - 0.37 \right) \right)^{-1} ; 1.0 \right] \quad (8.15)$$

where  $\varepsilon_t$  is tensile strain perpendicular to the crack. It should be noted that only  $f_c$  is reduced by the above factor, while  $\varepsilon_{cl}$  remains unchanged.

### Concrete-CFRP laminate interface

The behaviour of the concrete-to-laminate interface described below is suitable mainly for externally bonded laminates with strong (stiff) adhesives, where the failure of connection is induced by cracking in the concrete layer near the adhesive. It can be assumed that for actively or passively strengthened flexural elements the normal forces to the laminate-concrete connection are rather small. Thus, the constitutive relationships between the normal and tangential tractions and relative displacements are uncoupled, i.e. the normal traction  $t_n$  depends only on the relative normal displacement  $\bar{u}_n$ , and the tangential traction  $t_t$  is the function of only  $\bar{u}_t$ , where  $\bar{u}_t$  is the relative displacement in the tangential direction (the concrete - laminate slip). The definitions of  $t_n$ ,  $t_t$ ,  $\bar{u}_n$ ,  $\bar{u}_t$  are presented in Fig. 8.15.

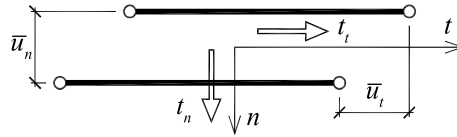


Fig. 8.15. Tractions and the relative displacement in the concrete-to-laminate interface

In the normal direction, the traction-relative displacement law is linear:

$$t_n = K_n \bar{u}_n \quad (8.16)$$

where:  $K_n$  is the normal stiffness of the interface. The local traction-slip behaviour in tangential direction is described by the function:  $t_t = g_t(\bar{u}_t)$ ,  $g_t$  is defined following (Lu et al., 2005) (see Fig. 8.16):

$$g_t = \begin{cases} K_{te}\bar{u}_t & 0 \leq \bar{u}_t \leq \bar{u}_{te} \\ t_{max}\sqrt{\frac{\bar{u}_t}{\bar{u}_{t0}}} & \bar{u}_{te} < \bar{u}_t \leq \bar{u}_{t0} \\ t_{max}e^{-\alpha\left(\frac{\bar{u}_t}{\bar{u}_{t0}}-1\right)} & \bar{u}_{t0} < \bar{u}_t \leq \bar{u}_{t,res} \\ t_{res,p} & \bar{u}_t > \bar{u}_{t,res} \end{cases} \quad (8.17)$$

where:  $t_{max}$  is maximum traction,  $\bar{u}_{t0}$  is the slip associated with  $t_{max}$ ,  $\alpha$  is a material constant that describes the post critical slope of function  $g_t$ .

If the linear material behaviour is assumed for slips from the range of  $\langle 0, \bar{u}_{te} \rangle$ .  $K_{te}$  is the initial stiffness and  $\bar{u}_{te} = 0.04\bar{u}_{t0}$ . Based on (Finckh and Zilch, 2012), for slips greater than  $\bar{u}_{t,res}$ , a constant residual traction  $t_{res,p}$  is assumed. The residual traction  $t_{res,p}$  reflects friction between concrete chunks at the fracture plane in the laminate-concrete connection. The slip  $\bar{u}_{t,res}$  is calculated from the equation:

$$\bar{u}_{t,res} = \bar{u}_{t,max} \left[ 1 - \frac{1}{\alpha} \ln \left( \frac{t_{res,p}}{t_{max}} \right) \right] \quad (8.18)$$

The incremental constitutive relationship of the laminate-concrete connection has the following form:

$$\bar{u}_{t,res} = \bar{u}_{t,max} \left[ 1 - \frac{1}{\alpha} \ln \left( \frac{t_{res,p}}{t_{max}} \right) \right] \quad (8.19)$$

where:

$$\Delta t = K \Delta u \quad (8.20)$$

$$\Delta t = \begin{bmatrix} \Delta t_n \\ \Delta t_t \end{bmatrix}, \quad \Delta \bar{u} = \begin{bmatrix} \Delta \bar{u}_n \\ \Delta \bar{u}_t \end{bmatrix}, \quad K = \begin{bmatrix} K_n & 0 \\ 0 & K_t(\bar{u}_t) \end{bmatrix} \quad (8.21)$$

The stiffness in tangential direction is defined by:

$$K_t = \frac{\Delta g_t}{\Delta \bar{u}_t} \tag{8.22}$$

The stiffness describes the constitutive law only for monotonic bond-slip behaviour. The complete physical law should also describe material behaviour in unloading conditions or unloading and reloading with opposite sign. This is important for structures that were severely cracked before strengthening or severe cracks appeared after applying the FRP reinforcement. The laminate is bonded in the vicinity of the crack edge, which is shown in Fig. 8.17. where local slips between cracks are presented. If the loading process is continued, slips of one sign dominate. Thus, the unloading/reloading with opposite sign process occurs near one crack (Fig. 8.17.). For slips  $\bar{u}_{te} < \bar{u}_t^{max}$ , where  $\bar{u}_t^{max}$  is the maximum slip reached in loading history, the damages (microcracks) in the microstructure of concrete near the surface are minor and plastic slips do not occur. Thus, unloading bond-slip path is directed towards the origin, as proposed in (Finckh, 2012) – see Fig.8.15. In this case, the secant stiffness in tangential direction is substituted by the equation:

$$K_{t1} \frac{t_t(\bar{u}_t^{max})}{\bar{u}_t^{max}} \tag{8.23}$$

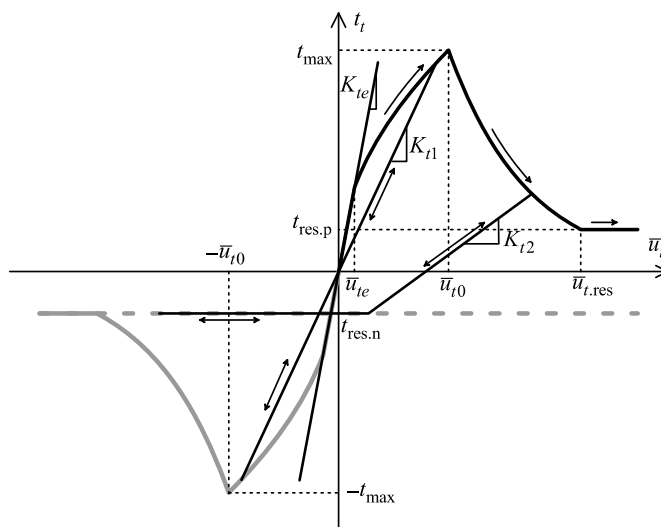


Fig. 8.16. Concrete-to-laminate traction-slip law

If, during further loading, slip  $-\bar{u}_t^{max}$  is reached, the bond-slip path follows the negative counterpart of  $g_t$ . The experimental evidence presented in (Ko and Sato, 2007; Zhang and Kanakubo, 2014) shows that if the maximum slip  $\bar{u}_t^{max}$  exceeds  $-\bar{u}_{t0}$  in the loading process, plastic slips occur. The secant stiffness in the tangential direction is given by the formula proposed in (Ko and Sato, 2007):

$$K_{t2} = \max \left[ a_1 \left( \frac{\bar{u}_t^{max}}{\bar{u}_{t0}} \right)^{q2}, g_t \frac{\bar{u}_t^{max}}{\bar{u}_t} \right] \quad (8.24)$$

where  $a_1$  and  $a_2$  are material constants determined empirically in (Ko and Sato, 2007).  $K_{t2}$  cannot be less than stiffness  $K_{t1}$  obtained for slips greater than  $\bar{u}_{t0}$  – see Fig. 8.16. This assumption prevents the model from nonphysical behaviour in the form of plastic slips with opposite sign in the unloading process.

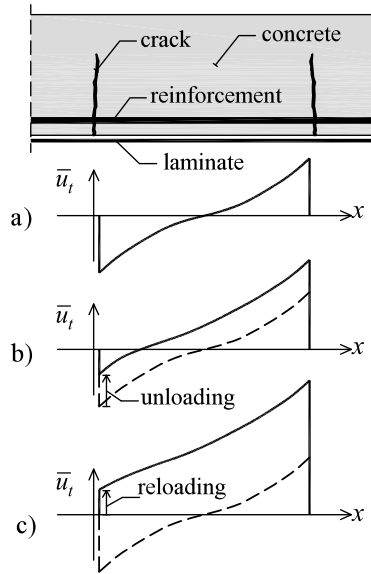


Fig. 8.17. Local laminate to concrete bond mechanism between cracks

Moreover, according to (Ko and Sato, 2007), if the maximum slip  $\bar{u}_t^{max}$  reached in the loading process is greater than  $\bar{u}_{t0}$  and, subsequently, when the unloading and reloading process with the opposite sign occurs, the maximum traction that can be reached is equal to  $t_{res,n}$  – see Fig. 8.17. This is coherent

with the near surface cracking mechanism simulated in (Lu et al., 2005b), where macrocracks near the concrete surface exist for significant slips. Only the residual forces in the interface are possible at these regions, as they are caused by friction in concrete between macrocracks.

The proposed approach to modelling the interface behaviour of externally bonded FRP laminates is not a standard material model available in the material library of used software (TNO DIANA). Due to this fact, the constitutive model was implemented using a user-supplied subroutine (USRIFC). The interface model was validated by performing two tests: an “one element” test and a cyclically loaded and unloaded anchorage test.

The first numerical test is presented in Fig. 8.18. The model consists of two 2D, eight-node elements connected by the six-node interface element. The vertical and horizontal displacements of the element No 1 are constrained at the element’s free edges. The relative displacement  $\bar{u}_t$  between 2D elements is obtained by the horizontal translation of the element No 2. The material parameters for the bond-slip relationship are taken from (Ko and Sato, 2007) as for the specimen C14 (  $t_{max} = 2.93MPa$  ,  $\alpha = 0.17$  ,  $\bar{u}_{t0} = 0.11mm$  ,  $t_{res,p} = t_{res,n} = 0.69MPa$  ,  $a_1 = 22GPa/m$  and  $a_2 = -0.93$  ). The load was applied in five sequences. During the first sequence the element No 2 was moved to  $\bar{u}_t = \bar{u}_{t0} = 0.11mm$  , then unloaded to zero and again loaded to  $\bar{u}_{t0}$  (sequence A-B-A- B in Fig. 8.18a). Next the element No 1 was moved to  $\bar{u}_t = 0.22mm$  , unloaded and reloaded to the same value (sequence B-C-A-C). In the third cycle No 2 element was moved to  $\bar{u}_t = 0.6mm$  , then unloaded and reloaded (sequence C-D-E-D in Fig. in Fig. 8.18b). Afterward the element No 2 was moved to  $\bar{u}_t = 1.2mm$  , then reloaded and loaded with opposite sign to  $\bar{u}_t = 0.25mm$  (sequence D-F-G). The last cycle started from  $\bar{u}_t = -0.25mm$  to  $\bar{u}_t = 1.6mm$  , then unloaded and reloaded again to  $\bar{u}_t = -0.25mm$  (sequence G-F-H-G).

The results of calculations presented in Fig. 8.18 indicate that the interface model correctly reproduces the monotonic traction-slip behaviour.

The second test is presented in Fig. 8.19. This is the anchorage test reported in (Ko and Sato, 2007) and performed on C14 specimen. The specimen’s dimensions are given in Fig. 8.19 and a detailed description of the test procedure can be found in (Ko and Sato, 2007). Mechanical parameters adopted in calculations are the same as for the first test. The specimen was loaded and unloaded in a few cycles up to the failure. The numerical model of the interface correctly reproduces experimental data both for monotonic and cyclic loads – see Fig. 8.20. At the beginning of the loading process the stiffness of the model is slightly underestimated. For the loading level above 17 kN discrepancies between the experiments and calculations are minor. The stiffness degradation

and plastic slips are correctly described, however, the model is unable to reflect the hysteresis phenomenon observed in the experiment.

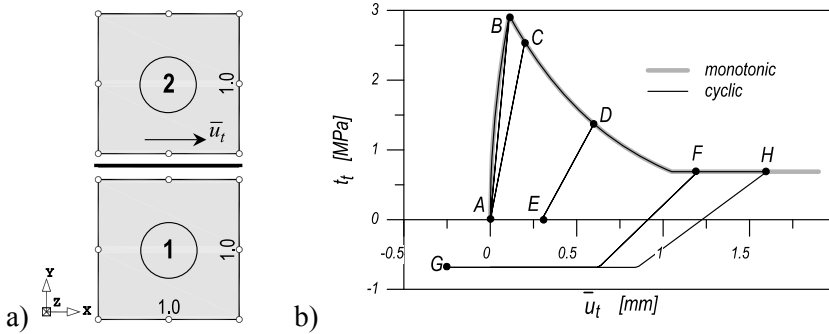


Fig. 8.18. Interface “one element” test: a) FEM model, b) results of calculations

Additionally, in Fig. 8.19 the distributions of traction along the bonding length for three loading levels are presented. The first load level (6.7 kN) is associated with attaining the maximum traction  $t_{max}$  at the point A. For the next load levels (19.0 kN and 22.1 kN) the pick  $t_{max}$  moves towards the anchorage end. After reaching the maximum load the snap-back behaviour is observed in the simulations – compare Fig. 8.20.

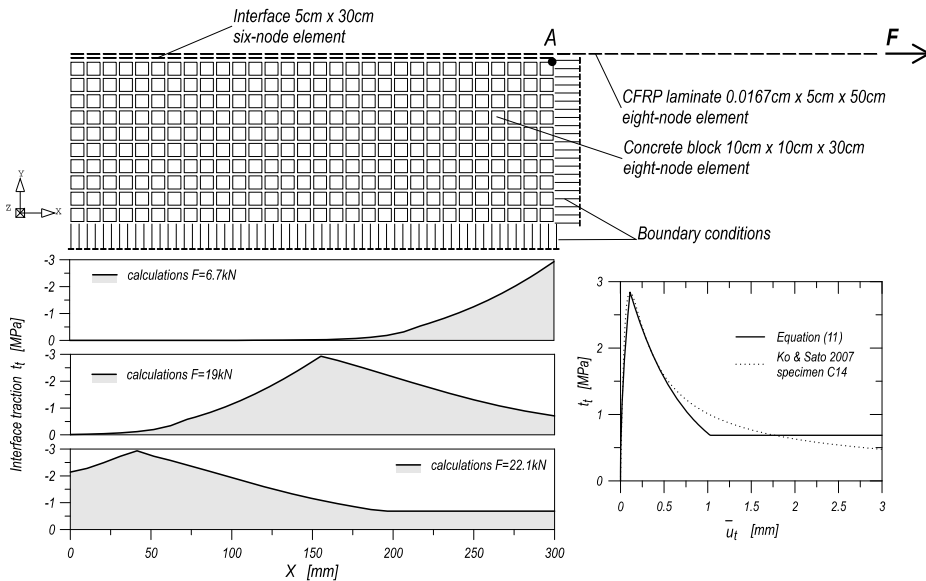


Fig. 8.19. FEM model for Ko & Sato (2007) anchorage test (specimen C14)

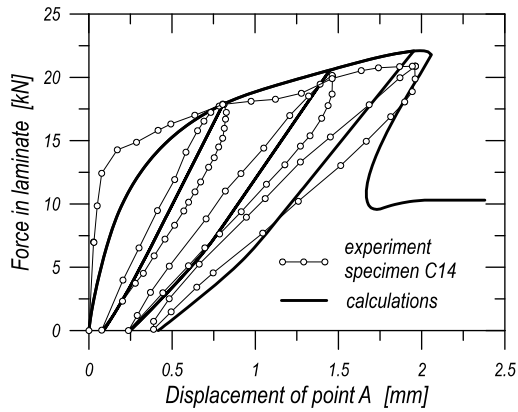


Fig. 8.20. Ko &amp; Sato (2007) anchorage test (C14) – experiment vs. calculations

Table 8.6. Mechanical parameters for the concrete-CFRP laminate interface

Element	$K_{t0}$	$K_n$	$t_{max}$	$\bar{u}_{t0}$	$\alpha$	$t_{res,p}^*)$	$a_1$	$a_2$
	[GPa/m]	[GPa/m]	[MPa]	[mm]	[-]	[MPa]	[GPa/m]	[-]
B12-a	$3.85 \cdot 10^2$	$4.0 \cdot 10^2$	3.2	0.042	0.27	0.65	63.7	-1.07
B12-a-e	$3.85 \cdot 10^2$	$4.0 \cdot 10^2$	2.8	0.036	0.21	0.50	74.8	-1.07
B16-a	$3.85 \cdot 10^2$	$4.0 \cdot 10^2$	2.5	0.032	0.18	0.27	83.4	-1.07
B16-a-e	$3.85 \cdot 10^2$	$4.0 \cdot 10^2$	4.3	0.056	0.46	0.50	46.9	-1.07

\*)  $t_{res,n} = -t_{res,p}$

The interface parameters adopted in the calculations of the beams are presented in Tab. 8.6. A part of the mechanical parameters (i.e.  $t_{max}$ ,  $t_{res,p} = -t_{res,n}$ ) shown in Tab. 8.6. were calibrated by a trial-and-error procedure in order to obtain the best agreement between the numerical simulations and experiments. On the basis of calibrated  $t_{max}$  the rest of mechanical parameters for the monotonic bond-slip law (i.e.  $\bar{u}_{t0}$ ,  $\alpha$ ,  $K_{te}$ ) were calculated according to the formulas in (Lu et al., 2005a). The parameters for the unloading behaviour ( $a_1, a_2$ ) are taken from (Ko and Sato, 2007) as the mean value for the specimens C14 to C19. It should be pointed out that the calibrated values for  $t_{max}$  are near the lower limit of experimental findings described in the literature on the subject and collected in (Ko et al., 2014). This effect is probably due to the fact that the experimental values of  $t_{max}$  were obtained for bonding tests carried out on the concrete specimens without any earlier preloading (usually it is a virgin concrete block). The concrete in the analysed beams was subjected to tensile stresses due to shrinkage in the vicinity of bottom

reinforcement and mechanical preloading. The CFRP laminate was applied to the concrete cover with damages, i.e. microcracks, that influenced on the  $t_{max}$  values.

### ***Concrete-CFRP laminate traction-slip law in the bonding region***

The anchorage system consisted of a steel plate mechanically fastened to the beam. The laminate was glued to the concrete and to the steel plate. The experimentally observed failure of the anchorage system was the laminate sliding from under the steel plate. Due to the lack of experimental evidence concerning the local tangential traction-slip behaviour of such bonding system type, the elastic perfectly plastic constitutive relationship was stipulated for this region, as shown in Fig. 8.21.a.

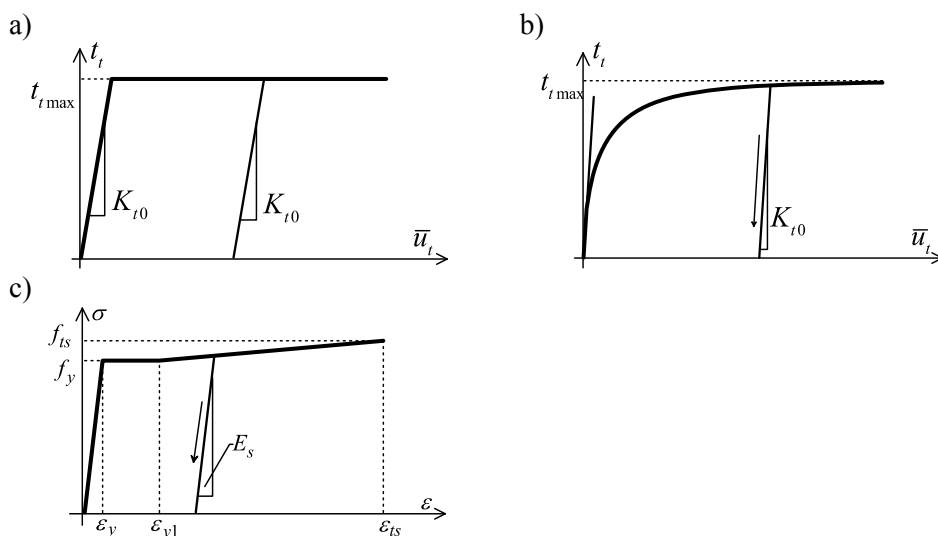


Fig. 8.21. a) bond-slip relationship in the mechanical anchorage region (steel plates), b) bond-slip model for the steel-concrete interface, c) uniaxial stress-strain relationship for reinforcing steel

The tangent and normal stiffness was assumed to be equal to  $3.85 \cdot 10^2$  GPa/m and  $4.0 \cdot 10^2$  GPa/m, respectively. The maximum traction in tangent direction  $t_{max}$  was 7.1 MPa.

***Bond-slip between steel reinforcement and concrete, constitutive model for reinforcing steel and CFRP***

The bond-slip behaviour of the tensile reinforcement is described according to (Shima et al., 1987) and presented in Fig. 8.21. Traction  $t_t$  and the relative bar – concrete slip is governed by the following exponential equation:

$$t_t = a_{nb} t_{tmax} \left[ 1 - e^{\left( \frac{-40\bar{u}_t}{D} \right)^{0.6}} \right] \quad (8.25)$$

where  $t_{max} = 0.9 f_c^{2/3} MPa$ ,  $D$  is the diameter of the tensile reinforcement bar and  $a_{nb}$  is equal to the number of tensile bars,  $a_{nb} = 4$ . The mechanical parameters for this bond-slip behaviour were calculated on the basis of the mean concrete strength given in Tab. 8.5. High penalty stiffness was assumed in the normal direction to the bar.

The constitutive model for steel is unambiguously defined by the uniaxial stress-strain relationship. The elastic-plastic with linear kinematic hardening model was assumed – Fig. 8.21.c. The mechanical parameters for steel adopted in the calculations were determined on the basis of experimental tests (Kotynia et al., 2013a) and are summarised in Tab. 8.7.

Table 8.7. Mechanical parameters of reinforcing steel used in the calculations

Element	Type of reinforcement	Steel series	Diameter of bars	$E_s$	$f_y$	$f_{ts}$	$\varepsilon_y$	$\varepsilon_{y1}$	$\varepsilon_{ts}$
			[mm]	[GPa]	[MPa]	[MPa]	[‰]	[‰]	[‰]
B12-a	t	A	12	191.1	511.4	594.5	2.68	25	100
	c, s	A	8	200.7	583.1	650.5	2.91	25	100
B12-a-e	t	B	12	191.3	539.6	627.5	2.82	25	100
	c, s	B	8	186.1	416.2	734.1	2.24	10	75
B16-a	t	C	16	198.0	595.0	672.0	3.01	23	100
	c, s	C	8	196.4	555.8	646.0	2.83	10	50
B16-a-e	t	C	16	198.0	595.0	672.0	3.01	23	100
	c, s	C	8	196.4	555.8	646.0	2.83	10	50

*t* – tensile reinforcement, *c* – compression reinforcement, *s* – stirrups

The linear elastic behaviour of CFRP laminate was assumed for strains less than the rupture strain of the laminate ( $\varepsilon_{fu} = 16.5‰$ ). The elastic modulus  $E_{CFRP}$  was equal to 173 GPa and the tensile strength of the laminate

$f_{fu} = 2857 \text{ MPa}$ . The calculations were terminated after reaching the strain limit  $\varepsilon_{fu}$ , which reflects the rupture of the tape.

### 8.2.3. Strategy of numerical simulations

#### 8.2.3.1. Loadings

Four loading schemes can be distinguished in the laboratory tests that were also considered in the numerical calculations. These loading schemes include: the dead weight, shrinkage of concrete, prestressing applied to laminates, external preloading and additional loading in the form of concentrated forces. The loading conditions were applied in the sequences that followed the experimental loading program described in (Kotynia et al., 2013a).

The dead weight was modelled as mass forces at each node of the finite element mesh. The concentrated load ( $F$ ) was replaced by a local, uniformly distributed load over the width of 0.1 m. The resultant of this load was equal to  $F$ , and its locations are shown in Fig. 8.13.

Since the shrinkage of concrete was not directly measured in a laboratory test, the kinetics of shrinkage strain  $\varepsilon_{cs}(t)$  was assumed to be as stipulated in (EN 1992-1-1:2004, 2004). Due to the fact that the autogenous shrinkage effects take place when the elastic properties of concrete are not fully developed, the only shrinkage to be considered was mean drying shrinkage. Similarly, the effect of nonuniform shrinkage distribution associated with nonuniform moisture field in the specimen's cross-section can be neglected. All elements were tested at least 70 days after removing formworks. Taking this fact into consideration as well as the shape of the specimen's cross-section, it is clear that the differences of drying shrinkage strain between the middle and external fibres of the cross-section (as the result of moisture gradients) are negligible and they did not induce a stress field in the specimens at the time when the tests were performed.

The prestress was modelled as the uniform load  $\sigma_{fp}$  applied to the ends of the CFRP laminate. The value of  $\sigma_{fp}$  was calibrated to obtain the initial strain in laminate  $\varepsilon_{fp}$  (i.e. the strain after immediate losses due to slips in anchors and prestress-induced deformations) equal to the strain measured in the tests (see Tab. 8.4.).

#### 8.2.3.2. Numerical procedure

An incremental iterative procedure was employed to obtain a solution for the analysed structures and loading programs. The computational process was controlled by increments of external loads and prestress. For load levels close to

the failure load (approximately 80% of the experimental failure load), the force controlled procedure was changed to the arc-length method. A vertical displacement of the node located at the top surface of the beam in the axis of symmetry was the control parameter for the arc-length method. For each load increment, the equilibrium between internal and external forces was calculated using the Newton–Raphson procedure. The residual forces and displacements norms were used as the convergence criteria.

The laboratory experiments contained several stages that had to be precisely reflected in the numerical simulations. Therefore, a phased analysis was used in the calculations. The following phases were taken into consideration:

- Phase I – reinforced concrete element without strengthening. The following model components were activated in this phase: concrete matrix elements, steel reinforcement and kinematic boundary conditions. The initial loads were applied in the successive sequences as: shrinkage, dead weight and preloading (if appropriate).
- Phase II – prestressing. CFRP laminate elements were added to the components of Phase I. The prestressing was applied at the end of the laminate.
- Phase III – transfer of the prestress force to the anchorage system. In this phase, all concrete-laminate interface elements were added to the model. In the case of preloaded elements (beams B12-a-e, B16-a-e), additional supports were activated at the location of the concentrated forces. These supports model the temporary displacements interlocks introduced in the experiments during prestressing of preloaded specimens (in the experiments these supports were realized using timber columns that blocked deflections during strengthening).
- Phase IIIa – removing the additional supports. This phase concerns only the preloaded beams.
- Phase IV – applying additional loading on the beams until the occurrence of failure. All model components from Phase III excluding the temporary supports were active in this phase of the analysis.

### **8.2.3.3. Validation of the numerical model**

The main goal of comparative analysis is validation of the proposed numerical model and the adopted mechanical parameters. In this comparative analysis, all quantities measured during experiments were taken into consideration, i.e. the maximum load bearing capacities, vertical displacements in the midspan, mean compressive and tensile strains in concrete averaged over the zone of constant curvature and mean strains of the laminate averaged over the same zone. Moreover, the analysis includes comparison with calculated

reference beams, i.e. non-strengthened beams and beams strengthened in the passive manner, i.e. without prestress. This provides the opportunity to analyse the influence of prestressing on the strengthening effectiveness in both the ultimate limit state (ULS) and the serviceability limit state (SLS).

The calculated and the experimental load bearing capacities are compared in Tab. 8.8. The experimental and calculated values differ less than 5%. Additionally, Tab. 8.8. shows the calculated load capacities of the reference specimens that were used to obtain strengthening efficiency ratios. The strengthening efficiency  $\eta_A$  related to a non-strengthened (RC) specimen is between 41% to 103%. For the passive type of strengthening, the strengthening efficiency  $\eta_P$  is lower and ranges from 32% to 76%. Comparison of  $\eta_A$  and  $\eta_P$  ratios indicates that, for ULS, the prestress affects more the elements with a lower steel reinforcement ratio. It is worth noting that the ultimate load for passively strengthened elements was achieved for significantly greater deformations – compare  $a_A$  and  $a_P$  values in Tab. 8.8.

Tab. 8.8.. Experimental vs. calculated ultimate load and calculated strengthening efficiencies

Element	$2F_{u,exp}$ [kN]	$2F_{u,A}$ [kN]	$\frac{2F_{u,exp}}{2F_{u,A}}$	$2F_{u0}$ [kN]	$2F_{u,P}$ [kN]	$\eta_A$	$\eta_P$	$a_A$ [mm]	$a_P$ [mm]
B12-a	53.0	52.3	101%	25.8	45.3	103%	76%	183	249
B12-a-e	49.0	51.7	95%	28.5	43.6	81%	53%	242	272
B16-a	74.4	73.9	101%	48.8	73.0	51%	50%	200	321
B16-a-e	72.0	71.5	101%	50.5	66.9	41%	32%	166	299

$F_{u,exp}$  – experimental ultimate load for strengthened specimen,  $F_{u,A}$  – calculated ultimate load for strengthened specimen,  $F_{u,0}$  – calculated ultimate load for RC reference specimen,  $F_{u,P}$  – calculated ultimate load for passively strengthened reference specimen,  $\eta_A = \frac{F_{u,A} - F_{u,0}}{F_{u,0}}$  – strengthening efficiency of prestressed specimens,  $\eta_P = \frac{F_{u,P} - F_{u,0}}{F_{u,0}}$  – strengthening efficiency for nonprestressed specimen,  $a_A$  - midspan displacement for active strengthened beams at ultimate load,  $a_P$  - midspan displacement for passive strengthened beams at ultimate load

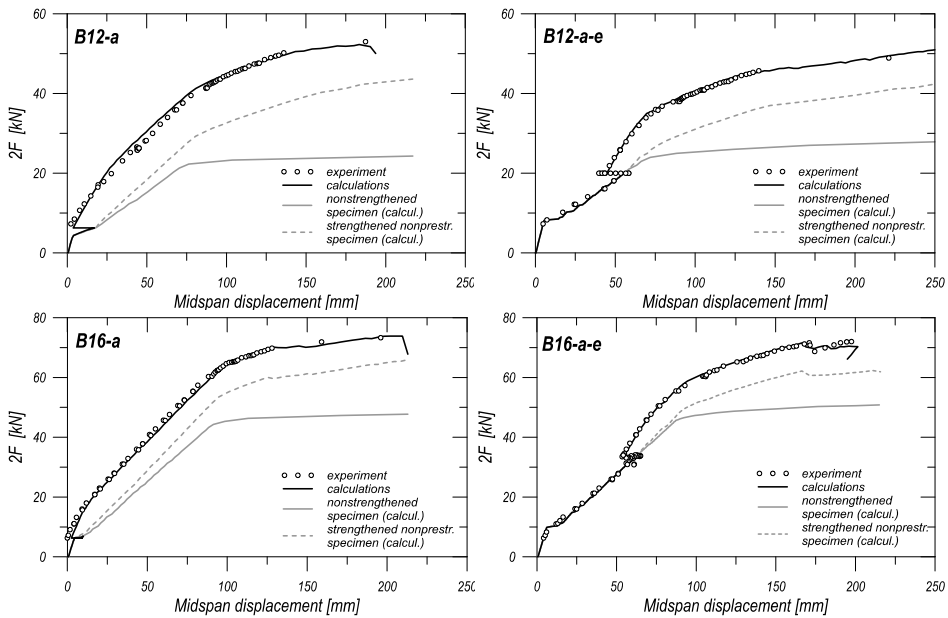


Fig. 8.22. Calculated and test charts of load – displacement

The comparison of the calculated and experimental load-displacement curves is shown in Fig. 8.22. These results are in a very good agreement for the whole loading range and throughout all the experimental stages. The numerical model is able to reproduce reduction of stiffness due to cracking at the first stage of experiment (preloading stage), then correctly reflects the stiffness recovery due to prestressing and finally predicts the decrease of stiffness as a result of crack development, yielding of steel and slips between the laminate and concrete. High accuracy in the simulations of the beams behaviour was achieved both for the specimens strengthened under self-weight (Fig. 8.22.b and c) and for the beams preloaded at the level of above 70% of the ultimate load capacity of the non-strengthened beam (reference RC specimen) – Fig. 8.22.b and d. When we compare the calculated displacements of actively and passively strengthened elements, we can see clearly that prestressing strongly influences the behaviour of specimens. Active strengthening introduces reverse displacements, prevents stiffness degradation at the low loading levels and also postpones the yielding of steel, which is especially important for highly preloaded elements.

The good predictive performance of the model is also demonstrated in Fig. 8.23. and Fig. 8.24. These figures present the comparison of experimental and predicted mean strains in the CFRP laminate as well as in the concrete tension and compression zones. In the case of concrete, the strains were measured at the distance of 35 mm from the specimen’s top and bottom surfaces. The model correctly reproduces changes in the CFRP strain gradients due to development

of cracks and the yielding of steel. Fig. 8.23. also shows strains in the reference beam, i.e. the one that was strengthened but not prestressed.

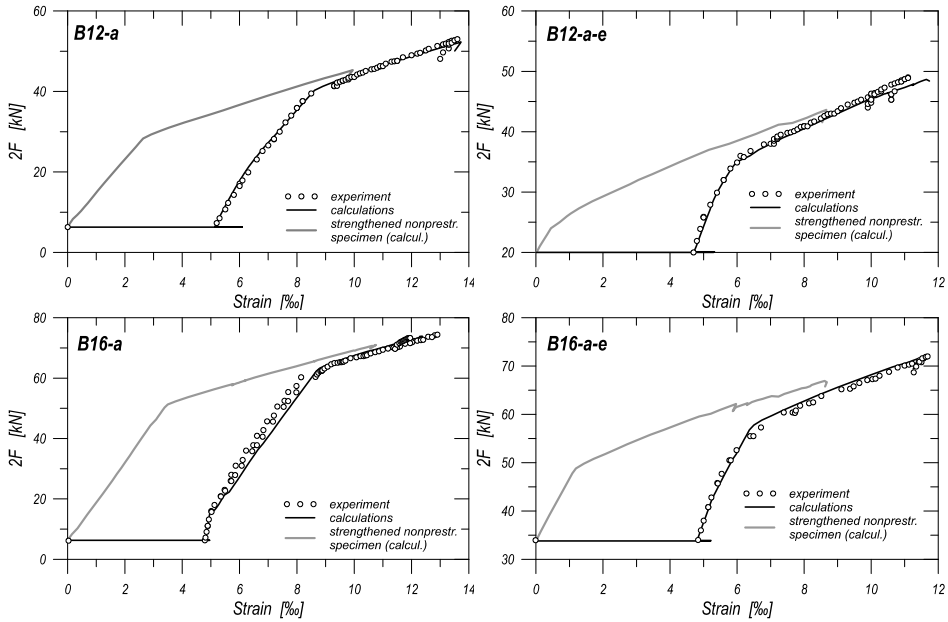


Fig. 8.23. Calculated and test charts of load - CFRP strain

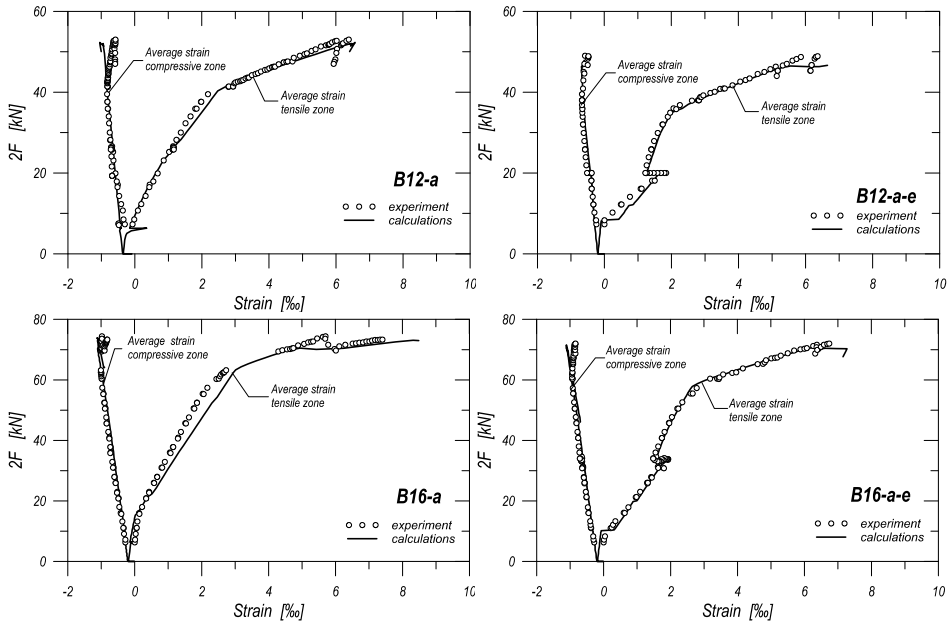


Fig. 8.24. Calculated and test charts of load - concrete strain

Chosen nonlinear finite element models

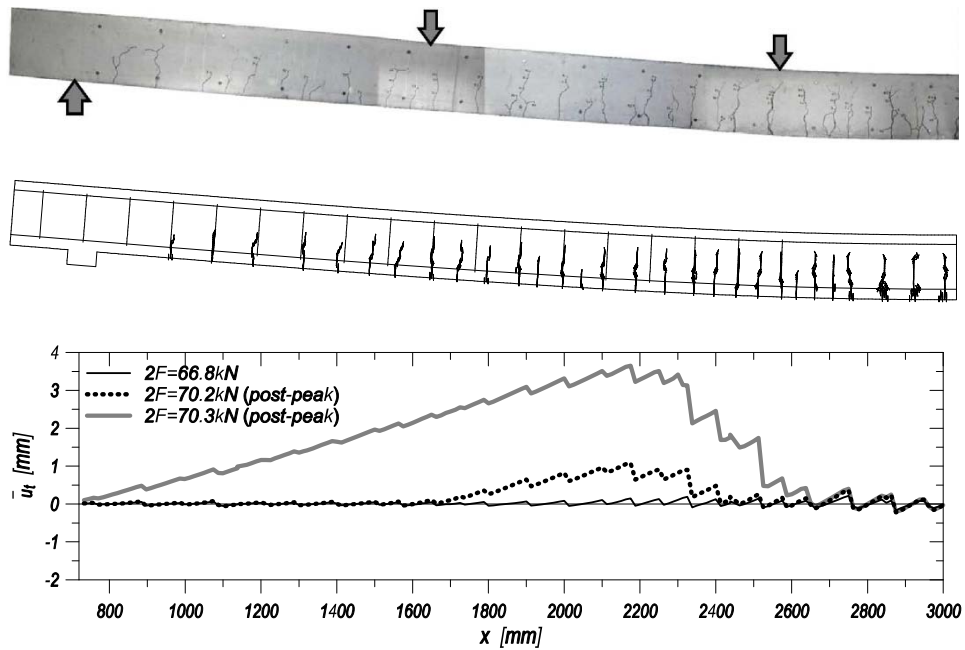


Fig. 8.25. Beam B16-a-e: a) experimental crack path after failure, b) predicted crack path after failure, c) local slips between concrete and CFRP laminate for different load stages

In all cases the ultimate CFRP strain of non-prestressed specimens is lower than the one for the actively strengthened beam. The differences between the ultimate strains, however, are less than the prestressing strain  $\varepsilon_{fp}$ . Apparently, these differences can be attributed to the fact that the slips between the concrete and laminate for comparable load levels are more developed in the actively strengthened specimens and provide slightly worse bonding conditions than in the case of the passively strengthened counterpart.

Experimentally and numerically obtained crack patterns for specimen B16-a-e at the ultimate load are shown in Fig. 8.25.a and b. The cracks in Fig. 8.25. are presented in the form of line sections at integration points perpendicular to the direction of the strain  $\varepsilon_n$  and they indicate the zones of fracture damage localization. The lines are visible only if the cracks have the width greater than 0.1 mm, i.e. if  $\varepsilon_n h \geq 0.1\text{mm}$ . The fracture damages localize mainly near the stirrups (where the first cracks appeared). For load levels close to the ultimate load, additional cracks appeared, usually between stirrups. A similar crack development process was observed in the experiments – see Fig. 8.25.a.

Fig. 8.25.c. presents development of slips  $\bar{u}_i$  in the concrete-laminate interface between the anchorages. For the loads near the failure, high slips of one sign are propagated from the location of the middle loading point towards the anchorage. The plastic flow in the anchorage was noticed following development of slips in the middle zone of the laminate. This precisely simulates the failure mode which was observed in the experiments – the intermediate crack debonding (IC) failure followed by sliding of composite from the anchorages.

#### 8.2.4. Parametric study

Table 8.9. Material and structural parameters considered in the parametric study

Element	Concrete class	$A_{s1}$	$b_F$	$E_{CFRP}$	$2F_{u0}$ $M_{u0}^*$	$\frac{2F_p}{2F_{u0}}$ $\frac{M_{u0}^*}{M_{u0}}$ [%]	$\sigma_{fp}$ % $f_{ju}$	Load scheme	$t_{max}$	$2F_u$ $M_u^*$	$\varepsilon_{f,max}$	$\eta_{ef}$
BPS-01	C30/37	4ø16	0.1	173.6	46.7	20	50	4F	3.60	75.5	14.91	90
BPS-02	C30/37	4ø16	0.1	173.6	46.7	40	50	4F	3.60	72.9	14.15	86
BPS-03	C30/37	4ø16	0.1	173.6	46.7	60	50	4F	3.60	70.1	13.51	82
BPS-04	C30/37	4ø16	0.1	173.6	46.7	20	20	4F	3.60	66.8	10.20	62
BPS-05	C30/37	4ø16	0.1	173.6	46.7	40	20	4F	3.60	63.9	9.16	56
BPS-06	C30/37	4ø16	0.1	173.6	46.7	60	20	4F	3.60	63.2	9.03	55
BPS-07	C60/75	4ø16	0.1	173.6	50.8	20	50	4F	5.74	85.8	16.49	100
BPS-08	C60/75	4ø16	0.1	173.6	50.8	40	50	4F	5.74	84.4	16.49	100
BPS-09	C60/75	4ø16	0.1	173.6	50.8	60	50	4F	5.74	83.3	16.49	100
BPS-10	C60/75	4ø16	0.1	173.6	50.8	20	20	4F	5.74	75.6	11.74	71
BPS-11	C60/75	4ø16	0.1	173.6	50.8	40	20	4F	5.74	74.6	11.51	70
BPS-12	C60/75	4ø16	0.1	173.6	50.8	60	20	4F	5.74	74.9	11.86	72
BPS-13	C60/75	4ø16	0.1	173.6	50.8 91.4	40 40	35	4F	5.74	80.2 144.4	14.29	87
BPS-14	C60/75	4ø16	0.15	173.6	50.8	40	35	4F	5.42	98.4	15.57	95
BPS-15	C60/75	4ø16	0.20	173.6	50.8	40	35	4F	5.11	117.4	16.49	100
BPS-16	C60/75	4ø16	0.1	225.3	50.8	40	1000 MPa	4F	5.74	82.2	11.94	n/a
BPS-17	C60/75	4ø16	0.1	121.3	50.8	40	1000 MPa	4F	5.74	76.7	17.94	n/a
BPS-18	C60/75	4ø12	0.1	173.6	31.6	40	35	4F	5.74	63.5	14.94	91
BPS-19	C60/75	4ø20	0.1	173.6	75.3	40	35	4F	5.74	100.4	13.08	79
BPS-20	C60/75	4ø16	0.1	173.6	50.8	40	35	4F	7.46	83.0	15.58	95
BPS-21	C60/75	4ø16	0.1	173.6	50.8	40	35	4F	4.02	74.8	12.21	74
BPS-22	C60/75	4ø16	0.1	173.6	91.4	40	35	2F	5.74	136.4	12.91	78
BPS-23	C60/75	4ø16	0.1	173.6	91.4	40	35	q	5.74	154.3	16.49	100

### Chosen nonlinear finite element models

$A_{s1}$  – steel reinforcement,  $b_F$  – laminate width,  $E_{CFRP}$  – elastic modulus of the laminate,  $f_{fu}$  – tensile strength of the laminate,  $2F_{u0}$  – failure load of non-strengthened specimen,  $M_{u0}$  – ultimate bending moment of non-strengthened specimen,  $2F_p$  – preloading,  $M_p$  – bending moment at preloading,  $4F$ ,  $2F$ ,  $q$  – load configuration respectively: 4 forces (as in experiment), 2 forces each 2.0 m from support, uniformly distributed load,  $2F_u$  – ultimate load,  $M_u$  – ultimate bending moment of the strengthened specimen,  $\varepsilon_{f,max}$  – strain in laminate at failure load,  $\eta_{ef} = \varepsilon_{f,max} / \varepsilon_{fu}$  – strain efficiency,  $\varepsilon_{fu}$  – rupture strain of laminate

The comparative analysis described in the previous section confirms the high predictive potential of the proposed numerical model. The main goal of this section is a parametric study that constitutes a supplementary analysis of the experimental tests (Kotynia et al., 2013a). The following parameters are taken into consideration, as well as their influence on the load bearing capacity and failure mode of actively strengthened beams: concrete class, steel and composite reinforcement ratios, elastic properties of the composite, bond strength between laminate and concrete, and load configurations. Additionally, the effect of preloading and prestressing ratios was also studied. Tab. 8.9. shows the list of the material and structural parameters that were considered in this parametric study.

Table 8.10. Mechanical parameters for concrete and bond-slip interface

Concrete class	C30/37 $b_F = 10cm$	C60/75 $b_F = 10cm$ , $b_F = 15cm^\#$ , $b_F = 15cm^{##}$
$f_c$	30	60
$f_{ct}$	2.0	3.2
$E_c$	32.8	39.1
$G_{fc}$	$10^4$	$10^4$
$G_{ft}$	80	115
$K_{t0}$	$3.85 \times 10^2$	$3.85 \times 10^2$
$K_n$	$4.0 \times 10^2$	$4.0 \times 10^2$
$t_{max}$	3.60	5.74, 5.42 <sup>#</sup> , 5.11 <sup>##</sup>
$\bar{u}_{t0}$	0.047	0.074, 0.070 <sup>#</sup> , 0.066 <sup>##</sup>
$\alpha$	0.34	0.86
$t_{res,p}^*$	0.68	0.41
$a_1$	56.1	34.2, 36.7 <sup>#</sup> , 39.0 <sup>##</sup>
$a_2$	-1.07	-1.07
*) $t_{res,n} = -t_{res,p}$		

Two classes of concrete were considered – C30/37 and C60/75 (EN 1992-1-1:2004, 2004). These concrete classes represent normal strength concrete and high performance concrete and they were selected to model different types of expected failure modes, i.e. failure governed by crushing of concrete in a compression zone associated with IC debonding of composite or failure governed only by bond-slip strength or laminate rupture. Tab. 8.10. shows the mechanical parameters of the analysed concrete types. Since the bond-slip behaviour depends on fracture properties of concrete, the adopted parameters for the traction-slip law are also shown in Tab. 8.10. These parameters were determined on the basis of (Ko and Sato, 2007) –  $t_{max}$ ,  $\bar{u}_{tmax}$ ,  $\alpha$ ; (Lu et al., 2005) –  $a_1$ ,  $a_2$  and (Finckh and Zilch, 2012) –  $t_{res,p}$ ,  $t_{res,n}$ . The stress-strain behaviour for steel reinforcement was taken as for C series steel shown in Tab. 8.7.

Three levels of preloading were considered – 20%, 40% and 60% of a non-strengthened specimen's ultimate load. The calculations were performed for two prestressing levels equal to  $20\%f_{fu}$  and  $50\%f_{fu}$ . Fig. 8.26. illustrates the results of the numerical simulations. The load capacities and maximum laminate strain are listed in Tab. 8.9. (elements BPS-01 to BPS-12). The results of calculations showed that the preloading has moderate influence on the load bearing capacity. In the case of normal strength concrete, the decrease in ultimate load was 5%-7% (beams BPS-01 to BPS-06). For high performance concrete, the differences were even smaller and did not exceed 3% (beams BPS-07 to BPS-12). Generally, the higher the preload level, the softer response of the specimen was observed. This is the result of accumulated damages (cracks) for beams with higher preload at strengthening. As expected, three failure mechanisms were obtained in the simulations. The first failure mode relied on simultaneous laminate slipping and concrete crushing and was pertinent to structures made of the normal concrete class. The next two failure modes were obtained for high performance concrete (C60/75). For the low prestress level ( $20\%f_{fu}$ ), the failure was governed by the laminate debonding mechanism, whereas the prestress equal to  $50\%f_{fu}$  resulted in the rupture of the composite.

Regardless of the mechanism involved in the failure, prestress has a significant effect on the ultimate load – see Fig. 8.26. For two considered concrete classes, the increase of the ultimate load was 37% to 47%, respectively, for concrete C30/37 (BPS-05) and C60/75 (BPS-11) and the prestress level of  $20\%f_{fu}$ . For prestress of  $50\%f_{fu}$ , the increase in the load bearing capacity was 56% (C30/37 – BPS-02) to 66% (C60/75 – BPS-08). The increase in the strain efficiency ratio  $\eta_{ef}$  for the specimens made of high performance concrete is attributed to better bonding properties between this type of concrete and laminate.

## Chosen nonlinear finite element models

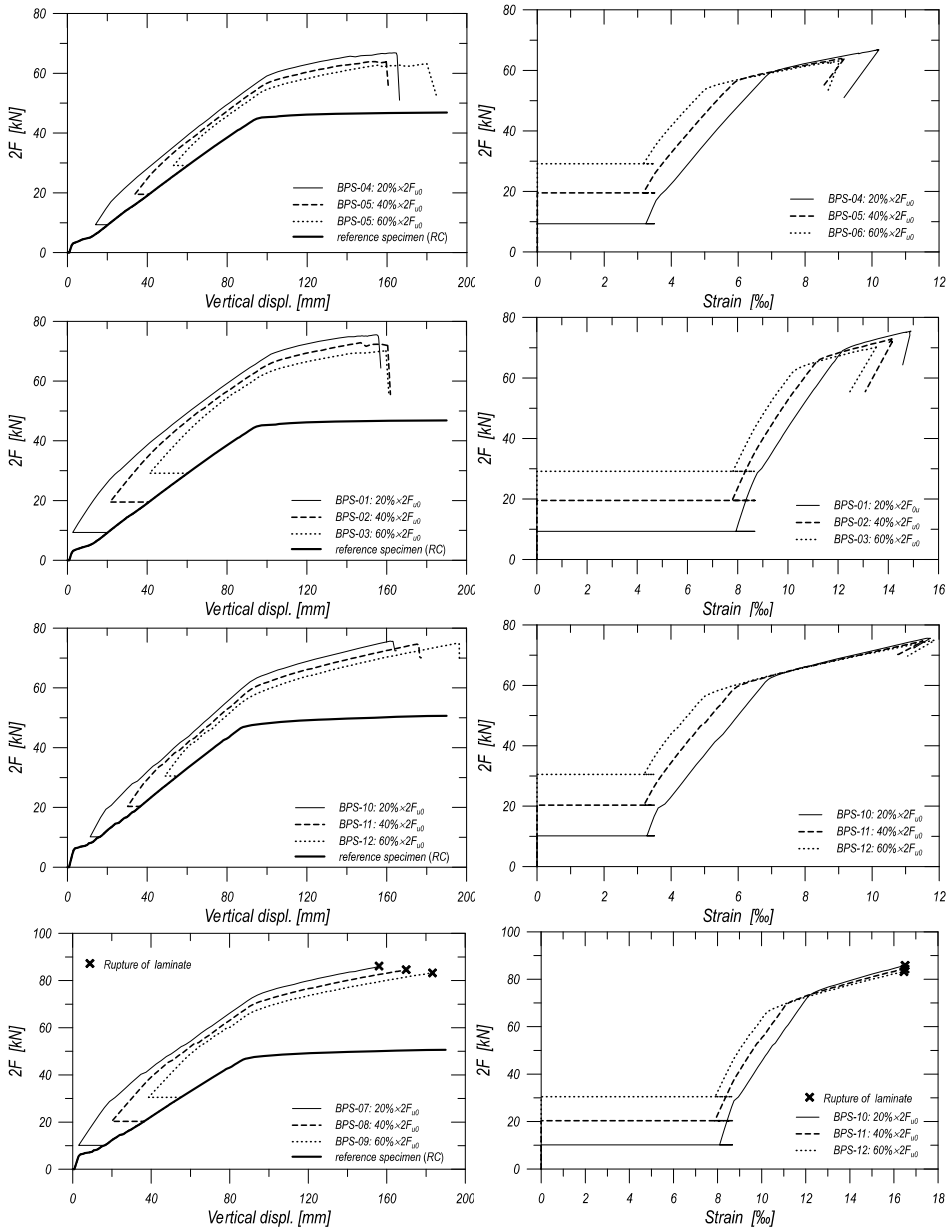


Fig. 8.26. Effect of preloading on load-displacement (the left column) and load-CFRP strain behaviour (the right column): a) C30/37 class and  $\sigma_{fp} = 20\%f_{fu}$ , b) C30/37 class and  $\sigma_{fp} = 50\%f_{fu}$ , c) C60/75 class and  $\sigma_{fp} = 20\%f_{fu}$ , d) C60/75 class and  $\sigma_{fp} = 50\%f_{fu}$

Fig. 8.28. presents the effect of concrete class on load-displacement and load-CFRP strain behaviour. The calculations were made for the specimens with preloading equal to 40% and prestress equal to  $20\%f_{fu}$  – elements BPS-05 (C30/37) and BPS-11 (C60/75). The beam made of concrete class C60/75 had the failure load 17% higher than the structure made of normal concrete. The increase in the failure load as well as the better strain efficiency ratio  $\eta_{ef}$  for the specimen made of high performance concrete is the result of better bond-slip properties for the concrete-laminate interface.

The elastic modulus of concrete also plays a minor role here. Specimens made of high performance concrete had lower deflections and thus less developed concrete-laminate slips for comparable load levels. The coupled effects of better traction-slip properties and lower deflections resulted in higher IC debonding failure load for the high performance concrete beam.

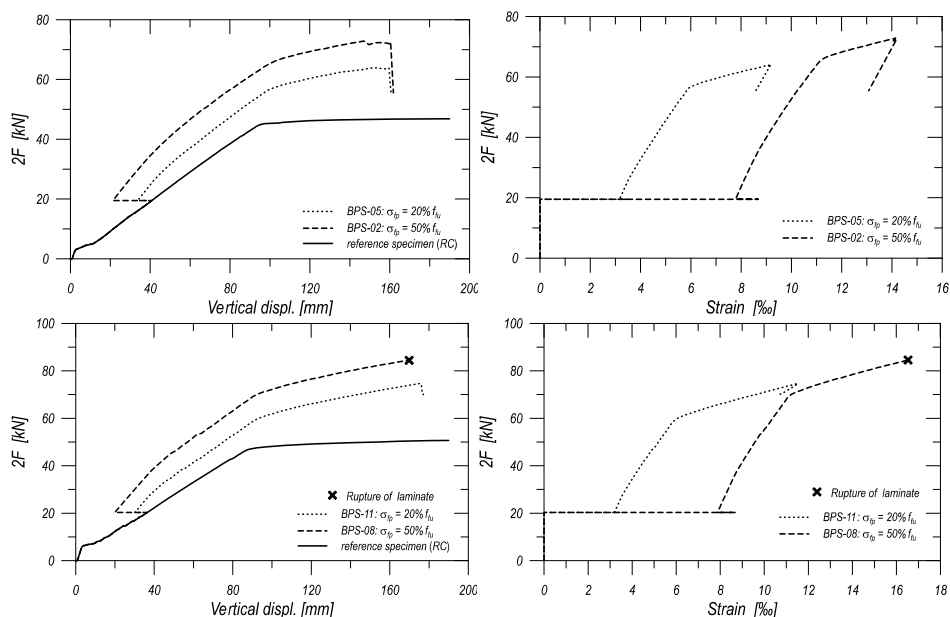


Fig. 8.27. Effect of prestressing on load-displacement (left column) and load-CFRP strain behaviour (right column): a) C30/37 concrete class: b) C60/75 concrete class

Fig. 8.29. shows the comparison of load-displacement and load-composite strain diagrams for three different laminate widths, i.e.  $b_f = 10\text{cm}$  (BPS-13),  $b_f = 15\text{cm}$  (BPS-14),  $b_f = 20\text{cm}$  (BPS-15). The effect of  $b_f/b_c$  ratio, where

## Chosen nonlinear finite element models

$b_c$  is the width of a beam, was taken into account in the calculations according to the model in (Lu et al., 2005) – compare Tab. 8.9. The obtained numerical results are quite obvious.

The increase of the ultimate load between corresponding elements was almost proportional to the increase of width – see Tab. 8.9. This is the effect of proportionally higher prestress load in the beams with  $b_F$  of 15cm and 20cm.

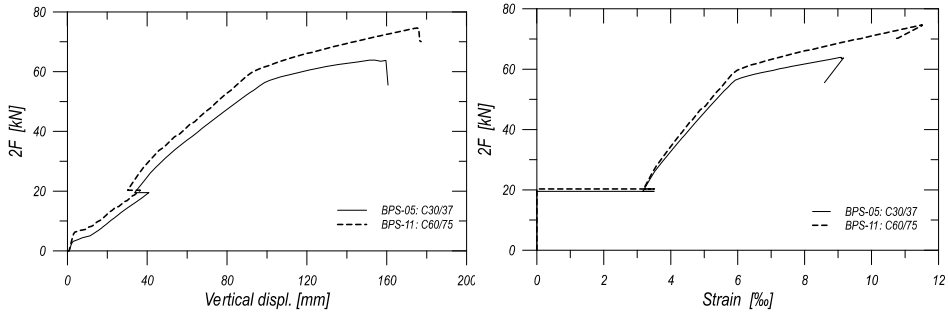


Fig. 8.28. Effect of concrete class: a) displacements, b) CFRP strains

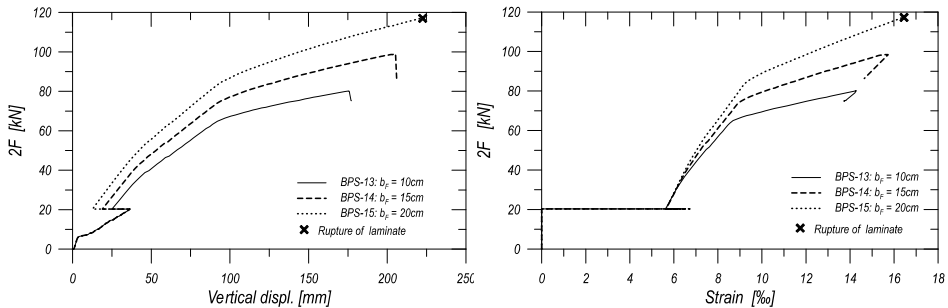


Fig. 8.29. Effect of the laminate width: a) displacements, b) CFRP strains

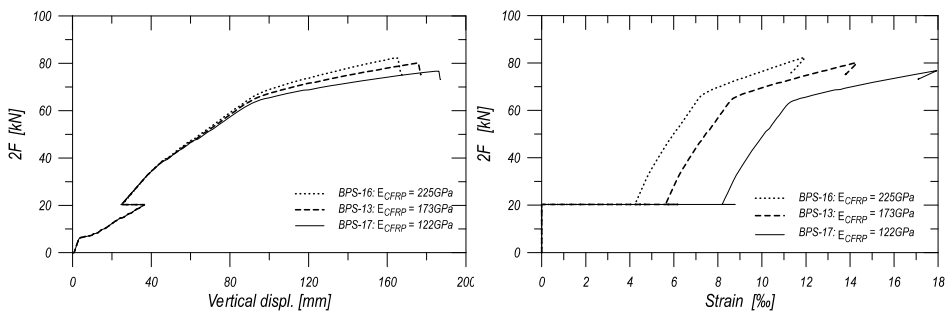


Fig. 8.30. Effect of the laminate elastic modulus: a) displacements, b) CFRP strains

The slightly better stiffness conditions for beams BPS-14 and BPS-15 in comparison with BPS-13 also influence the strain efficiency ratio  $\eta_{ef}$ . The reduction of displacements decreased the concrete-laminate slips. Therefore, for element BPS-15, the ultimate strain in the laminate was attained, even though the initial laminate strain was quite low (5.8‰).

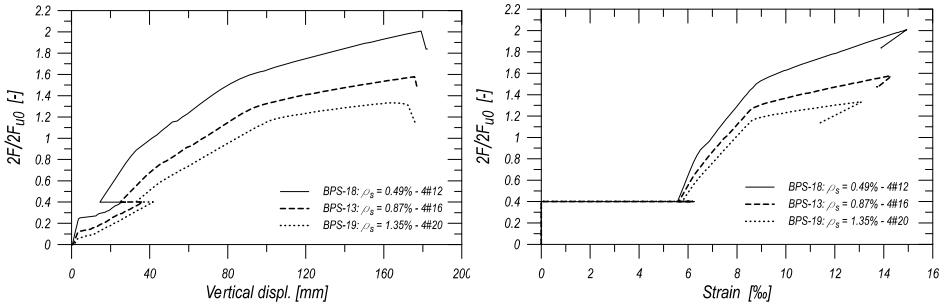


Fig. 8.31. Effect of the steel reinforcement ratio: a) displacements, b) CFRP strains

The elastic modulus of composite  $E_{CFRP}$  has minor effect on load–displacement behaviour and the ultimate load. Fig. 8.29. presents a comparison of the numerical results for three different  $E_{CFRP}$ : the reference one that has the same value as in the experiments (BPS-13) and two others, equal to 70% (BPS-17) and 130% (BPS-16) of the reference elastic modulus. The minor increase in load bearing capacity of elements BPS-13 and BPS-16, when compared to specimen BPS-17, is the result of slightly stiffer behaviour of these beams, especially after yielding of steel.

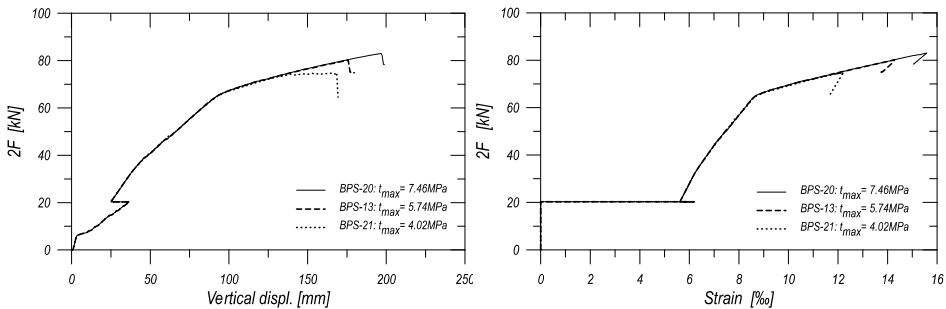


Fig. 8.32. Effect of  $t_{max}$ : a) displacements, b) CFRP strains

The influence of steel reinforcement ratio  $\rho_s$  on the behaviour of actively strengthened beams was analysed on the basis of specimens BPS-18

(  $\rho_s = 0.49\%$  ), BPS-13 (  $\rho_s = 0.87\%$  ) and BPS-19 (  $\rho_s = 1.35\%$  ). High performance concrete (C60/75) was adopted for all the beams, with preloading up to 40% of the non-strengthened specimen's ultimate load and prestress in the laminate equal to  $35\%f_{fu}$ .

The cross-section geometry, configuration of compressive reinforcement and stirrups as well as concrete covers remained the same for all specimens. The results of calculations are presented in Fig. 8.31. The IC debonding failure mode was observed in all the specimens. The absolute values of the ultimate load increase were similar for each case: 31.9 kN (BPS-18), 29.6 kN (BPS-13), 25.1 kN (BPS-19), however, for the specimens with higher  $\rho_s$  the increase in the load bearing capacity was slightly lower. This effect can be explained by the fact that structures with higher  $\rho_s$  ratio underwent more severe cracking at the preloading stage. Thus, the bonding conditions of the laminate in the middle zone of the beam were worse for these elements. This effect also resulted in the lower ultimate composite strain attained at the failure – see Fig. 8.31.b and Tab. 8.9.

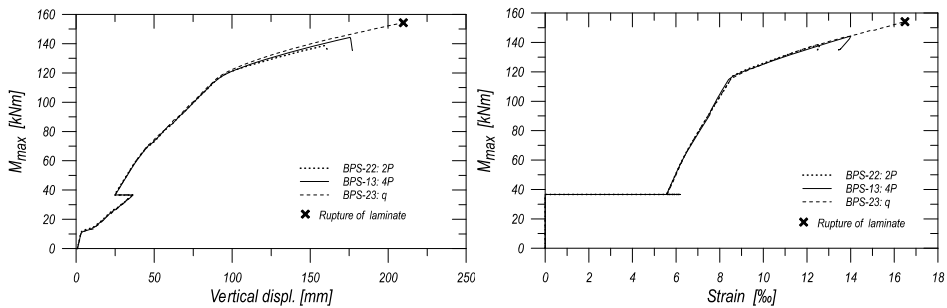


Fig. 8.33. Effect of loading configuration: a) displacements, b) CFRP strains

Fig. 8.32. shows the influence of the maximum tangential traction  $t_{max}$  on load capacity and behaviour of strengthened beams. For the bond-slip law three values of  $t_{max}$  were considered: 5.74MPa (  $t_{max,ref}$  ) – BPS-13, 4.02MPa (  $0.7t_{max,ref}$  ) – BPS-21 and 7.46 (  $1.3t_{max,ref}$  ) – BPS-20.

It should be mentioned that only maximum strength  $t_{max}$  was changed, whereas the other parameters remained the same as specified in Tab. 8.10. For the load levels below 80% of the ultimate load,  $t_{max}$  did not have any influence on load-displacement and load-CFRP strain behaviour. The differences were evident when severe slips started to develop. Comparing the results for the specimens BPS-20 and BPS-21 it can be stated that maximum tangential traction

$t_{max}$  has very moderate influence on the ultimate load capacity – 86% increase in  $t_{max}$  resulted only in 16% increase of the ultimate load. The possible explanation for this result is that the effective bond length for the considered bond-slip relationship was greater than the crack spacings for the load close to the failure load. Thus, the bonding effectiveness is substantially reduced and the maximum tangential traction  $t_{max}$  cannot be fully utilized.

The last issue analysed in this parametric study is the configuration of loads along the span. Three types of loading schemes were considered: 4 concentrated forces on the span following the experimental configuration (BPS-13), uniformly distributed load (BPS-23) and 2 concentrated forces symmetrically located, each at the distance from the nearest support equal to 2.0 m (BPS-22). Each specimen was preloaded prior to strengthening in order to obtain 40% of the ultimate bending moment of a non-strengthened beam at the critical section (i.e. the section with the maximum bending moment). The results are shown in Fig. 8.33 and in Tab. 8.9. It can be concluded from this figure that the load bearing capacity and failure mode strongly depend on the load configuration. The IC debonding failure mechanism occurred for the elements with the concentrated loads (beams BPS-13 and BPS-22), whereas the beam with uniformly distributed load (beam BPS-23) failed because of rupture of the laminate. The maximum increase in the ultimate bending moment is equal to 10% (between beams BPS-22 and BPS-23) and was the result of considerably less shear stresses (caused by the shear force) between concrete and the laminate in the zone of maximum curvatures. For beams BPS-13 and BPS-22, the maximum bending moment and maximum shear zones exist near the concentrated forces, which increases shear stresses in the laminate-concrete interface. Therefore, the development of severe slips in specimens BPS-13 and BPS-22 occurred for a lower bending moment than in the case of the beam with uniformly distributed load (BPS-23).

### **8.2.5. Conclusions**

The main goal of the presented analysis was to develop an efficient numerical model for actively strengthened flexural reinforced concrete structures. A two-dimensional plane stress model was developed, capable of simulating all stages of strengthening of a structure and capturing the nonlinear behaviour of constituent materials, i.e. cracking and crushing of concrete, reinforcement yielding. An uncoupled interface physical relationship was proposed and programmed to reflect the proper behaviour of a concrete-to-laminate connection. A parametric study was performed for the calibrated model that shows the influence of different material parameters and structural features on

load-displacement behaviour, strengthening efficiency factor, failure modes and load bearing capacities of the analysed beams. The following conclusions can be drawn from the comparative analysis of the experimental and numerical results as well as from the carried out parametric study:

- Application of prestressed CFRP laminates is an efficient technique of strengthening RC flexural members, irrespective of the preloading level before strengthening.
- Although the preloading levels in two experimentally examined beams exceeded the serviceability limit states prior to strengthening, the application of prestressed CFRP laminates resulted in a significant reduction of deflections and strains due to subsequently applied loads. The prestressing technique led to partial recovery of beam stiffness similar to specimens without preloading.
- The comparison of experimental and computational results confirms a good predictive performance of the FEM model in terms of the flexural response of RC beams strengthened with pretensioned CFRP laminates over the range covering preloading state, strengthening process, up to the failure. It is useful for analysis of crack propagation.
- The calculations show that prestressing increases the load bearing capacity in comparison with passively strengthened elements. The obtained strengthening efficiency ratios are greater for structures with less reinforcing steel ratios both for prestressed elements (this was also confirmed experimentally) and passively strengthened ones.
- The performed parametric study considerably broadened the scope of the investigated cases in comparison with the experimental campaign (Kotynia et al., 2013a). The simulations showed that preloading has a moderate effect on the load bearing capacity. It was also demonstrated that, for elements made of high strength concrete and with high pretension levels, the CRFP rupture failure mode may occur. The full strength of laminate can be utilized for such elements.
- The CFRP laminate width has important influence on load bearing capacity due to a greater prestressing force applied to the concrete section and a greater tensile force reached at failure. It is also worth noting that the laminate-rupture failure mode was obtained for the widest analysed CFRP tape.
- The influence of CFRP elastic modulus on load–displacement and load-bearing capacity is very moderate.
- The parametric study confirms the experimental observation concerning the strengthening efficiency of structures with different reinforcing steel ratios. It can be observed that the lower the reinforcing steel ratio is, the higher the reached level of strengthening efficiency.

- The maximum tangential traction between concrete and laminate  $t_{max}$  has a moderate influence on load-displacement behaviour and load capacity.
- The numerical simulations show that loading configuration strongly influences load bearing capacity and failure mode of the analysed specimens. The beam with uniformly distributed load performed much better than the ones loaded in the concentrated manner. This is the effect of additional shear stresses near the zone of maximum curvatures that exist in the case of structures with concentrated forces. Moreover, full utilisation of CFRP laminates was attained in the case of a beam with uniformly distributed load, while comparable elements with concentrated forces failed, due to the IC debonding mechanism.

## 9. Conclusions

The main aim of this book is to present development of research in the field of flexurally–strengthened RC members with adhesively–bonded FRP materials on the external surface of concrete.

The purpose is to explain problems referring to the phenomenon of bond losing between FRP and concrete at variable levels of loads, static scheme of the structure, the existing steel reinforcement and FRP reinforcement ratio.

A detailed analysis of variable parameters governing the bond losing between FRP and concrete shows complexity of this problem.

The Author indicated a strong effect of non-axial action on the FRP reinforcement, which was justified during last decade in a few publications that started a new direction in research of FRP-to-concrete bond behaviour.

This book summarizes new trends in the knowledge on theoretical models based on the complex phenomenon of bond effecting by concrete strength and surface preparation before the strengthening process. It points out that the previous empirical models should be revised for the new more, advanced, models considering complex problems of bond behaviour effected mainly by the stiffness of RC member and their curvature changes in the sagging and hogging regions. The main concept of this book is to justify benefits based on economy and effectiveness of structural strengthening, with the use of more accurate design approaches. The idea to introduce advanced models in comparison with the simplified ones is to change the existing conservative approaches for more economically–efficient design.

This book steers for the scientific approaches and shows tendency of changes in designing FRP–strengthened RC members, referring to the ultimate and serviceability limit states. It should be emphasized that the main difference between the internal reinforcement and externally–bonded reinforcement lies in different completely different bond behaviour between both types of reinforcement, which indicates different bond conditions to the concrete and consequently different bond length of steel and FRP reinforcement. This justifies the opinion that the full tensile strength of the EB FRP reinforcement cannot be achieved (without any anchorage system). This is the main assumption in design of structural strengthening RC members in flexure. Sometimes there are erroneous opinions about risky design of FRP strengthening, which misleads of designers. If one understands the structural strengthening assumptions and model approaches, there is no cause for concern in designing FRP structural strengthening on RC members.

The Author is fully convinced of the benefits and superiority of the advanced model proposed by DafStb (2014) named as “*more accurate model*” or “*intermediate crack element*” model based on the analysis of bond strength transmission at the segments of the RC member between cracks. This is the only model considering the vertical *contact pressure of concrete on the EB FRP* reinforcement bringing an increase in the bond strength. The superiority of this model over other advanced published models resulted in introducing this approach into the new guidelines in *fib* Bulletin 90.

Chapter 7 seems to be more practical for design purposes. This chapter presents Author’s own parametric analysis performed for RC slabs and beams considering different stiffness of the last one. The nomograms can be useful for designers to assess, in a simple way, strengthening efficiency in variable configurations of steel and FRP reinforcement ratio. The computer software used for this analysis considers materials and geometry variability with reference to the preloading effects before strengthening and variable FRP prestressing strain. It could be very useful for engineers to assess strengthening efficiency of variable geometry of RC cross sections and variable existing steel reinforcement ratio in tension and compression. The Author is still working on a separate guidebook with exercises for designers, which considers variable cases of RC structures strengthened in flexure with non-prestressed and prestressed FRP materials. This guidebook will consider two calculated methods: simplified and more accurate to justify superiority of the advanced method over the simplified one.

## References

1. Abdel Baky, H. M., Ebead, U. A., Masmoudi, R., and Neale, K. W., 2004. Analysis of the flexural response of FRP-strengthened concrete beams. *Advanced composite materials in bridges and structures*, M. El-Badry and L. Dunaszegi, eds., Canadian Society for Civil Engineering.
2. ACI 318-95, 1999. *Building Code Requirements for Structural Concrete (318-95) and Commentary (318R-95)*. American Concrete Institute (ACI), Fifth Printing, Michigan, USA.
3. ACI 440.2R-08, 2008. American Concrete Institute, *Guide for the design and construction of externally bonded FRP systems for strengthening concrete structures*. MI, USA.24.
4. Adhikary, B. B., Mutsuyoshi, H., 2001. Study on the bond between concrete and externally bonded CFRP sheet. *Proc., 6th Int. Symp. on Fiber Reinforced Polymer Reinforcement for Concrete Structures (FRPRCS-5)*, 1, 371-378.
5. ADINA, 2004. *Automatic dynamic incremental nonlinear analysis: Finite element software version 8.2*, ADINA R & D, Inc., Watertown, Mass.
6. Ahmed, O., van Gemert, D., 1999. Effect of longitudinal carbon fiber reinforced plastic laminates on shear capacity of reinforced concrete beams. In: Dolan CW, Rizkalla SH, Nanni A, editors. *Proceedings of the Fourth International Symposium on Fiber Reinforced Polymer Reinforcement for Reinforced Concrete Structures*. Maryland, USA, 933-943.
7. Ahmed, O., van Gemert, D., Vanderwalle, L., 2001. Improved model for plate end shear of CFRP strengthened RC beams. *Cement & Concrete Composites*, 23(1), 3-19.
8. Ajdukiewicz, A., Hulimka, J., 2010. Strengthening and rehabilitation of a heating plant chimney in Poland. *Case Studies of Rehabilitation, Repair, Retrofitting, and Strengthening - Series: Structural Engineering Documents*, Vol. 12, Chapter 6, IABSE, Zurich, 81-94.
9. Alam, M. S., Kanakubo, T., Yasojima, A., 2012. Shear-peeling bond strength between continuous fiber sheet and concrete. *ACI Structural Journal*, 109(1), 75-82.
10. Andrä, H.P., König, G., Maier, M., 2001. Einsatz vorgespannter Kohlefaser-Lamellen als Oberflächenspannglieder. *Beton- und Stahlbetonbau*, 96(12).
11. Andrä, H.P., König, G., Maier, M., 2002. First applications of CFRP tendons in Germany, IABSE Symposium Melbourne, Australia, CD.
12. Aram, M. R., Czaderski, C., Motavalli, M., 2008. Effects of gradually anchored prestressed CFRP strips bonded on prestressed concrete beams. *Journal of Composites for Construction*, 12(1), 25-34.
13. Arduini, M., Nanni, A., 1997. Behavior of pre-cracked RC beams strengthened with carbon FRP sheets. *Journal of Composites for Construction*, ASCE, Vol. 1 (2), 63-70.

14. AS 3600, 1988. Concrete Structures, AS 3600, Standards Australia, Sydney, Australia.
15. Aslam, M., Shafiqh, P., Jumaat, M.Z., Shah, S.N.R., 2015. Strengthening of RC beams using prestressed fiber reinforced polymers - A review. *Construction and Building Materials*, vol. 82, 235–256.
16. Bank, L.C., 2006. Composites for construction. *Structural Design with FRP Materials*. John Wiley & Sons, New Jersey
17. Bank, L.C., Borowicz D.T., Arora D., Lamanna A.J., Ray J.C., Velazquez G.I., 2004. Strengthening of concrete beams with fasteners and composite material strips – scaling and anchorage issues. Report ERDC/GSL TR-04-5, US Army Corps of Engineers, 154.
18. Bartosik, T., Kałuża, M., 2010. Strengthening of reinforced concrete structures with CFRP materials, selected examples of the field applications. XXV National Workshops for Construction Designer. Szczyrk 2010, CD. [Wzmocnianie żelbetowych konstrukcji budowlanych materiałami CFRP, wybrane przykłady realizacji. XXV Ogólnopolskie Warsztaty Pracy Projektanta Konstrukcji. In Polish]. Szczyrk, CD (in Polish).
19. Bazant, Z. P., Planas, J., 1997. Fracture and size effect in concrete and other quasi-brittle materials. Boca Raton: Florida, CRC Press.
20. Belarbi, A., Hsu, T.T.C., 1995. Constitutive laws of softened concrete in biaxial tension compression. *ACI Structural Journal*, 92(5), 562–73.
21. Berset, T., Schwegler, G., Trausch, L., 2002. Verstärkung einer Autobahnbrücke mit vorgespannten CFK-Lamellen. *tec21*, 128, 27–29.
22. Bilotta, A., Ceroni, F., Nigro, E., Pecce M., 2011b. Design by testing of debonding load in RC element strengthened with EBR FRP materials. 10th International Symposium on Fiber Reinforced Polymer Reinforcement for Reinforced Concrete Structures, Tampa, Florida, USA. April 2-4, 2011.
23. Bilotta, A., Faella, C., Martinelli, E., Nigro, E., 2011a. Indirect identification method for bilinear bond-law relationship. *Journal of Composites for Construction*, ASCE.
24. Bilotta, A., Faella, C., Martinelli, E., Nigro, E., 2012. Indirect identification method of bilinear interface laws for FRP bonded on a concrete substrate. *Journal of Composites for Construction*, 16, 171–184, ISSN: 1090-0268.
25. Bilotta, A., Faella, C., Martinelli, E., Nigro, E., 2013. Design by testing procedure for intermediate debonding in EBR FRP strengthened RC beams. *Engineering Structures*, 46, 147–154.
26. Bizindavyi, L., Neale, K.W., 1999. Transfer lengths and bond strengths for composites bonded to concrete *Journal of Composites for Construction* ASCE, 153–160.
27. Blontrock, H., Taerwe, L., Vanwalleghem, H., 2002. Bond testing of externally glued FRP laminates at elevated temperature. In *Proceedings of the International Symposium Bond in Concrete: from research to standards*, Budapest, 648–654.

---

## References

---

28. Bonacci, J.F., Maalej, M., 2000. Externally bonded fiber-reinforced polymer for rehabilitation of corrosion damaged concrete beams. *ACI Structural Journal*, 97(5), 703-711.
29. Brandt, A.M., 1996. O zastosowaniu uzbrojenia i sprężania konstrukcji prętami, ciągłymi taśmami z materiałów kompozytowych. XLII Konferencja naukowa Komitetu Inżynierii Lądowej i Komitetu Nauki PZiTb, Kraków – Krynica, 169-174. In Polish
30. Brosens, K., van Gemert, D., 1997. Anchoring stresses between concrete and carbon fibre reinforced laminates. In *Proceedings of the 3rd International Symposium on Non-Metallic (FRP) Reinforcement for Concrete Structures*, Japan Concrete Institute, Sapporo, 1, 271-278
31. Casadei, P., Galati, N., Parretti, R., Nanni, A., 2003. Strengthening of a bridge using two FRP technologies. *Field application of FRP reinforcement: Case Studies*. ACI Convention, Boston, Rizkalla, S., and Nanni A., Editors, ACI Special Publication, No. 215, American Concrete Institute, Farmington Hills, MI, 219-237.
32. Ceroni, F., Garofano, A., Pecce, M., 2014. Modelling of bond behavior in masonry elements externally bonded with FRP materials, in press on *Composite part B*, Elsevier
33. Ceroni, F., Pecce, M., 2002. Bond behaviour of R.C. elements externally reinforced with FRP laminates. In *Proceedings of the International Symposium Bond in Concrete—from research to standards*. Budapest, 622-629. ISBN 963-420-714-6
34. Ceroni, F., Pecce, M., Matthys, S., Taerwe, L., 2008. Bond tests on concrete elements with CFRP and anchorage systems. *Composites: Part B*, Elsevier, 39, 429-441
35. Chajes, M.J., Finch, W.W.Jr., Januszka, T.F., and Thonson, T.A.Jr., 1996. Bond and force transfer of composite material plates bonded to concrete. *ACI Struct. Journal*, 93(2), 295-303.
36. Chajes, M.J., Thomson, T.A., Januszka, T.F., Finch, W.W. Jr., 1994. Flexural strengthening of concrete beams using externally bonded composite materials. *Construction and Building Materials*, 8(3), 191-201.
37. Chen, J. F., Teng, J. G., 2001. Anchorage strength models for FRP and Steel Plates bonded to concrete. *ASCE Journal of Structural Engineering*, 127(7), 784-791.
38. Chen, J. F., Teng, J. G., 2003. Shear capacity of FRP-strengthened RC beams: FRP debonding. *Construction and Building Materials*, 17, 27-41.
39. Chen, J. F., Yang, Z. J., Holt, G. D., 2001. FRP or steel plate-to-concrete bonded joints: effect of test methods on experimental bond strength. *Steel Composite Structures*, 1(2), 231-244.
40. Chen, J.F., Yuan, H., Teng, J.G., 2007. Debonding failure along a softening FRP-to-concrete interface between two adjacent cracks in concrete members. *Engineering Structures*, 29(2), 259-70.

41. CNR-DT 200, 2004. Guide for the Design and Construction of Externally Bonded FRP Systems for Strengthening Existing Structure. National Research Council, Advisory Committee on Technical Recommendations for Construction.
42. Cornelissen, H.A.W., Hordijk, D.A., Reinhardt, H.W., 1986. Experimental determination of crack softening characteristics of normalweight and lightweight concrete. *Heron*, 31(2), 45–56.
43. Cruz, J.M.S., Barros, J.A.O., 2002. Bond behaviour of carbon laminate strips into concrete by pullout bending test. In *Proceedings of the International Symposium “Bond in Concrete — from research to standards”*, Budapest, 614–621.
44. Czaderski, C., 2012. Strengthening of reinforced concrete members by prestressed, externally bonded reinforcement with gradient anchorage. Ph.D. thesis, ETH Zürich.
45. Czaderski, C., Martinelli, E., Michels, J., Motavalli, M., 2012. Effect of curing conditions on strength development in an epoxy resin for structural strengthening. *Composites: Part B— Engineering*, 43(2), 398–410.
46. Czaderski, C., Motavalli, M., 2007. 40-Year-old full-scale concrete bridge girder strengthened with prestressed CFRP plates anchored using gradient method. *Composites: Part B Engineering*, 38(7–8), 878–886.
47. Czarnecki, L., Emmons, P.H., 2002. Repair and protection of concrete structures. Polish Cement Publication. [Naprawa i ochrona konstrukcji betonowych. Polski Cement], Kraków. (in Polish).
48. DAfStb-Guideline: Strengthening of concrete members with adhesively bonded reinforcement. Deutscher Ausschuss für Stahlbeton, 2012, English version, Beuth, Berlin, 2014.
49. Dai, J., Ueda, T., Hiroki, O., Sato, Y., 2003. Experimental study on the mix-mode fracture of FRP sheet-concrete interface. *JCI International Symposium on Latest Achievement in Technology and Research on Retrofitting Concrete Structures, Interface Mechanics and Structural Performance*, Kyoto, Japan, 121–128.
50. Dai, J.G., Ueda, T., 2003. Local bond stress slip relations for FRP sheetsconcrete interfaces. In: *Proc. of 6th international symposium on FRP reinforcement for concrete structures*. Singapore: World Scientific Publications, 143–152.
51. De Borst, R., 1987. Smearred cracking, plasticity, creep and thermal loading - a unified approach. *Computer Methods in Applied Mechanics and Engineering*, 62(1), 89–110.
52. De Lorenzis, L., Miller, B., Nanni, A., 2001. Bond of Fiber-Reinforced Polymer Laminates to Concrete. *ACI Materials Journal*. 98-M29, 256–264.
53. Derkowski, W., 2005. Fatigue life resistance of bent RC sections strengthened with carbon fibre reinforced strips. [Trwałość zmęczeniowa zginanych przekrojów żelbetonowych wzmocnionych taśmami z włókien węglowych], Krakow University of Technology Ph.D. thesis. (in Polish).

---

## References

---

54. Deuring, M., 1993. Verstärken von Stahlbeton mit gespannten Faserverbundwerkstoffen, Eidgenössische Material prüfungs und Forschungsanstalt EMPA, EMPa – Bericht, 224, Dübendorf, Switzerland.
55. Deuring, M., 1994. Brandversuche an nachtraglich verstärkten tragern aus beton. Research Report EMPA No. 148'795, Dubendorf: Swiss Federal Laboratories for Materials Testing and Research.
56. DIN EN 1992-1-1, 2011. Eurocode 2: Design of concrete structures – Part 1-1: General rules and rules for buildings; German version EN 1992-1-1:2004S AC:2010. Deutsches Institut für Normung.
57. Ebead, U. A., and Marzouk, H., 2005. Tension-stiffening model for FRP-strengthened RC concrete two-way slabs. *Mater. Struct.*, 38, 193–200.
58. Ebead, U. A., Neale, K. W., 2007. Mechanics of fibre-reinforced polymer–Concrete interfaces. *Canadian Journal of Civil Engineering*, 34, 367–377.
59. Ebead, U. A., Neale, K. W., and Bizindavyi, L., 2004. On the interfacial mechanics of FRP-strengthened concrete structures. *FRP composites in civil engineering—CICE 2004*, R. Seracino, ed., Balkema Publications, Rotterdam, The Netherlands, 351–359.
60. Ehsani, M. R., and Saadatmanesh, H., 1990. Fibre composite plates for strengthening bridge beams. *Composite Structures*, 15, 343–355.
61. El-Hacha, R., 2000. Prestressed CFRP sheets for strengthening concrete beams at room and low temperatures, Ph.D. Thesis, Queen's University, Department of Civil Engineering, Kingston, Ontario, Canada, 525.
62. El-Hacha, R., Aly, M.Y.E., 2013. Anchorage system to prestress FRP laminates for flexural strengthening of steel-concrete composite girders. *Journal of Composites for Construction*, 17 (3), 324–335.
63. El-Hacha, R., Green, M. F., Wight, R.G., 2004a. Flexural behaviour of concrete beams strengthened with prestressed carbon fibre reinforced polymer sheets subjected to sustained loading and low temperature. *Canadian Journal of Civil Engineering*, 31(2), 239–252.
64. El-Hacha, R., Wight R.G., Green, M.F., 2001. Prestressed fiber-reinforced polymer laminates for strengthening structures. *Progress in Structural Engineering and Materials*, 3, 111-121.
65. El-Hacha, R., Wight, R.G., Green, M.F., 2003. Innovative system for prestressing fiber-reinforced polymer sheets. *ACI Structural Journal*, 100(3), 305–313.
66. El-Hacha, R., Wight, R.G., Green, M.F., 2004b. Prestressed carbon fiber reinforced polymer sheets for strengthening concrete beams at room and low temperatures. *Journal of Composites for Construction*, 8(1), 3–13.
67. EN 1992-1-1:2004, 2004. Eurocode 2: Design of concrete structures – Part 1-1: General rules and recommendations for buildings.

68. Faella, C., Martinelli, E., & Nigro, E., 2008. Formulation and Validation of a Theoretical Model for Intermediate Debonding in FRP Strengthened RC Beams. *Composites Part B*, 39(4), 645–655. ISSN 1359-8368
69. Faella, C., Martinelli, E., Nigro, E., 2002. Aderenza tra calcestruzzo e fogli di FRP utilizzati come placcaggio di elementi inflessi. Parte II: modelli teorici ed elaborazioni numeriche. Atti del XIV Congresso C.T.E., Bologna.
70. Faella, C., Martinelli, E., Nigro, E., 2003. Interface behaviour in FRP plates bonded to concrete: experimental tests and theoretical analyses. In *Proceedings of the International Conference on Advanced Materials for Construction of Bridges, Buildings and other Structures—III*, Davos (Svizzera), 7–12 September 2003.
71. Feenstra, P.H., de Borst, R., 1993. Aspects of robust computational modeling of plain and reinforced concrete. *Heron*, 38(4), 3–76.
72. Ferracuti, B., Savoia, M., Mazzotti, C., 2007. Interface law for FRP-concrete delamination. *Composite Structures*, 80(4), 523–531
73. fib Bulletin 14, 2001. Externally Bonded FRP Reinforcement for RC Structures. Technical Report, Lusanne, Switzerland.
74. Finckh, W., 2012. Influence of member-specific effects on the design of reinforced concrete members strengthened using CFRP strips. PhD thesis, Technische Universität München, in German.
75. Finckh, W., Zilch, K., 2012. Strengthening and rehabilitation of reinforced concrete slabs with carbon-fiber reinforced polymers using a refined bond model. *Computer-Aided Civil and Infrastructure Engineering*, 27(5), 333–46.
76. Focacci, F., Nanni, A., Bakis, C. E., 2000. Local bond-slip relationship for FRP reinforcement in concrete. *Journal of Composites for Construction*, 4(1), 24–31.
77. Furtak, K., 1998. Strengthening of viaduct caps with carbon fibre reinforced polymer laminates. *Engineering & Construction Journal*. [Wzmocnienie oczepów wiaduktu drogowego taśmami kompozytowymi z włókien węglowych. *Inżynieria i Budownictwo*], 8, 435-437.
78. Furtak, K., 2014. Technical assessment of RC bridge after 12 years from structural strengthening with carbon fibre reinforced polymer laminates. *Archives of Civil Engineering Institute. Poznan University of technology*. [Ocena stanu technicznego żelbetowego mostu drogowego po 12 latach od wzmocnienia matami kompozytowymi. *ACE, Politechnika Poznańska*], 18, 17-26 (in Polish).
79. Gao, P., Gu, X., Mosallam, A.S., 2016. Flexural behavior of preloaded reinforced concrete beams strengthened by prestressed CFRP laminates. *Composite Structures*, 157, 33–50.
80. Garden, H. N., Holloway, L. C., 1998. An experimental study of the failure modes of reinforced concrete beams strengthened with prestressed carbon composite plates. *Composites: Part B—Engineering*, 29(4), 411–424.

## References

---

81. Garden, H.N., Holloway, L.C., Thorne, A.M., 1997. A preliminary evaluation of carbon fibre reinforced polymer plates for strengthening reinforced concrete members. *Proceedings of the Institution of Civil Engineers: Structures and Buildings*, 123(May), 127–42.
82. Garden, H.N., Holloway, L.C., Thorne, A.M., 1998a. The Strengthening and Deformation Behavior of Reinforced Concrete Beams Upgraded Using Prestressed Composite Plates. *Materials and Structures*, 31(208), 247-258.
83. Garden, H.N., Quantrill, R.J., Holloway, L.C., Thorne, A.M., Parke, G.A.R., 1998b. An experimental study of the anchorage length of carbon fibre composite plates used to strengthen reinforced concrete beams. *Construction and Building Materials*, 12, 203–19.
84. Ghorbani, M., Mostofinejad, D., Ardalan Hosseini, A., 2017. Experimental investigation into bond behavior of FRP-to-concrete under mixed-mode I/II loading, *Construction and Building Materials*, 132, 303–312
85. Górski, M., Krzywoń, R., Hulimka, J., Ajdukiewicz, A., Majewski, S., 2002. Development of design rules for structural strengthening of RC structures with CFRP sheets. Final scientific report on the research project. [Opracowanie zasad obliczania wzmocnień konstrukcji betonowych za pomocą mat z włókien węglowych. Raport końcowy z realizacji projektu badawczego nr 7 T07E 011 18. Gliwice]. (in Polish)
86. Grace, N.F., Sayed, G.A., Soliman, A.K., Saleh, K.R., 1999. Strengthening reinforced concrete beams using fiber reinforced polymer (FRP) laminates. *ACI Structural Journal*, 96(5), 865–74.
87. Grace, N.K., Sayed, G.A., 2003. Construction and evaluation of full-scale CFRP prestressed concrete DT-girder. *Proc. of Fiber-Reinforced Polymer Reinforcement for Concrete Structures*, Singapore, 1281-1290.
88. Guadagnini, M., Serbescu, A., Palmieri, A., Matthys, S., Bilotta, A., Nigro, E., Ceroni, F., Czaderski, C., Olia, S., Szambo, Z., Balazs, G., & Mazzotti, C., 2012. Round robin test on the bond behaviour of externally bonded frp systems to concrete. In *Proceedings of CICE 2012, 6th International Conference on FRP Composites in Civil Engineering*, Rome, Italy, CD ROM, 13–15.
89. Guo, Z.G., Cao, S.Y., Sun, W. M., Lin X.Y., 2005. Experimental study on bond stresses-slip behaviour between FRP sheets and concrete. In Chen & Teng (Eds.), *Proceedings of the International Symposium on Bond Behaviour of FRP in Structures*, BBFS 2005, 77–83.
90. Gutowski, T., Łagoda, G., Łagoda, M., 2003. Structural strengthening with prestressed CFRP laminates. *Building Materials Journal*. [Wzmacnianie konstrukcji żelbetowych przy użyciu wstępnie naprężonych taśm kompozytowych z włókien węglowych. *Materiały Budowlane*], 7, 55-56 (in Polish).
91. Haghani, R., Al-Emrani, M., 2014. A New Method and Device for Application of Bonded Pre-stressed FRP Laminates. *Proceedings of the Second Intl. Conf. on Advances in Civil and Structural Engineering - CSE 2014*.

92. Harmanci, Y. E., 2013. Prestressed CFRP for structural retrofitting—experimental and analytical investigation. M.Sc. thesis, ETH Zürich.
93. Hiroyuki, Y., Wu, Z., 1997. Analysis of debonding fracture properties of CFS strengthened member subject to tension. *Non-Metallic (FRP) Reinforcement for Concrete Structures.*, Proc., 3rd Int. Symp., Japan Concrete Institute, Sapporo, 1, 287–294
94. Hollaway, L.C., Leeming, M.B., 1999 *Strengthening of reinforced concrete structures using externally-bonded FRP composites in structural and civil engineering.* CRC Press, England.
95. Holzenkaempfer, P., 1994. *Ingenieurmodelle des verbundes geklebter bewehrung fur betonbauteile.* Dissertation. TU Braunschweig (in German).
96. Hordijk, D.A., 1991. Local approach to fatigue of concrete. Ph.D. thesis. Delft University of Technology.
97. Horiguchi, T., Saeki, N., 1997. Effect of test methods and quality of concrete on bond strength of CFRP sheet. In *Proceedings of International Symposium on Non-metallic (FRP) reinforcement for concrete structures*, Sapporo, Japan, Japan Concrete Institute, 1, 265–270.
98. Huang, Y., Wu, J.H., Yen, T., Hung, Ch., Lin, Y., 2005. Strengthening reinforced concrete beams using prestressed glass fiber-reinforced polymer—Part I: Experimental study. *Journal of Zhejiang University SCIENCE*, 6A(3), 166–174.
99. Husemann, U. and Budelmann, H., 2009. Increase of the Bond Capacity of Externally Bonded CFRP-Plates on RC-Structures Due to Self-Induced Contact Pressure, In: *Proceedings of the 9th International Symposium on Fibre Reinforced Polymers in Reinforced Concrete Structures (FRPRCS 9)*, Sydney, Australia.
100. Ichimasu, H., Maruyama, M., Watanabe, H., Hirose, T., 1993. RC Slabs strengthened by bonded carbon FRP plates Part 2- Application. *International Symposium on Fiber-Reinforced-Polymer Reinforcement for Concrete Structures*, ACI Publication SP 138-25, Detroit, Michigan, USA, eds. Nanni, A. and Dolan, C.W., 957-970.
101. Iovinella, I., Prota, A., Mazzotti, C., 2013. Influence of surface roughness on the bond of FRP laminates to concrete, *Construction and Building Materials*, 40, 533–542.
102. Jansen, D.C., Shah, S.P., 1997. Effect of length on compressive strain softening of concrete. *Journal of Engineering Mechanics*, 123(1), 25–35.
103. Jansze, W., 1997. *Strengthening of RC Members in Bending by Externally Bonded Steel Plates.* PhD Thesis, Delft University of Technology, Delft.
104. JCI, 2003. Japan Concrete Institute. Technical report of technical committee on retrofit technology. In *Proceedings International Symposium on Latest Achievement of Technology and Research on Retrofitting Concrete Structures.*
105. Jones, R., Swamy, N., 1983. In situ strengthening of concrete structural members using epoxy bonded steel plates. Department of Civil & Structural Engineering, University of Sheffield, UK, 251–255.

---

## References

---

106. Jones, R.M., 1999. *Mechanics of Composite Materials*. 2nd ed. Taylor & Francis, Philadelphia, PA.
107. JSCE, 2001. Recommendations for the upgrading of concrete structures with use of continuous fiber sheets. *Journal of Concrete Engineering, Series 41*, Japanese Society of Civil Engineers, Tokyo.
108. Kachlakev, D.I., Barnes, W.A., 1999. Flexural and shear performance of concrete beams strengthened with fiber reinforced polymer laminates. *Proc. of the Fourth International Symposium on Fiber Reinforced Polymer Reinforcement for Reinforced Concrete Structures, (FRPRCS-4)*, Baltimore, Maryland, 959-972.
109. Kaiser, H.P., 1989. Strengthening of reinforced concrete with epoxy bonded carbon fibre plastics. Ph.D. thesis. ETH nr 8918, ETH, Zurich Ch-8092 Zurich/Switzerland.
110. Kałuża, M., 2004. Selected problems of strengthening of RC structures with prestressed CFRP laminates. *Scientific Journals of the Silesian University of Technology*. [Wybrane problemy wzmacniania konstrukcji żelbetowych sprężonymi taśmami z włókien węglowych. *Zeszyty Naukowe Politechniki Śląskiej*], 102, 93-200 (in Polish).
111. Kałuża, M., Ajdukiewicz, A., 2008. Comparison of behaviour of concrete beams with passive and active strengthening by means of CFRP strips. *Architecture Civil Engineering Environment*, 1(2), 51-64.
112. Kamiński, M., Trapko, T., Bywalski, Cz., 2006. Strengthening of RC structures using reinforced concrete. *XXI National Workshops for Construction Designer. Ustron 2006*. [Wzmacnianie konstrukcji żelbetowej przez konstrukcję żelbetową, *XXI Ogólnopolska konferencja Warsztat pracy projektanta konstrukcji*], Ustroń (in Polish).
113. Karbhari, V.M., Engineer, M., ECKEL II, D.A., 1997. On the durability of composite rehabilitation schemes for concrete: use of a peel test, *Journal of Materials Science*, 32(1), 147-156.
114. Katsumata, H., Kimura, K., Murahashi, H., 2001. Experience of FRP strengthening for Japanese historical structures. *Proc. Intern. Conf. FRP Composites in Civil Eng.*, Elsevier Science, New York, 2, 1001-1008.
115. Khalifa, A., Gold, W. J., Nanni, A., Aziz, A., 1998. Contribution of externally bonded FRP to shear capacity of RC flexural members. *Journal of Composites for Construction, ASCE*, 2(4), 195-203.
116. Kim, Y.J., Green, M.F., Wight, R.G., 2010a. Bond and short-term prestress losses of prestressed composites for strengthening PC beams with integrated anchorage. *Journal of Reinforced Plastics and Composites*, 29(9), 1277-1294.
117. Kim, Y.J., Green, M.F., Wight, R.G., 2010b. Effect of prestress levels in prestressed CFRP laminates for strengthening prestressed concrete beams: A numerical parametric study. *PCI Journal*, 55(2), 96-108.

118. Kim, Y.J., Longworth, J.M., Wight, R.G., Green, M.F., 2008a. Flexure of two-way slabs strengthened with prestressed or nonprestressed CFRP sheets. *Journal of Composites for Construction*, 12(4), 366–374.
119. Kim, Y.J., Shi, C., Green, M.F., 2008b. Ductility and cracking behavior of prestressed concrete beams strengthened with prestressed CFRP sheets. *Journal of Composites for Construction*, 12(3), 274–283
120. Kim, Y.J., Wight, R.G., Green, M.F., 2008c. Flexural strengthening of RC beams with prestressed CFRP sheets: Development of nonmetallic anchor systems. *Journal of Composites for Construction*, 12(1), 35–43.
121. Kim, Y.J., Wight, R.G., Green, M.F., 2008d. Flexural strengthening of RC beams with prestressed CFRP sheets: Development of nonmetallic anchor systems. *Journal of Composites for Construction*, 12(1), 35–43.
122. Ko, H., Matthys, S., Palmieri, A., Sato, Y., 2014. Development of a simplified bond stress-slip model for bonded FRP-concrete interfaces. *Construction and Building Materials*, 68, 142–57.
123. Ko, H., Sato, Y., 2007. Bond stress–slip relationship between FRP sheet and concrete under cyclic load. *Journal of Composites for Construction*, 11(4), 419–26.
124. Kotynia, R., 1999. Ductility and Load Capacity of Reinforced Concrete Members Strengthened with CFRP Strips. Ph.D. Dissertation Department of Civil Engineering, Architecture and Environmental Engineering, University of Lodz, Poland (in Polish), pp 215.
125. Kotynia R., 2011. Shear strengthening of RC beams with polymer composites. Dr of Science Habilitation Thesis, Lodz University of Technology, (in Polish) p. 310.
126. Kotynia, R., 2012. Bond between FRP and concrete in reinforced concrete beams strengthened with near surface mounted and externally bonded reinforcement, *Construction and Building Materials*, 32, 41–54,
127. Kotynia, R., Baky, H. A., Neale, K. W., Ebead ,U. A., 2008. Flexural Strengthening of RC Beams with Externally Bonded CFRP Systems: Test Results And 3-D Nonlinear FE Analysis, *Society Journal of Composites for Construction*, American Society of Civil Engineers, March / April 2008, Vol. 12, No. 2, ISSN: 1090-0268, Editor: Ch. E, Bakis. s. 190-201.
128. Kotynia, R., Kaminska, M. E., 2003. Ductility and failure mode of RC beams strengthened for flexure with CFRP.” Rep. No. 13, Dept. of Concrete Structures, Technical Univ. of Lodz, Poland.
129. Kotynia R., Lasek K. (2018) Strengthening efficiency of RC beams strengthened for flexure with prestressed CFRP laminates. [Efektywność zastosowania wstępnie naprężonych taśm CFRP do wzmacniania belek żelbetowych na zginanie], *Badania doświadczalne elementów i konstrukcji żelbetowych*, Report No 21, Wydawnictwo Katedry Budownictwa Betonowego Wydziału Budownictwa i Architektury Politechniki Łódzkiej, Łódź 2018.

---

## References

---

130. Kotynia, R., Lasek, K., Staśkiewicz, M., 2013a. Flexural behaviour of preloaded RC slabs strengthened with prestressed CFRP laminates. *Journal of Composites for Construction*, 18(3).
131. Kotynia, R., Staśkiewicz, M., & Lasek, K., 2013b. Efficiency analysis of strengthening of RC structures with prestressed CFRP composites. Paper presented at the APFIS 2013, Melbourne, Australia.
132. Kotynia, R., Walendziak, R., Stoecklin, I., Meier, U., 2011. RC slabs strengthened with prestressed and gradually anchored CFRP strips under monotonic and cyclic loading, *Journal of Composites for Construction*, 15(2), 168–180.
133. Kubica, J., Hulimka, J., Kałuża, M., 2010. Specification of strengthening of concrete and masonry Structures with composite materials. [Specyfika wzmacniania konstrukcji betonowych i murowych materiałami kompozytowymi. *Inżynieria i Budownictwo*], nr 5-6, s. 260-267.
134. Labossière, P., Neal, K.W., Rochette, P., Demers, M., Lamothe, P., Lapierre, P., Desgagne, G., 2000. Fiber reinforced polymer strengthening of Sainte-Emilie-de-l'Energie Bridge: design, instrumentation, and field testing. *Canadian Journal of Civil Engineering*, 27(5), 916-927.
135. Labossière, P., Neale, K.W., Martel, S., 1997. Strengthening with composite materials practical applications in Quebec. Proc. of the US-Europe Workshop on Recent Advances in bridge Engineering: Advanced Rehabilitation, Durable Materials, Non-destructive Evaluation, and Management, eds. Meier, U., and Betti, R., Dubendorf and Zurich, 11, 89-96.
136. Łagoda, G., Łagoda, M., 2009, Strengthening steel bridge across Vistula River in Poland. The Proceedings of the 33rd IABSE Symposium: Sustainable Infrastructure Environment Friendly, Safe and Resource Efficient, Bangkok, Thailand.
137. Łagoda, M., 2002. Recommendations for strengthening of bridge structures with externally bonded reinforcement. [Zalecenia dotyczące wzmacniania konstrukcji mostowych przez przyklejanie zbrojenia zewnętrznego. IBDIM]. Warszawa (in Polish)
138. Łagoda, M., 2005. Strengthening of bridge structures with externally bonded elements. [Wzmacnianie mostów przez doklejanie elementów. Monografia 322, seria *Inżynieria Lądowa*], Politechnika Krakowska, Kraków (in Polish).
139. Lam, L., Teng, J.G., 2001. Strength of cantilever RC slabs bonded with GFRP strips. *Journal of Composites for Construction*, ASCE, 5(4), 221–7.
140. Lamanna, A.J., Bank, L.C., Scott, D.W., 2004. Flexural strengthening of RC beams by mechanically attaching FRP strips. *Journal of Composites for Construction*, ASCE, 8 (3), 203-210.
141. Lasek, K., 2015. Efficiency of flexural strengthening of reinforced concrete elements with pretensioned CFRP. PhD thesis, Lodz University of Technology. In Polish.
142. Lees, J. M., Burgoyne, C. J., 1999. Experimental study of influence of bond on flexural behavior of concrete beams pretensioned with aramid fiber reinforced plastics. *ACI Structural Journal*, 96(3), 377–385.

143. Lees, J. M., Winistörfer, A. U., Meier, U., 2002. External prestressed carbon fiber-reinforced polymer straps for shear enhancement of concrete. *Journal of Composites for Construction*, 6 (4), 249–256.
144. Liu, I. S. T., Oehlers, D. J., Seracino, R., 2007. Study of intermediate crack 983 debonding in adhesively plated beams. *Journal of Composites for Construction*, 11(2), 175–183.
145. Liu, I.S.T., Oehlers, D.J., Seracino, R., 2006. Moment redistribution in FRP and steel plated reinforced concrete beams. *Journal of Composites for Construction*, 10(2), 115–24.
146. Lu, X.Z., Teng, J.G., Ye, L.P., Jiang, J.J., 2005a. Bond-slip models for FRP sheets/plates externally bonded to concrete. *Engineering Structures*, 27 (6), 920–937
147. Lu, X.Z., Ye, L.P., Teng, J.P., Jiang, J.J., 2005b. Meso-scale finite element model for FRP sheets/ plates bonded to concrete. *Engineering Structures*, 27(4), 564–75.
148. Maeda, T., Asano, Y., Sato, Y., Ueda, T., Kakuto, Y., 1997. A study on bond mechanism of carbon fiber sheet. In *Proceedings of the 3rd International Symposium on Non-Metallic (FRP) Reinforcement of Concrete Structures*, 1, October.
149. Malek, A.M., Saadatmanesh, H., Ehsani, M.R., 1998. Prediction of failure load of R/C beams strengthened with FRP plate due to stress concentration at the plate end. *ACI Structural Journal*, 95(1), 142–52.
150. Mapei, 2018. Sistema di rinforzo strutturale composto da lamina pultrusa in fibra di carbonio ad elevata resistenza e resine epossidiche di incollaggio (FRP). Coperto da Certificato di Idoneità Tecnica all'impiego n°2467/2018. Classi C150/2300 - C190/1800 - C200/1800
151. Markeset, G., Hillerborg, A., 1995. Softening of concrete in compression - localization and size effects. *Cement and Concrete Research*, 25(4), 702–8.
152. Matana, M., Nanni, A., Dharani, L., Silva, P., Tunis, G., 2005. Bond performance of steel reinforced polymer and steel reinforced grout. In *Proceedings of the International Symposium on Bond Behaviour of FRP in structures*, Honk Kong, 125–132.
153. Matthews, F. L., Rawlings, R. D., 1994. *Composite materials: engineering and science*, Chapman & Hall
154. Matthys, S., Taerwe, L., Janssens, J., 2004. Repair and strengthening of reptile building of the Antwerp zoo. *Proc. of First International Conference on Innovative Materials and Technologies for Construction and Restoration*, V. 2, Lecca, Italy, 653–663.
155. Mazzotti, C., Bilotta, A., Carloni, C., Ceroni, F., D'Antino, T., Nigro, E., Pellegrino, C., 2016. Bond between EBR FRP and concrete, in: *Design procedures for the use of composites in strengthening of reinforced concrete structures*, Springer, Dordrecht, 39–96.

## References

---

156. Mazzotti, C., Savoia, M., Ferracuti, B., 2005. A New Set-Up for FRP-Concrete Stable Delamination Test. In C. K. Shield & J. P. Busel (Ed.), *Proceedings of 7th International Symposium FRP Reinforcement for Concrete Structures*, Kansas City, Missouri, 165–180. 3 Bond Between EBR FRP and Concrete 93.
157. Mazzotti, C., Savoia, M., Ferracuti, B., 2007. Mode II fracture energy and interface law for FRP–concrete bonding with different concrete surface preparations. In *Proceedings of FRAMCOS 6. FRAMCOS 6—Fracture Mechanics of Concrete and Concrete Structures*. Catania, Italy, 2, 1249–1257.
158. MC-Bauchemie, 2005: Instrukcja stosowania taśm MC-DUR CFK i kleju do taśm MC-DUR 1280.
159. McSweeney, B. M., Lopez, M. M., 2005. FRP-Concrete Bond Behavior: A Parametric Study Through Pull-Off Testing. In C. K. Shield & J. P. Busel (Eds.), *Proceedings of the 7<sup>th</sup> International Symposium FRP Reinforcement for Concrete Structures*, Kansas City, Missouri, pp. 441–460.
160. Megachemie, 2011: NEOXE System wzmacniania konstrukcji budowlanych materiałami kompozytowymi, Karta techniczna, Wydanie 02/PL
161. Meier, U., 1997. Bridge repair with high performance composite materials. *Material und Technik*, 4, 125-128.
162. Meier, U., 1992. Carbon fibre-reinforced polymers: Modern materials in bridge engineering. *Structural Engineering International*, 2, 7-12.
163. Meier, U., 1995a. Strengthening of structures using carbon fibre/epoxy composites. *Construction and Building Materials*, 9(6), 341-351.
164. Meier, U., 1995b. Nachträgliche Verstärkung von Bauwerken mit CFK-Lamellen, SIA/EMPA Dokumentation D 0128, Editor: Swiss Society of Engineers and Architects (SIA), Zürich, Switzerland.
165. Meier, U., Deuring, M., Meier, H., Schwegler, G., 1993. Strengthening of structures with advanced composites. *Alternate materials for the reinforcement and prestressing of concrete*, J.L. Clarke, editor, Blackie Academic and Professional, Glasgow.
166. Meier, U., Stöcklin, I., 2005. A novel carbon fiber reinforced polymer (CFRP) system for post-strengthening. Paper presented at the ICCRRR, Cape Town, South Africa.
167. Menegotto, M., Monti, G., 2005. Strengthening concrete and masonry with FRP – A new code of practice in Italy. *Proc. of the Int. 5th AMCM2005 Conference*, Gliwice-Ustron, Poland CD.
168. Michalak, B., 2000. *Mechanics of elastic plates and coatings*. [Mechanika sprężystych płyt i powłok, Warszawa, PWN (in Polish).
169. Michels, J., Czaderski, C., Motavalli, M., 2011. Prestressed CFRP for structural strengthening. Paper presented at the 1st SMAR conference, Dubai, UAE.
170. Michels, J., C. Czaderski, Hüppi M., 2012b. *Vorgespannte CFK-Lamellen mit Gradientenverankerung - Manual für Verarbeiter und planende Ingenieure*, Version Januar 2012. S&P Clever Reinforcement und Empa, Switzerland.

171. Michels, J., Czaderski, C., El-Hacha, R., Brönnimann, R., Motavalli, M., 2012a. Temporary bond strength of partly cured epoxy adhesive for anchoring prestressed CFRP strips on concrete. *Composite Structures*, 94(9), 2667–2676.
172. Michels, J., Martinelli, E., Czaderski, C., Motavalli, M., 2014a. Prestressed CFRP strips with gradient anchorage for structural concrete retrofitting: Experiments and numerical modelling. *Polymers*, 6, 114–131.
173. Michels, J., Sena Cruz, J., Czaderski, C., Motavalli, M., 2013. Structural strengthening with prestressed CFRP strip with gradient anchorage. *Journal of Composites for Construction*, 17(5), 651–661.
174. Michels, J., Staśkiewicz, M., Czaderski, C., Lasek, K., Kotynia, R., Motavalli, M., 2014b. Anchorage resistance of CFRP strips externally bonded to various cementitious substrates. *Composites: Part B—Engineering*, 63, 50–60.
175. Miller, B., Nanni, A., 1999. Bond Between CFRP Sheets and Concrete Congress. In *Proceedings ASCE 5th Materials Cincinnati, Ohio*, 240–247.
176. Monti, G., Liotta, M.A., 2007. Tests and design equations for FRP-strengthening in shear. *Journal of Construction and Building Materials*, 21 (4), 799-809.
177. Monti, M., Renzelli, M., Luciani, P., 2003. FRP adhesion in uncracked and cracked concrete zones. In: *Proc. of 6th international symposium on FRP reinforcement for concrete structures*. Singapore: World Scientific Publications, 183–192.
178. Mossakowski P., 2006. FRP bars for reinforcing concrete structures. *Rods and Bridges Journal*. [Pręty z kompozytów polimerowych z włóknami do zbrojenia betonowych konstrukcji inżynierskich. *Drogi i mosty*], s. 35-52.
179. Motavalli, M. Czaderski, C., 2007. FRP Composites for Retrofitting of Existing Civil Structures in Europe: State-of-the-Art Review in *COMPOSITES & POLYCON*, American Composites Manufacturers Association, 2007.
180. Motavalli, M., Czaderski, C., Pfyl-Lang, K., 2011. Prestressed CFRP sor strengthening of reinforced concrete structures: Recent developments at Empa, Switzerland. *Journal of Composites for Construction*, 15(2), 194–204.
181. Mukhtar, F.M., Faysal, R.M., 2018. A review of test methods for studying the FRP-concrete interfacial bond behaviour. *Construction and Building Materials*, 169, 877–887
182. Naaman, A., 1999. Repair and strengthening of reinforced concrete beams using CFRP laminates. Testing and Research Section, Construction and Technology Division, Research Project No. RC-1372, University of Michigan, Department of Civil and Environmental Engineering.
183. Nakaba, K., Kanakubo, T., Furuta, T., Yoshizawa, H., 2001. Bond behaviour between fiber-reinforced polymer laminates and concrete. *ACI Structural Journal*, 98(3), 359–367.
184. Nakamura, H., Higai, T., 2001. Compressive fracture energy and fracture zone length of concrete. In: Shing BP, editor. *Modeling of inelastic behavior of RC structures under seismic loads*. American Society of Civil Engineers, 471–87.

## References

---

185. Nanni, A., 1993. Fiber-Reinforced-Plastic (FRP) reinforcement for concrete structures: properties and applications, *Developments in Civil Engineering*, Vol. 42, Elsevier, Amsterdam, The Netherlands, 450.
186. Nanni, A., 1995. Concrete repair with externally bonded FRP reinforcement: Examples from Japan, *Concrete International*, 23.
187. Nanni, A., Di Ludovico, M., Parretti, R., 2004. Shear strengthening of a PC bridge girder with NSM CFRP rectangular bars. *Advanced Structural Engineering*, 7 (4), 97–109.
188. Neale, K. W., Ebead, U. A., Abdel Baky, H. M., Elsayed, W. E., and Godat, A., 2005. Modelling of debonding phenomena in FRP-strengthened concrete beams and slabs. Bond behaviour of FRP in structures, J. F. Chen and J. G. Teng, eds., *Int. Institute for FRP in Construction*, Hong Kong, 45–54.
189. Neubauer, U., 2000. Verbundtragverhalten geklebter Lamellen aus Kohlenstofffaser-Verbundwerkstoff zur Verstärkung von Betonbauteilen. Dissertation, Institut für Baustoffe, Massivbau und Brandschutz, TU Braunschweig, Heft 150.
190. Neubauer, U., Rostasy, F. S., 1997. Design aspects of concrete structures strengthened with externally bonded CFRP plates. Proc., 7th Int. Conf. on Struct. Faults and Repairs, ECS Publications, Edinburgh, Scotland, 2, 109–118.
191. Neubauer, U., Rostasy, F.S., 1999. Bond failure of concrete fiber reinforced polymer plates at inclined cracks-experiments and fracture mechanics model. In: Proc. of 4th international symposium on fiber reinforced polymer reinforcement for reinforced concrete structures, SP-188. Farmington Hills (MI), ACI, 369–82.
192. Neubauer, U., Vom Berg, W., Onken, P., 2007. Structural strengthening with a new system of prestressed CFRP strips. Paper presented at the FRPRCS-8, Patras, Greece.
193. Nguyen, D.M., Chan T.K., Cheong H.K., 2001. Brittle failure and bond development length of CFRP-concrete beams. *Journal of Composites for Construction*, ASCE, 5(1), 12–7.
194. Niedermeier, R., 1996. Stellungnahme zur Richtlinie für das Verkleben von Betonbauteilen durch Ankleben von Stahlflaschen—Entwurf März 1996. Schreiben 1390 vom 30.10.1996 des Lehrstuhls für Massivbau, Technische Universität München, Munich, Germany (in German).
195. Niedermeier, R., 1997. Gemischte Bewehrung bei klebarmierten Bauteilen. In: *Zilch, K. (Hrsg.): Münchner Massivbau-Seminar*.
196. Nitereka, C., and Neale, K. W., 1999. Analysis of reinforced concrete beams strengthened in flexure with composite laminates. *Canadian Journal of Civil Engineering*, 26, 646–654.
197. Noakowski, P., 1988. Nachweisverfahren für Verankerung, Verformung, Zwangsbeanspruchung und Rissbreite. Kontinuierliche Theorie der Mitwirkung des Betons auf Zug. Rechenhilfen für die Praxis. Schriftenreihe des DAfStb No. 394, Beuth, Berlin.

198. Oehlers, D. J., Park, S. M., Mohamed, Ali M.S., 2003. A structural engineering 1025 approach to adhesive bonding longitudinal plates to RC beams and slabs. *Composites 1026 Part A: Applied Science and Manufacturing*, 34(9), 887-897.
199. Oehlers, D.J., 1992 Reinforced concrete beams with plates glued to their soffits. *Journal of Structural Engineering*, ASCE 1992, 118(8), 2023–38.
200. Oehlers, D.J., Liu, I., Seracino, R., 2007. A generic design approach for EB and NSM longitudinally plated RC beams. *Construction and Building Materials*. 21(4), 697-708
201. Oehlers, D.J., Moran, J.P., 1990. Premature failure of externally plated reinforced concrete beams. *Journal of Structural Engineering*, ASCE, 116(4), 978–95
202. Oehlers, D.J., Visintin, P. and Lucas, W., 2015. Flexural strength and ductility of 1 FRP-plated RC beams: Fundamental mechanics incorporating local and global IC 2 debonding. *Journal of Composites for Construction*, 20(2), p.04015046. 3 10.1061/(ASCE)CC.1943-5614.0000610
203. Olivito, E., Pecce, R., Poggi, M.C., 2009. Experimental round robin test on FRP concrete bonding. In *Proceedings of FRP RCS9, Sydney, Australia*, 13–15.
204. Oudah, F., El-Hacha, R., 2012. A new ductility model of reinforced concrete beams strengthened using Fiber Reinforced Polymer reinforcement. *Composites Part B Engineering*, 43(8), 3338–3347.
205. Pan, J.L., Chung, T.C.F., Leung, C.K.Y., 2009. FRP debonding from concrete beams under various load uniformities. *Advances in Structural Engineering*, 12(6), 807–19.
206. Paško, P., Siwowski, T., 2016. Strengthening of steel bridge with prestressed CFRP laminates. *Bridges Journal*. [Wzmocnienie mostu stalowego wstępnie naprężonymi taśmami CFRP. Mosty, 3] (in Polish).
207. Pellegrino, C., Modena, C., 2009a. Flexural strengthening of real-scale RC and PRC beams with End-Anchored Pretensioned FRP Laminates. *ACI Structural Journal*, 106(3), 319-328
208. Pellegrino, C., Modena, C., 2009b. Influence of axial rigidity on FRP-concrete bond behavior: an analytical study. *Advances in Structural Engineering*, 12(5), 639–649.
209. Pellegrino, C., Tinazzi, D., Modena, C., 2008. Experimental study on bond behavior between concrete and FRP reinforcement. *Journal of Composites for Construction*, ASCE 12(2), 180–189.
210. Piątek, B., 2017. New strengthening technology of strengthening concrete structures with prestressed CFRP laminates. [Nowa technologia wzmacniania konstrukcji betonowych naprężanymi taśmami CFRP, Ph.D. thesis, Technical University of Rzeszów (in Polish).
211. Piątek, B., Siwowski, T., 2016a Investigation of strengthening effectiveness of reinforced concrete bridge with prestressed CFRP strips, *Roads and Bridges*, 15/2016, 301–314.

## References

---

212. Piątek, B., Siwowski, T., 2016b. Mechanical anchorage effect on strengthening efficiency of RC beams strengthened with CFRP laminates. *Engineering & Construction Journal*. [Wpływ kotwienia mechanicznego taśm CFRP na efektywność wzmocnienia belek żelbetonowych] *Inżynieria i Budownictwo*] 12/2016, 659-662 (in Polish).
213. Piątek, B., Siwowski, T., 2017. Research on the new CFRP prestressing system for strengthening of RS structures. *Architecture Civil Engineering Environment – ACEE*, 10(3), 81-87.
214. Quantrill, R. J., Hollaway, L. C., 1998. The flexural rehabilitation of reinforced concrete beams by the use of prestressed advanced composite plates. *Composites Science and Technology*, 58 (8), 1259–1275.
215. Rabinovitch, O., 2004. Fracture mechanics failure criteria for RC beams strengthened with FRP strips—a simplified approach. *Composite Structures*, 64, 479–492.
216. Rabinovitch, O., Frostig, Y., 2001. Delamination failure of RC beams strengthened with FRP strips—A closed-form high-order and fracture mechanics approach. *Journal of Engineering Mechanics.*, 127(8), 852–861.
217. Radomski, W., 2005. Strengthening of concrete bridge structures with FRPs. *Building Materials Journal*. [Wzmacnianie betonowych konstrukcji mostowych za pomocą wyrobów z polimerów zbrojonych włóknami. *Materiały Budowlane*, 4] (in Polish).
218. Rahimi, H., Hutchinson, A., 2001. Concrete beams strengthened with externally bonded FRP plates. *Journal of Composites for Construction, ASCE*, 5(1), 44–56.
219. Raof, M, Hassanen, M.A.H., 2000. Peeling failure of reinforced concrete beams with fibre-reinforced plastic or steel plates glued to their soffits. *Proceedings of the Institution of Civil Engineers: Structures and Buildings*, 140(August), 291–305.
220. Raof, M, Zhang, S., 1997. An insight into the structural behaviour of reinforced concrete beams with externally bonded plates. *Proceedings of the Institution of Civil Engineers: Structures and Buildings*, 122(November), 477–92.
221. Ritchie, P.A., Thomas, D.A., Lu, L.W., Conelly, G.M., 1991. External reinforcement of concrete beams using fibre reinforced plastics. *ACI Structural Journal*, 88(4), 490–500.
222. Roberts, T.M., 1989. Approximate analysis of shear and normal stress concentrations in the adhesive layer of plated RC beams. *The Structural Engineer*, 67(12), 229–33.
223. Rosenboom, O., Rizkalla, S., 2008. Modeling of IC debonding of FRP-strengthened concrete flexural members. *Journal of Composites for Construction*, 12(2), 168–79.
224. Ross, C.A., Jerome, D.M., Tedesco, J.W., Hughes, M.L., 1999. Strengthening of reinforced concrete beams with externally bonded composite laminates. *ACI Structural Journal*, 96(2), 212–20
225. Rots, J.G., 1988. Computational modeling of concrete fracture. Ph.D. thesis. Delft University of Technology.

226. S&P, 2019. CFRP laminates in epoxy resin. [Taśmy kompozytowe z włókien węglowych zatopionych w matrycy z żywicy epoksydowej] (in Polish).
227. Saadatmanesh, H., Ehsani, M.R., 1991. RC beams strengthened with GFRP plates. I. Experimental study. *Journal of Structural Engineering, ASCE*, 117 (11), 3417–33
228. Saadatmanesh, H., Malek, A.M., 1998. Design guidelines for flexural strengthening of RC beams with FRP plates. *Journal of Composites for Construction, ASCE*, 2(4), 158–64.
229. Sand, B., Remlo, H., 2001. RC beams with externally bonded CFRP: Finite element modelling of delamination failure. Doc. No. NTAS F2001-32, Interreg Nordkaotten Institute.
230. Savoia, M., Bilotta, A., Ceroni, F., Di Ludovico, M., Fava, G., Ferracuti, B., Mazzotti C., Nigro, E., Olivito, R., Pecce, M., Poggi, C., 2009. Experimental Round Robin test on FRP-concrete bonding, *Proceedings of FRPRCS-9, Sydney, Australia, July 2009, 1-4, on CD.*
231. Savoia, M., Ferracuti, B., Mazzotti, C., 2003. Nonlinear bond-slip law for FRP-concrete interface. In *Proceedings of the conference FRPRCS-6, Singapore.*
232. Sayed-Ahmed, E. Y., Bakay, R., Shrive, N. G., 2009. Bond strength of FRP laminates to concrete: State-of-the-art review, *Electronic Journal of Structural Engineering*, 9, 45–61.
233. Schlaich, M., Zwingmann, B., Liu, Y., Goller, R., 2012. Zugelemente aus CFK und ihre Verankerungen. *Bautechnik*, 89(12), 841–850.
234. Schwegler, G., 1994. Verstärken von Mauerwerk mit Hochleistungsfaserverbundwerkstoffen, *Dissertation, EMPA - Bericht Nr 229.*
235. Sebastian, W. M., 2001. Significance of midspan debonding failure in FRP-plated 1040 concrete beams. *Journal of Structural Engineering*, 127(7), 792-798.
236. Seim, W., Hörman, M., Karbhari, V., Seible, F., 2001. External FRP poststrengthening of scaled concrete slabs, *Journal of Composites for Construction*, 5(2), 67–75.
237. Seracino, R., Jones, N.M., Page, M.W., Ali, M.S.S., Oehlers, D.J., 2007a. Bond strength of near-surface mounted FRP-to-concrete joints. *Journal of Composites for Construction, ASCE*, 11 (4), 401-409.
238. Seracino, R., Raizal Saifulnaz, M.R., Oehlers, D.J., 2007b. Generic debonding resistance of EB and NSM plate-to-concrete joints, *Journal of Composites for Construction*, 11 (1), 62–70.
239. Serbescu, A., Guadagnini, M., Pilakoutas, K., 2013. Standardised double-shear test for determining bond of FRP to concrete and corresponding model development. *Composites Part B Engineering*, 55, 277–297.
240. Seręga, Sz, Kotynia, R., Lasek, K., 2018. Numerical modelling of preloaded RC beams strengthened with prestressed CFRP laminates. *Engineering Structures* 176:917-934.

---

## References

---

241. Shahawy, M., Chaallal, O., Thomas, E.B., Adnan, E., 2001. Flexural strengthening with carbon fiber-reinforced polymer composites of preload full-scale girders. *ACI Structural Journal*, 98 (5), 735–743.
242. Shahawy, M.A., Arockiasamy, M., Beitelman, T., Sowrirajan, R., 1996. Reinforced concrete rectangular beams strengthened with CFRP laminates. *Composites: Part B*, 27B, 225–33.
243. Sharif, A., Al-Sulaimani, G.J., Basunbul I.A., Baluch M.H., Ghaleb B.N., 1994. Strengthening of initially loaded reinforced concrete beams using FRP plates. *ACI Structural Journal*, 91(2), 160–8.
244. Shima, H., Chou, L.L., Okamura, H., 1987. Micro and macro models for bond in reinforced concrete. *J Fac Eng Univ, Tokyo (B)*, 22, 133–94.
245. Sieńko, R., Dyduch, K., Derkowski, W., 2006. Strengthening RC structures by prestressing. XXI National Workshops for Construction Designer. Ustron 2006. [Wzmacnianie konstrukcji żelbetowych przez sprężenie. XXI Ogólnopolska Konferencja Warsztat Pracy Projektanta Konstrukcji, Szczyrk], 27-63 (in Polish).
246. Sika® CarboDur®, 2016. CFRP laminates for structural Strengthening. [Taśmy z włókien węglowych do wzmocnień konstrukcji, Sika® CarboDur®]. Karta informacyjna produktu (in Polish).
247. Siwowski T., Piątek B., 2014. Research on the new bridge strengthening system with prestressed CFRP strips. The Proceedings of the International Symposium on Life-Cycle Civil Engineering (IALCCE 2014). Tokyo, Japan.
248. Siwowski T., 2012b. Prestressing CFRP laminates. Strengthening concrete Structures. [Sprężone taśmy CFRP. Wzmacnianie mostów betonowych. Mosty, 5] (in Polish).
249. Siwowski, T., 1997. Strengthening technology of RC Bridges with FRP laminates. [Technologia wzmacniania mostów żelbetowych taśmami kompozytowymi. Konf. Naukowo-Techniczna Mosty w drodze do XXI wieku], 743 – 752 (in Polish).
250. Siwowski, T., 2006. Road Bridges. Part I. [Część I. Magazyn Autostrady, 10/2006, wydanie specjalne - jesień 2006, Mosty - konstrukcja, wyposażenie, utrzymanie, 30-38, Część II. Magazyn Autostrady, 11/2006, 67-72] (in Polish).
251. Siwowski, T., 2012a. CFRP materials for Strengthening concrete Bridges. [Materiały kompozytowe CFRP stosowane we wzmacnianiu mostów betonowych, Mosty, 4, 24-29] (in Polish).
252. Siwowski, T., 2015. Bridge Engineering. Selected Issues. p. 190.
253. Siwowski, T., Kaleta, D., Rajchel, M., Wlasak, L., 2017. The first Polish road bridge made of FRP composites. *Structural Engineering International*, 27(2), 308-314.
254. Siwowski, T., Michałowski, J., Błażewicz, S., 2009. New prestressing system for strengthening bridges with CFRP laminates. [Nowy system sprężania taśm kompozytowych CFRP do wzmacniania mostów. Konf. Naukowo-Techniczna Awarie Budowlane XXIV, Szczecin-Międzyzdroje], 947-960 (in Polish).

255. Siwowski, T., Michałowski, J., Błażewicz, S., 2010. New prestressing system for strengthening RC structures with CFRP laminates. [Nowy system sprężania taśm kompozytowych CFRP do wzmacniania konstrukcji żelbetowych. Inżynieria i Budownictwo, 3], 152-156 (in Polish).
256. Siwowski, T., Michałowski, J., Błażewicz, S., 2010. New prestressing system for strengthening RC structures with CFRP laminates. [Nowy system sprężania taśm kompozytowych CFRP do wzmacniania konstrukcji żelbetowych. Inżynieria i Budownictwo, tom LXVI, 3, 152-156 (in Polish).
257. Siwowski, T., Radomski, W., 1998. First national application of FRP laminates for bridge Strengthening. [Pierwsze krajowe zastosowanie taśm kompozytowych do wzmocnienia mostu. Inżynieria i Budownictwo], 7, 382 – 388 (in Polish).
258. Siwowski, T. Radomski, W., 2015. The Polish experience in bridge strengthening with CFRP composites. Third Conference on Smart Monitoring, Assessment and Rehabilitation of Civil Structures SMAR 2015, Antalya.
259. Siwowski, T., Żółtowski, P., 2012. Strengthening Bridges with Prestressed CFRP Strips. SSP – Journal of Civil Engineering, 7(1), 2012.
260. Smith S.T., Teng J.G., Interfacial stresses in plated beams. Engineering Structure 2001, 23(7):857-871.
261. Smith, S.T., Teng, J.G., 2002a. FRP-strengthened RC beams. I: Review of debonding strength models. Engineering Structures; 24(4):385–95.
262. Smith, S.T., Teng, J.G., 2002b. FRP-strengthened RC beams. II: Assessment of debonding strength models. Engineering Structures; 24(4):397–417.
263. Smith, S.T., Teng, J.G., 2003. Shear-bending interaction in debonding failures of FRP-plated RC beams. Advances in Structural Engineering, 6(3), 183–99.
264. Spadea, G., Bencardino, F., Swamy, R.N., 1998. Structural behavior of composite RC beams with externally bonded CFRP. Journal of Composites for Construction, ASCE, 2(3), 132 -137.
265. Stöcklin, I., Meier, U., 2003. Strengthening of concrete structures with prestressed and gradually anchored CFRP strips. Proc. 6th Int. Symp. FRP Reinforcement for Concrete Structures, FRPRCS-6, K.H. Tan ed., World Scientific, Singapore, 1321-1330.
266. Swamy, R.N., Lynsdale, C.J., Mukhopadhya, P., 1996. Effective strengthening with ductility: use of externally bonded plates of non-metallic composite materials. Proc. of Second International Conference on Advanced Composite Materials in Bridges and Structures, ACMBS II, ed. El-Badry, M.M., Montréal, Canada, 481-488.
267. Swamy, R.N., Mukhopadhya, P., 1999. Debonding of carbon-fibre reinforced polymer plate from concrete beams. Proc. of the Institution of Civil Engineers: Structures and Buildings, 134, 301–17.
268. Taerwe, L., Khalil, H., Matthys, S., 1997. Behaviour of RC beams strengthened in shear by external CFRP sheets. Proc. of the Third International Symposium Non-Metallic (FRP) Reinforcement For Concrete Structures, 1, 483–90.

---

## References

---

269. Takahashi, Y., Sato, Y., Ueda, T., Maeda, T., and Kobayashi, A., 1997. Flexural behaviour of RC beams with externally bonded carbon fibre sheet. *Proc., Non-Metallic (FRP) Reinforcement for Concrete Structures*, JCI, 1, 327–334.
270. Takeda, K, Mitsui, Y, Murakami, K, Sakai, H, Nakamura, M., 1996. Flexural behaviour of reinforced concrete beams strengthened with carbon fibre sheets. *Composites Part A*, 27A, 981–7.
271. Täljsten, B., 1994. Strengthening of existing concrete structures with epoxy bonded plates of steel or fibre reinforced plastics. Doctoral Thesis, 1994:152, Luleå University of Technology, 290.
272. Täljsten, B., 1996 Strengthening of concrete prisms using the plate bonding technique. *Int. J. Fract.*, 82, 253–266
273. Täljsten, B., 1997a. Strengthening of concrete structures for shear with bonded CFRP fabrics. *Recent Advances in Bridge Engineering*, U. Meier and R. Betti, 67-74.
274. Täljsten, B., 1997b. Strengthening of Beams by Plate Bonding”, *ACI Journal of Materials in Civil Engineering*, 9(4), 206-212.
275. Tanaka, T., 1996. Shear resisting mechanism of reinforced concrete beams with CFS as shear reinforcement. Graduation thesis, Hokkaido University, Japan.
276. Technical Report no 55, 2000. Design guidance for strengthening concrete structures using fiber composite materials. Concrete Society, London.
277. Teng, J.G., Chen, J.F., Simth, S.T., Lam, L., 2002. FRP-strengthened RC structures. UK: John Wiley & Sons Ltd., Chichester (UK), ISBN 0-471-48706-6.
278. Teng, J.G., Lu, X.Z., Ye, L.P., Jiang, J.J., 2004. Recent research on intermediate crack-induced debonding in FRP-strengthened RC beams. *Advanced composite materials in bridges and structures*, M4. El-Badry and L. Dunaszegi, eds., Canadian Society for Civil Engineering.
279. Teng, J.G., Smith, S.T., Yao, J., Chen, J.F., 2003. Intermediate crack-induced debonding in beams and slabs. *Construction and Building Materials*, 17(6–7), 447–62.
280. Teng, J.G., Yuan, H., Chen, J.F., 2006. FRP-to-concrete interfaces between two adjacent cracks: theoretical model for debonding failure. *International Journal of Solids and Structures*, 43(18–19), 5750–78.
281. TNO DIANA BV., DIANA, User’s Manual.
282. Triantafillou, T. C., Deskovic, N., 1991. Innovative prestressing with FRP sheets. Mechanics of short-term behavior. *Journal of Engineering Mechanics*, 117(7), 1652–1672.
283. Triantafillou, T. C., Deskovic, N., Deuring, M., 1992. Strengthening of concrete structures with prestressed fiber reinforced plastic sheets. *ACI Structural Journal*, 89(3), 235–244.

284. Triantafillou, T.C., Antonopoulos, C.P., 2000. Design of concrete flexural members strengthened in shear with FRP, *Journal of Composites for Constructions*, 4 (4), 198–205.
285. Triantafillou, T.C., Plevris, N., 1992. Strengthening of RC Beams with Epoxy-Bonded Fiber-Composite Materials. *Materials and Structures*, 25(4), 201-211
286. Tumialan, G., Belarbi, A., Nanni, A., 1999. Reinforced concrete beams strengthened with CFRP composites: failure due to concrete cover delamination. Department of Civil Engineering, Center for Infrastructure Engineering Studies, Report No. CIES-99/01, University of Missouri-Rolla, USA: 1999.
287. Tyfo<sup>®</sup> UC Composite Laminate Strip System, 2015.
288. Ueda, T., Sato, Y., Asano, Y., 1999. Experimental study on bond strength of continuous carbon fiber sheet. In *Proceedings of 4th International Symposium on Fiber Reinforced Polymer reinforcement for Reinforced Concrete structure*, 407–16.
289. Uji, K., 1992. Improving Shear capacity of existing reinforced concrete members by applying carbon fiber sheets. *Transactions of the Japan Concrete Institute*, 14, 253-266.
290. Van Gemert, D., 1980. Force transfer in epoxy-bonded steel–concrete joints. *International Journal of Adhesion and Adhesives*, 1, 67–72.
291. van Mier, J.G.M., Shah, S.P., Arnaud, M., Balayssac, J.P., Bascoul, A., Choi, S., et al., 1997 Strainsoftening of concrete in uniaxial compression. *Materials and Structures*, 30(4), 195–209.
292. Varastehpour, H., Hamelin, P., 1997. Strengthening of concrete beams using fiber-reinforced plastics. *Materials and Structures*, 30, 160–6.
293. Vecchio, F.J., 1989. Nonlinear finite element analysis of reinforced concrete membranes. *ACI Structural Journal*, 86(1), 26–35.
294. Vecchio, F.J., 1990. Reinforced concrete membrane element formulations. *Journal of Structural Engineering*, 116(3), 730–50.
295. Vecchio, F.J., Collins, M.P., 1993. Compression response of cracked reinforced concrete. *Journal of Structural Engineering*, 119(12), 3590–610.
296. Vonk, R.A., 1992. Softening of concrete loaded in compression. Ph.D. thesis. Eindhoven University of Technology.
297. Wan, B., 2002. Study of the Bond Between FRP Composites and Concrete. Ph.D. Dissertation, University of South Carolina, Department of Civil and Environmental Engineering
298. Wang, C.Y, Ling, F.S., 1998. Prediction model for the debonding failure of cracked RC beams with externally bonded FRP sheets. In: *Proceedings of the Second International Conference of Composites in Infrastructure (ICCI)*, Arizona, USA, 548–562.
299. Wight, R.G., Green, M.F., Erki, M-A., 2001. Prestressed FRP Sheets for Post-strengthening Reinforced Concrete Beams., *Journal of Composites for Construction*, 5(4), 214-220.

---

## References

---

300. Wong, R. S. Y., Vecchio, F. J., 2003. Toward modelling of reinforced concrete members with externally bonded fibre-reinforced polymer composites. *ACI Structural Journal*, 100(1), 47-55
301. Wu, H.CH., Eamon, Ch.D., 2017. *Strengthening of Concrete Structures Using Fiber Reinforced Polymers (FRP): Design, Construction and Practical Applications*, Woodhead Publishing series and Structural Engineering
302. Wu, Z. S., Iwashita, K., Hayashi, T., Higuchi, T., Murakami, S., Koseki, Y., 2003. Strengthening prestressed-concrete girders with externally prestressed PBO fiber reinforced polymer sheets. *Journal of Reinforced Plastics and Composites*, 22(14), 1269–1286
303. Wu, Z. S., Yuan, H., Yoshizawa, H., Kanakubo, T., 2001. Experimental/analytical study on interfacial fracture energy and fracture propagation along FRP-concrete interface. *ACI International SP-201-8*, 133–52.
304. Xue, W., Tan, Y., Zeng, L., 2010. Flexural response predictions of reinforced concrete beams strengthened with prestressed CFRP plates, *Composite Structures*, 92, 612-622.
305. Yang, D.-S., Park, S.-K., Neale, K. W., 2009. Flexural behaviour of reinforced concrete beams strengthened with prestressed carbon composites. *Composite Structures*, 88(4), 497-508.
306. Yang, H., Wu, Z. S., Yoshizawa, H., 2001. Theoretical solutions on interfacial stress transfer of externally bonded steel/composite laminates. *J. Structural Mechanics and Earthquake Engineering, JSCE*, 18(1), 27–39.
307. Yao, J., 2004. Debonding failures in RC beams and slabs strengthened with FRP plates. Ph.D. thesis. The Hong Kong Polytechnic University.
308. Yao, J., Teng, J. G., Chen, J. F., 2005. Experimental study on FRP-to-concrete bonded joints. *Composites Part B Engineering*, 36, 99–113.
309. Yao, J., Teng, J.G., 2007. Plate end debonding in FRP-plated RC beams-I: experiments. *Engineering Structures*, 29(10), 2457–71.
310. Yeong-soo, S., Chadon, L., 2003. Flexural behavior of reinforced concrete beams strengthened with carbon fiber-reinforced polymer laminates at different levels of sustaining load. *ACI Structural Journal*. 100 (2), 231–240.
311. Yu, P., Silva, P. F., Nanni, A., 2008. Flexural strength of reinforced concrete beams strengthened with prestressed carbon fiber-reinforced polymer sheets—Part II. *ACI Structural Journal*, 105(1), 11–20.
312. Yuan, H., Wu, Z., 1999. Interfacial fracture theory in structures strengthened with composite of continuous fiber." *Proc., Symp. Of China and Japan: Sci. and Technol. of 21st Century*, Tokyo, Sept.,142–155.
313. Yuan, H., Teng, J. G., Seracino, R., Wu, Z. S., Yao, J., 2004. Full-range behavior of FRP-to-concrete bonded joints. *Engineering Structures*, 26(5), 553–564.
314. Zhang, S., Raoof, M., Wood, L.A., 1995. Prediction of peeling failure of reinforced concrete beams with externally bonded steel plates. *Proceedings of the Institution of Civil Engineers: Structures and Buildings*, 110, 257–68.

315. Zhang, S., Raoof, M., Wood, L. A., 1997. Prediction of peeling failure of reinforced concrete beams with externally bonded plates. Proc., Inst. of Civ. Engrs., Struct. and Build., London, 122, 493–496.
316. Zhang, W., Kanakubo, T., 2014. Local bond stress-slip relationship between carbon fiber reinforced polymer plates and concrete under fatigue loading. ACI Structural Journal, 111(4), 955–965.
317. Zhou, Y. W., Wu, Y. F., & Yun, Y., 2010. Analytical modeling of the bond-slip relationship at FRP-concrete interfaces for adhesively-bonded joints. Composites: Part B, 41, 423–433
318. Zilch, K., Niedermeier, R., Finckh, W., 2010. Bauteilspezifische Effekte aus die Verbundkraftübertragung von mit aufgeklebten CFK-Lamellen verstärkten Betonbauteilen. Bauingenieur, 85, 97-104.
319. Zilch, K., Niedermeier, R., Finckh, W., 2011. Sachstandbericht Verstärken von Betonbauteilen mit geklebter Bewehrung. Schriftenreihe des DAfStb No. 591, Beuth, Berlin.
320. Zilch, K., Niedermeier, R., Finckh, W., 2012. Praxisgerechte Bemessungsansätze für das wirtschaftliche Verstärken von Betonbauteilen mit geklebter Bewehrung – Verbundtragfähigkeit unter statischer Belastung. Schriftenreihe des DAfStb No. 592, Beuth, Berlin.
321. Zilch, K., Niedermeier, R., Finckh, W., 2014. Strengthening of Concrete Structures with Adhesively Bonded Reinforcement Design and Dimensioning of CFRP Laminates and Steel Plates. BetonKalender. Wilhelm Ernst & Sohn, Berlin.
322. Ziraba, Y.N., Baluch, M.H., Basunbul, I.A., Sharif, A.M., Azad, A.K., Al-Sulaimani, G.J., 1994. Guidelines towards the design of reinforced concrete beams with external plates. ACI Structural Journal, 91(6), 639–46.

ISBN 978-83-7283-996-1

